Study of the Influence of the Different Synthesis Parameter on the Structure, Morphology, Bonding and Properties of the Graphene oxide (GO), Reduced graphene oxide and Graphene/alumina Nanocomposites

By

Demudubabu Dommisa

Reg: No: 10ENPT08

in partial fulfillment of the requirement for the award of the degree of

Doctor of Philosophy In

Nanoscience and Technology

Supervisor

Dr. Raj Kishora Dash



2017

School of Engineering Sciences & Technology, University of Hyderabad, Hyderabad, India – 500046



CERTIFICATE

This is to certify that the thesis entitled Study of the influence of the different synthesis parameter on the structure, morphology, bonding and properties of the graphene oxide (GO), reduced graphene oxide and graphene/alumina nanocomposites Submitted by Demudubabu Dommisa bearing registration number 10ENPT08 in partial fulfillment of the requirements for award of Doctor of Philosophy in the School of Engineering Sciences and Technology is a bonafide work carried out by him under my supervision and guidance.

This thesis is free from plagiarism and has not been submitted previously in part or in full to this or any other University or Institution for award of any degree or diploma.

Parts of this thesis have been:

- A. published in the following publications:
 - i. Demudubabu.D, Raj Kishora Dash "Effect of the precursor graphite on the structure and morphology of graphite oxide and reduced graphene oxide Advanced Materials Letters2017, 8(3), 315-321 Ch. 4
 - ii. R. K. Dash and Demudu Babu, "Size Effects on the Morphology and Stability of Nanoparticles", BVDU Res. J. Vol. X, No. 1, p. 59-63 (2013).
- B. presented in the following conferences:
- 1. D. Babu and R. K. Dash, "Influence of graphite size on the structural, optical, and thermal properties of graphite oxide and reduced graphene oxide synthesis by modified Hummers Method" International conference on Materials science & Technology, March 2016 at University of Delhi (2016).
- 2. N. Nischal, D. Babu and R. K. Dash, "Fabrication of r-GO bismuth telluride thermoelectric Nanocomposite for energy harvesting applications", ICFM -2016, IIT Kharagpur, 23-24th, Dec, 2016.
- 3. D. Babu and R. K. Dash, "Size Effects on the Morphology and Stability of Nanoparticles", International Conference on Nanotechnology, NANOCON-2012, Bharati Vidyapeeth University, Pune, India, 18-19 October, 2012.

Further, the student has passed the following courses towards fulfillment of coursework requirement for Ph.D.

| Course Code | Name | Credits | Pass/Fail |
|-------------|----------------------|---------|-----------|
| NT601 | Research Methodology | 4 | Pass |

and was exempted from doing coursework (recommended by Doctoral Committee) on the basis of the following courses passed during his M.Tech. program (in Int. M.Tech./Ph.D. program) and the M.Tech.degree was awarded:

| Course Code | Name | Credits | Pass/Fail |
|-------------|---|---------|-----------|
| NT401 | Phase Transformation and Thermodynamics | 4 | Pass |
| NT402 | Characterization of Materials | 4 | Pass |
| NT403 | Seminar | 2 | Pass |
| NT404 | Design and Selection of Engineering Materials | 4 | Pass |
| NT405 | Nanomaterials Synthesis and Characterization Laboratory | 4 | Pass |
| NT406 | Concepts of Nano Science and Technology | 4 | Pass |
| NT407 | Synthesis and Applications of Nanomaterials | 4 | Pass |
| NT451 | Nano Biotechnology | 4 | Pass |
| NT452 | Mechanical Behavior of Nanomaterials | 4 | Pass |
| NT453 | Modeling and Simulation | 4 | Pass |
| NT454 | Powder Metallurgy and Ceramics | 4 | Pass |
| NT455 | Surface Engineering and Advanced Nanofabrication Technologies | 4 | Pass |
| NT456 | MEMS and NEMS | 2 | Pass |
| NT457 | Laboratory | 4 | Pass |
| NT458 | Seminar | 2 | Pass |
| NT601 | Research Methodology | 4 | Pass |

Supervisor Dean of School

Declaration

I hereby declare that the work reported in this Ph.D. dissertation entitled, "Study of the influence of

the different synthesis parameter on the structure, morphology, bonding and properties of the

graphene oxide (GO), reduced graphene oxide and graphene/alumina nanocomposites"

submitted to University of Hyderabad for the award of Doctor of Philosophy in Nano Science and

Technology is original and was carried out by me during my tenure as a Ph.D. scholar under the

supervision of Dr. Raj Kishora Dash, Assistant Professor at the University of Hyderabad, INDIA.

This dissertation has not formed the basis for the award of any degree, diploma, associateship,

membership or similar title of any university or institution. Finally, plagiarism of this dissertation

has been checked and satisfied the requirements.

Demudubabu Dommisa

SCHOOL OF ENGINEERING SCIENCES & TECHNOLOGY,

University of Hyderabad,

Hyderabad-500046,

INDIA.

Place: HYDERABAD

Date:

3

Acknowledgment

I would like to express the most sincere gratitude and heartfelt appreciation to the project supervisor, Associate Professor Dr. Raj Kishora Dash, for his concern, guidance and understanding rendered throughout this work, especially for his invaluable support and patience.

I am also grateful to the staff of the Centre for nanotechnology, for their assistance in the characterization of samples in Raman spectroscopy, TEM and UV- VIS Spectroscopy.

Finally, I would like to thank my family for their understanding and encouragement throughout my academic pursuit.

List of publications

- 1. Demudubabu.D, Raj Kishora Dash "Effect of the precursor graphite on the structure and morphology of graphite oxide and reduced graphene oxide", *Advanced Materials Letters*, 8(3), 315-321(2017).
- 2. R. K. Dash and Demudu Babu, "Size Effects on the Morphology and Stability of Nanoparticles", *BVDU Res. J.* Vol. X, No. 1, p. 59-63 (2013).
- 3. R. K. Dash and Demudu Babu, "Influence of the n and p-type Si on the formation of graphene oxide thin films by electrophoresis deposition", *Journal of Materials Science: Materials in Electronics* (submitted).
- 4. R. K. Dash and Demudu Babu, "Size-dependent Phase and Morphological Transformation of Alumina Nanoparticles", *J. Materials Research Express* (under review)
- 5. R. K. Dash and Demudu Babu, "Electrical conductive and exotic graphene oxide by controlling the oxidation reaction temperature in Hummers method" (Final draft to submit soon)
- 6. R. K. Dash and Demudu Babu, "Influence of different additivities on the formation of reduced graphene oxide-gamma-alumina nanocomposites by colloidal mixing", (under preparation to submit)

PAPERS PRESENTED INTERNATIONAL CONFERENCES

- 1. D. Babu and R. K. Dash, "Influence of graphite size on the structural, optical, and thermal properties of graphite oxide and reduced graphene oxide synthesis by modified Hummers Method" International conference on Materials science & Technology, March 2016 at University of Delhi (2016).
- 2. N. Nischal, D. Babu and R. K. Dash, "Fabrication of r-GO bismuth telluride thermoelectric Nanocomposite for energy harvesting applications", ICFM -2016, IIT Kharagpur, 23-24th, Dec, 2016.
- 3. D. Babu and R. K. Dash, "Size Effects on the Morphology and Stability of Nanoparticles", International Conference on Nanotechnology, NANOCON-2012, Bharati Vidyapeeth University, Pune, India, 18-19 October, 2012.

Abstract

Graphene is an emerging material due to its unique properties such as electrical, mechanical, optical, chemical and thermal properties and hence it has a lot of potentials to use in several applications. The graphene oxide is generally defined as a single layer of graphene with oxygen functional groups present in basal planes and edges of the graphene structures. These functional groups are mostly hydroxyl, epoxide, ketone and carboxyl on the surface of graphene layer at basal plane and edges. Therefore, GO is easily dispersible in water and other organic solvents and hence, mostly applicable in different forms such as thin films, composites and hybrid materials. Composites are novel type materials and have unique properties than host matrix. Graphene can be used in the composite material as filler to develop novel composites which have novel and unique properties. Comparative other nanomaterial graphene is more suitable for making the nanocomposite because of easy synthesis process of graphene with large-scale production for industrial application. To prepare the graphene-based composite mostly used graphene derivatives, it has tunable electrical and optical properties, based on the composite properties the applicationsFrom the recent literature, we have concluded that graphene oxide can be synthesized by a chemical process which is a simple, costeffective and more economical. Further, the obtained GO can be reduced by using suitable reducing agents to obtain reduced graphene oxide(RGO), which has a lot of potentials to be used in several applications. However, most of current studied mainly focus on the synthesis of the graphene oxide and the corresponding reduced graphene oxide by using one size graphite precursor material (~45µm). Therefore, the impacts of the different size graphite precursors (very smaller to a larger size) as starting material for synthesis of GO and RGO and the details study of the oxidation process, structure, Morphology, bonding characteristics etc are not addressed to our best knowledge. Therefore, there is a lack of clear understanding of the influence of different sizes graphite precursor on the synthesis of GO and RGO by a chemical process. Thus, these issues and challenges need to be addressed. Further, the oxidation reaction temperature is a key factor for controlling the properties of the GO, and further, the quality of RGO obtain from the as-synthesized GO. Hence, the influence of the reaction temperature of the oxidation process need to be addressed and a more details investigation of its effects on the structure, morphology, bonding to be required. Moreover, the reduction of GO to RGO is generally carried out in a few solutions, so more work is still required to understanding the solution effects on the reduction of GO to RGO.

In the second part of literature review part, we have thoroughly searched all the recent literature on the synthesis and characterization of the graphene/alumina nanocomposite for its potential to be utilized as potential materials for several applications such as energy, storage devices, capacitors, memory devices and so.on. Though, there are several existing syntheses processes has been reported by several groups and also mentioned that electrical and mechanical properties can be improved by

fabrication of the graphene alumina nanocomposite. It is observed that most of the reported work has chosen the α – phase alumina nanoparticles to synthesize the nanocomposites due to the stable phase of the alumina. Also, few reported work are existing, where they have prepared alumina by choosing the alumina precursor to synthesize the alumina by chemical processes such as sol-gel method, finally fabricating the graphene/alumina nanocomposites. Moreover, the most of the reported work mainly focuses on the fabrication of the bulk materials by SPS process and then to investigate the different properties of the nanocomposites.

Therefore, to the best of our knowledge, still, there is a lacking of clearly understanding the graphene /alumina nanocomposite structure, morphology, and bonding characteristics, when γ – phase alumina is employed as matrix material insisted of α – phase alumina. Further, the as the obtained powder form of the graphene /alumina nanocomposite need to be studied in details, as these powder form can be used as starting material for thin films formation, for another hybrid material synthesis and also for utilizing as filler material for more complex hybrid material fabrication.

Thus there are still more challenges are there to clearly understand the GO and RGO synthesis process by a chemical method and also for fabrication of graphene /alumina nanocomposites for effectively using these materials for mass production and also for several practical applications.

In this thesis research work, the influence of the synthesis parameters such as oxidation reaction temperature (low and high) on the structure, morphology, bonding and properties of the graphene oxide(GO) and the corresponding chemically and thermally reduced graphene oxide(RGO) was studied by using the standard Modified Hummers synthesis method. In the second part of the thesis work, the influence of the different sizes source graphite on the synthesis of graphene oxide (GO) and corresponding reduced graphene oxide (RGO) was investigated by choosing the optimum synthesis parameters as obtained from the first part of the research work. The impacts of host graphite powder sizes on the structure, morphology, disorder, bonding and properties were also investigated by using the different analytical instruments. In the final part of the thesis work, a set of six GO/RGO-Al₂O₃ nanocomposite was synthesized by choosing γ -phase Al₂O₃ using the colloidal mixing process and the effects of the different additives such as HCl, Hydrazine hydrate and without any additives were investigated. The corresponding nanocomposites structure, morphology, bonding, interface and thermal stability were investigated by using different analytical instruments such as XRD, FESEM, TEM, FT IR, Raman spectroscopy and TGA/DTA for understanding the nanocomposite formation.

Graphene oxide was synthesized by varying the reaction temperature (low and high) by using the equal ratios of graphite, H₂SO₄, NaNO₃ and KMnO₄. All the samples were analyzed by using the XRD, FT IR, Raman, TEM, FESEM, UV and TGA/DTA for structural, molecular & bonding characteristics, morphological and thermal analysis. Experimental results indicated that oxidation reaction temperature has an effective role in the synthesis of GO. It was observed that low-temperature reaction showed the good quality of graphene oxide(GO) with better structural, less disorder and 2-3 layers of GO as compared to the higher reaction temperature. Further, the

corresponding reduced graphene oxide (RGO) was obtained by using hydrazine hydrate and thermal reduction process, and experimental results confirmed that the RGO which was obtained by using the lower reaction temperature GO showed less disorder, more graphical structure, flat type and 2-3 layers as compared to the GO obtained at higher temperature.

Three different sizes graphite precursor (2-15 µm, <45 µm, and 170-840µm,) were oxidized by MHM method and then corresponding RGO were synthesized by the hydrazine hydrate reduction process. The experimental results indicated that the smaller size precursor graphite was fully oxidized in comparison to the large size graphite as source material. Hence, oxidation of graphite to graphene oxide is size depended on the source graphite and also showed better quality of reduced graphene oxide than other sizes. Further, from the TGA and DTA analysis, it is observed that different weight loss and different exothermic peak position in the graphite oxide which suggest that weight loss also depends on the size graphite due to the oxidation rate. UV spectroscopy analysis shows different abortion peaks which indicated that all the sizes graphite oxidized differently. Hence, the precursor graphite size has a key role in the synthesis of GO and corresponding RGO.

A set of six GO/RGO-Alumina nanocomposites were prepared by colloidal mixing process by varying the reaction temperature (at RT and 80^{0} c) and different additives such as HCL and hydrazine hydrate. From all the analytical analysis results such as XRD, FESEM, FTIR, Raman, TEM is TGA and DTA, it was concluded that only when hydrazine hydrate was used as an additive GO was reduced during the synthesis process and RGO – Al2O3 nanocomposite was formed. All other cases GO – Al2O3 nanocomposites formed. Hence, RGO-Alumina nanocomposite can be synthesized by using hydrazine hydrate as an additive during fabrication process by using a smaller size γ -phase alumina nanoparticles.

Different GO/RGO- Al2O3 nanocomposites were synthesized by using the optimum process parameters as obtained by varying the wt% GO (0.5, 1, 3, 5, 10 and 20 wt %) and all the samples were analyzed by using XRD, FT IR, Raman and TEM. Experimental results indicated that as the GO content increases more disorder and less agglomeration of the alumina nanoparticles are observed. Further, it was seen that as the GO content increases the oxygen-related function groups are removed because of more interaction between the GO and alumina nanoparticles.

In this thesis work, GO/RGO- alumina nanocomposites were synthesized and formation of the graphene-alumina nanocomposite was confirmed based on the structural, bonding, morphological and TGA/DTA analysis, however still to use such nanocomposites in practical application such as energy storage, memory devices and other applications, properties such as mechanical, catalytic and electrical are needed to be addressed. Therefore, the future scope of this thesis works to investigate the electrical, mechanical properties and the percolation threshold in order to utilize this nanocomposite for practical memory devices and energy applications.

Contents

Chapter 1 – Introduction

Chapter 2 – Literature review

- 2.1 Recent Literature review
- 2.2. Current challenges and issues
- 2.3 Motivation and objective of the thesis
- 2.4 Thesis outline

Chapter 3 – Influence of the chemical synthesis parameters on the structural, morphology, bonding and thermal properties of GO and RGO synthesis by MHM

- 3.1 Introduction
- 3.2 Effect of reaction temperature (low temperature) on the synthesis of GO and RGO by MHM
- 3.2 Effect of reaction temperature (at higher temperature) on the synthesis of the GO by MHM
- 3.3 Effect of solvents on the reduction of graphene oxide reduction (rgo)
- 3.4 Conclusion

Chapter 4 – Influence of the precursor graphite size on the structure, morphology, and bonding characteristic of the graphene oxide and reduced graphene oxide

- 4.1 Introduction
- 4.2 Synthesis of graphite oxide by different sizes precursor graphite
- 4.3 Synthesis of graphene oxide by chemical reduction process
- 4.4 Characterization of GO and RGO
- 4.5 Conclusion

$Chapter \ 5-Influence \ of \ synthesis \ parameters \ on \ the \ synthesis \ of \ GO/RGO-Alumina \ Nanocomposite \ by \ colloidal \ mixing \ process$

- 5.1 Introduction
- 5.2 Source graphite oxide and alumina nanoparticles for synthesis of nanocomposites
- 5.3 Preparation of GO-alumina nanocomposites by colloidal mixing process
- 5.4 Structural analysis by XRD
- 5.5 Bonding characteristic by FTIR
- 5.6 UV Spectroscopy analysis
- 5.7 TGA and DTA analysis
- 5.8 Morphological analysis by FESEM
- 5.9 Structural and Morphological analysis by TEM
- 5.10 Raman analysis
- 5.11 Conclusion

Chapter 6 - Influence of GO wt% in the formation of RGO-Al₂O₃ Nanocomposite

- 6.1 Introduction
- 6.2 Preparation of different GO wt% in the formation of RGO-Al₂O₃ Nanocomposite
- 6.3 Structural analysis by XRD
- 6.4 Bonding characteristic by FTIR
- 6.5 Raman analysis
- 6.6 Structural and Morphological analysis by TEM
- 6.7 Conclusion

Chapter 7 – Conclusions, Limitations, and Scope of Future Work

References

Chapter 1

Introduction

1.1 Why choose nanotechnology

The idea of nanotechnology was given by the Richard Feynman in his talk "There's Plenty of Room at the Bottom." In this talk, he had described the process of the individual molecules and atoms. After ten years, the first nanotechnology term was used by Proof. Nario Taniguchi for his experimental work. Now -a- days people have been explored in the Nanotechnology research due to the excellent properties exhibited by materials in the range of 1-100nm size. These materials drastically different from the bulk materials [1] because of such nanomaterials possess high surface area to volume ratio. Currently, vigorous research is going on globally to study the excellent novel phenomena and properties of nanoscale materials for understanding the fundamental science and also for technological applications [2-18]. Nanotechnology is an interdisciplinary subject, deals with physics, chemistry, biology, materials, and different branch of engineering. Different types of nanomaterials are existing such as 0D (nanoparticles, quantum dots and clusters [19-21]), 1D (nanotubes, nanowires and nanorods 22-25]) and 2D materials(nanocoatings and nano-thin films [26-30]. Therefore, nanomaterials and nanotechnology have become an emerging area for both fundamental understandings and for practical application of the materials at the nanoscale. Out of several types of nanomaterials like metals, ceramics, polymers, and carbon-based nanomaterials such as carbon nanotubes, carbon fibers, and graphene are emerging as key advanced materials for future advanced technologies [5-45].

1.2 Carbon-based Materials

Among all of these nanomaterials, carbon-based nanomaterials are showing unique properties such as physical, optical, mechanical, chemical and electrical properties [31]. These materials show

different allotrope form such as graphite, amorphous carbon, fullerene, CNT, and graphene because of SP² and SP³ hybridization. [32].

Graphite

Graphite is naturally formed of carbon. It has a layer and planar 3D structure of hexagonal crystal structure. It has lattice parameter 0.142nm, and the interplanar distance between the layers is 0.335nm. In this material, the carbon atoms bind together by Van der Wall forces with sp² hybridization. This material is very soft and good electrical conductor [33-36].

Amorphous carbon

Amorphous carbon is soot and black form of carbon. It does not have any crystal structure because of carbon atoms are randomly arranged. This material can be used in inks, paints and industrial rubber filler [37-39].

Fullerene

There are more than 30 forms of fullerene. It looks like a soccer ball and also called C60 molecules. It has 60 carbon atoms with pentagonal and hexagonal carbon rings in which no two pentagons share an edge, but hexagonal rings are shared with edges. In this material, each carbon atoms covalently bonded to the three adjacent carbon atoms. Its diameter is around 1nm. Its hardness is more than diamond and can be used in drug delivery and antioxidants [40-41].

Carbon Nano Tube (CNT)

CNT materials are one form of the fullerene (0D), where the fullerene is elongated as cylindrical with a diameter in nm, micro or millimeter length. Therefore it is a 1D material and appears in a hollow cylinder with a curved sheet of the graphitic layer. The carbon atoms are bonded with sp² hybridization. The CNTs can be classified as single-walled(SWCNT), double walled (DWCNT) and multi-walled carbon nanotubes(MWCNT). This material shows extraordinary properties, such as high electrical conductivity, high tensile strength, ductility, thermal conductivity and chemical stability [42-43]. Hence, there are several possible applications and few of them are also commercialized.

Graphene

The single atomic thin layer of graphite is called graphene. It is a 2D material and formed with sp2 hybridization of carbon atoms arranged in honeycomb hexagonal lattice manner. Recently graphene is a most emerging material due to its unique properties such as electrical, mechanical, chemical, physical, thermal and optical properties [44-45]. Some of the carbon allotropes can be obtained through the graphene sheet, such as fullerene can be formed by graphene sheet wrapped up into the 0D material, it can be rolled into 1D and formed CNT and stacked of graphene sheets to form 3D graphite. Different types of allotropic form of graphene are shown in Fig 1.1.

1.3 Graphene synthesis

There are several synthesis processes to obtain graphene such as mechanical exfoliation, epitaxial growth, CVD method and chemical methods. These methods are briefly discussed in this section.

1.3.1 Mechanical exfoliation

In 2004, Konnstaintin Novoselov and Audre Geim reported single layer of graphene by using the mechanical cleavage [46-49]. In this method, two steps are involved such as the first one is splitting of graphite repeatedly by using scotch tape and secondly small species are dissolved in acetone and finally deposited these pieces onto the silicon substrate. This process is shown in Fig.1.2. This synthesis method has few drawbacks due to the small species of graphene sheet size and obtained product is also small quantity. So, it cannot be applicable for the industrial applications, but this method was used fully for the studying the fundamental research for accurate properties of graphene because the obtained graphene did not contain any defects.

1.3.2 Epitaxial growth

In this method, graphene layers are grown on the silicon carbide (SiC) substrate at high temperature i.e. around 1100°C [51-58]. After growing the graphene layers are separated from the substrate by using the etching process. This method is very expensive and time-consuming also. This process is shown in Fig. 1.3.

1.3.3 Chemical Vapour Deposition (CVD)

By using CVD method, large-scale production of graphene films can be obtained, but it needs the elevated temperatures operating through the precursor such as hydrocarbon gas [59-64]. Also, this

process requires a metal catalyst such as Cu, Ni and finally transfer process. This method can be limited to the industrial applications due to expensive process. Because of deals with costly deposition and transfer process. However, the quality of graphene is very excellent for electronic devices.

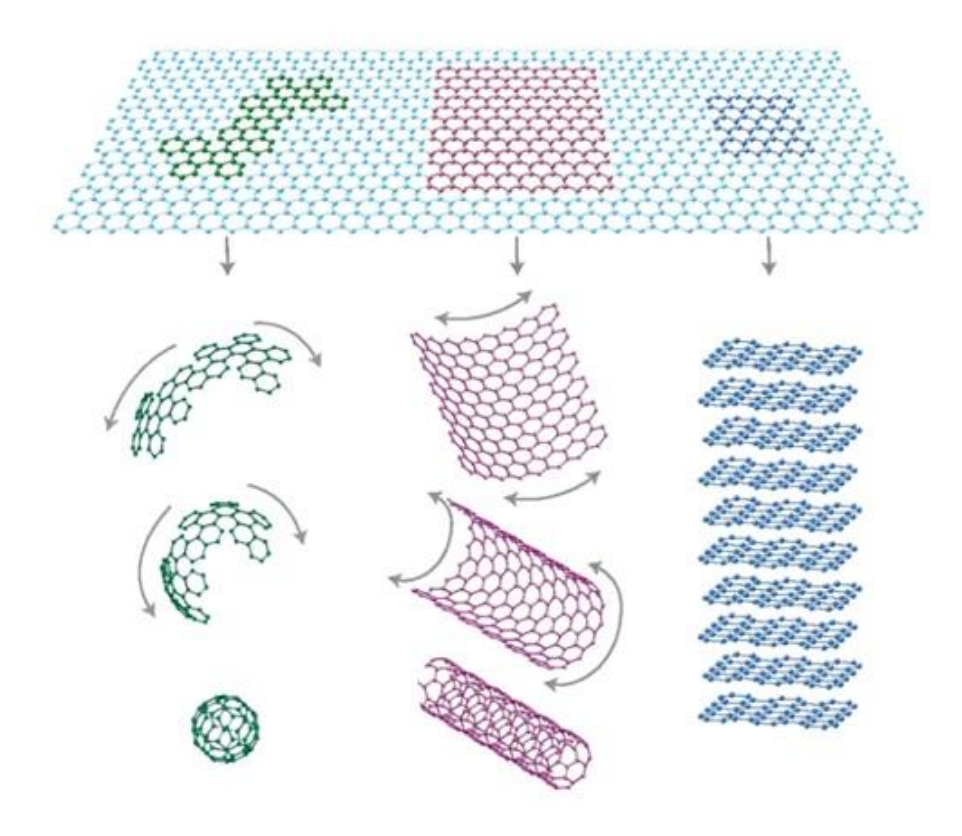


Fig.1.1 Different types of allotropes from graphene [45].



Fig.1.2. Mechanical cleavage process by using the scotch tape [50].

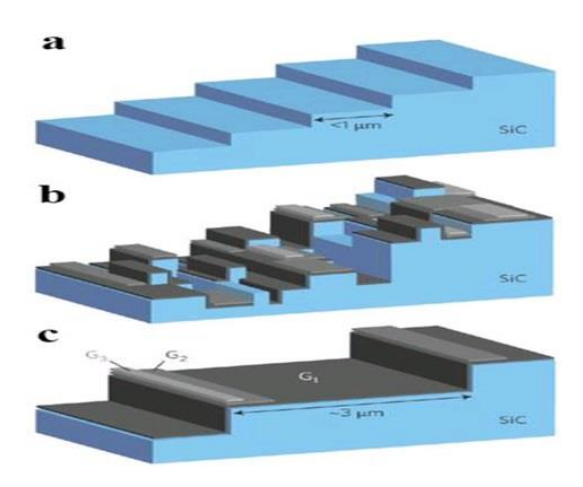


Fig. 1.3 Epitaxial growth of graphene layers on SiC substrate(a) pure SiC(b), graphitized SiC (c), Morphology graphene obtained from the surface in high-pressure argon [51]

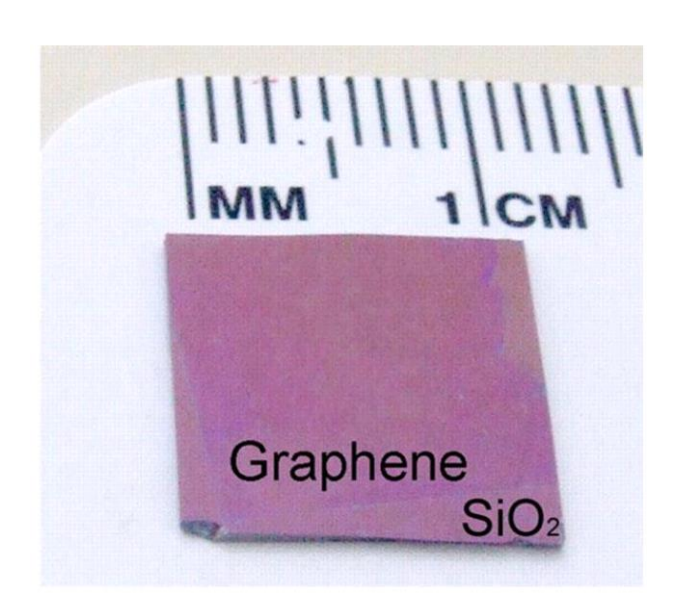


Fig. 1.4 Graphene films obtained by Chemical Vapour Deposition [59].

1.3.4 Chemical Method

Generally, this process requires graphite as source materials and by using chemical process graphene is synthesized. Several types process are already reported such as Brodie [65], Staudenmaier [68] and Hummer's method [70].

Brodie method [65-67]

In 1859, Benjamin Brodie studied the reaction of the graphite with strong oxidation agents such as chlorates, and the obtained material was known as graphite acid ($C_{11}H_4O_5$ with C/O ratio 2.2). This method has few drawbacks due to the formation of more quantity of ClO_2 gas during the reaction and also these gases are very explosives.

L. Staudenmaier[68-69]

This process is modified from the Brodie method using the Sulphuric acid into the mixture of nitric acid and potassium chlorate of Brodie method.

Hummer's method[70-75]

In 1958, Hummer and Offerman successfully prepared the graphite oxide without chlorate by using the KMnO4. This process was known as Hummers method and still, mere research is in progress to improve to improve this process. Such as improved Hummers method, NaNO₃ free modified Hummers method. Fig.1.5 shows the comparisons between all these three methods of preparation of graphene oxide. The following section deals with the properties of the graphene.

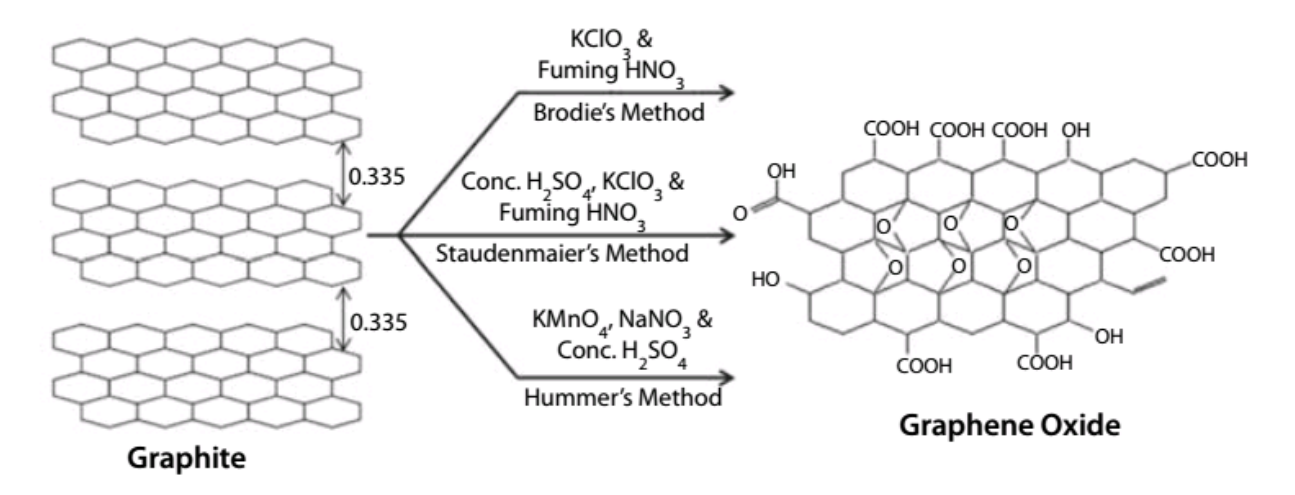


Fig.1.5 Schematic illustration of Brodie's method, Staudenmaier's method and Hummers' method to prepare graphene oxide [76].

1.4 Properties of graphene

Graphene can be utilized in a wide range of applications due to its excellent and unique properties such as optical, electrical, chemical, physical, electronic, Quantum Hall Effect, Mechanical and thermal properties.

1.4.1 Optical properties[77-82]

Graphene has sp^2 hybridization of carbon atoms arranged in honeycomb lattice structure as shown in Fig 1.6 (a). The optical properties of graphene are mainly due to the free electrons in the P_Z orbital

that can form π bonds covalently. These bonds can form as bonding and antibonding due to the overlapping of P_Z orbitals so that properties of graphene depends on the electronic band structure of the graphene. In Fig. 1.6 (a), a1 and a2 represent lattice vectors and values are $a1=a/2(3, \sqrt{3})$ and $a2=a/2(3,-\sqrt{3})$. where a=1.42Å is the distance between two carbon atoms and $\delta 1=a/2(1, \sqrt{3})$, $\delta 2=a/2(1, -\sqrt{3})$ and $\delta 3=-a(1,0)$ are the nearest neighbor real space vectors. As shown in Fig. 1.6 (b) the Brillouin zone vectors points in the graphene unit cell. It has two atoms in this figure b1, and b2 are reciprocal lattice vectors these can be written as $b1=2\pi/a((1,\sqrt{3}),b2=2\pi/a((1,-\sqrt{3}))$ and k and k' are the Dirac points which are massless. Which is also represents the momentum space vectors $k=(2\pi/3a,2\pi/3\sqrt{a})$ and $k'=k=(2\pi/3a,-2\pi/3\sqrt{a})$. This electronic structure is mainly responsible for the optical properties of graphene. In the graphene, the absorption of the graphene is active in the infrared region and due to the π - bonds of carbon atoms. Therefore, it possesses 97% of transmittance for single-layer of graphene and varies as the no.of layers increases.

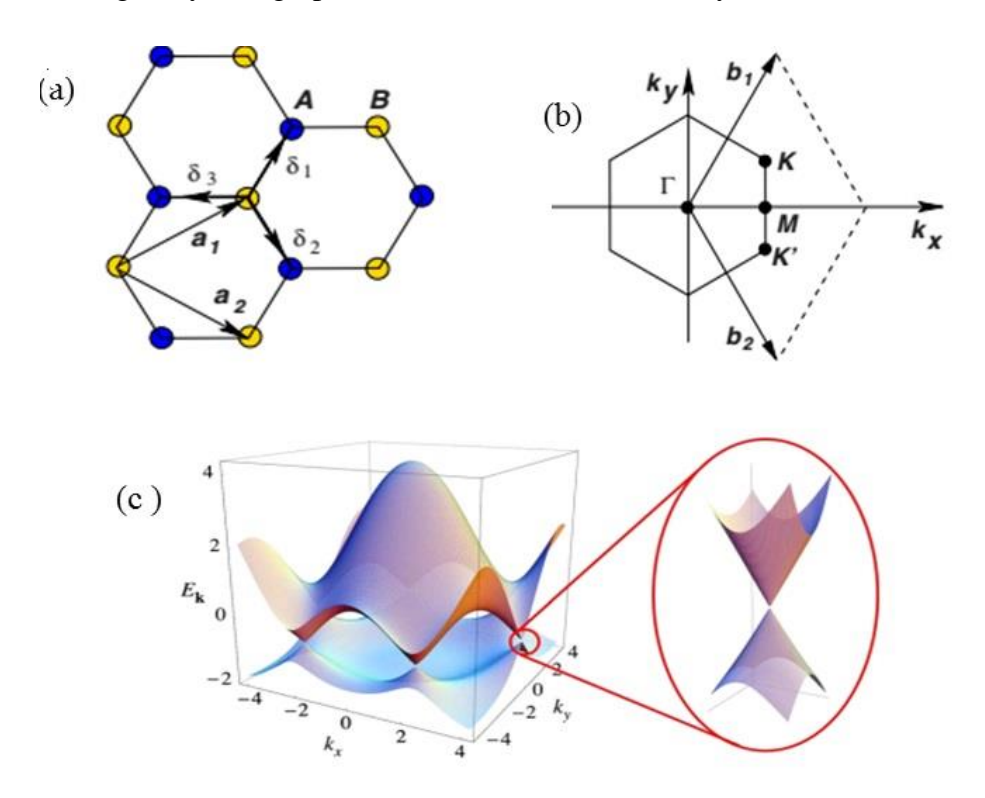


Figure.1.6 (a) Honeycomb lattice structure of graphene, (b) Graphene Brillouin zone and (c) Band structure of graphene [77].

1.4.2 Electrical properties[83-89]

Graphene consists of massless Dirac points, and hence there is no band gap so, it consists of more free electrons and shows higher conductivity. The band gap can be tuned by different graphene

derivatives useful in transistors and high-frequency application of the electronic devices. Also, due to π – electrons it shows unique electrical properties.

1.4.3 Mechanical properties[90-94]

Still today graphene is the strongest material comparative other material like diamond and also 300 times stronger than steel material. It consists of higher Young's modulus i.e 1.07Pa [90] and very high fracture strength i.e 130GPa[90] such values depend on the quality of graphene and vary with different derivative graphene and structure. It has been also reporting that it shows the less tensile strength of chemically reduced graphene and can be improved ceramic composites and used in optoelectronic applications. Graphene is very stretchable and thus it makes this promising material for using in different applications.

1.4.4 Thermal conductivity[95-100]

The thermal conductivity of graphene is very high due to the less mass of Dirac fermions and strong anisotropic bonding of carbon atoms and this material exhibits very high thermal conductivity than CNT, graphite, and diamond [95]. The reported thermal conductivity value was 3000-5300 of Single-layer graphene [96]. The next section describes the different applications of graphene.

1.5 Applications of Graphene

Graphene is an emerging material due to its unique properties such as electrical, mechanical, optical, chemical and thermal properties and hence it has a lot of potentials to use in several applications. As shown in Fig. 1.7, some of the applications of the graphene are described the following subsections.

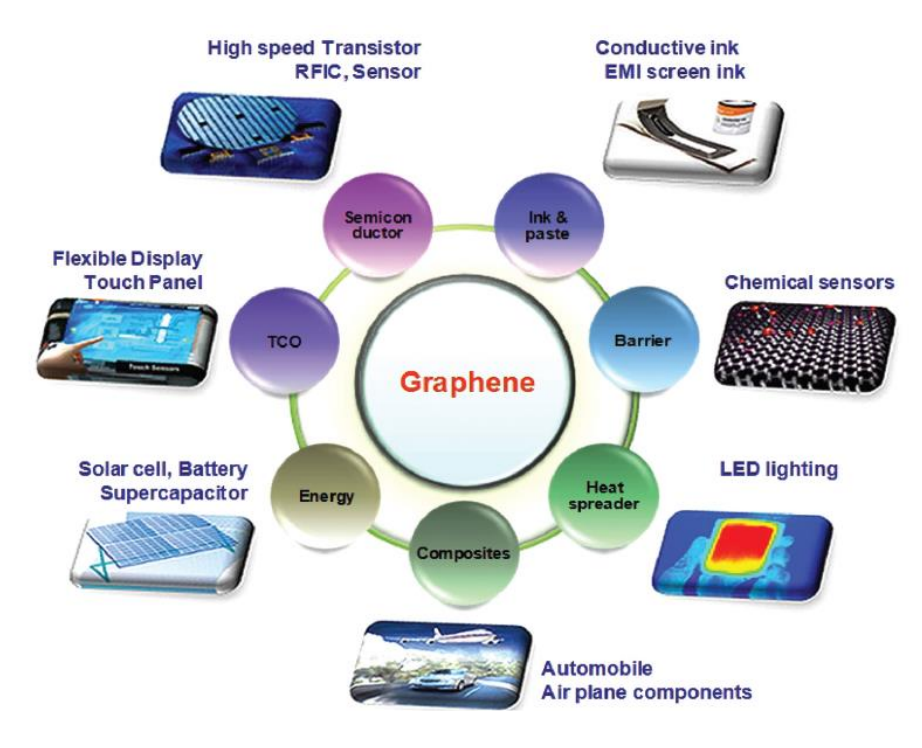


Fig. 1.7 Graphical illustration of wide range possibility applications of the graphene[101]

Electronic devices

More than 50 years onwards semiconducting devices are developed based on the Moor's law [102] for integrated circuit technology based on Si – band technology. These dives are now limiting the scaling law to fabricate transistors and can use up to 2020. Therefore, new materials are needed to overcome the future challenges for transistors devices. In this context, graphene can be chosen an alternative due to its unique properties such as high electron mobility and blastic transport. These features are more attractive for transistor applications. In 2007, Melinda.Y.H, et al. [103] first developed GNR – FET device by using the e- beam lithography and oxygen plasma etching. J.B.Oostinga et al. [104] developed the double – gate graphene device, and they have reported that device Mobilities can be reached to 230000cm2/V/S. This value represents the ballistic transport over micron length scales. Figure 1.8 shows the graphene electronic device.

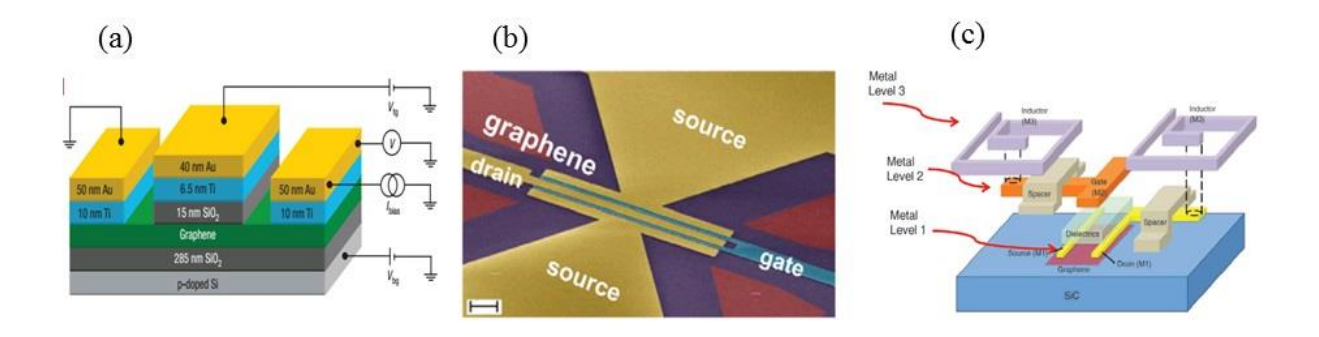


Fig.1.8 (a) The double – gate graphene device[104], (b) Radio-frequency graphene field-effect transistor[105,106] and (c) Graphene integrated circuit[107].

Photonics and Optoelectronics[108-114]

Graphene exhibits peculiar optical properties such as absorption of independent wavelength, tunable bands gaps, and more charge carriers, because of these properties graphene can be utilized to develop photonic devices.

Sensors[115-123]

Sensors are an emerging technology and have a lot of potentials to use a wide range of application such as aerospace, healthcare, automation, biomedical, devices, energy, space and some applications etc. there are several different types sensors are available such as a mass sensor, force, chemical, electrical sensors, biosensors and so on.Nowadays graphene-based sensors are emerging as a new area of research and several groups are actively working to develop new types sensors by using graphene as sensing material. For example, graphene-based sensors used in high-frequency devices. This frequency range was detected by the graphene-based sensors. Different graphene-based sensors shown in Fig.1.9. for this purpose very high efficient sensors those are cost-effective, energy efficient, easily integrate to other devices, is required for future technology.

Flexible Electronics[125-129]

Still, to date, most of the electronic devices are developed by using the rigid material. However, if flexible materials are used then such devices are foldable, lightweights and long-lasting. Hence graphene can be used as flexible materials for the development of flexible electronic device because of flexible and transparent properties of graphene. Also, this material is more useful to fabricate

flexible device because of transformation making the human touchable device. The graphene-based flexible devices are shown in Fig. 1.10.

Energy storage and Conversion [130-140]

Due to the current energy crisis, alternative energy is required for running all day to day electronic devices, cell phones, home applications, automobile etc to develop energy storage and conversion devices through the fabricating batteries, capacitors, and fuel cell. Nowadays, more research is carried on graphene-based energy storage application due to its high surface area. However comparative traditional based material device to the graphene-based material, have high complicated fabrication process and high-cost effect. Graphene-based thermo–electronic device is shown in Fig.1.11.

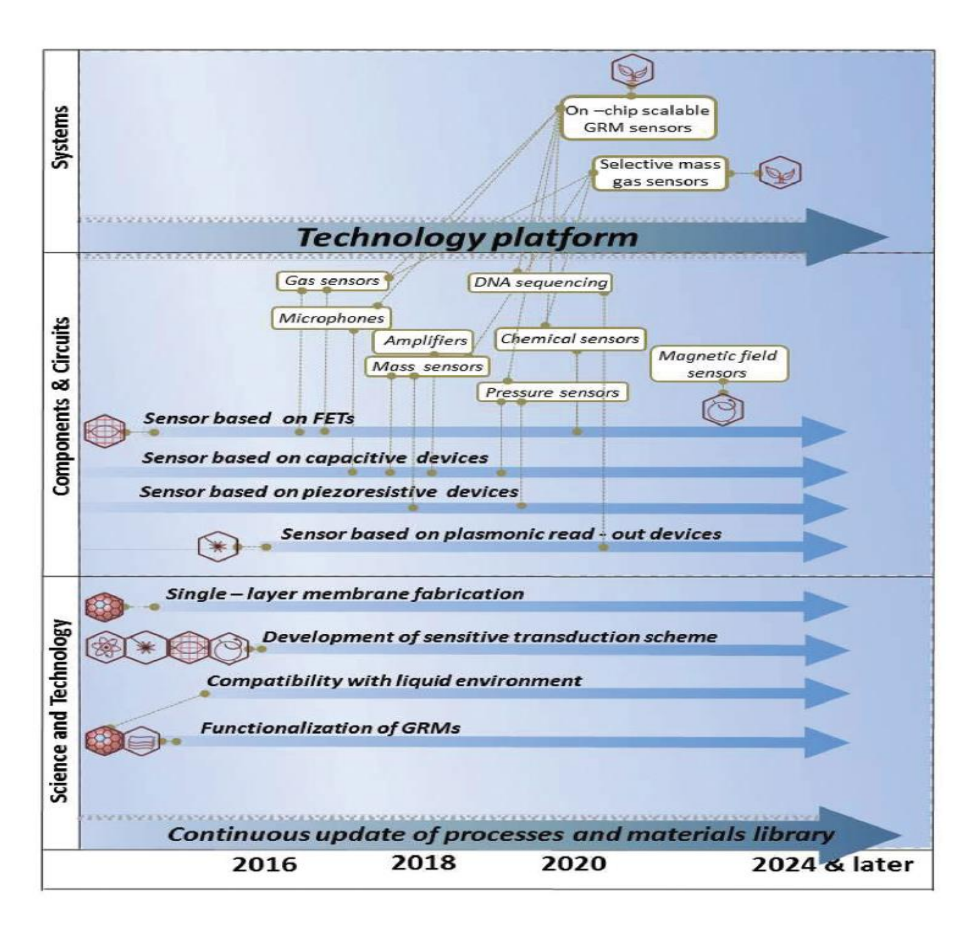


Fig. 1.9. Different Graphene-based sensors with time [124]

Composites [141-150]

Composites are novel type materials and have unique properties than host matrix. Graphene can be used in the composite material as filler to develop novel composites which have novel and unique properties. Comparative other nanomaterial graphene is more suitable for making the nanocomposite because of easy synthesis process of graphene with large-scale production for industrial application. To prepare the graphene-based composite mostly used graphene derivatives, it has tunable electrical and optical properties, based on the composite properties the applications [141-150].

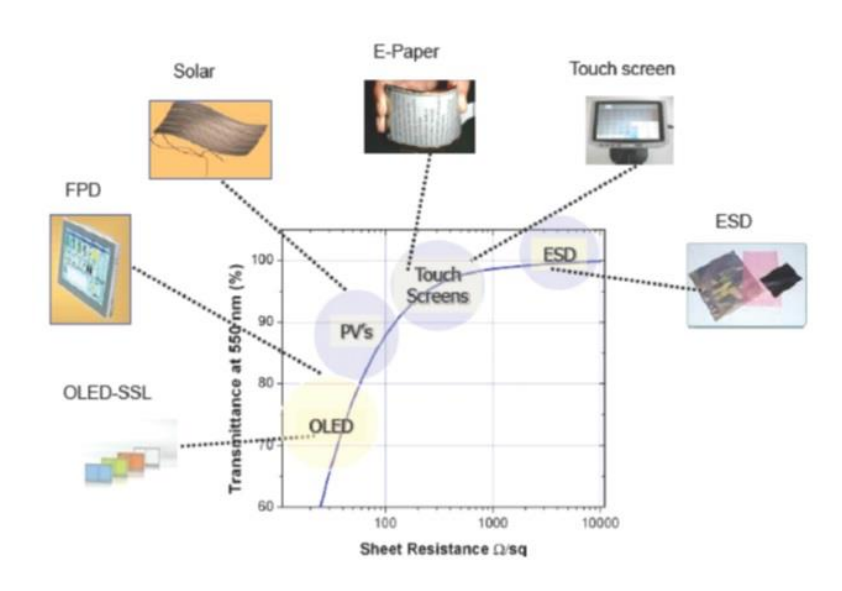


Fig. 1.10. Graphene-based flexible devices [129]

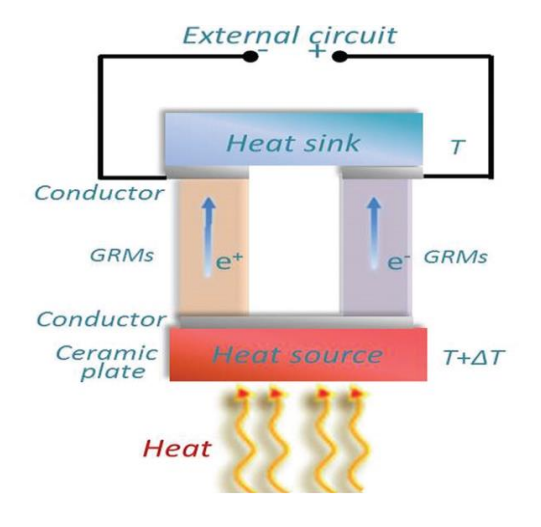


Fig. 1.11 shows the energy conversion diagram [140]

1.5 Conclusions

This chapter deals with the basic introduction of nanomaterials and nano techniques, synthesis of graphene by different processes, properties of the graphene and finally current utilization of graphene in different applications. Next chapter involves the current literature review, current challenges, and objective of this thesis work.

Chapter 2

Literature Review

2.1 Literature review

This chapter describes the up-to-date literature review on the chemical synthesis of graphene oxide, reduced graphene oxide and GO/Al₂O₃ or RGO/Al₂O₃. Final section deals with the current challenges and issues in these areas, objective and outline of this future's work.

2.2 Literature review on synthesis Graphene Oxide (GO) by chemical Method.

The graphene oxide is generally defined as a single layer of graphene with oxygen functional groups present in basal planes and edges of the graphene structures. These functional groups are mostly hydroxyl, epoxide, ketone and carboxyl on the surface of graphene layer at basal plane and edges [151]. The arrangement of these groups and mechanism of GO is explained by different models. In 1930 Thiele et al.[152] had proposed a structural model. In this model the oxygen-containing the functional group, OH attach to the carbon atoms with a covalent bond as shown in Fig. 2.1 and they had proposed a formula for graphene oxide like C₆O₃H₃. In 1934 Hofmann et al.[153], had proposed that the epoxy groups are attached to the graphene oxide. These bond are weak showed as shown in Fig. 2.1. In 1947 Ruess et al. [154], had proposed a where model the hydroxyl groups present on the basal plane of GO as shown in Fig. 2.1. In 1957 Clauss et al. [155] explained the presence of carbonyl and hydroxyl groups on the graphene sheet as shown in Fig. 2.1. After 60 years later, Nakajima et al.[156] showed the GO structure model as a similar to the Thiel model but a change in formula $C_8(OH)_4$ for the $C_6(OH_3)$ of Thiele model which shown in Fig. 2.1. However, still to date, the mechanism of graphene oxide is unclear. Basically, the graphene oxide is synthesized by chemical methods which involve the oxidized agents such as KClO₃ and KMnO₄ and form ClO₂ and MnO₇ in the presence of con.H₂SO₄/HNO₃. Then the reactive species such as MnO₃⁺ penetrate into the interlayer spacing between the two positively charged graphite layers. Recently, Ayrat.M. Dimiev et al.[157], have explained the graphene oxide mechanism, by reporting that the complete oxidation process happens by three steps, each step is independent of each other. In the 1st step, graphite is mixed with H₂SO₄, and followed by the stirring. In this step, H₂SO₄ and molecules and HSO₄⁻ ions can occupied between the graphite layers. This stage of material is represented as graphite intercalated compound (GIC). This reaction can be completed within 3-5 minutes only. In the 2nd step, the oxidizing agent is added to 1st step material (GIC), then the oxidized agent form ions or molecule (for example if KMnO₄, is chosen then it form MnO₇ and MnO₃⁺). These diffuse in between the graphite layers and remove the intercalated molecule or reactants. Also, it reacts with the carbon atoms to form new types of C-O bonding. This stage material is called as oxidized graphite. This material consists of C-axis ordered form of the graphite. This process generally takes a long time (hours to days). In the 3rd stage, PGO is exfoliated by the water, and individual graphene oxide (GO) can be obtained. These three steps are shown in Fig. 2.2.

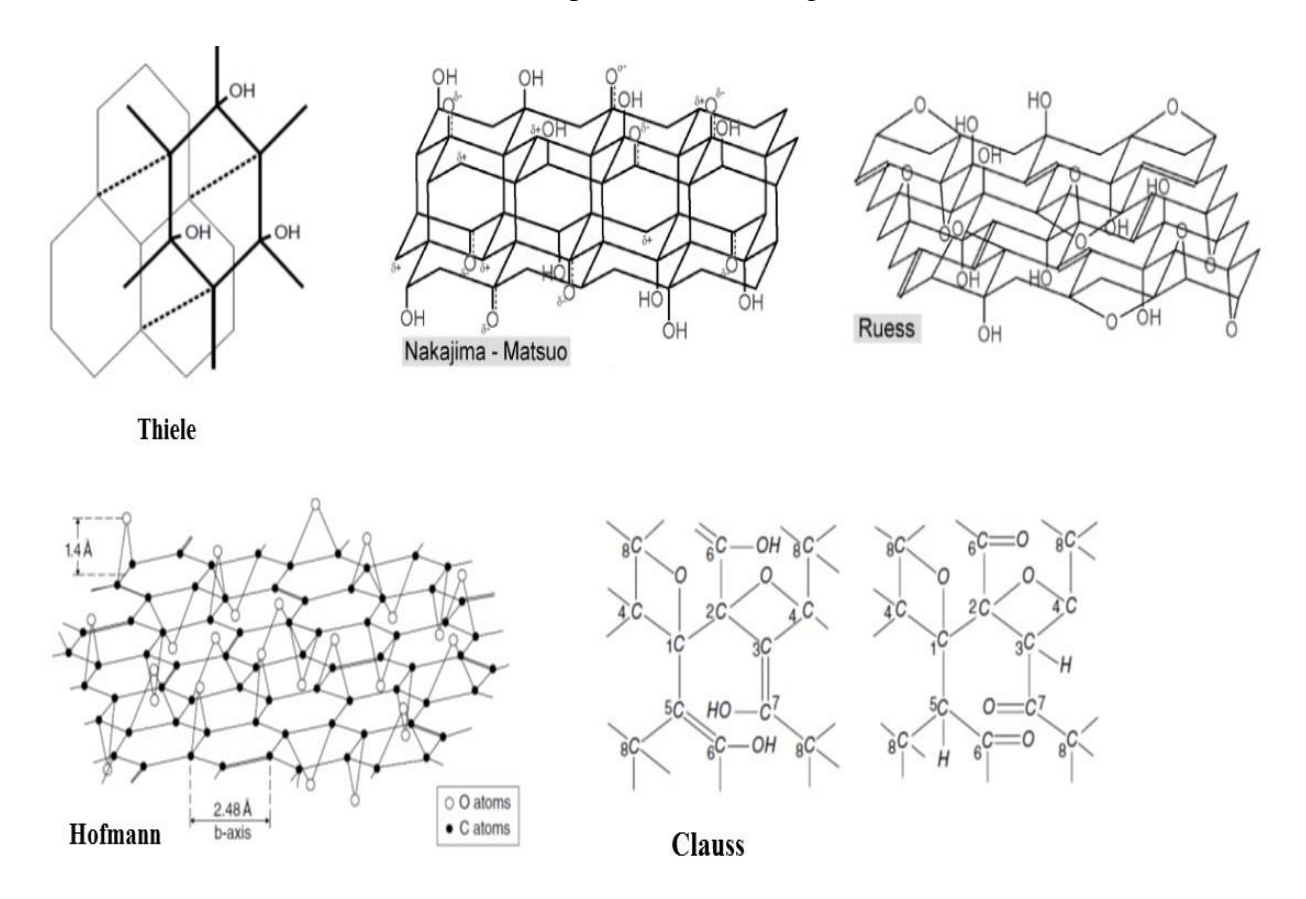


Fig. 2.1 Different oxidation models of graphene oxide as proposed in the literature [152-156].

Still, to date, graphene oxide mechanism is unclear because of variation in the formation of the oxygen functional groups. These functional groups attached to the graphene sheet mostly depends on the oxidation process method, reaction temperature, reaction time, variation in the oxidizer agent quantity and percentage of oxidation (fully oxidized or partially oxidized). Gongkai Wang et al.[158] have studied the structural and optical behavior of the different degree oxidation of the graphene oxide. They have prepared GO by different methods and using the graphite size is 20µm.

The structural analysis is carried out by the XRD and shown in Fig.2.3 (a), in which the graphite with $2\theta=26.5^{\circ}$, d= 0.336nm and $2\theta=9^{\circ}$, 10° , and 11.1° with d=0.979, 0.880 and 0.799nm for the No-1, No-2, No-3 samples respectively. No-4 sample has $2\theta=26.4^{\circ}$ with d= 0.338nm. From these results, it clear that No-1 sample shows a high degree of oxidation comparative to the other samples, and also No-4 sample shows very low intensity compared to graphite so that it consists of less functional groups.

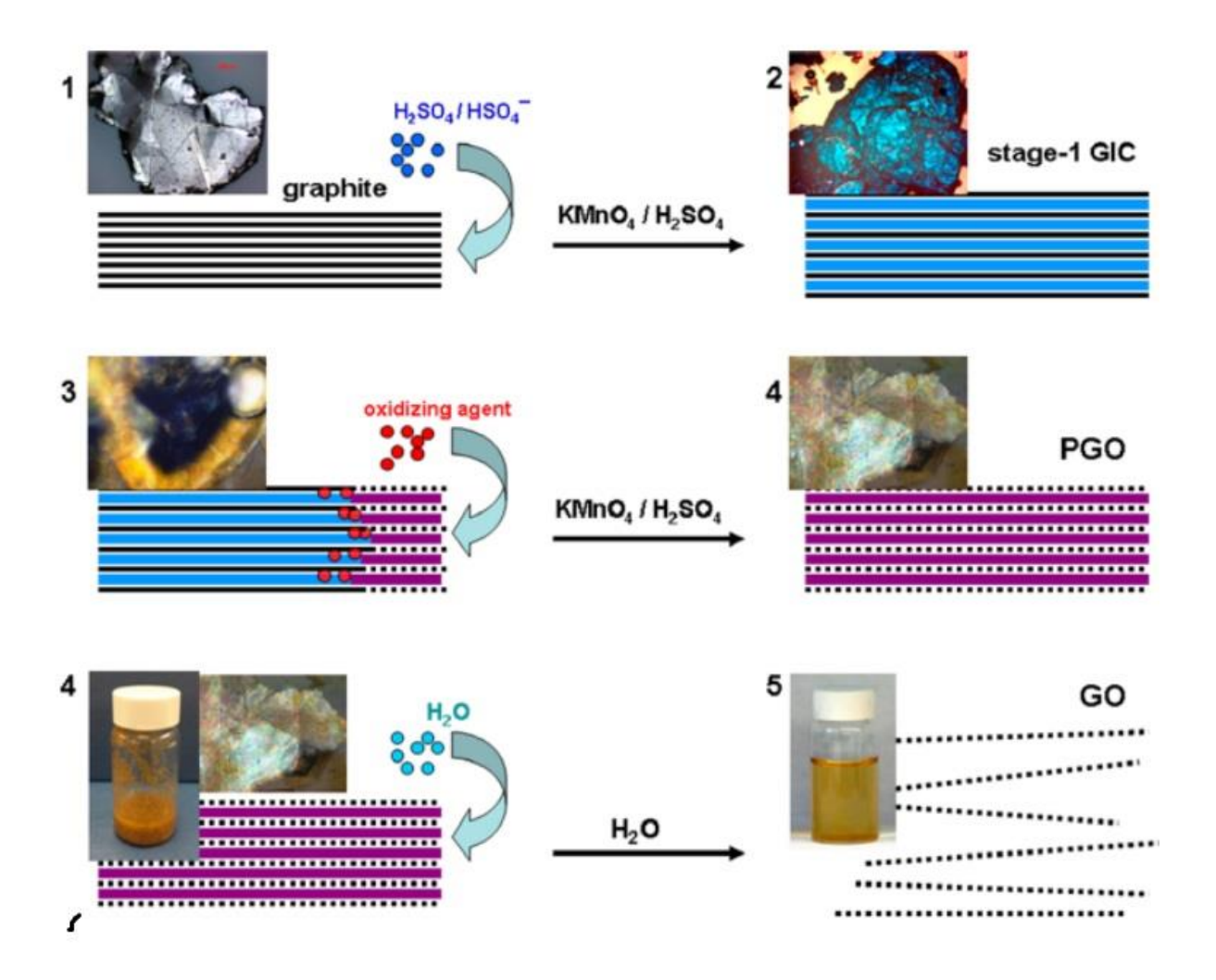


Fig.2.2. Graphene oxidation formation involves three different steps[157].

. The optical characteristics were observed by UV spectroscopy as shown in Fig.2.3(b). The π - π * transition peaks appear at 232,235,237 and 261nm for the No-1, No-2, No-3 and No-4 samples respectively. The increases in the wavelength represent the increases π – electrons. They have indicated that least wavelength peak samples need high energy and also observed that first three samples show the shoulder peak at 300nm (n- π *) and 4th sample do not have this peak.

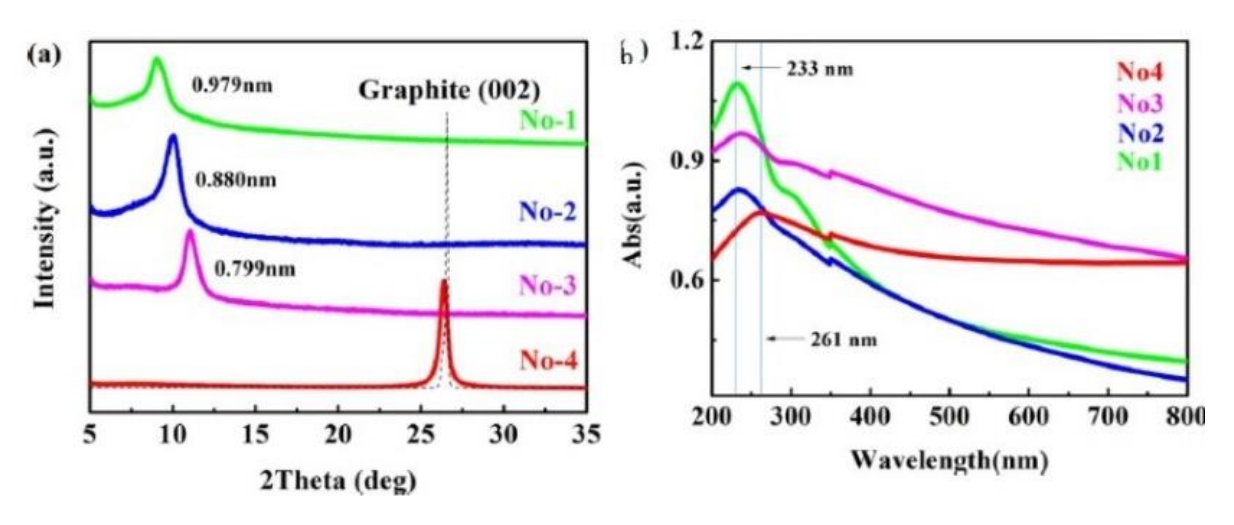


Fig.2.3.(a) XRD pattern and (b) UV spectroscopy of different degree oxidation of GO[158].

Jesus Guerrero et al.[159] have studied the different oxidation degree of the graphene oxide by Hummers method. In this work, the variation in the degree of oxidation was obtained by the changing the synthesis parameters such as NaNO₃, KMnO₄, reaction temperature and reaction time as shown in Table 2.1. From the results, they have mentioned that all samples consist of nearly same C/O ratios and the formation of oxygen functional groups have different intensity analyzed by the FTIR spectra. These functional groups mostly impact the structural, optical and electrical properties of graphene oxide. Recently in 2016, Tong Hun Kang et al.[160] have reported the hidden second oxidation step of the Hummers Method. In this .work, they mentioned that two steps are involved in preparing the graphene oxide and all synthesis parameters are listed in Fig.2.4. They also mentioned that oxidation depends on reaction temperature and time. Also, it is indicated that defects are formed in the 2nd stage of oxidation process at high temperature. In their process, it has been also reported that more oxidation occurs at the 2nd stage due to the increase in the temperature during the 2^{nd} stage. However, in step1 only partial oxidation occurs with the presence of unoxidized C = Cbonds carbon atoms. The optical properties are changed in both the oxidation steps. In the step1, the peak position appears at the higher wavelength in UV spectrum that means π - π * absorption peak appearance at 233nm. Which further indicates the undamaged conjugated structure in GO. In the case of step 2, oxidation, the absorption peak shifts to lower wavelength at 231nm at 45°C, when the temperature increases further, the peak position decreases to 228nm at 95°C. Which indicates a reduction of graphite domain. The $n-\pi^*$ transition peak also increases with an increase in the temperature during step2 oxidation which represents the increases of carbonyl bonds C=O. From the FTIR analysis, they have also observed that when the temperature increases in step 2 oxidation process, O-H groups increases and hence the peak intensity increases more at 3440cm-1, which indicates that during this process more hydroxyl groups are formed. However, the epoxy groups formation reduces as shown in Fig.2.5. Therefore, the material obtained at the step 2 oxidation, easily disperse than step1 oxidation material. The interlayer distance decreases further due to the presence of the hydrogen bonding.

Table.2.1. Different synthesis parameters for GO preparation by using Hummers method [159].

| | NaNO ₃ (g) | KMnO ₄ (g) | Residence | Residence | Residence |
|----------------|-----------------------|-----------------------|-----------|-----------|-----------|
| | | | time@5℃ | time@35℃ | time@98℃ |
| Sample | | | (min) | (min) | (min) |
| O ^a | 0.50 | 3 | 120 | 30 | 30 |
| 1 ^b | 0.25 | 3 | 120 | 30 | 30 |
| 2 ^b | 0.75 | 3 | 120 | 30 | 30 |
| 3 ^b | 0.50 | 1.5 | 120 | 30 | 30 |
| 4 ^b | 0.50 | 4.5 | 120 | 30 | 30 |
| 5° | 0.50 | 3 | 60 | 30 | 30 |
| 6° | 0.50 | 3 | 180 | 30 | 30 |
| 7° | 0.50 | 3 | 120 | 15 | 30 |
| 8° | 0.50 | 3 | 120 | 45 | 30 |
| 9° | 0.50 | 3 | 120 | 30 | 45 |

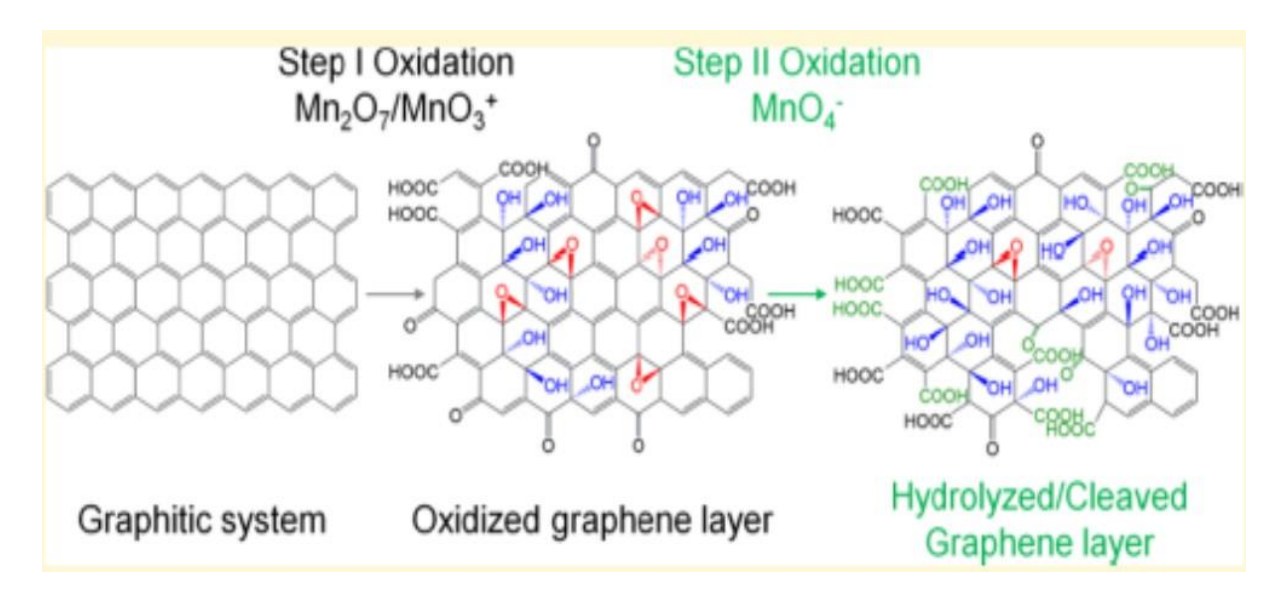


Fig. 2.4. Mechanism of the graphite oxide in step2 oxidation[160]

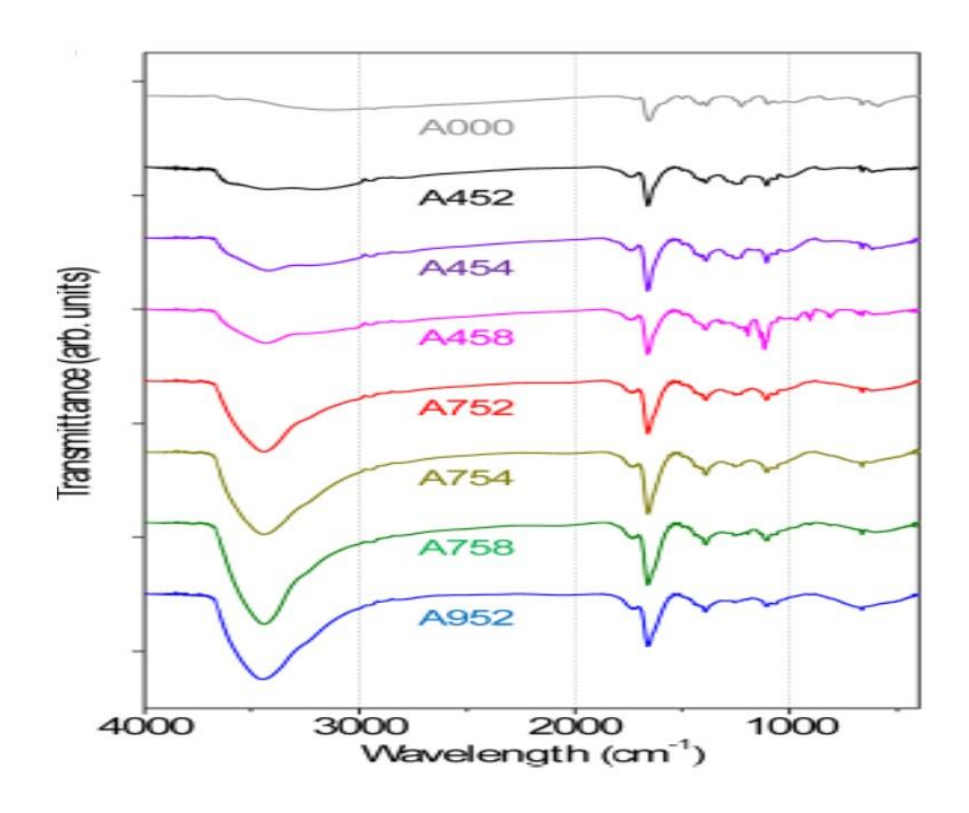


Fig .2.5 FTIR Spectrum for the step1 and step 2 oxidation process[160]

2.3 Litterature review on Reduced graphene oxide(RGO)

We already described the graphene synthesis methods in section 2.1. Out of all the methods, chemical method represents the graphene oxide which provides the different properties in comparison to the others method due to the oxygen functional groups. These groups disturb the conjugated structure of graphite lattice [161-162]. Then, the graphene oxide behaves as an insulator and exhibits the resistance $\sim 10^{12} \,\Omega/\mathrm{qs}$ or higher[163-164]. Since, graphene exhibits the excellent electrical, mechanical, thermal and optical properties due to the sp² conjugated carbon atoms, hence, graphene can be obtained from the graphene oxide by removing of oxygen functional groups. The process of removing the oxygen functional groups is known as reduction process, and obtained graphene is called as reduced graphene oxide. So that it can retain the original sp² conjugated carbon atoms. There are different reduction methods available for the reduction of graphene oxide to obtain graphene by restoring the sp² hybridized carbon atoms and improve the conductivity of material [161-162]. Such as thermal reduction, chemical reduction, and multi-step reduction. Xingfa Gao et al.[165] have studied the reduction mechanism of graphene oxide reduction by hydrazine and thermal reduction by the density functional theory. They have mentioned that the graphene oxide has two types of epoxy groups represents A and A', and attach to the interior and edge of the

aromatic domain. Another two types are hydroxyl groups and attached same as epoxide groups and represented as B and B', the carbonyl and carboxyl groups are attached at edges of the graphene sheet and represent as C and D respectively. These groups arrangement is shown in Fig.2.6. In this work, they have mentioned that only epoxy oxide groups are removed by hydrazine and the mechanism was very well explained. However, the removal of hydroxyl groups mechanism is not explained. By hydrazine treatment, the epoxy groups are removed through three routes as shown in Fig.2.7. and shown as route 1,2 and 3. The hydroxyl removal path is shown in Fig. 2.7 like route 4 and 5. The carbonyl and carboxyl path is shown in figure 2.7 as route 6 and 7 respectively.Ning-Jing Song et al.[166], have reported the thermal and mechanical properties of thermally reduced graphene oxide thin films. In this work, GO was prepared by modified Hummers method and thin films were prepared then heated to a different temperature such as 800°C,900°C,1000°C,1100°C and 1200°C in a nitrogen atmosphere. They observed that when the temperature increases the thermal conductivity also increases, as shown in Fig.2.8 (a). whereas Young's modulus (stiffness Fig 2.8(b)) decreases and after 900°C, no further reduction in Young's modulus. Similarly, tensile strength decreases with temperature and suddenly increase at a 1200°C heat treated GO thin film.

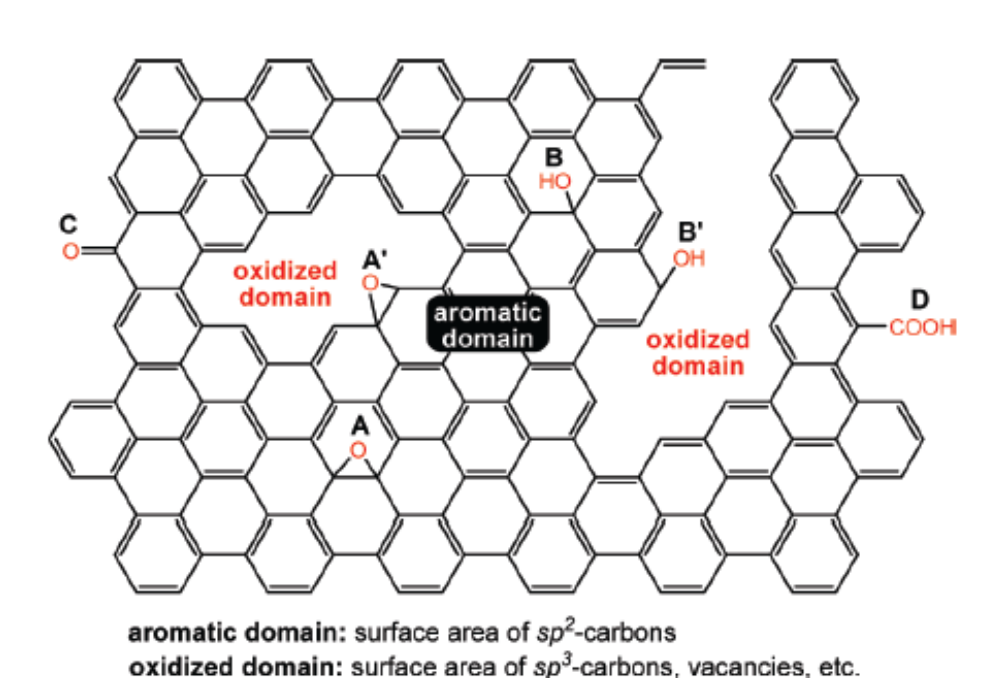


Fig. 2.6 .The oxygen-related functional groups in Graphene oxide [165].

The chemically reduced graphene oxide (RGO) can be synthesized by using different reducing agents. Out of these, the most used reducing agent is hydrazine. Therefore, in this section, we have included more literature on the reduction of GO to RGO by using hydrazine. S.Stankovich et

al.[167] have studied the electrical conductivity of the graphene oxide reduction by hydrazine hydrate. In this work, they have taken the GO solution in DIW and reduced at 1000C by hydrazine hydrate. They have reported the electrical conductivity is $2x10^2$ s/m of the RGO. This value is for better than GO with 5 order more. Dan Li et al.[168] have developed the large-scale graphene synthesis by without surfactant. In this work, they have observed the charge of graphene by zeta potential, GO and RGO have a negative charge, but RGO has less charge than GO. Both GO and RGO has shown the negative charge which indicates that after reduction with hydrazine, still carboxylic and hydroxyl groups are present. They have investigated the effect of lower and higher quantity of the hydrazine in the reduction oxygen functional groups of GO. They have reported that RGO dispersion is decreased with increasing the hydrazine quantity. In this work, they have also mentioned that RGO dispersion depends on the PH of the solution and also observed that the UV absorption depends on the reduction time. When the reduction time is increased the observation peak is also shifted to the higher wavelength (231nm to 271nm). This indicates that band structure can be modified for different applications. T.T.Dang et al.[169] have studied the effect of the reduction temperature by using hydrazine monohydrate as reducing agent. They have reported that the electrical conductivity depends on the temperature which also depends on the variation in C/O ratio. In this work, they have prepared the GO by the MHM and then followed by the microwaveassisted thermal expansion. They have seen that the optical absorption changes when the temperature increases, the intensity of absorption peak also increases. Prerna Bansal et al.[170], have reported the effect of the temperature on the RGO for the structural and optical properties. In this work, they have prepared GO by improved Hummers method by using the graphite size ~45µm and reduction by hydrazine hydrate at a different temperature such as 80 and 95°C in the water solvent. They have mentioned that at a high reduction temperature RGO can be reduced with fewer defects. However, at high temperature, the obtained RGO show a smaller optical gap as analyzed by UV – spectroscopy.

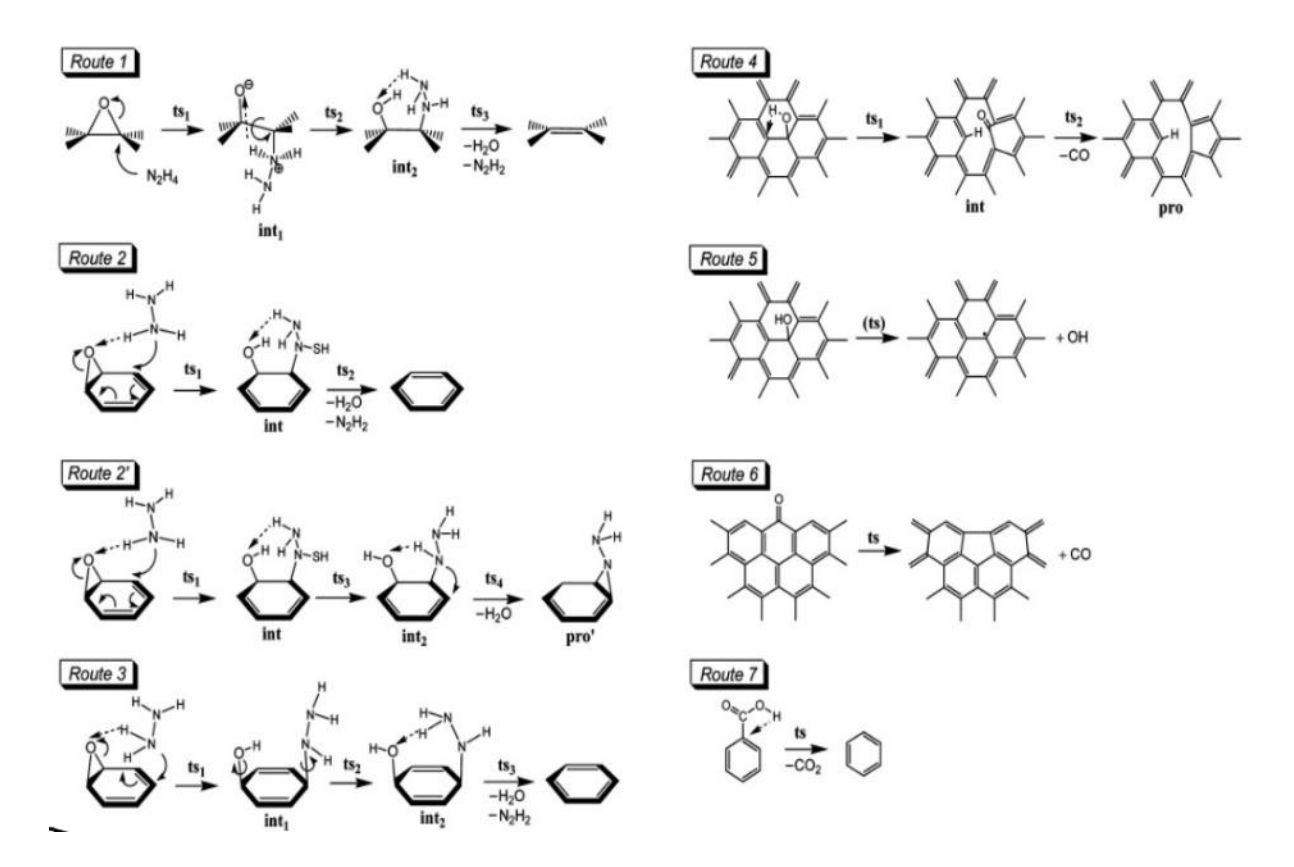


Fig. 2.7 the reduction mechanism to obtain reduced graphene oxide (RGO) from graphene oxide (GO)[165].

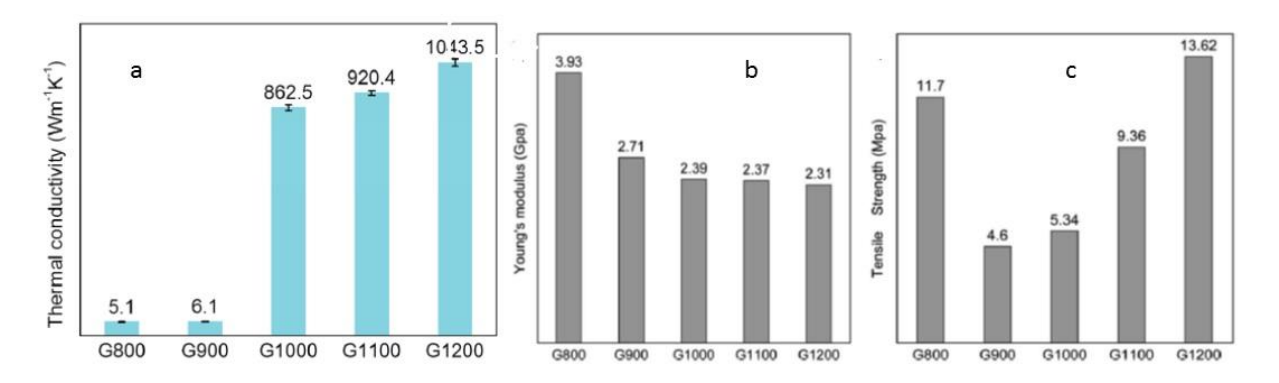


Fig. 2.8. (a) Thermal conductivity, (b) Young's modulus and (c) tensile strength of the GO thin film heated at a different temperature.[166]

2.4 Literature review on source graphite size effect on the GO and RGO synthesis:

Graphene oxide(GO) is produced by the chemical method by oxidizing the graphite precursor in a suitable oxidizing agent. This chemical method can be used to produce a large-scale production of graphene. But the production of GO depends on the source of the graphite, the size of the graphite and crystallite size of the graphite. Cristina Botas et al. [61] have studied the effect of the parent graphite on the structure of graphene oxide. In this work, they have used two synthetic graphite such as flow domains and mosaics which are represented by G1 and G2 respectively and the GOs was synthesized by the modified Hummers method. In this work, they have reported that the smaller crystallite size of the graphite of GO consists of more carboxylic groups those are present at the edges of the sheets but in the case of larger size crystallite GO, more epoxy groups are attached to the basal plane of the sheets as shown in Fig. 2.9.

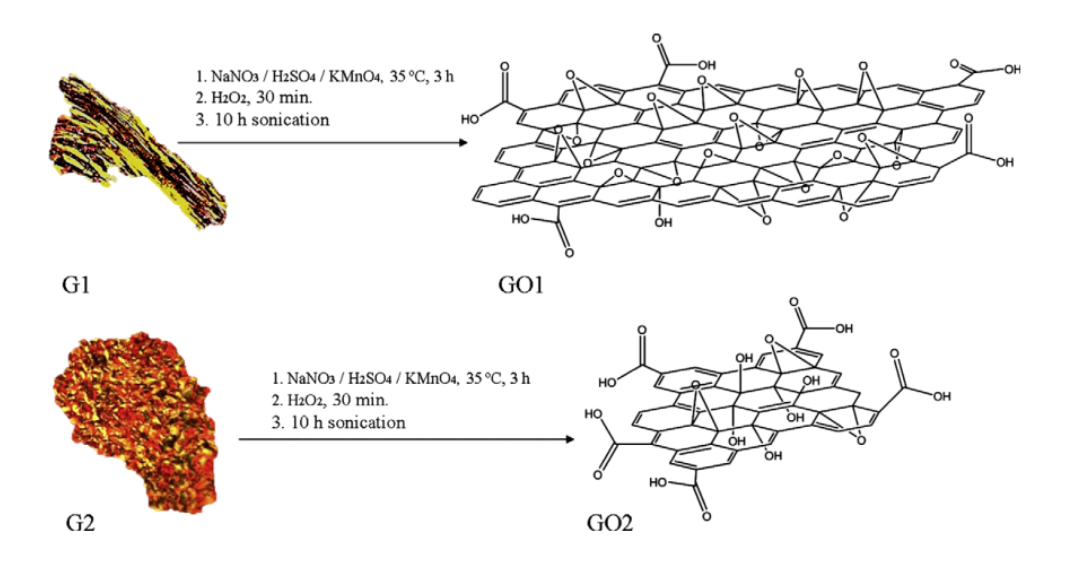


Fig. 2.9. Influence of the graphite source sizes on the GO structure [171].

Cristina Botas et al[172], have reported that the larger crystallites are more favorable for exfoliation, which has large sheets yield within shorter sonication time comparison to the smaller crystallite size as shown in Fig.2.10 and also have mentioned that the yielding is independent of the oxygen content in the graphene oxide. In 2014 Minh-Hai Tran et al. [173] have studied the graphite size effect on the electrochemical performing of the reduced graphene oxide reduction by using the hydrazine. In this, they have used the natural graphite source with different graphite size such as 20, 74 and 149µm, they have synthesized the GO by using modified Brodie method and then followed by reduction with the low and high quantity of hydrazine. They have mentioned that among all the

graphites, larger size graphite has more crystalline than smaller size as analyzed by XRD. They have also reported that the reduction process depends on the size of the graphite. In which the graphite oxide synthesized from the smaller size graphite shows more reduction than the graphite oxide synthesized by using larger size graphite. The reduction of the graphite oxide can influence the electrochemical properties for using in the energy storage applications.

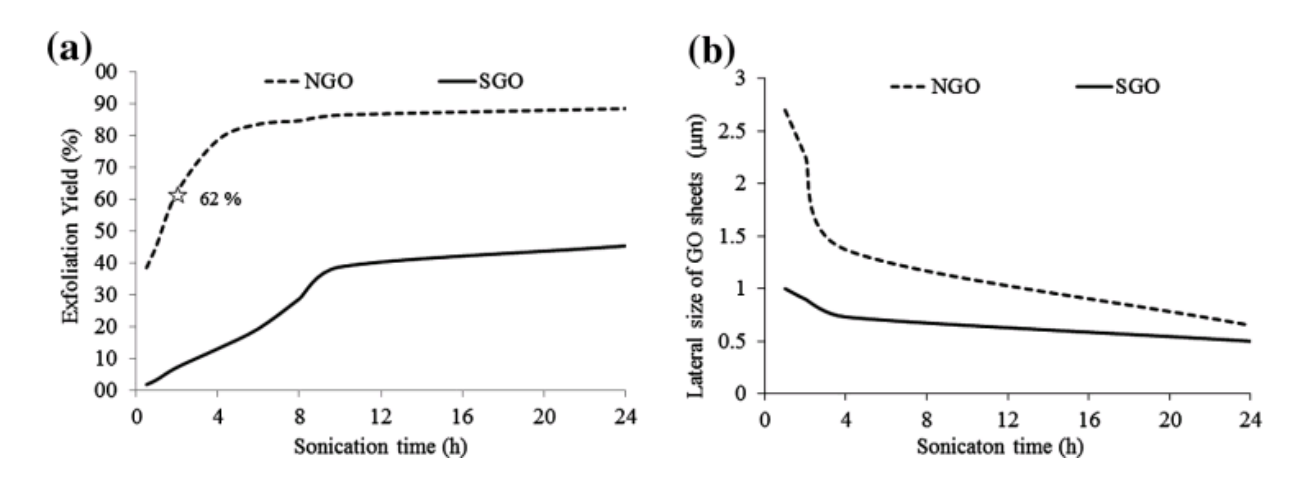


Fig .2.10. Size effect the source graphite on the exfoliation yield of GO by varying the sonication time [172].

Haiyang Xian et al. [174] have investigated the size and structure of the graphene oxide prepared by modified Hummers method using the natural graphite flakes with different sizes such as -200, -100,+150,+80 and +50 mesh. In this work, they have observed that the obtained graphene oxide sheet size is smaller than graphite size and also mentioned that the graphite particle size impacts the oxidation process. Smaller particle size graphite can be easily oxidized, it contains more defects, and large size particles contains fewer defects. Haoran Yu et al. [175] have studied the importance of the raw graphite size to the capacitive properties of the graphene oxide. In this work, they have chosen different graphite size of natural graphite. Such as 2000mesh, 800mesh, and 100mesh. The graphite oxide was prepared by modified Hummers method. They have reported that the I_D/I_G ratio is all most same for the three samples from the Raman analysis and the interplanar distance are 0.782nm,0.789nm and 0.811nm for the 2000mesh,800mesh, and 100mesh respectively. These results indicated that the larger size of the graphite, GO possess higher interplanar distance than smaller particles size of graphite GO due to the presence of the hydrogen bonding of the intercalated water molecule. They have also reported that larger size graphite GO. They have

measured the specific surface area 32,89and 62m²g⁻¹ of 2000mesh, 800mesh and 100mesh respectively. Since, smaller size shows the high surface area, but in this case, smaller graphite size GO showed less surface area because of agglomeration or damage of structure due to the contains the more oxygen functional groups, forming of hydrogen bonding in the intercalated water molecules. The surface area can be improved by the freeze-drying of the GO material then removal of the water molecules. They have also observed that equivalent series resistance is same for all the three samples, but charge transfer decreases with increasing the graphite size. They have also reported that the large size graphite such as 100mesh and 800mesh size, have faster and slow diffusion ions which form the different pore size distribution. They have reported that the specific capacitance 94.4, 33.1 and 11.7F for the 100mesh, 800mesh, and 2000mesh respectively as shown in Fig. 2.11 (a). The 800mesh sample shows a high surface area, but it has less capacitance because it has more charge transfer. Therefore, the capacitance depends on the specific surface area, pore structure, and electrical conductance of the GO. They have also studied specific capacitance with the cycle numbers and shown in Fig. 2.11 (b), that indicates that the all three samples have good stability up to 1500 cycles.

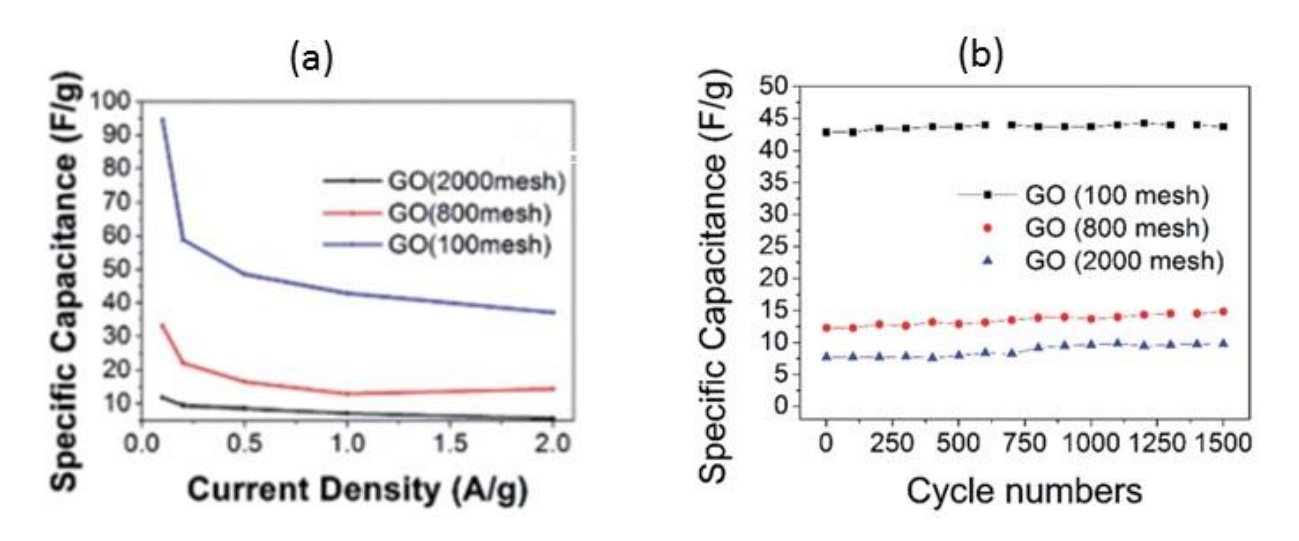


Fig .2.11. (a) The specific capacitance vs current density in 6M KOH, (b) the specific capacitance vs cycle numbers for the GO synthesized by different sizes source graphite [175].

2.5 Literature review of Alumina /Graphene (Al₂O₃/GO or Al₂O₃/RGO) nanocomposites

K.Wang et al. [176] have synthesized the graphene nanosheet/alumina composite by using the SPS (Spark Plasma Sintering) method. In this process, they have initially prepared GO by MHM, and then, 20g of α alumina nanoparticles (particles 72nm size) was dispersed in 100ml of water. After that, the solution was Sonicated for 30mints as shown in Fig 2.12(b) then the GO solution (as shown in Fig 2.13(a)) was slowly added to the alumina solution with stirring then obtained material was reduced using the hydrazine monohydrate at 60° C for 24h. Finally, the composite powder was sintered by SPS at 1300° C.

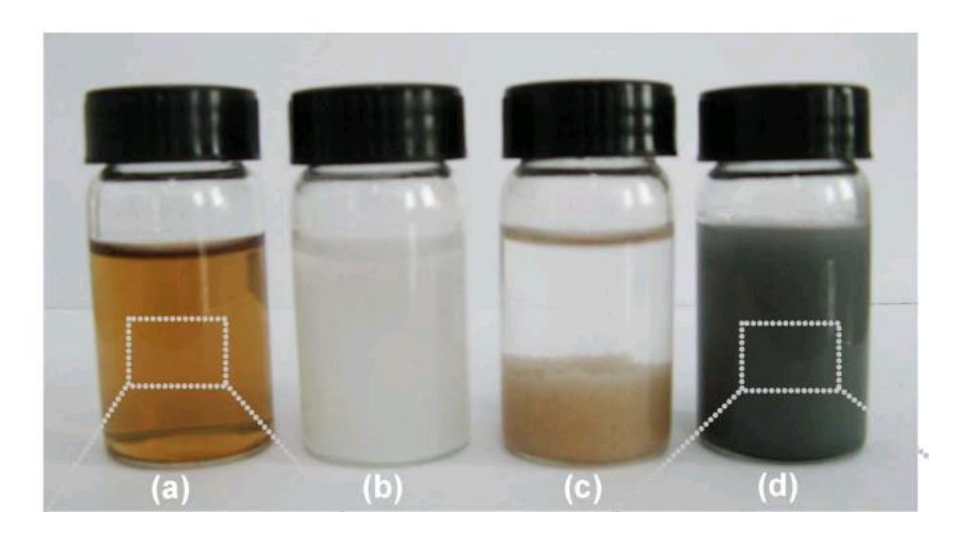


Fig 2.12. (a) GO solution, (b) alumina solution, (c) mixed solution of GO and alumina and (d) reduced graphene –alumina composite.[176].

In this work, they have reported the mechanical and electrical properties such as fracture toughness and electrical conductivity by using the four-point probe method. They have reported that fracture toughness is $5.21 MPam^{-2}$ and electrical conductivity is $172 Sm^{-1}$. As shown in Fig.2.13, they have mentioned the agglomeration of GO with alumina. The structural study was done by the XRD of graphene /alumina composite shown in Fig 2.14 [176]. They have observed that the composite exhibits the higher angle shift compare to the pure alumina due to the residuals stress because of diffusion of carbon atoms into alumina grains.

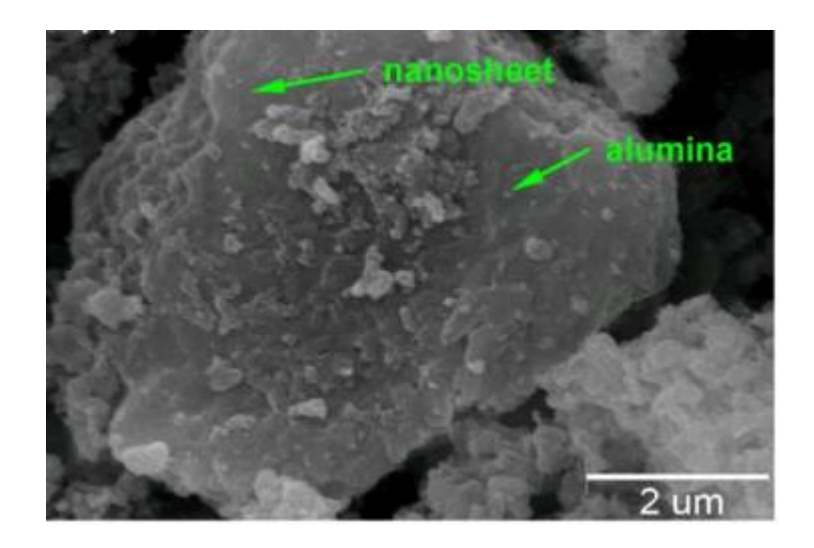


Fig. 2.13 Shows the SEM image of graphene/alumina in powder form [176]

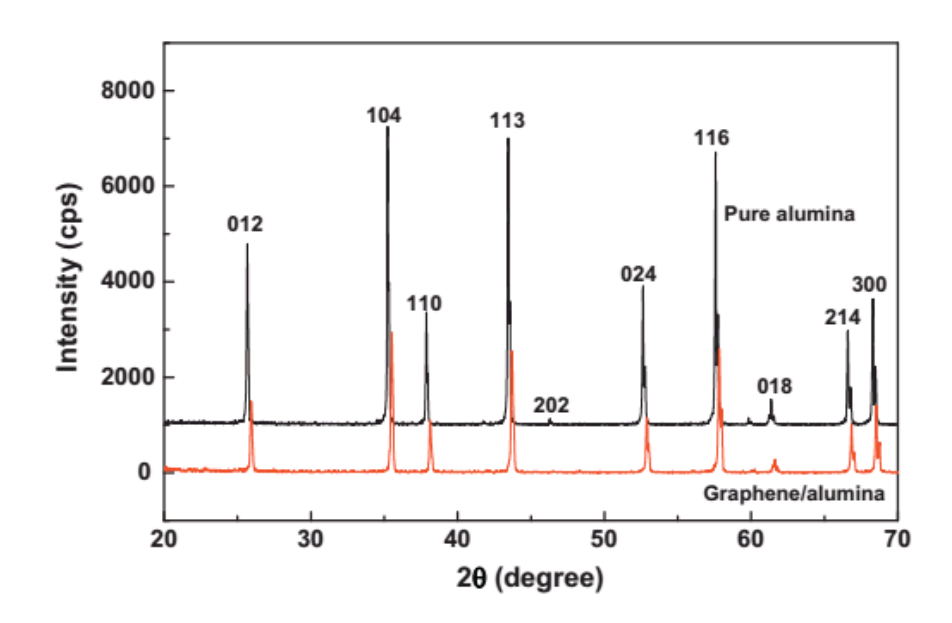


Fig.2.14 XRD pattern of alumina/graphene nanocomposite and pure alumina[176].

Yuchi Fan et al. [177] have prepared the few-layer graphene /alumina nanocomposite by using the titration method then followed by SPS. In this work, they have to synthesized GO used by MHM and chosen α - alumina (particle 200nm size). In this process, they have prepared low and high GO content nanocomposite and sintered at 1300° C. Figures 2.15 and 2.16 showed the morphology of low and high content of GO for FG / alumina nanocomposite by SEM and TEM respectively. They have reported that GO thin sheet wrapped on the alumina surface. They have also studied the structural change by Raman, as shown in Fig. 2.17.

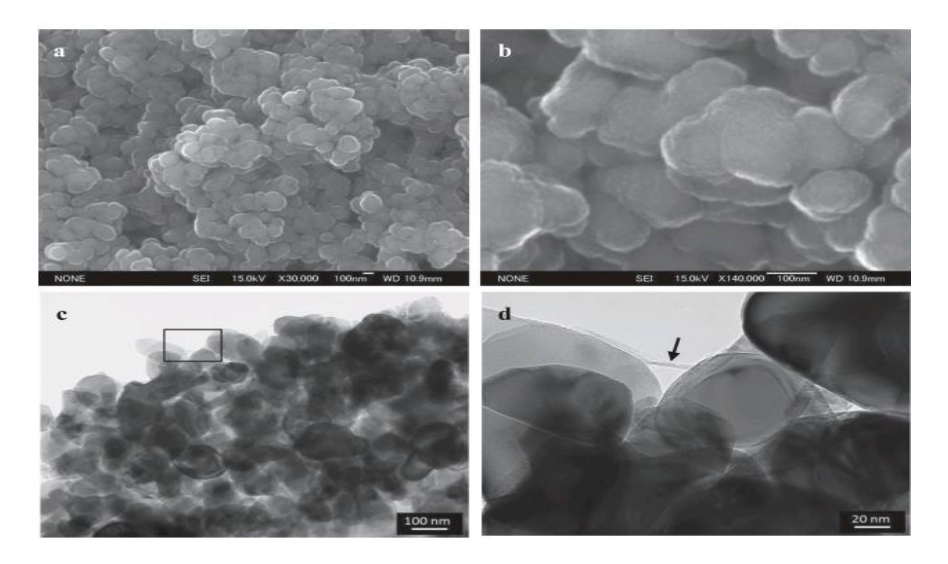


Fig 2.16. The morphology of graphene /alumina nanocomposite for low content (1.92wt. %) of GO.(a) and (b) shows the SEM images of low and higher magnification respectively and (c) and (d) TEM images of low and higher magnification of c image box location respectively [177].

They have also studied the structural change by Raman, as shown in Fig. 2.17. All the samples show the defects bands due to the high-temperature sintering process. (as shown in Fig.2.17) The electrical properties and the percolation threshold value was also found at 0.38 vol% of FG/ alumina nanocomposite and seen that the electrical conductivity increases with the increasing the GO content. They have observed the type of charge carriers by Hall Effect measurement and mentioned that at a low content of GO it behaves as p-type and at high content GO it has n-type charge carriers, as shown in Fig 2.18. Harshit Porwal et al.[178] have reported the synthesis of the graphene reinforced alumina nanocomposite by SPS method. In this process, graphene was prepared by liquid exfoliation method by sonication using a different solution such as NMP and DMF and taken α-alumina particle size was 200nm which was added to the graphene solution and then finally ball milled. The obtained powder was sintered at 1350°C by SPS. In this process, they have used the different content of the graphene, to investigate the mechanical properties such as fracture toughness by chevron notch and indentation methods. These results are shown in Fig 2.19.

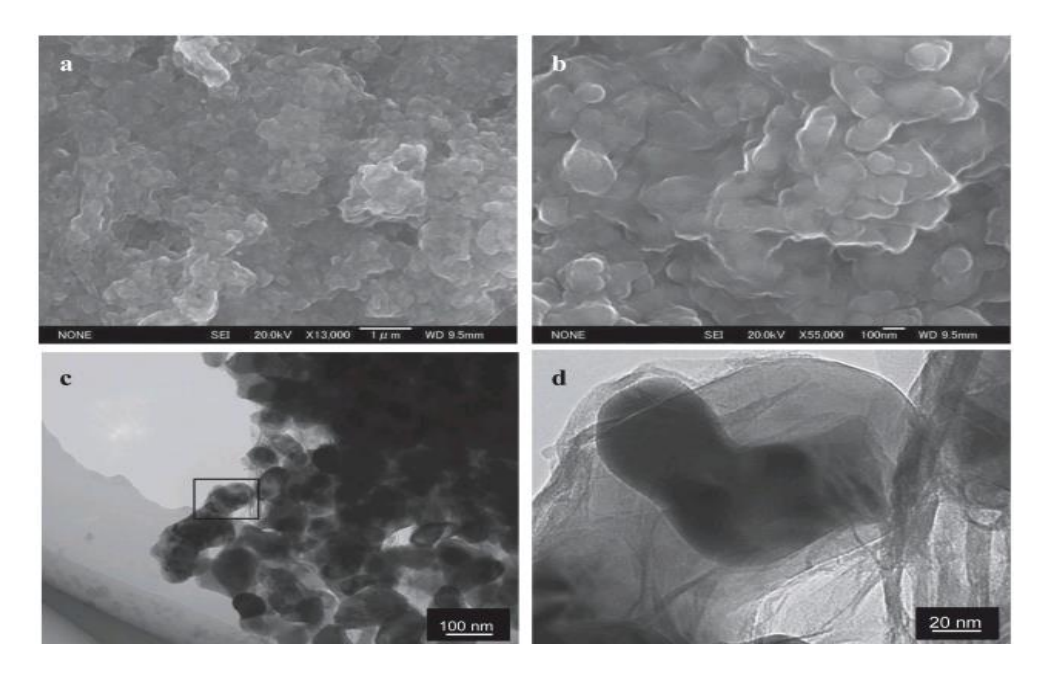


Fig 2.16. The morphology of graphene /alumina nanocomposite for high content (11.5wt. %) of GO. a and b shows the SEM images of low and higher magnification respectively and c and d TEM images of low and higher magnification of c image box location respectively[177].

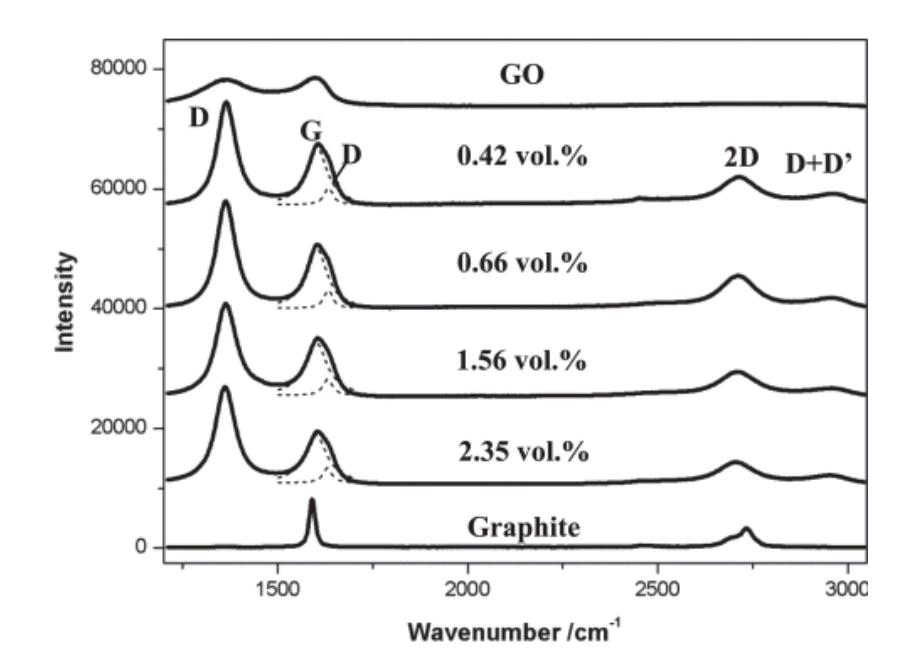


Fig 2.17. Raman spectra of different GO content of FG/ alumina nanocomposite with graphite and GO[177].

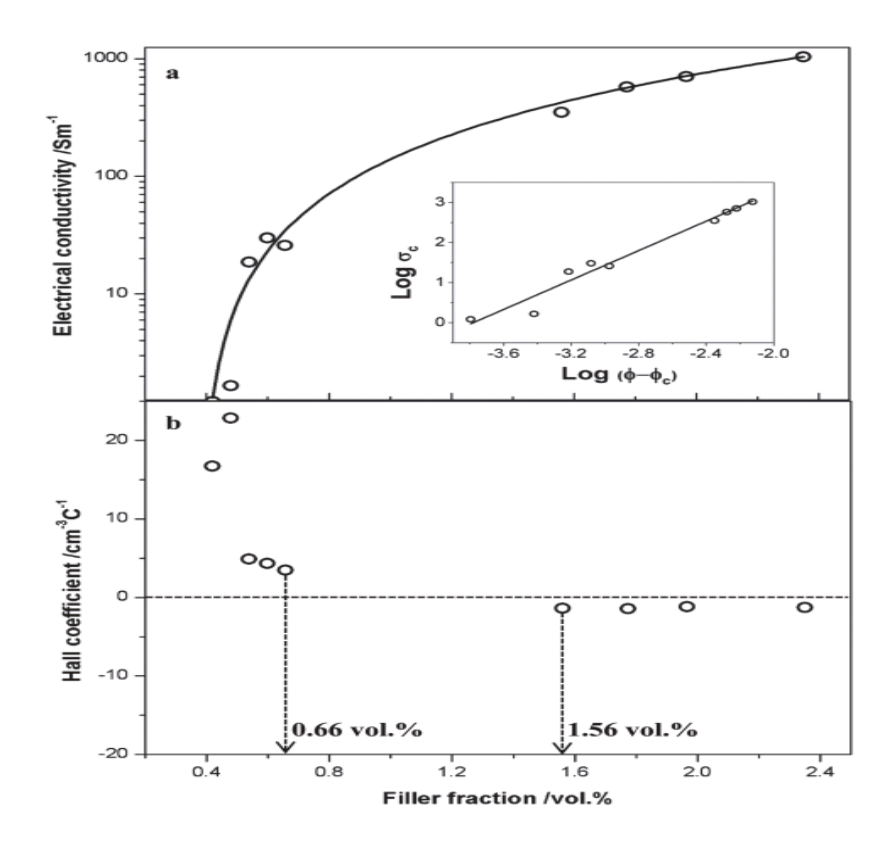


Fig 2.18. (a) Electrical conductivity and (b) Hall coefficient (RH) plotted against filler volume fraction for FG/Al_2O_3 nanocomposites [177].

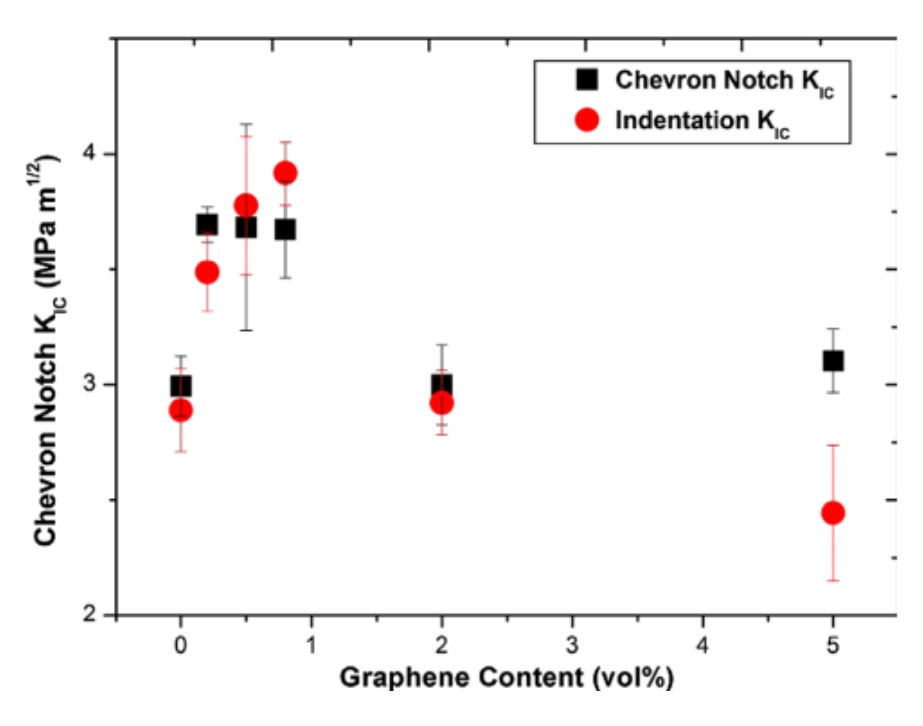


Fig. 2.19. The fracture toughness with respective to different graphene content of the alumina /graphene nanocomposite[178].

From the Fig.2.19, it is observed that the fracture toughness increases initially up to 0.8 vol% then decrease with increasing graphene content. It is seen that at 5 vol% of the graphene content, fracture toughness value is very low, because of the info connected graphene network which forms weak interface, so the indentation method measure only the local toughness values which give the lower values. Hence indentation method is not suitable for the higher graphene content nanocomposites. Agnieszka. M.T. and Andrzej. R.O.[179], have developed the RGO/Al2O3 nanocomposite by the dry sol-gel method. This process is showed in Fig 2.20.In this work, they have studied the morphological and surface area of the nanocomposites. The Fig.2.21 and 2.22 show the morphology of the RGO/alumina nanocomposite by SEM and EDS. The alumina nanoparticles are uniformly decorated on the surface of RGO sheet. The RGO/alumina nanocomposite consists of a high surface area (242.4 m²/g) in comparison to the GO surface area (227.8 m²/g). in this process, the molecular linker is not needed and incorporate very fewer impurities in the obtained nanocomposite. They have reported that this nanocomposite can be utilized as catalytic, sensor, energy storage and optoelectronic applications.

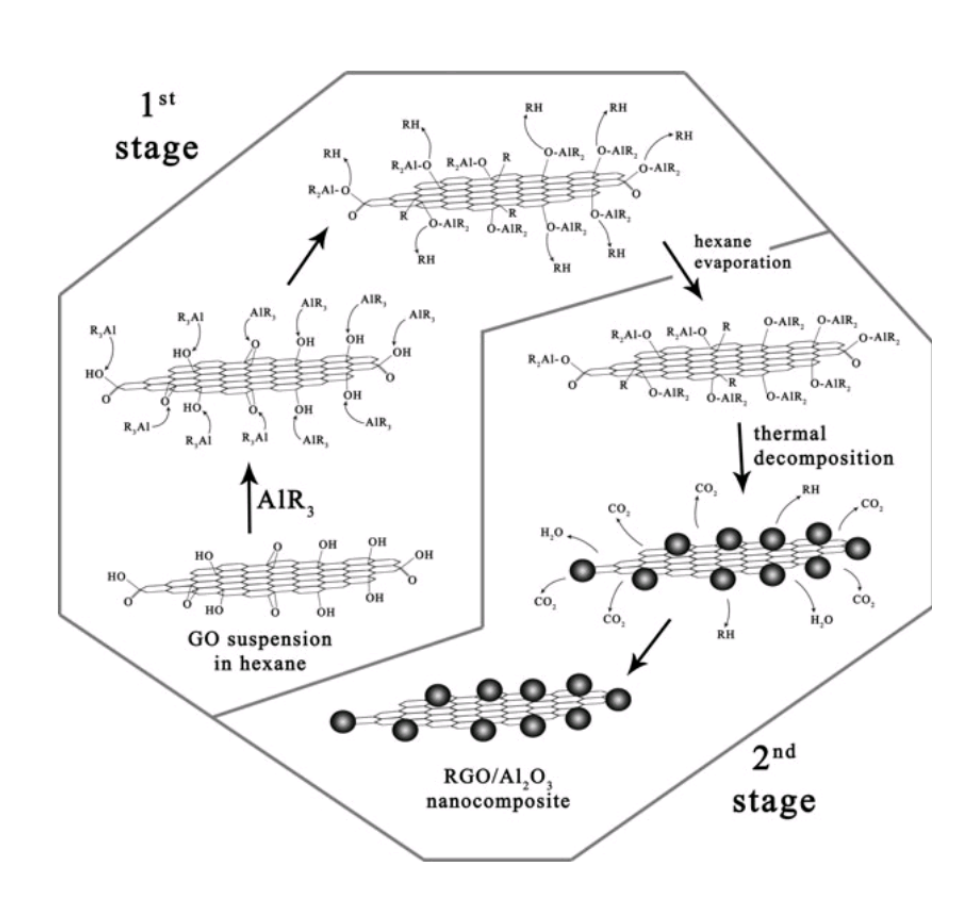


Fig.2.20. Synthesis process of RGO/alumina nanocomposite by dry sol-gel [179].

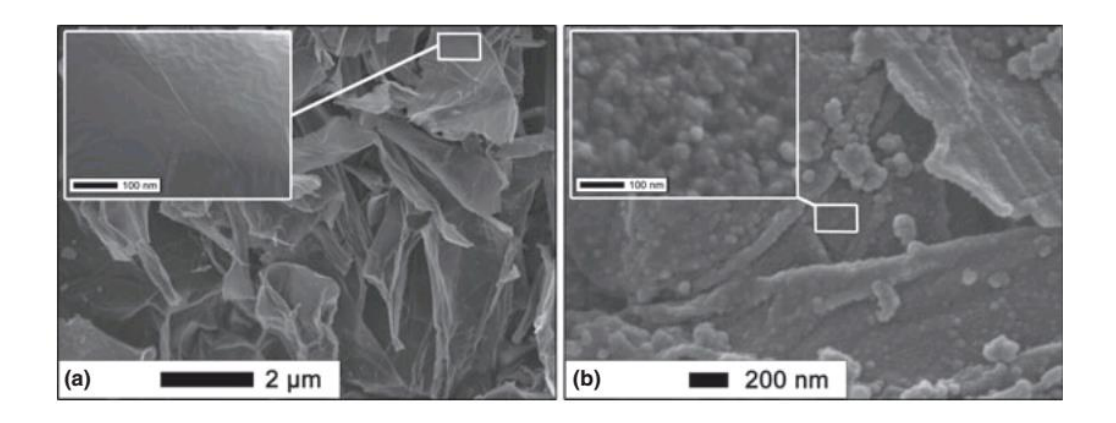


Fig .2.21(a) and (b) SEM images of GO and RGO/alumina nanocomposite respectively [179]

Ben Lee et al[180] have investigated the mechanical properties of the RGO/alumina composite which was prepared by the molecular level mixing process. In this process initially, they have prepared GO by MHM then mixed with alumina precursor Al(NO₃)₃.9H₂O and stirred for 12h. Finally, the sample was heated at 100°C and the finally sample again heated at 300°C to obtain RGO/amorphous alumina nanocomposite. After that the power was ball milled for 12h then sintered at 1400°C by SPS is shown in Fig 2.23 (a). they have observed that the alumina phase changes in the nanocomposite as shown in the Fig 2.23 (b). there are three stages of phase change occurs for the obtained alumina/graphene nanocomposite with variation in the temperature case shown in Fig2.23(b). In the first stage, amorphous alumina/graphene composite is formed. In the second stage

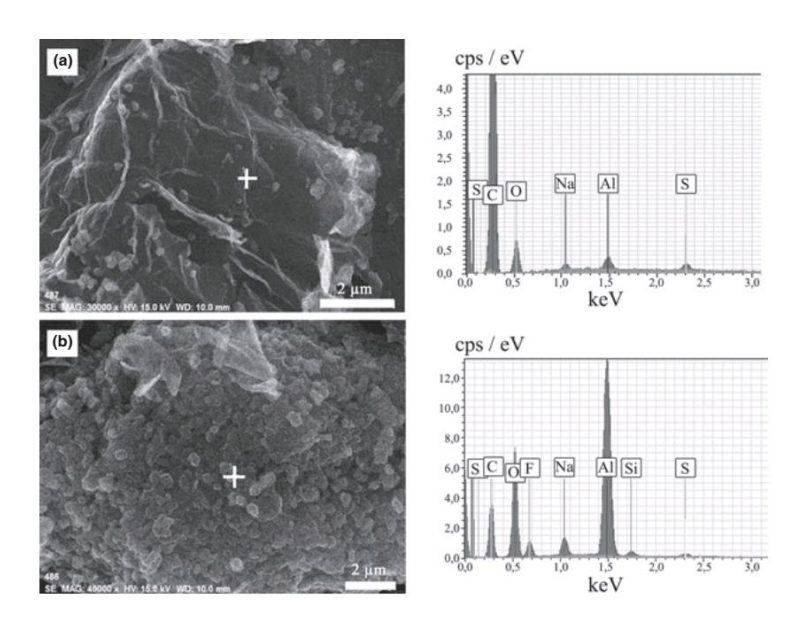


Fig 2.23. Shows the SEM images of RGO/alumina with EDS corresponding the different places (a) is EDS on the RGO surface and (b) shows the at alumina point[179].

 γ -phase, alumina and 3^{rd} stage α -phase alumina are present in the nanocomposite. They have also studied the mechanical properties of the nanocomposite with varying the RGO content in RGO/alumina composite, as shown in Fig 2.24(a). It is seen from the Fig 2.24(a), that has the RGO content increased 0 to 3 vol% the hardness also increases from 2008 to 2294HV of RGO/alumina composite and flexural strength also increases from 350 to 425MPa. Fracture toughness also increases with increasing the GO content as shown in Fig 2.24 (b) [180].

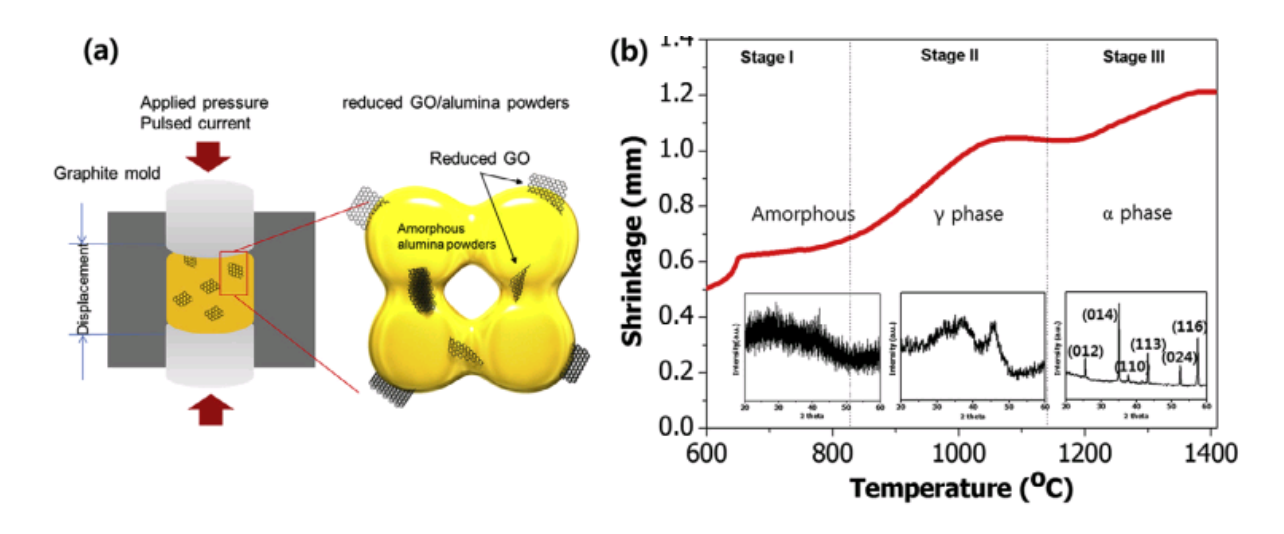


Fig. 2.23. (a) Schematic diagram of SPS process for preparing the reduced GO/alumina composite (b) SPS behavior of composite material (RGO/alumina) with temperature [180].

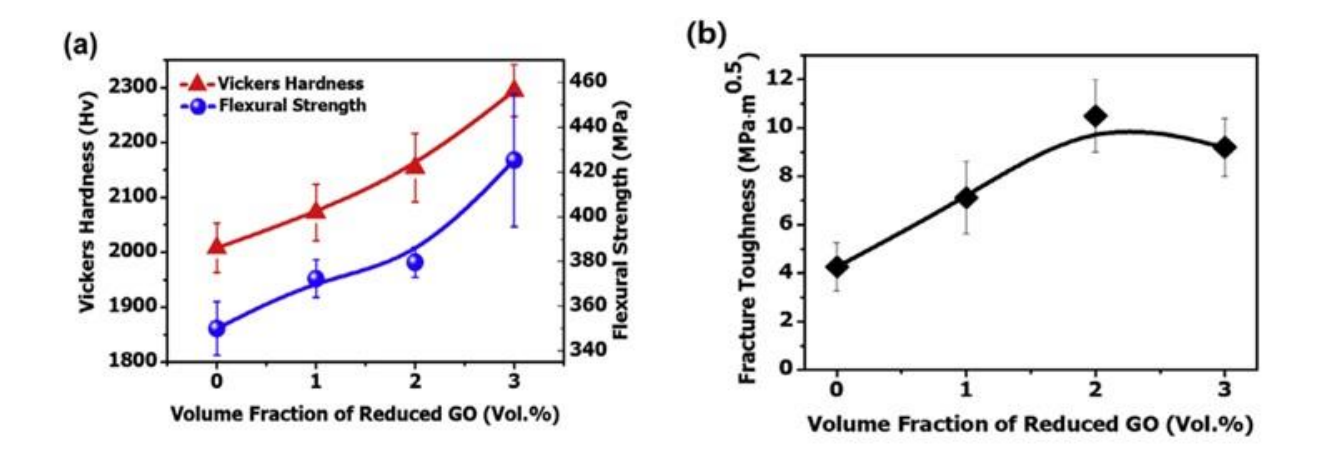


Fig 2.24 (a) Vickers hardness and (b) fracture toughness of the Al₂O₃/RGO[180].

A.M.Jastrzebska et al [181] have synthesized the RGO/alumina (40wt% of GO) core-shell nanocomposite based on their previous report [179] changing the alumina precursor and GO dispersed solution, and this process is shown in fig 2.25. In this work, they have investigated the structural, morphological and electrostatic properties of RGO/Al₂O₃ nanocomposite and the obtained material is confirmed by Raman and FIR analysis. Which indicates that the quality of RGO/Al₂O₃ nanocomposite as shown in Fig 2.26 (a) and (b) respectively [181]. The morphological study was done by using the SEM and as shown in Fig. 2.27. As shown in Fig. 2.27, RGO/Al₂O₃ nanocomposite is not agglomerated as compare to the individual alumina nanoparticles agglomeration because of the high surface area of the nanoparticles[181]. The structural analysis results from the TEM and XRD confined that the alumina nanoparticles are in the γ -phase due to the low temperature (at 300°C) synthesis process. The electrostatic properties are measured by using the zeta potential, for the different solutions such as DIW, electrolyte and drinking water for the GO, alumina and RGO/Al₂O₃ nanocomposite and have observed that these materials show the different charge properties as shown in figure 2.28.

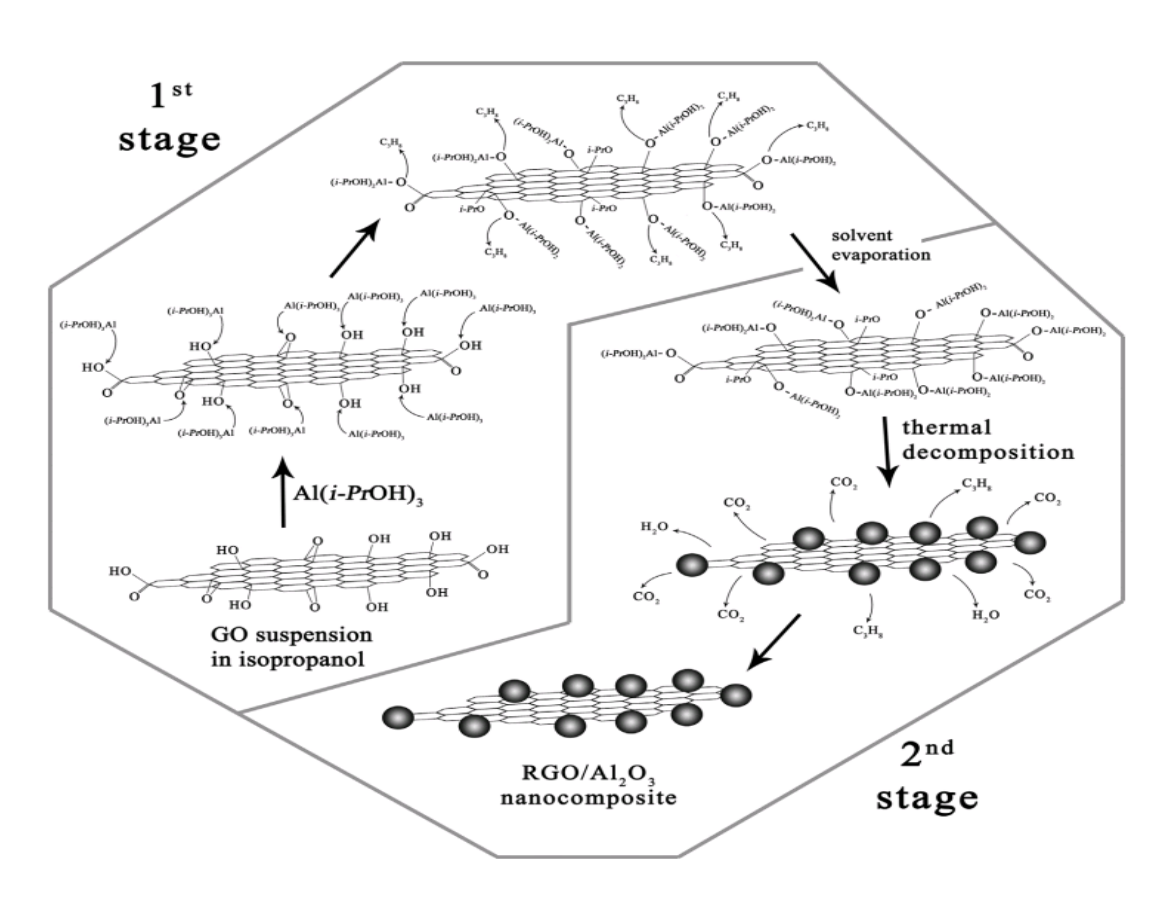


Fig. 2.26. Shows the dry sol-gel method for to prepare RGO/Al₂O₃ nano composite[181].

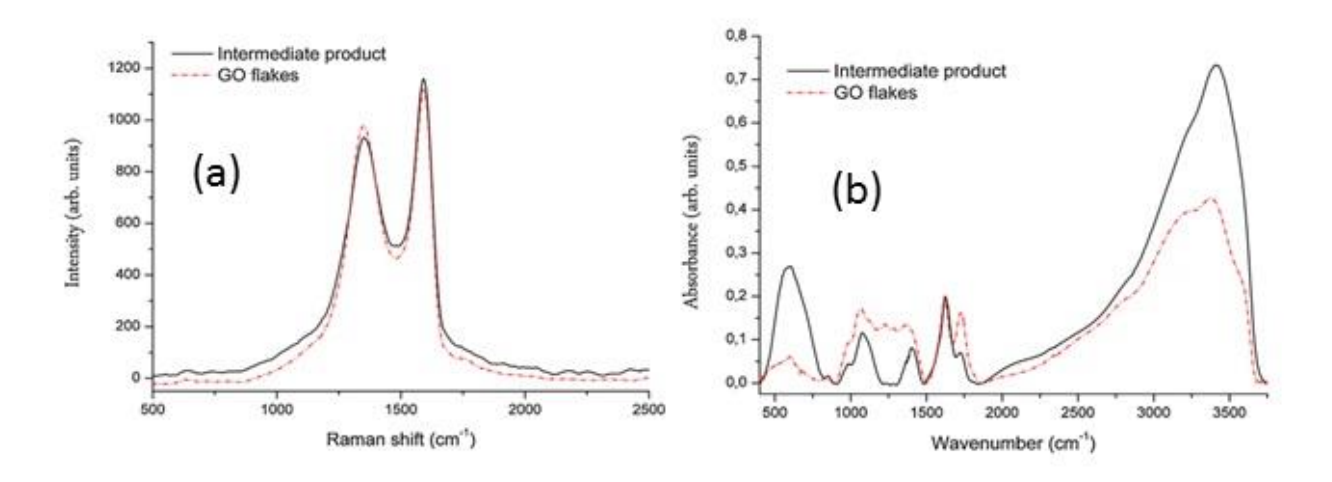


Fig. 2.27. (a) Raman spectra and (b) FTIR spectrum of RGO/Al₂O₃ nano composite[181].

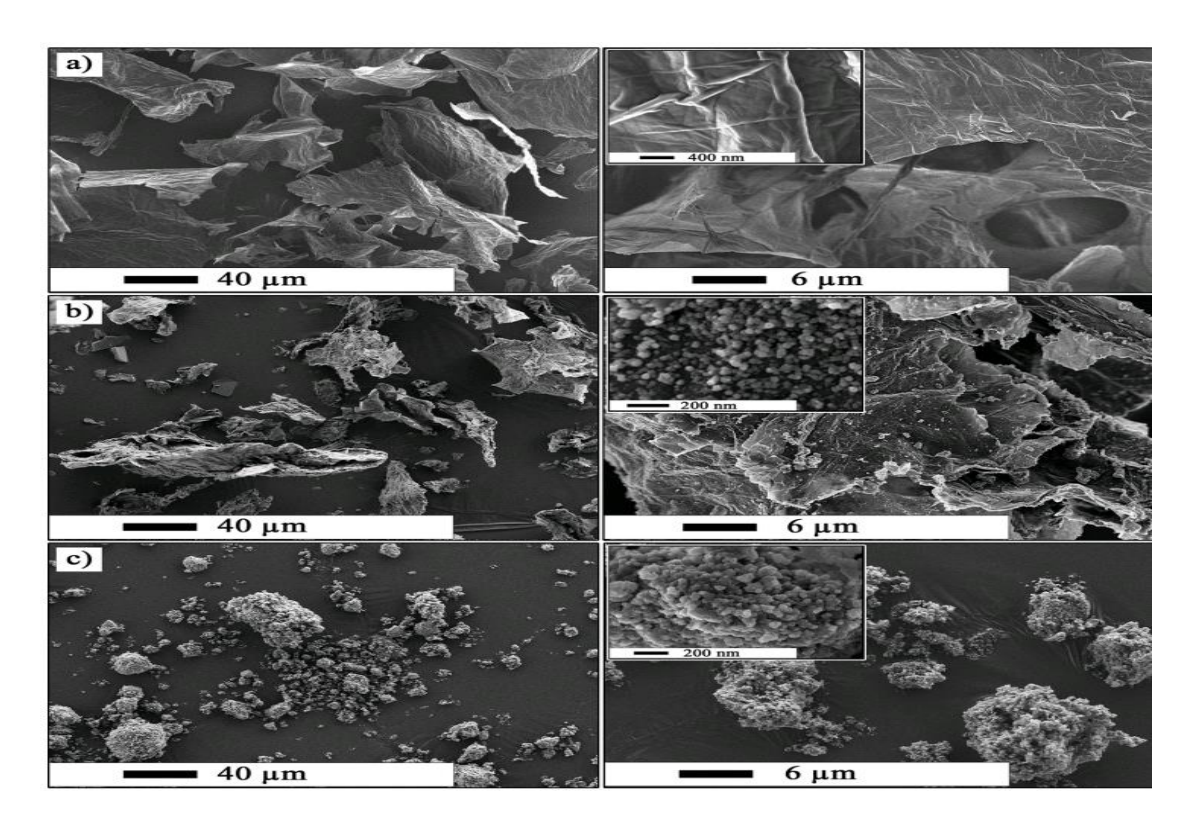


Fig. 2.28. SEM images of (a) GO flakes,(b) RGO/alumina nanocomposite and (C) alumina Nano powder[181]

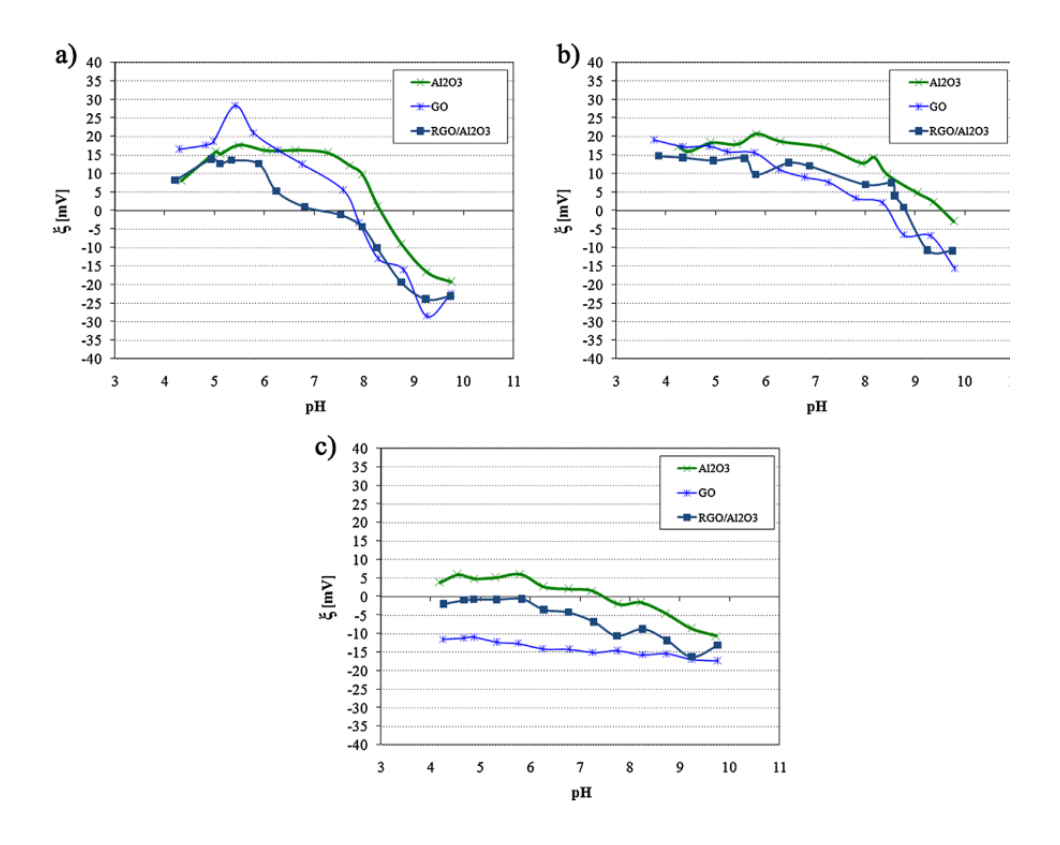


Fig . 2.29. Shows the zeta potential curves of (a) distill water,(b) electrolyte, (c) drinking water for the GO, alumina, RGO/Al_2O_3 nano composite[181].

Their results indicated that RGO/Al₂O₃ is not an electrically conductive but can be useful in the capacitance, charge screening and energy storage capacity applications. Kaleem Ahmad et al [182] have investigated the electrical and dialectical properties of alumina/ graphene nanocomposite. In this work, they have prepared the GO by MHM and then reduced thermally at high-temperature 1000°C and represent as TRGNS, and dispersed in isopropanol simultaneously by sonication and stirring for 30min. Then, they have taken the alumina (200nm) particles dispersed in isopropyl alcohol sonication stirred for 30min, finally slowly added to the TRGNS solution, followed by sonication and stirring for 30min at the same time. Then this solution was ball milled for 24h, and then the obtained material slurry was dried in hot water at 80°C, dried at 90°C for 12h. They have sintered this material at 1550°C by SPS. This process showed in the figure 2.29. In this process, they have prepared graphene /alumina composite with different content 0 to 5 vol% of the TRGNS.

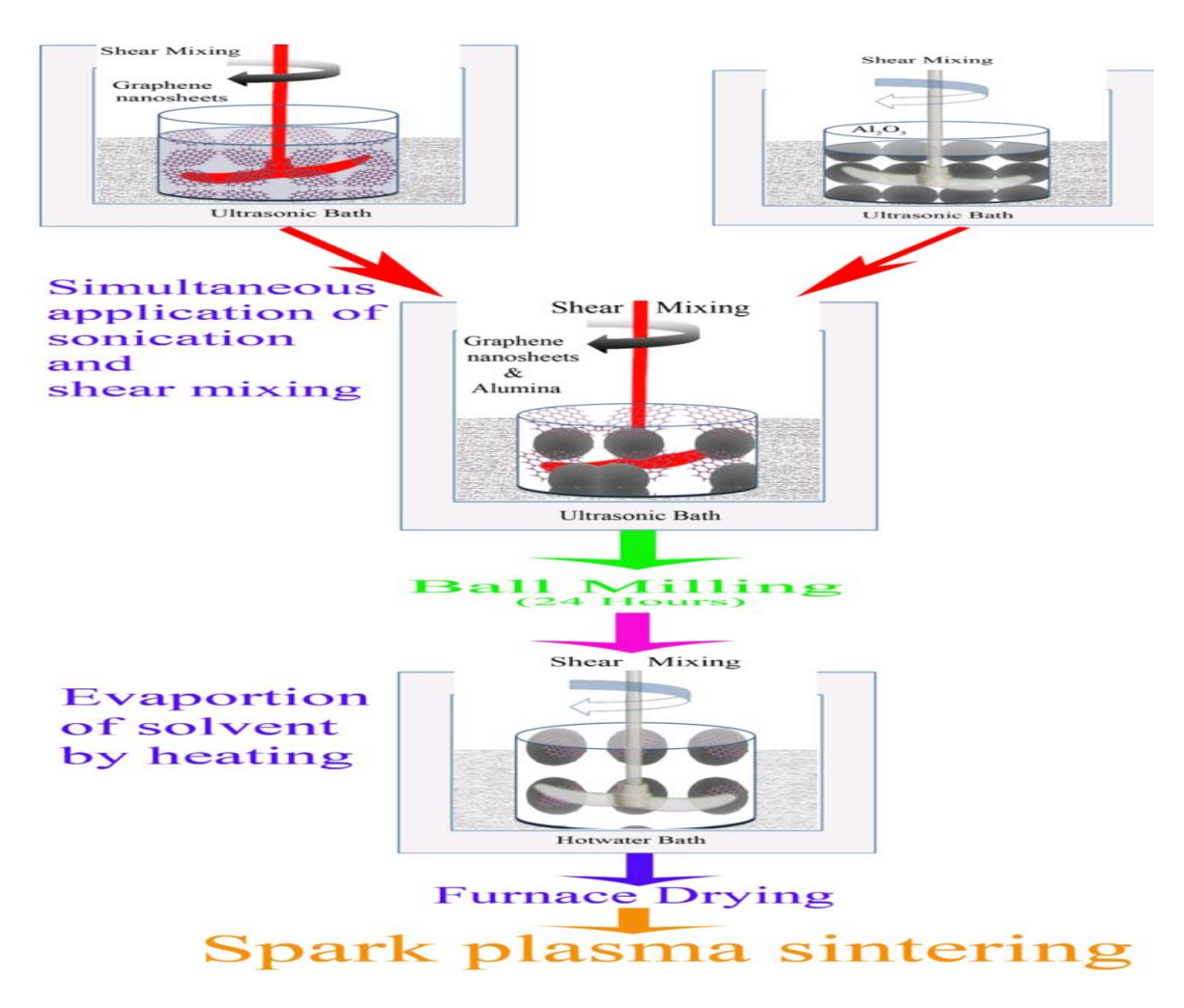


Fig. 2.30. Synthesis graphene/alumina nanocomposite by colloidal mixing process and SPS[182].

The morphology is shown in figure 2.30, for low content of the TRGNS in graphene/alumina composite, as shown in the Fig. 2.30, thin graphene network and high content show the thick graphene network through the alumina boundaries. They have measured the DC conductivity of the graphene/alumina composite, for varying % graphene as a filler as shown in Fig.2.31(a) Which indicates that the DC increases when the graphene content increases in the composite, up to 0.74 vol% and then saturates. They have also shown the temperature depends on the DC conductivity of the graphene/alumina composite for 1.5 vol% of the graphene as shown Fig. 2.31(b) and composite have a linear increment of the conductivity with temperature, but in case of 1.5, vol% the partly increment is observed because in the 5 vol % nanocomposite the electrons can be transformed between interconnected of graphene sheets due to the thick network graphene sheets. Therefore 5vol% content of graphene shows the more metallic behavior in comparison to that of 1.5 vol% of graphene content in the graphene/alumina nanocomposite. Fig 3.31(d) shows the frequency and dielectric constant with different graphene content in graphene/alumina composite. This result

indicates that the dielectric constant increases with increase in graphene content of graphene/alumina nanocomposite due to the reduced oxygen functional groups. They have reported that these materials can be used in communication, space, defines and automobile industry due to the tunable electrical conductivity.

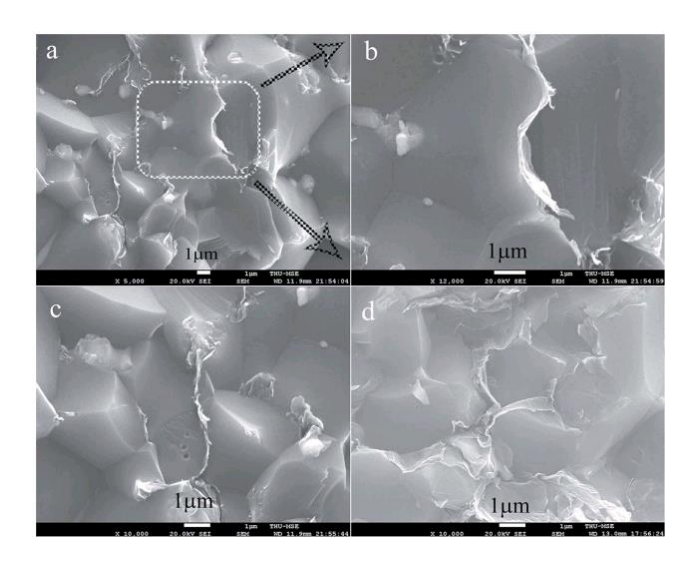


Fig. 2,31. SEM images of the graphene/alumina nanocomposite after sintering , (a) 1vol% graphene/alumina composite ,(b) thin graphene network in the alumina for 1vol% , (c) 1.51vol% graphene/alumina composite and (d) thick graphene network in alumina for 1vol% [182].

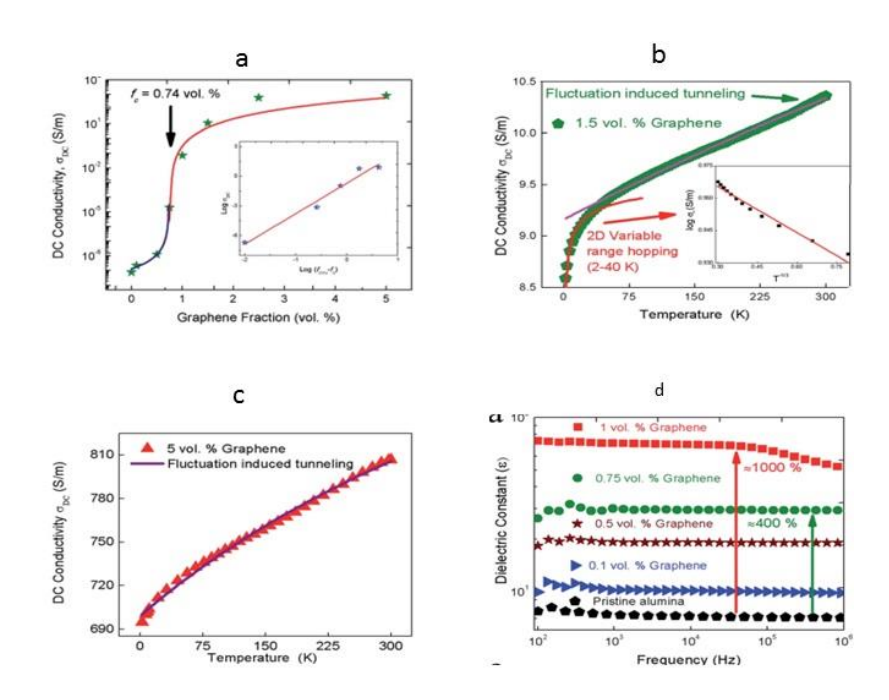


Fig. 2.32. (a) DC conductivity of the graphene/alumina nanocomposite vol% of the grain as pillar, (b) DC conductivity of the 1.5 vol% graphene content composite with varying the temperature, (c) DC conductivity of the 5 vol% graphene content nanocomposite with varying the temperature and (d) frequency vs dielectric constant with different graphene content in graphene/alumina composite[182].

2.6 Current challenges and issues

From the recent literature, we have concluded that graphene oxide can be synthesized by a chemical process which is a simple, cost-effective and more economical. Further, the obtained GO can be reduced by using suitable reducing agents to obtain reduced graphene oxide(RGO), which has a lot of potentials to be used in several applications. However, most of current studied mainly focus on the synthesis of the graphene oxide and the corresponding reduced graphene oxide by using one size graphite precursor material (~45µm). Therefore, the impacts of the different size graphite precursors (very smaller to a larger size) as starting material for synthesis of GO and RGO and the details study of the oxidation process, structure, Morphology, bonding characteristics etc are not addressed to our best knowledge. Therefore, there is a lack of clear understanding of the influence of different sizes graphite precursor on the synthesis of GO and RGO by a chemical process. Thus, these issues and challenges need to be addressed. Further, the oxidation reaction temperature is a key factor for controlling the properties of the GO, and further, the quality of RGO obtain from the as-synthesized GO. Hence, the influence of the reaction temperature of the oxidation process need to be addressed and a more details investigation of its effects on the structure, morphology, bonding to be required. Moreover, the reduction of GO to RGO is generally carried out in a few solutions, so more work is still required to understanding the solution effects on the reduction of GO to RGO.

In the second part of literature review part, we have thoroughly searched all the recent literature on the synthesis and characterization of the graphene/alumina nanocomposite for its potential to be utilized as potential materials for several applications such as energy, storage devices, capacitors, memory devices and so.on. Though, there are several existing syntheses processes has been reported by several groups and also mentioned that electrical and mechanical properties can be improved by fabrication of the graphene alumina nanocomposite. It is observed that most of the reported work has chosen the α – phase alumina nanoparticles to synthesize the nanocomposites due to the stable phase of the alumina. Also, few reported work are existing, where they have prepared alumina by choosing the alumina precursor to synthesize the alumina by chemical processes such as sol-gel method, finally fabricating the graphene/alumina nanocomposites. Moreover, the most of the reported work mainly focuses on the fabrication of the bulk materials by SPS process and then to investigate the different properties of the nanocomposites.

Therefore, to the best of our knowledge, still, there is a lacking of clearly understanding the graphene /alumina nanocomposite structure, morphology, and bonding characteristics, when γ –

phase alumina is employed as matrix material insisted of α – phase alumina. Further, the as the obtained powder form of the graphene /alumina nanocomposite need to be studied in details, as these powder form can be used as starting material for thin films formation, for another hybrid material synthesis and also for utilizing as filler material for more complex hybrid material fabrication.

Thus there are still more challenges are there to clearly understand the GO and RGO synthesis process by a chemical method and also for fabrication of graphene /alumina nanocomposites for effectively using these materials for mass production and also for several practical applications.

2.7 The motivation and objective of the thesis

The main objective of this thesis work is to investigate the influence of the oxidation reaction temperature (at lower and also higher temperature), and other synthesis parameters on the structure, morphology, bonding characteristics of the GO and RGO synthesis by chemical method mainly modified Hummers Method (MH). The second objective is to study the impact of the γ phase alumina as matrix material for the synthesis of graphene/alumina nanocomposite. Further, the influence of the different additives on the synthesis process, structure, morphology, and bond formation of the GO/RGO alumina nanocomposite are invetsigated for obtaining a potential nanocomposite material for using as catalytic, sensor, energy storage and optoelectronic applications.

2.8 Thesis outline

Chapter 1 deals with the introduction of the nanomaterials, nanotechnology and graphene properties and applications. Chapter 2 involves the current literature review, challenges, and issues. Chapter 3 deals with the influence of the chemical synthesis parameters on the structural, morphology, bonding and thermal properties of GO and RGO synthesis by MHM. Chapter 4 deals with the influence of the precursor graphite size on the structure, morphology, and bonding characteristic of the graphene oxide and reduced graphene oxide. Chapter 5 deals with the influence of synthesis parameters on the synthesis of GO/RGO-Alumina Nanocomposite by the colloidal mixing process. Chapter 6 deals with the influence of GO wt% in the formation of RGO-Al₂O₃ Nanocomposite. Finally, chapter 7 describes the conclusions, limitations, and scope of future work.

Chapter-3

Influence of the chemical synthesis parameters on the structural, morphology, bonding and thermal properties of GO and RGO synthesis by MHM

3.1 Introduction

This chapter deals with the study of the impact of different chemical synthesis's parameters such as oxidation temperature with equal ratios(1:3:23 for graphite: KMnO₄: H₂SO₄) and the synthesis are represent as reaction 1, reaction 2 and reaction 3. These reactions are reduced by the chemical (using the hydrazine hydrate) and thermal reduction.

3.2 Effect of reaction temperature (low temperature) on the synthesis of GO and RGO by MHM

3.2.1 Materials

Graphite (\geq 99.99% Sigma-Aldrich) used was having a particle size of \leq 45 μ m, Sodium Nitrate (NaNO3, 99.0% Sigma-Aldrich). Potassium Permanganate (KMnO4, 99.5% Merck) and concentrated Sulphuric acid (abt. 98%) Hydrogen Peroxide (30%) was purchased from SDFCL India. DI water was also used for this reaction.

3.2.2 Synthesis of GO at three different lower reaction temperature

Graphite oxide was synthesized from graphite powder by modified Hummer's method. graphite powder was first added into the concentrated H2SO4 and NaNO3 taken in the 2000ml beaker in Ice bath string for few mints. Under stirring, the mixture was cooled to 5°C using an ice bath. KMnO4 was then gradually added under cooling and stirring, and also keep the temperature below 5°C, then removing the Ice bath and stirring for at RT on the hot plate. Increased temperature RT to the different temperature shown on the table and stirring. The increased temperature to 98°C during the high-temperature stage adding the DI water at 98°C stirred and further diluted with DI

water. After that, 30% H₂O₂was added to the mixture to reduce the residual KMnO₄. After washing with DI water several times and 35% HCl 2times used (each time 80ml) until pH value reached to 7, the as-obtained graphite oxide (GO) was collected by centrifuging and filtering and drying. The resulting graphite oxide (GO) was dried at 100°C for12 h in a vacuum oven the synthesis parameters showed in table 3.2.1. These graphite oxide samples are thermally reduced at 300°C in a furnace in air condition. All the synthesis carried out in the same ratio of graphite: KMnO₄: H₂SO₄ in 1:3:23.

Table 3.2.1. Graphite oxide synthesis parameters by MHM (Graphite : KMnO₄: H₂SO₄ :: 1:3:23)

| Parameter | Reaction 1 | Reaction 2 | Reaction 3 |
|--------------------------------|---------------|-------------------|---------------|
| | (1:3:23) | (1:3:23) | (1:3:23) |
| Graphite | 4gm | 2gm | 5gm |
| H ₂ SO ₄ | 92ml | 46ml | 115ml |
| NaNO ₃ | 2gm | 1gm | 2.5gm |
| KMnO ₄ | 12gm | 6gm | 15gm |
| Stirring time | 2h | 1h | 1h |
| Temperature and | 45°C | 40°C | 35°C |
| stirring time | 15h | 15h | 2h |
| DIW & Stirring time | 184ml & 30min | 92ml & 15min | 230ml & 15min |
| DIW & H2O2 | 560ml & 40ml | 280ml & 20ml | 700ml & 50ml |
| HCl | 80ml | 80ml | 80ml |
| Drying temperature & | 100°C & 12h | 100°C & 12h | 100°C & 12h |
| Time | | | |

3.2.3 Synthesis of reduced graphene oxide (RGO)

Graphite oxide was taken in a beaker and 500ml DI water was poured then sonicated for an obtained clearer solution. Then Hydrazine hydrate was added to the graphene oxide solution then heated 120°C and stirring. This experimental was going on hotplate by using the vegetable oil both. After completion of the reaction, we observed that in the DIW, the solution appearing in black colored but the material looked like weight loss and formed on the surface of the solution. These samples were washed with DIW and obtained PH=7 and filtered with a vacuum pump and dried at 120°C in the

Oven for 12h and the reaction parameters are followed in table 3.2.2 and also these samples followed thermal reduction at 300° C.

Table 3.2.2: Parameters for synthesis of Reduced Graphene Oxide(RGO)

| parameter | Reaction(1) | Reaction(2) | Reaction(3) |
|--------------------------------------|---|---------------------------|------------------------|
| Graphite Oxide | 250mg | 250mg | 125mg |
| Distilled Water | 250ml | 250ml | 125ml |
| Sonication for clear solution | 30min | 30min | 15min |
| Hydrazine Hydrate(72-82%) | 10ml | 10ml | 5ml |
| Temperature | 120°C | 120 ⁰ C | 120°C |
| String Time | 6h | 4h | 6h |
| Observation | Solution :cleared separation of material | Solution , black coloured | solid |
| pH | 10 | 10-11 | 7 |
| Washing with Distilled Water & pH | 3 days & 7 | 4 days & 7 | |
| Dried in Oven. | 120 ⁰ C&12h | 120 ⁰ C&12h | 120 ⁰ C&12h |

3.2.4 Structural analysis by XRD

Fig.3.2.1 shows the graphite pattern of XRD. The graphite has interplanar distance is d=0.334nm at 2θ=26.6 and crystallite size was measured by the from the brags law, D= 23.08nm and the peak of intensity is 44280(a.u). the shape of the peak is very very narrow which represents the layers are arranged in regular and exhibits the big size of the crystallite size due to the low FWHM value is 0.3593°. Fig.3.2.2. (a) shows the XRD pattern of the combined plot of graphite oxides for all reaction (1),2 and 3 and their corresponding peak positions, interplanar distance d (calculated by using the Brag's law) and crystallite size D (by using the Scherr formula) showed in table 3.2.3. We observed that the graphite basal plane (002) was shifted to the higher interplanar distance for all samples (showed in table 3.2.3) due to the oxygen functional groups attached to the graphite layers which indicates the complete oxidation happened. But three samples show the different peak

positions such as $2\theta = 12.3,12.6$ and 13.5 and also the corresponding interplanar distances are 0.72,0.696 and 0.655nm of reaction (1),2 and 3 graphite oxide respectively.

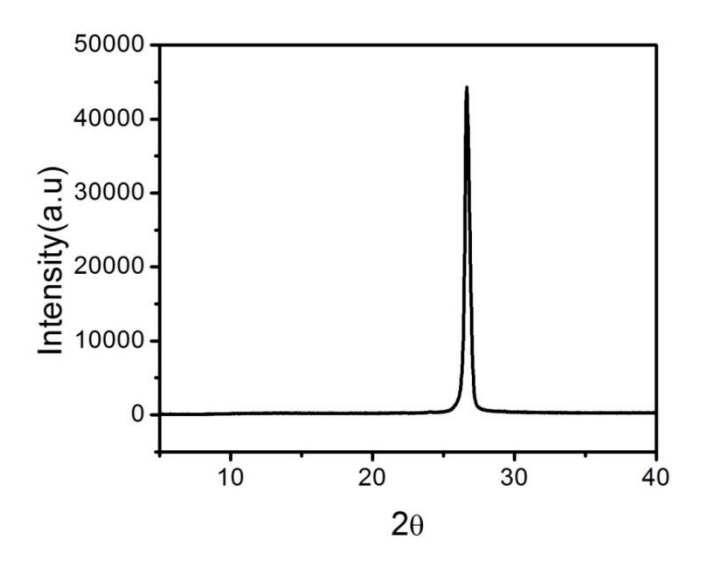


Fig. 3.2.1. XRD pattern of graphite (size 45µm).

So that these samples have may be different oxygen functional groups or these samples have different quantity of similar functional groups. Even though we are using equal ratios of reaction agents, these samples show the different interplanar distances. This may happen due to the reaction conditions such as temperature and time. Because the synthesis is done at different temperature 45,40 and 35°C and also reaction time was 15h,15h, and 2h for reaction (1),2 and 3 respectively. So that we clearly observed that when changing the slight variation in temperature oxidation levels are different for equal ratios of graphite: KMnO₄: H₂SO₄ and also observed that when reaction time was same for reaction 1 and 2 with different temperature, reaction 1 shows the more oxygen functional groups indication by the due to the higher interplanar distance. These samples are dried at 100°C for 12h, that means mostly water molecules are may be removed so that these graphite oxide samples have fewer water moles in the samples. So that these samples can exhibit different oxygenrelated groups or depends on the number of similar functional groups. The crystallite sizes of these samples have different showed in table 3.2.3. the reaction 1 and 2 have nearly same such as 5.8 and 6.1nm and reaction 3 has crystallite size is 4.8 nm. Even we are using the same size of graphite (<45µm) with equal ratios of synthesis agents, these samples show the different crystallite sizes so that the crystallite size varying with the reaction temperature. The reaction 1 and 2 have similarly crystallite size but variation in their intensity. Reaction 1 has more intensity than other two samples which indicates this sample may have more crystallinity than other two samples.

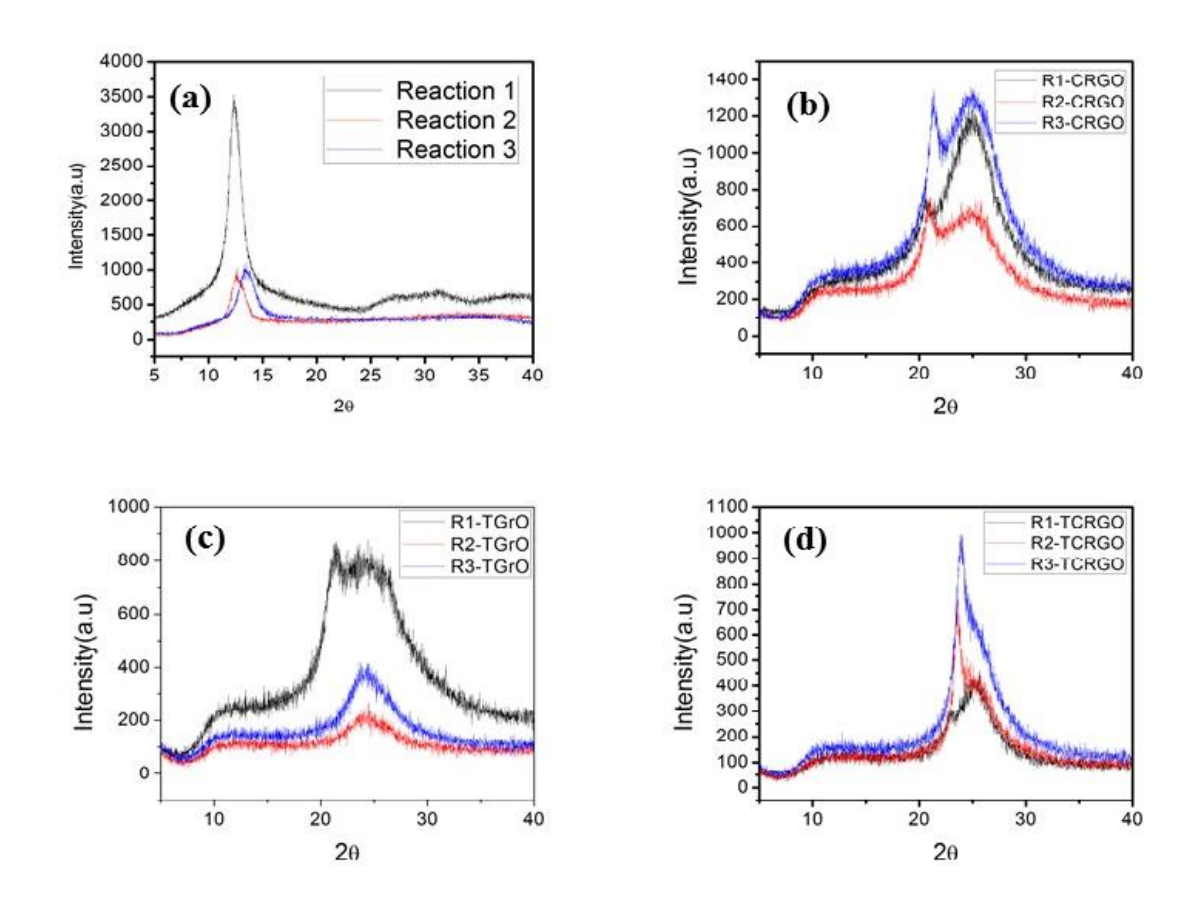


Fig.3.2.2 XRD pattern of the different graphene derivatives of reaction 1,2 and 3. (a) graphite oxides of reaction 1,2 and3, (b) chemically reduced graphene oxide of 1,2 and 3 reactions, (c) thermally reduced graphene oxide at 300^{0} Cof 1,2 and 3 reactions and (d) thermally reduced of the chemically reduced sample.

Table 3.2.3 XRD peak position, interplanar distance, and crystallite size of reaction 1, 2 and 3 for the graphite oxide

| Sample name | 2θ ⁰ | d nm | D nm | I (a.u) | Shape of the peak | FWHM ⁰ |
|----------------|------------------------|---------|---------|------------|-------------------|-------------------|
| GrO1 | 12.3 | 0.72 | 5.804 | 3390 | Semi Broadening | 1.42 |
| GrO2 | 12.6 | 0.696 | 6.09 | 930 | Broadening | 1.36 |
| GrO3 | 13.5 | 0.655 | 4.84 | 990 | More Broadening | 1.7 |

Figure 3.2.2. (b) shows the XRD pattern of the combined plot of chemically reduced graphene oxides for all reaction (1),2 and 3. Reduced oxygen functional groups by using the reducing agent such as hydrazine hydrate, the interplanar distance was decreased (shown in table 3.4). which indicates the oxygen functional groups are reduced. All three samples show the nearly same peak position at 21° represents the hydrocarbons presence and 25° peak indicates the formation of graphene structure. The broadening of the peaks represents the reduction in the size of the sp² domains in the graphene and also provide the information about the disorder of graphene layers. The broadening of the graphene peak gives the reduced of the no of layers of graphite, which represents the all three samples formation of the few-layer graphene but variation in their intensity which represents, these samples are may have different crystallinity.

Table 3.2.4 XRD peak position, interplanar distance, and crystallite size of reaction (1),2 and 3 for the chemically reduced graphene oxide(CRGO)

| Sample name | $2\theta^0$ | d nm | D nm | I (a.u) | Shape of the peak | FWHM ⁰ |
|----------------|-------------|----------------|---------|-----------------|-------------------------------|-------------------|
| CRGO1 | 20.5 25 | 0.4 0.357 | | 7 50 1200 | Semi Broadening Broadening | |
| CRGO2 | 20.9 25 | 0.425 0.357 | | 750 700 | Semi Broadening Broadening | |
| CRGO3 | 21 25 | 0.42 0.357 | | 1250 1300 | Semi Broadening Broadening | |

Figure 3.2.2. (c) shows the XRD pattern of the combined plot of thermally reduced graphene oxides for all reaction (1),2 and 3. Table 3.2.5 shows the corresponding the XRD values. From this table, we can say that the oxygen functional groups are removed from chemically reduced samples but variation in the formation of the hydrocarbon-related groups. The reaction 1 only showed the hydrocarbon-related groups and in reaction 2 and reaction 3 these groups are absent. The reaction 3 and 2 have same peak position that means same interplanar distance and the crystallite size also same but variation in the intensity showed in table 3.2.5.

Table 3.2.5. XRD peak position, interplanar distance, and crystallite size of reaction (1),2 and 3 for the thermally reduced graphene oxide(TRGO)

| Sample | $2\theta^0$ | d | D | I | Shape of the | $FWHM^0$ |
|--------|-------------|-------|-------|-------|--------------|----------|
| name | | nm | nm | (a.u) | peak | |
| | | | | | | |
| TRGO1 | 21 | 0.42 | | 853 | Broadening | |
| | 24.5 | 0.364 | ••••• | 790 | Broadening | |
| TRGO2 | 24.4 | 0.364 | 1.7 | 225 | Broadening | 4.99 |
| | | | | | | |
| TRGO3 | 24.4 | 0.364 | 1.7 | 400 | Broadening | 5 |
| | | | | | | |

Table 3.2.6 XRD peak position, interplanar distance, and crystallite size of reaction (1),2 and 3 for the thermally chemically reduced graphene oxide(TCRGO)

| Sample name | $2\theta^0$ | d nm | D nm | I (a.u) | Shape of the peak | FWHM ⁰ |
|----------------|-------------|---------------|---------|------------|---------------------------|-------------------|
| TCRGO1 | 22.9 25 | 0.389 0.57 | | 310 420 | Semi Broading Broading | |
| TCRGO2 | 23.6 | 0.376 | 2.08 | 730 | Broadening | 4.04 |
| TCRGO3 | 23.9 | 0.359 | 2.425 | 970 | sharp | 3.5 |

Fig.3.2.2. (d) shows the XRD pattern of the combined plot of thermally reduced of chemically reduced graphene oxides for all reaction (1),2 and 3. These samples show the structural deviation from the chemically reduced samples. In the case of chemical reduced samples shows the two peaks but double reduced samples show the single peak at $2\theta = 24$ and interplanar distance (d) = 20.36 nm.

3.2.5 Molecular structure and disorder by Raman analysis

Raman technique is mostly used for the carbon-based materials and also find out the quality of the graphene. In this work, we used the 532 nm LASER wavelength and all samples are in the powder form. Fig. 3.2.3 shows the Raman spectrum of graphite (<45µm size). It shows that more sharp peak at 1583cm⁻¹, which represents as G band arising from the E2g phonon mode of high-frequency first order mode. This is the most responsible for the "in-plane atomic displacement, the sharpness of the peak indicates it has large crystallite size and also this represents the sp2 carbon network of graphite. The Very weak intensity and sharp peak appearance at 1356cm⁻¹ represent as D band due to the aromatic rings of breathing mode and also this peak may be shows the defects or disorder and reduction of graphite domain size. One more weak peak appearance at 2452 cm⁻¹, indicates the second order Raman spectrum. Another important sharp peak at 2706 cm⁻¹, which represents a 2D band of an overtone of D band. From this peak to measure the no of layers by the intensity and

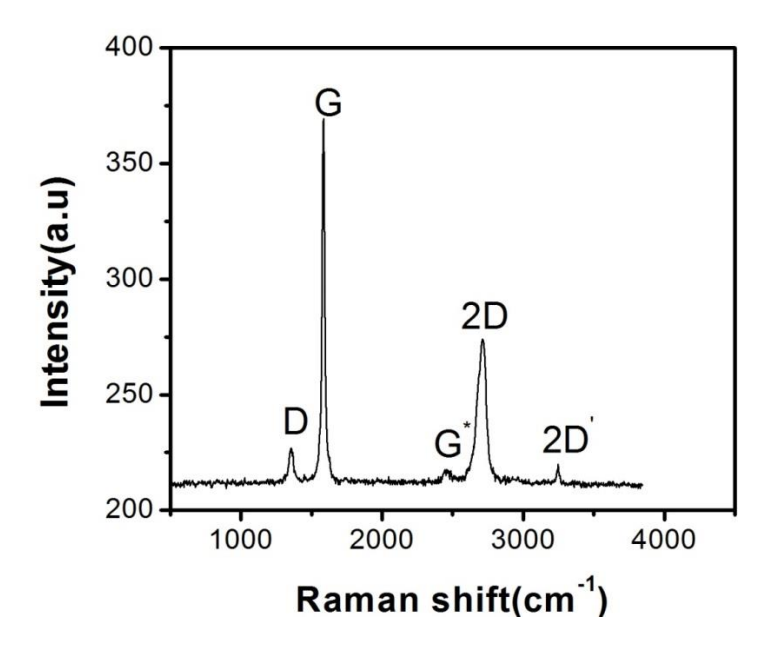


Fig. 3.2.3 Ramana spectrum of graphite (<45µm size)

shape of the peak. And also find out the graphene nature from the peak shift. One more second order weak peak appearance at 3246 cm⁻¹, which is an overtone of the 2D band and represent as 2D'. This mode "can allow without defects".

Fig. 3.2.4 (a) shows the Raman spectrum of reaction (1),2 and 3 of graphite oxides.which shows the broadening of the G peak and D band, this represents the oxidation was happened and all three samples show the suppressed of the 2D band, and also appearing the broad hump in this region. Comparative to graphite, these samples show the increase in I_D/I_G ratio of graphite oxide which indicates the change of graphite domain size may reduce and formation of the disorder . in all

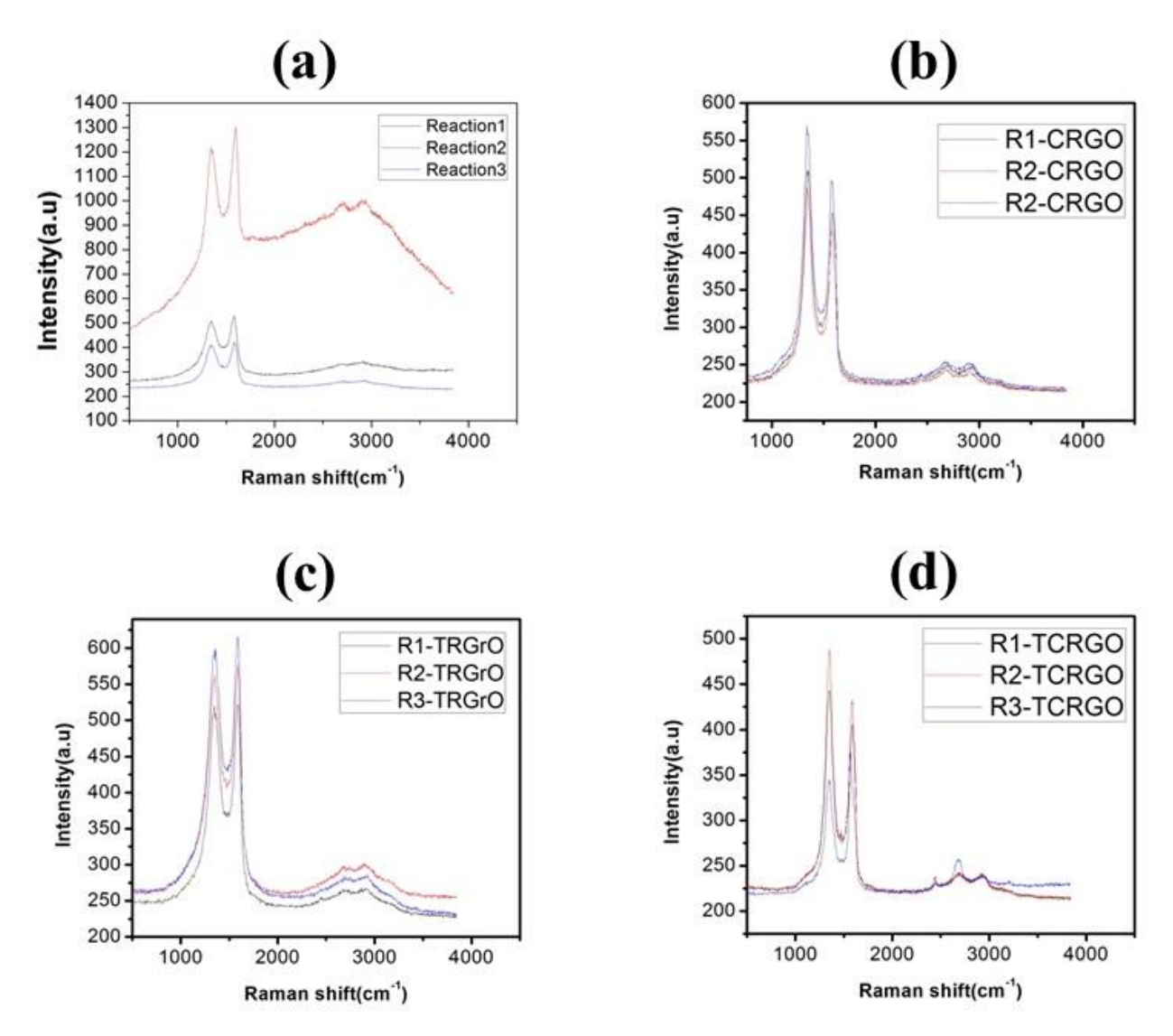


Fig .3.2.4. Raman spectrum of different graphene-based materials of Reaction 1,2, and 3. (a) graphite oxide of Reaction 1,2, and 3, (b) Reduced graphene oxide of Reaction 1,2, and 3, (c) thermally reduced graphite oxide of Reaction 1,2, and 3 and (d) thermally reduced of chemically reduced samples of Reaction 1,2, and 3.

three samples show the new peak appearance of the D+G band and disappearance of the G* and 2D' bands showed in Table 3.2.6. This indicates the out-of-plane related to the functional groups formed

in the graphite oxide. In the graphite oxide, the out-of-plane functional groups are carbonyl and carboxyl groups formed. In the Table 3.2.6 shows, the three reactions have different band position of G. In the case of reaction (1) shows the 1581cm-1, reaction (2) has 1597cm-1 and reaction three shows the 1586 cm-1. Generally, the graphite oxide case G band position was a redshift of the graphite position. In the reaction (1) shows the blueshift of the G peak which

Table. 3.2.6 Raman Analysis of GO for reaction 1, 2 and 3

| Sample name | D band cm ⁻¹ | G band cm ⁻¹ | 2D band cm ⁻¹ | G*band cm ⁻¹ | D+G band cm ⁻¹ | 2D'band cm ⁻¹ | $I_{ m D}/I_{ m G}$ | I _{2D} /I _G |
|---------------------|-------------------------------|----------------------------|-----------------------------|---|------------------------------|-----------------------------|---------------------|---------------------------------|
| R ₁ -GrO | 1343 | 1582 | ••••• | | 2910 | ••••• | 0.95 | |
| R ₂ -GrO | 1349 | 1597 | ••••• | •••• | 2910 | | 0.93 | |
| R ₃ -GrO | 1342 | 1587 | • • • • • • | • | 2919 | | 0.97 | |

Table.3.2.7 Raman Analysis of chemically reduced RGO for reaction 1, 2 and 3

| Sample name | D band cm ⁻¹ | G band cm ⁻¹ | 2D band cm ⁻¹ | G*band cm ⁻ | D+G band cm ⁻¹ | 2D'band cm ⁻¹ | I_D/I_G | $I_{\mathrm{2D}}/I_{\mathrm{G}}$ |
|---------------------|-------------------------------|----------------------------|--------------------------------|---------------------------|------------------------------|-----------------------------|-----------|----------------------------------|
| R ₁ -RGO | 1347 | 1586 | 2690 | 2437 | 2926 | ••••• | 1.12 | 0.55 |
| R ₂ -RGO | 1343 | 1580 | 2678 | 2445 | 2904 | ••••• | 1.13 | 0.57 |
| R ₃ -RGO | 1344 | 1582 | 2676 | 2436 | 2926 | | 1.15 | 0.51 |

indicates that it contains the less epoxy, hydroxyl and water molecules. The blueshift can happen when the double bond related functional formed. This may be happened to form a new peak appears at the D+G band and also a 2D band at 2670cm-1 which shows the blue shift from the graphite indicates that this material shows the graphene-related structure. Fig. 3.2.4 (b) shows the combined plot of chemically reduced graphite oxide by hydrazine hydrate and the band positions showed in table 3.2.7. We observed that these band positions are completely changed compared to the graphite oxide samples. Which indicates the reduction happened. The I_D/I_G ratios are changes like, increased comparative graphite oxides showed in the table, which means that the chemical reduction was introduced the defects or disorder or reducing the size of SP^2 domains or newly formed SP^2 carbon network. After reduction, the 2D band's intensity is increased and these bands are not observed in the graphite oxide samples but in this range, the broad hump was there. These samples have

different I_{2D}/I_G ratios, that means a different number of graphene layers are formed. These ratios are less thane graphite ratio and the 2D band positions are blueshift from the graphite 2D band position, which indicates these samples exhibit the graphene nature, removing the oxygen-related functional groups and obtained SP² carbon network. G* band appear in all samples, this band was absent in the graphite oxide samples. This band also observed in the source of graphite sample, so that these samples have recovered from graphitic nature. All three RGO samples show the G+D band positions this indicates the defects or disorder in the samples.

Fig. 3.2.4 (c) shows the graphite oxide samples are thermally reduced at 300° C in the air and the corresponding band positions showed in table 8. These samples are exhibits the band position and intensity variation, completely different from the graphite oxide and chemically reduced graphite oxide samples. These samples are not showing 2D band particularly comparative to CRGrO samples. We also observer that the I_D/I_G ratios are increased compared to graphite oxide sample and decreased with chemically reduced samples which mean that formation of SP^2 carbon domains may be larger size comparative CRGrO samples. G^* band is absent in these samples comparative chemically reduced graphite oxides and also G+D band was more intensity than CRGO samples. The G band position is red shifted compare to CRGO samples.

Table:3.2.8 Raman Analysis of thermally reduced RGO for reaction 1, 2 and 3

| Sample name | D band cm ⁻¹ | G band cm ⁻¹ | 2D band cm ⁻¹ | G*band cm ⁻¹ | D+G band cm ⁻¹ | 2D'band cm ⁻¹ | I _D /I _G | $ m I_{2D}/I_{G}$ |
|---------------------|----------------------------|----------------------------|--------------------------------|----------------------------|---------------------------------|---|--------------------------------|-------------------|
| R ₁ -GrO | 1347 | 1586 | ••••• | ••••• | 2903 | • | 0.99 | |
| At 300°C | | | | | | | | |
| R ₂ -GrO | 1350 | 1585 | | | 2932 | | 0.97 | |
| At 300°C | | | | | | | | |
| R ₃ -GrO | 1353 | 1591 | | | 2915 | | 1.003 | |
| At 300°C | | | | | | | | |

Table: 3.2.9 Raman Analysis of chemically and thermally reduced RGO for reaction 1, 2 and 3

| Sample name | D band cm ⁻¹ | G band cm ⁻¹ | 2D band cm ⁻¹ | G*band cm ⁻¹ | D+G band cm ⁻¹ | 2D'band cm ⁻¹ | I _D /I _G | I _{2D} /I _G |
|---|-------------------------------|----------------------------|--------------------------------|----------------------------|---------------------------------|-----------------------------|--------------------------------|---------------------------------|
| R ₁ -RGrO At 300 ⁰ C | 1348 | 1585 | 2686 | 2440 | 2927 | | 1.09 | 0.59 |
| R ₂ -RGrO At 300 ⁰ C | 1352 | 1585 | 2685 | 2440 | 2924 | ••••• | 1.1 | 0.56 |
| R ₃ -RGrO At 300 ⁰ C | 1345 | 1568 | 2682 | 2442 | 2938 | | 0.93 | 0.70 |

Fig. 3.2.4 (d) shows the thermally reduced at 300°C of chemically reduced samples, which represent as TCRGO. These samples different band position and intensity each other. G* band intensity was increased comparative to reaction 3 (TCRGO) of other samples and also this band was not observed in TRGrO samples. These samples have different 2D band position, intensity, and shape showed in Fig. 3.2.7 (d) and Table 3.2.9. The 2D band of reaction 1 and 2 of TCRGO samples have low intensity and broad hump comparative reaction 3, it has more intensity and sharp peak and also a well blue shift of band position comparative other two samples. This sample has less intensity band of the D+G band and also G band was well decreased to lower wave number, showed in table 3.2.9. The I_D/I_G ratio decreased comparative reaction 1 and2 of TCRGO but increased in I_{2D}/I_G ratio. So that reaction 3 of TCRGO is better reduction happen than reaction 1 and 2 of TCRGO. TCRGO samples showed different band position, intensity comparative other two methods such as chemically reduced (CRGO) and thermally reduced graphite oxide(TRGO).

3.2.6 Morphological analysis by FESEM

Fig. 3.2.5 (a), (b) and (c) shows the FESEM images of the morphology of the graphite oxide reaction(1),(2) and (3) respectively. All three samples are shown the good intercalated sheet-like morphology which indicated the oxidation successfully happened. Fig.3.2.5 (d), (e) and (f) shows the reduced graphene oxide(RGO) samples of reaction(1),(2) and (3) respectively. Three samples show the different morphology comparative to their oxidation samples. In this, all samples show the disorder and folding sheet-like morphology. These results agree with XRD and Raman results. the disorder may happen due to the new formation of the graphite domains, in the XRD shows the hydrocarbon templates and in the Raman ID/IG ratio increased so the RGO samples show the irregular shape sheets. Fig.3.2.5 (g), (h) and (i) shows the thermally reduced graphene

oxide(TRGO) samples of reaction(1),(2) and (3) respectively. Each figure shows the two different morphology showed by two areas indicated as 1 and 2. Area 1 shows the more transference sheets and area 2 has more exploited sheets. These samples show the different morphology comparative GrO and RGO samples. Fig. 3.2.5 (j), (k) and (l) shows the thermally reduced of chemically reduced graphene oxide(TCRGO) reaction(1),(2) and (3) respectively. These samples show the different morphology comparative to the CRGO and TGrO samples. In which the these have a sheet-like morphology.

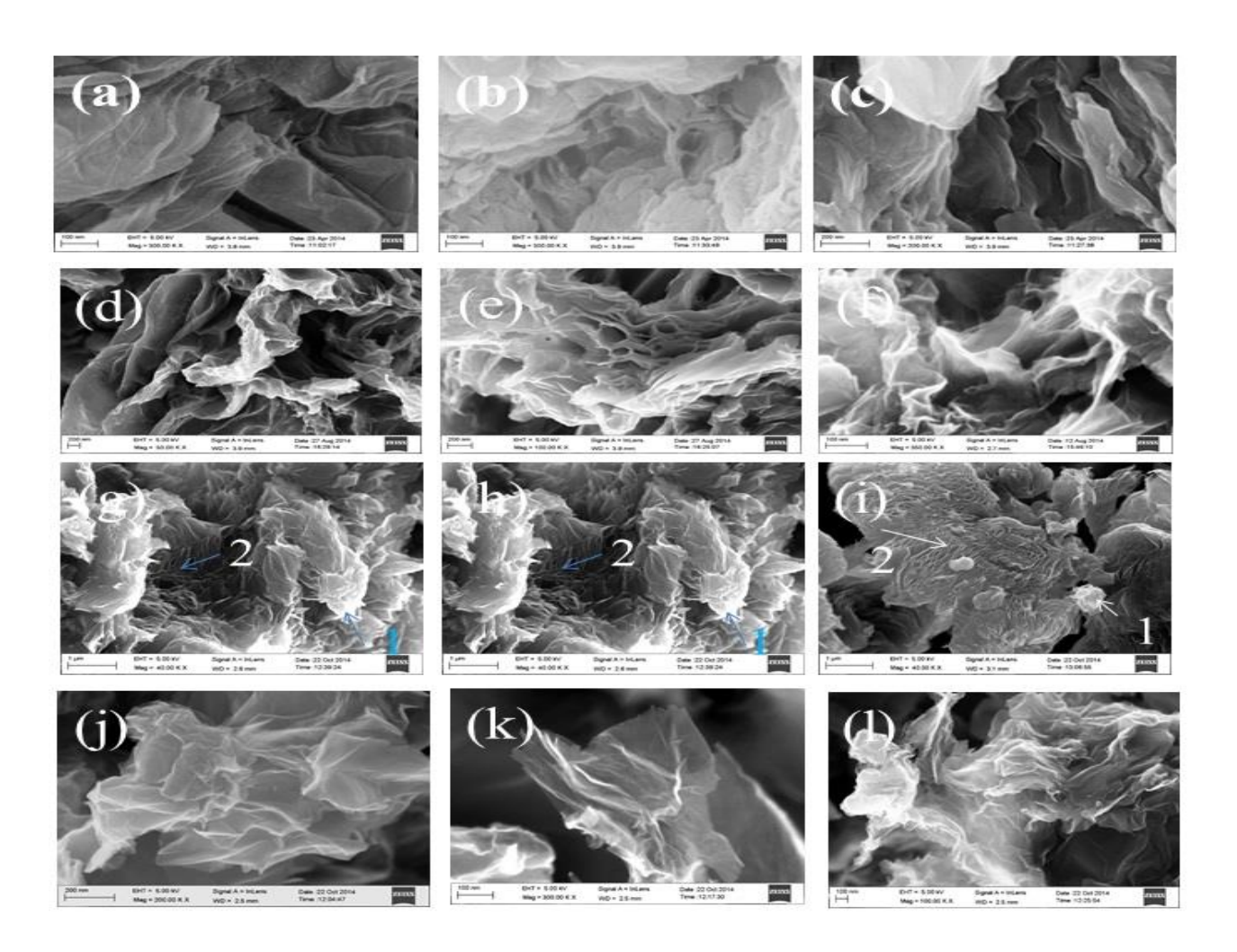


Fig.3.2.5 The typical FESEM images of graphite oxide (a).(b) and (c) for the) reaction(1),(2) and (3) respectively. (d),(e) and (f) are reduced graphene oxide(RGO) samples of reaction(1),(2) and (3) respectively. (g),(h) and (i) shows the thermally reduced graphene oxide(TRGO) samples of reaction(1),(2) and (3) respectively and (j), (k) and (l) shows the thermally reduced of chemically reduced graphene oxide(TCRGO) reaction(1),(2) and (3) respectively.

3.2.7 Morphology and structural Analysis by TEM

Transition electron microscopy(TEM), Model: FEI Technai G2S-Twin is also used for the studying morphology and structural properties. The operating acceleration voltage of TEM was 200kv. Fig. 3.2.6 shows the morphology and structure of the powder form of graphite oxide for all samples. In this Fig. 3.2.6 (a) shows the sheet-like and folding morphology of reaction 1 of graphite oxide. Fig. 3.2.6 (b) shows high-resolution transition electron microscopy (HRTEM) of reaction 1, in this, it shows the,<10 layer so this material represent as few-layer graphene oxide and Fig. 3.2.6 (c) is a selected area electron diffraction (SAED) reaction 1, it shows the less intensity diffraction spots in the inner ring this may happen due to the formation of the FLG. Crystallinity shows this material may have fewer water molecules and also has more sp² carbon network. This result may agree with the Raman results due to the blue shift of the G band.

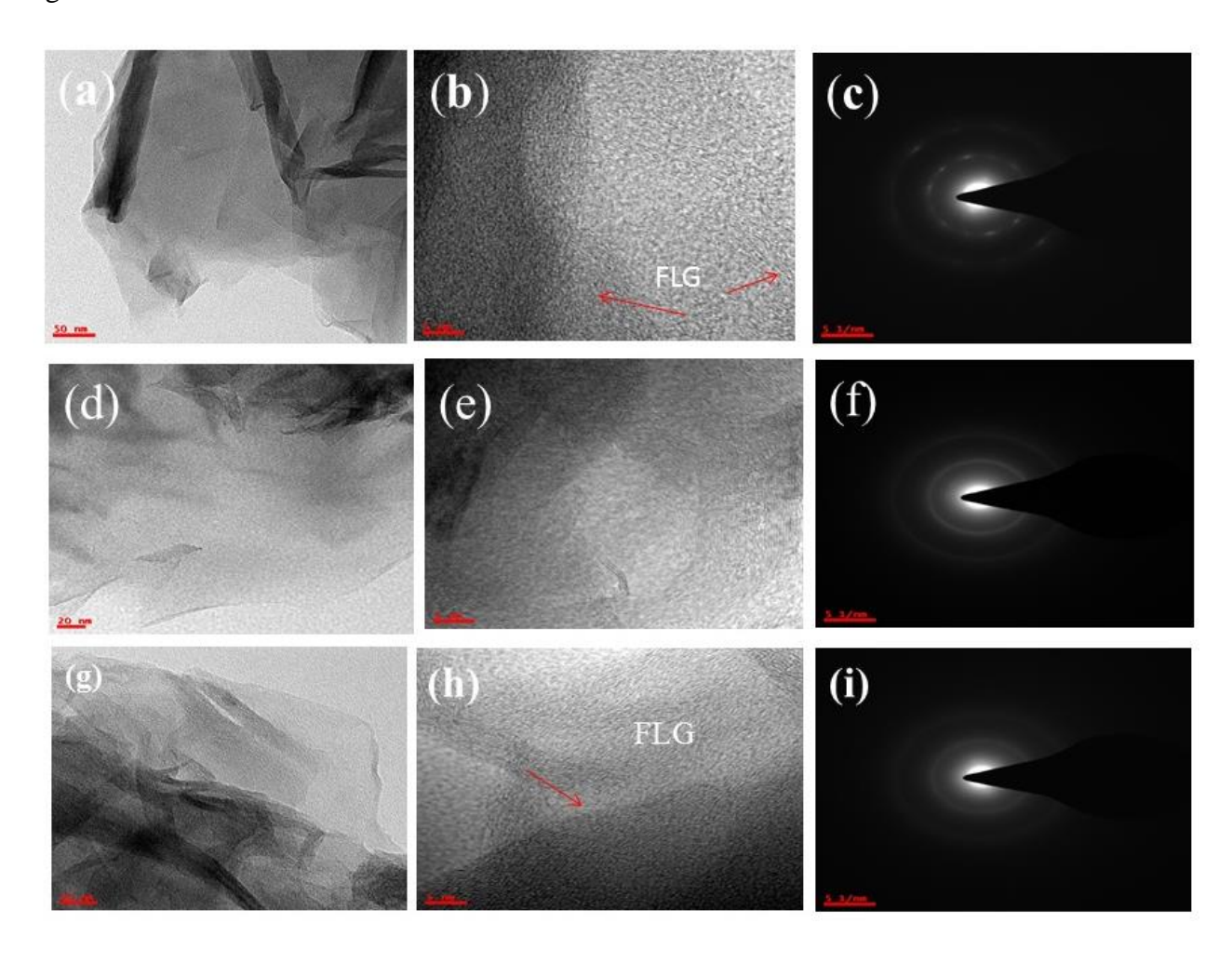


Fig. 3.2.6. TEM image of the graphite oxide for reaction(1),(2) and (3) (a) TEM image, (b) HRTEM image and (c) SAED of reaction (1), (d) TEM image, (e) HRTEM image and (f) SAED of reaction (2) and (g) TEM image, (h) HRTEM image and (i) SAED of reaction (3).

Fig. 3.2.6 (d) shows the TEM images of powder of the graphite oxide for the reaction(2). It appears as a thin sheet-like morphology with folding. Fig. 3.2.6(e) is HRTEM images of graphite oxide for the reaction(2), it clearly shows the FLG with a disorder of the graphite layers, which also indicates the overlapping of the layers. Fig. 3.2.6 (f) shows the SAED pattern of graphite oxide for the reaction(2), appearance like ring pattern which indicates that disorder of the layers due to the SP³ hybridization of oxygen-related functional groups. Generally, ring pattern indicates amorphous nature of the materials. But in the graphite oxide, the oxygen functional attached to the basal plane and edge with randomly, so that the ring pattern of the graphite may be happened due to the disorder, which means that more water molecules, hydroxyl and epoxy groups formed in this sample. Fig. 3.2.6(g) is the TEM image for the graphite oxide reaction (3) which is similar to the reaction (2) results but this sample has more folding than reaction(2). This sample has FLG with disorder shown in Fig. 3.2.6 (h) and Fig. 3.2.6(i) shows same as reaction (2) pattern like ie ring pattern.

Fig. 3.2.7(a) shows the TEM image of the reduced graphene oxide for reaction (1), this image clearly indicates the transference of the graphene oxide sheet, more folding of the sheets and restacking of the layers. Fig. 3.2.7(b) shows the HRTEM image, in this graphene layers formed in disorder with re-stacking of the layers. Fig. 3.2.7(c) shows the SAED pattern, the diffraction pattern indicates that polycrystalline nature. This pattern is comparative to the corresponding the graphite oxide, this sample shows the bright spots, which indicates that the crystalline nature is increased that means that removing of the sp³ related oxygen functional groups and formed the newly sp² hybridized carbon atoms in the sample. Fig. 3.2.7 (d) shows the TEM image of reaction (2) for the reduced graphene oxide. This image, reduced graphene oxide have more transference than corresponding the graphite oxide with more folding. From the HRTEM image shown in Fig. 3.2.7 (e), clearly observed that this sample contains the different layers such as 3 layers and 4 layers so that this sample has FLG and also this sample has restacking of the graphene layers. In Fig. 3.2.7 (f) shows SAED pattern RGO sample has the bright ring pattern, but in the case of corresponding the graphite oxide samples show the light intensity SAED pattern. Increased in the intensity indicates that, some of the oxygen functional groups are removed. Fig. 3.2.7 (g) represents the TEM images

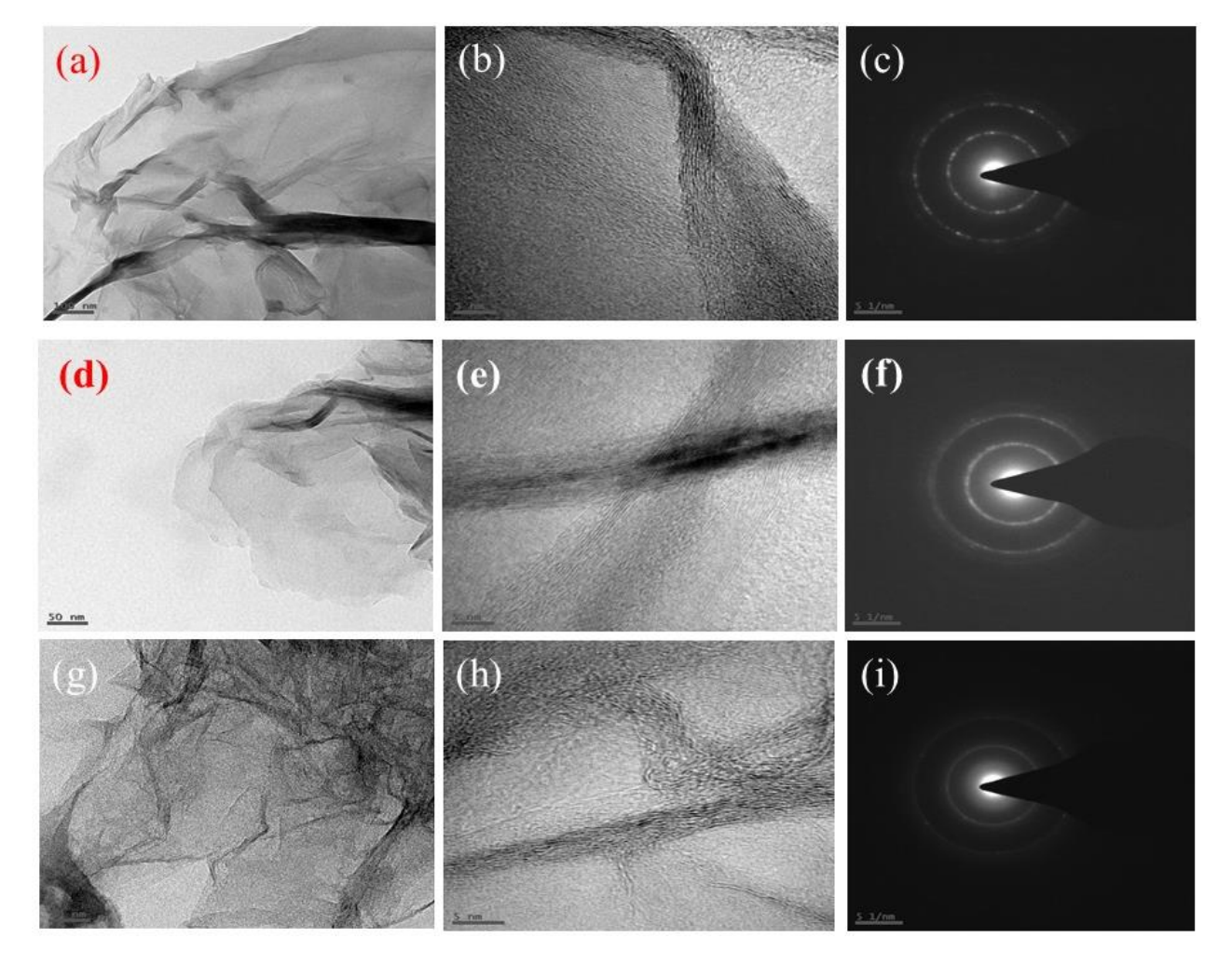


Fig. 3.2.7. TEM images of the chemically reduced graphene oxide of reaction(1),(2) and (3) (a) TEM image, (b) HRTEM image and (c) SAED of reaction (1), (d) TEM image, (e) HRTEM image and (f) SAED of reaction (2) and (g) TEM image, (h) HRTEM image and (i) SAED of reaction (3).

of reaction(3) for the chemically reduced graphene oxide. It shows the different morphology of the other two samples(reaction1 and 2 RGO samples. It has a very thin sheet-like morphology with more folding comparative other samples. The HRTEM image showed in Fig.3.2.7 (h), it has different layers, single, double, try and few layers reduced graphene oxide with more disorder. This results clearly showed in Fig. 3.2.7 (i) SAED pattern of the sample. Fig. 3.2.7 (i) has two rings formation with very low-intensity diffraction spots appearing in hexagonal position, this pattern takes at the very flat and thin place of reduced graphene oxide. The Very low intensity and hexagonal pattern represent the formation of singer layer graphene. Fig. 3.2.8 (a) shows the TEM images of the thermally reduced graphite oxide reaction (1). This image shows the very transference sheet-like morphology with more folding. In this image, we choose the different places and taken the SAED pattern for corresponding identification places showed in Fig. 3.2.8 (a) and the place

represents area 1,2,3 and 4. Area 1, looks like very thin transference graphene sheet without folding and the corresponding SAED pattern shows the hexagonal diffraction spots with low intensity which indicates the single layer graphene is formed. The 2nd area is very very less folding with transference place also shows the hexagonal diffraction spots with more intensity than area 1. In Fig. 3.2.8 (a), 3rd place indicates the more folding than a 1st and 2nd place which shows the SAED pattern disappearance of hexagonal pattern and formation of the polycrystalline with low and high-intensity spots, which means that the number of layers increased. 4th place represents the more folding than

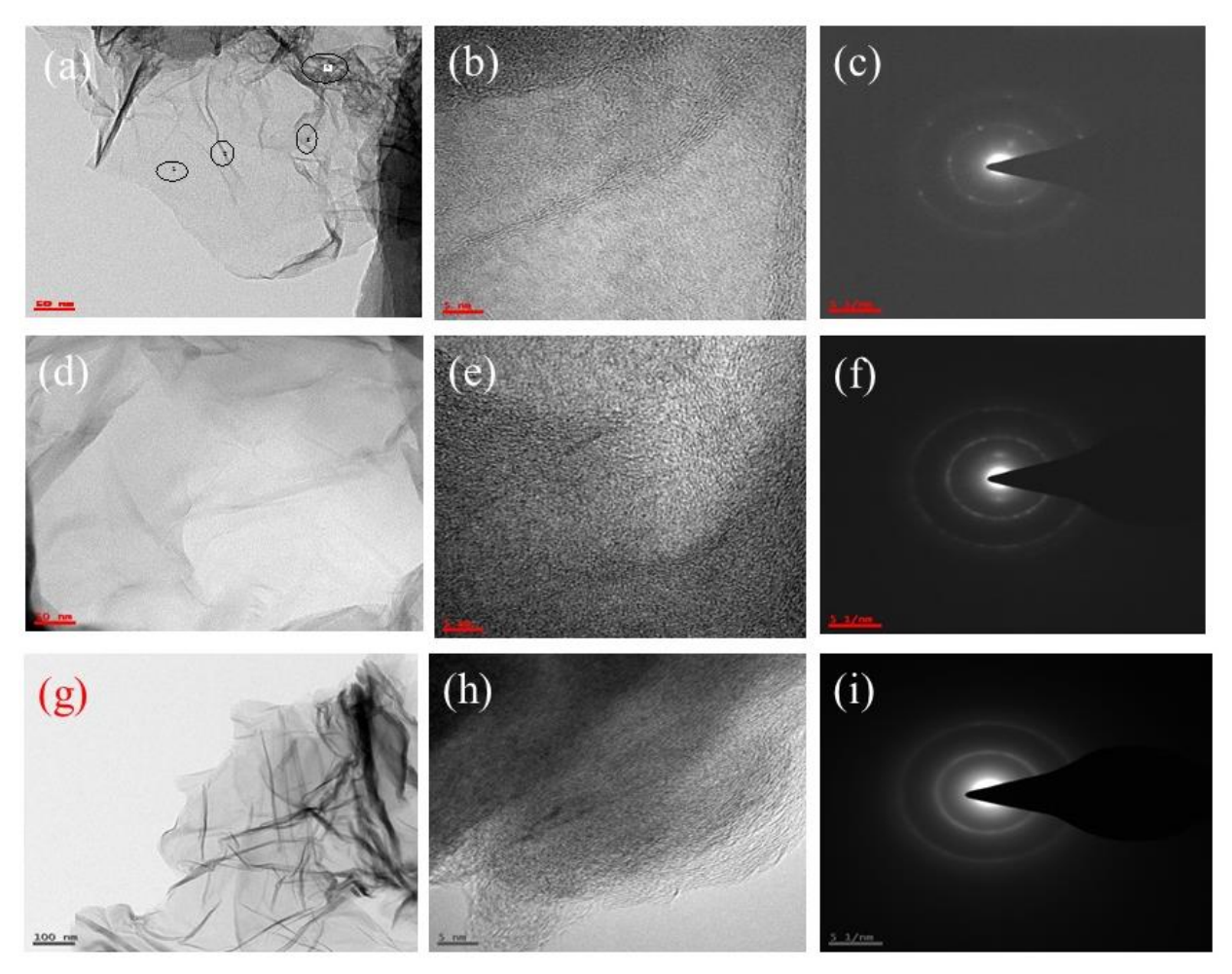


Fig. 3.2.8. TEM images of the thermally reduced graphene oxide of reaction(1),(2) and (3) (a) TEM image, (b) HRTEM image and (c) SAED of reaction (1), (d) TEM image, (e) HRTEM image and (f) SAED of reaction (2) and (g) TEM image, (h) HRTEM image and (i) SAED of reaction (3).

other places the corresponding the SAED the pattern indicates the more spots with high intensity. Fig.3.2.8 (b) shows the HRTEM image of the thermally reduced graphite oxide for the reaction (1). This image clearly shows the different layer formation in this sample, it contains the single layer to FLG.

Fig. 3.2.8 (d) represents the TEM image of thermally reduced graphite oxide for reaction (2). In this image observed that sheet-like morphology with more folding. Fig. 3.2.8 (e) and (f) are HRTEM and SAED for this samples, clearly which indicates that it more disorder of the sample. Fig. 3.2.8 (g) shows the TEM image,(h) is HRTEM image and (i) shows the SAED pattern of thermally reduced graphite oxide for reaction 3. These images clearly indicate that more transference and folding that means it has disorder nature of the sample.

3.2.8 Thermal analysis by TGA and DTA

Thermogravimetric Analysis (TGA), was very useful for to find out the different weight loss since we identify the synthesis reaction temperature conditions. This technique was one of the best, for the identification graphene-based materials. Fig. 3.2.9 (a) shows the TGA curve for the graphite oxide samples of reaction 1,2 and 3. These samples clearly show the different weight loss that means that may be different oxygen groups can form. The reaction 1 of graphite oxide sample shows the 8 % weight loss in the range of $52 - 120^{0}$ C, 6% weight loss at $120-204^{0}$ C and sudden weight loss is 23% occurred at $204 - 263^{0}$ C. From this temperature onwards there no sudden weight loss but the weight loss 26% is gradually decreased. The reaction 2 shows the 4% weight loss at $50 - 120^{0}$ C sharply decreased weight loss at $174 - 369^{0}$ C is 24% and after 500^{0} C temperature, the gradually decreased weight loss is 18 %. The reaction 3 of graphite oxide sample exhibits the 5% weight loss at the range is $50-160^{0}$ C, sudden weight loss 26% occurred at $160 - 269^{0}$ C and gradually decreased weight loss is 24% at $269 - 950^{0}$ C.

These graphite oxide samples such as reaction 1,2 and 3 show the different weight loss. Even though we dried at 100^{0} C, 50 - 120^{0} C range indicates absorbed water molecules or moisture of the samples and also in this range also reaction 1 show the more weight loss than other samples. this is clearly observed in XRD results due to the increase of the interplanar distance. All samples show the sudden weight loss at a range of $160 - 270^{0}$ C which indicates the oxygen-related functional groups and these groups eliminated as in the form of CO_2 , CO and stream . in this range reaction 3 has more weight loss than other samples. The gradually decreased weight loss at $>300^{0}$ C indicates the more stable oxygen-related function groups and break down of the carbon skeleton structure.

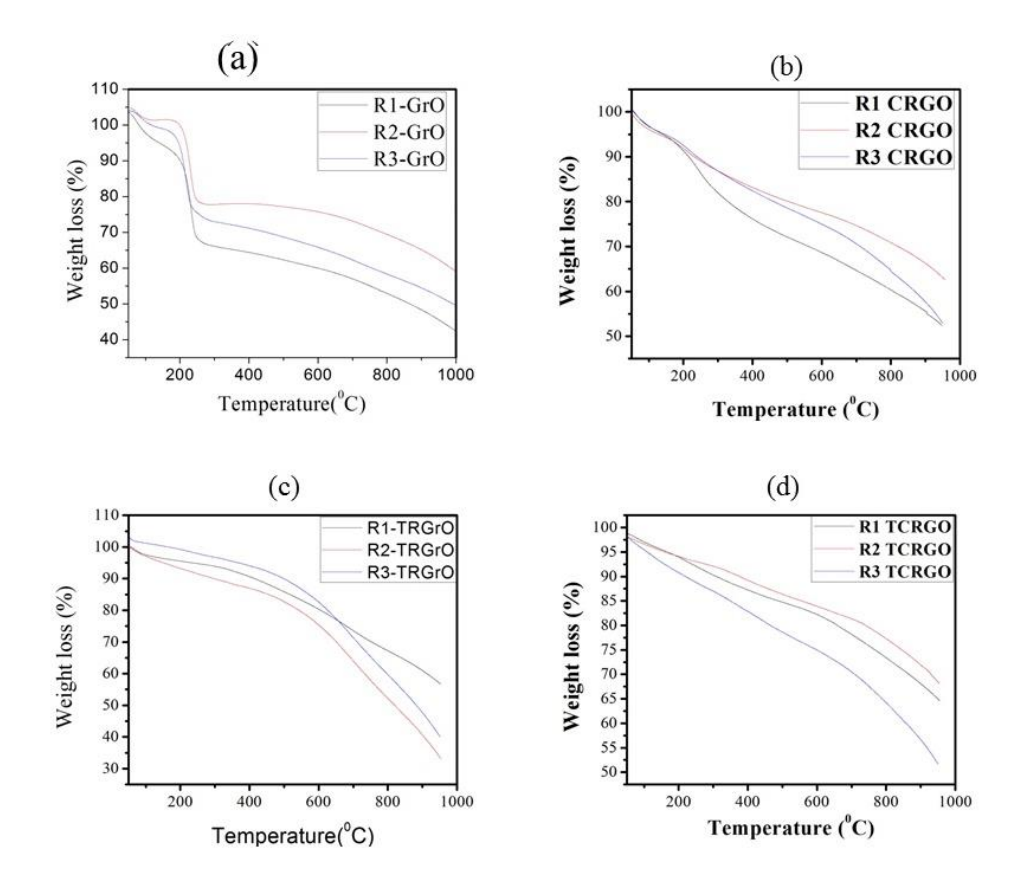


Fig .3.2.9. TGA curves of different graphene-based materials of Reaction 1,2, and 3. (a) graphite oxide of Reaction 1,2, and 3, (b) Reduced graphene oxide of Reaction 1,2, and 3, (c) thermally reduced graphite oxide of Reaction 1,2, and 3 and (d) thermally reduced of chemically reduced samples of Reaction 1,2, and 3.

Fig. 3.2.9 (b) showed TGA curve of the chemically reduced by hydrazine hydrate at 120°C in a DIW solvent and dried at 120°C for reaction 1,2 and 3. These samples do not show any sudden decrease of the oxygen-related functional groups. Fig. 3.2.9 (c) represents the reaction 1, 2 and 3, thermally reduced graphite oxide at 300°C and Fig. 3.2.9 (d) shows the thermally reduced of chemically reduced samples. Reduction of the samples shows the removal of the oxygen-related groups.

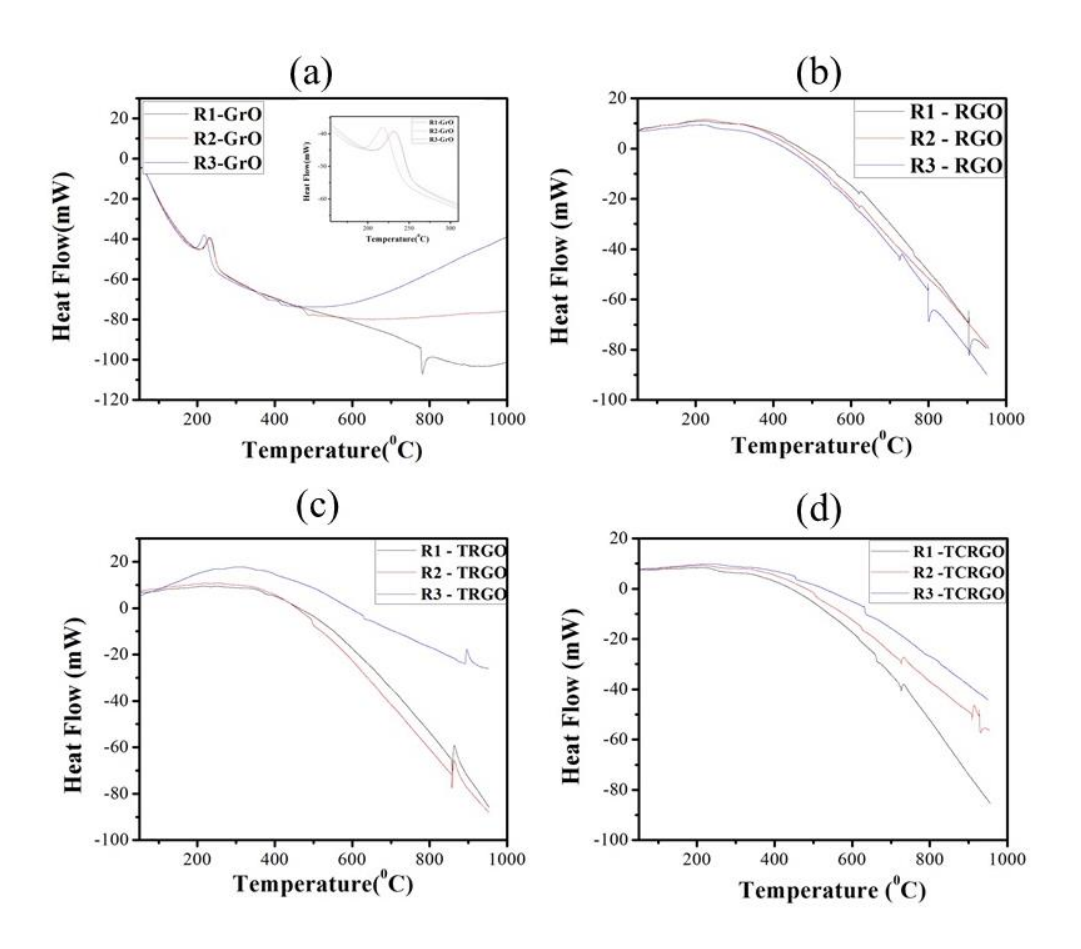


Fig .3.2.10. DTA curves of different graphene-based materials of Reaction 1,2, and 3. (a) graphite oxide of Reaction 1,2, and 3, (b) Reduced graphene oxide of Reaction 1,2, and 3, (c) thermally reduced graphite oxide of Reaction 1,2, and 3 and (d) thermally reduced of chemically reduced samples of Reaction 1,2, and 3.

Fig.3.2.10(a) shows the DTA curve of Graphite Oxide for the reaction 1,2,3. In which the DTA curves shows the different peak Exothermic peak positions. The reaction 1 has the Exothermic peak temperature range onset is 212°C and offset temperature point is 257°C and the peak position is 224°C. Reaction 2 has an Exothermic peak at 230°C and reaction 3 has an exothermic peak at 280°C. These samples also show the very small intents endothermic peaks at 781°C for the reaction 1. Reaction 2 has very small intensity endothermic peaks at 424°C and 486°C and Reaction 3 has 480°C. These Graphite Oxide samples show the different exothermic peaks which clearly indicates that these samples have different oxidation level. These endothermic peaks represent the decomposition of Oxygen-related functional group or combustion of these oxygen functions.

Fig.3.2.10(b) shows the chemically reduced Graphene Oxide DTA curve of reaction 1,2,3, Fig.3.2.10(c) shows the thermally reduced Graphite Oxide of DTA curve for the reaction 1,2,3 and Fig.3.2.10(d) shows the thermally reduced of chemically reduced Graphene Oxide for the reaction 1,2,3. The DTA curves of reduction samples show the very small endothermic peaks than Graphite

Oxide and the more intensity exothermic peaks are absent in the reduction samples so that we can conclude that all oxygen-related function groups are may be removed.

3.2.9 Compositional analysis (EDS)

Fig. 3.2.11 Shows the EDS analysis images of the graphite oxide (left side) samples of R1(a &b), R2(c &d) and R3 (e &f) respectively. Graphite oxide samples have C/O ratios (atomic %) for. R1 (2.1), R2 (1.94) and R3 (1.95) and also identified the sulfur (S) in all three samples with very less quantity of (0.1-0.5%) it this may be due to the impurity or during the synthesis coming from the H₂SO₄. All three samples show the nearly equal C/O ratios which indicate the all samples are fully oxidized. But these graphite oxide samples shows the different interplanar distance from the XRD analysis, different band position in Raman analysis and different weight loss and exotherm peak position observed in TGA and DTA analysis. So we concluded that these samples have equal C/O ratios even though the formation of the oxygen-related functional groups are different on the graphene oxide samples. Fig. 3.2.11 Shows the EDS analysis images of the chemically reduced graphene oxide ((right side) samples of R1(a &b), R2(c &d) and R3 (e &f) respectively, these

Energy Dispersive Spectroscopy (EDS) is very useful for the identification of elemental composition in the materials.

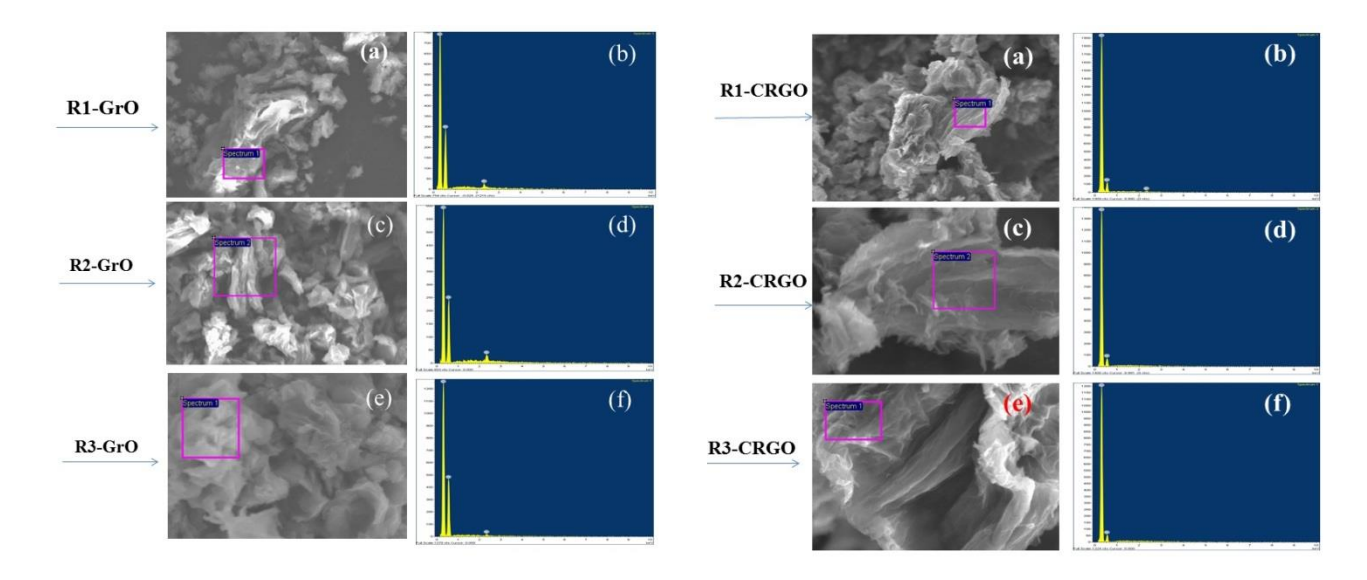


Fig. 3.2.11 EDS spectrum of the graphite oxide samples (left side) and chemically reduced samples (right side) of reaction 1,2 and 3 respectively.

samples have C/O ratios 6.8,8.5 and 12.1 of chemically reduced at 120°C by hydrazine hydrate in DIW as a solute. Comparative graphite oxide samples the C/O ratios are increases which indicate

the oxygen-related functional groups are removed. And also reaction 3 CRGO sample has more C/O ratio than other samples. So that, in the case of chemically reduced samples R3 sample is more effective to remove the oxygen-related function groups than other two samples. This result was supported by the TEM, TGA and DTA, and Raman.

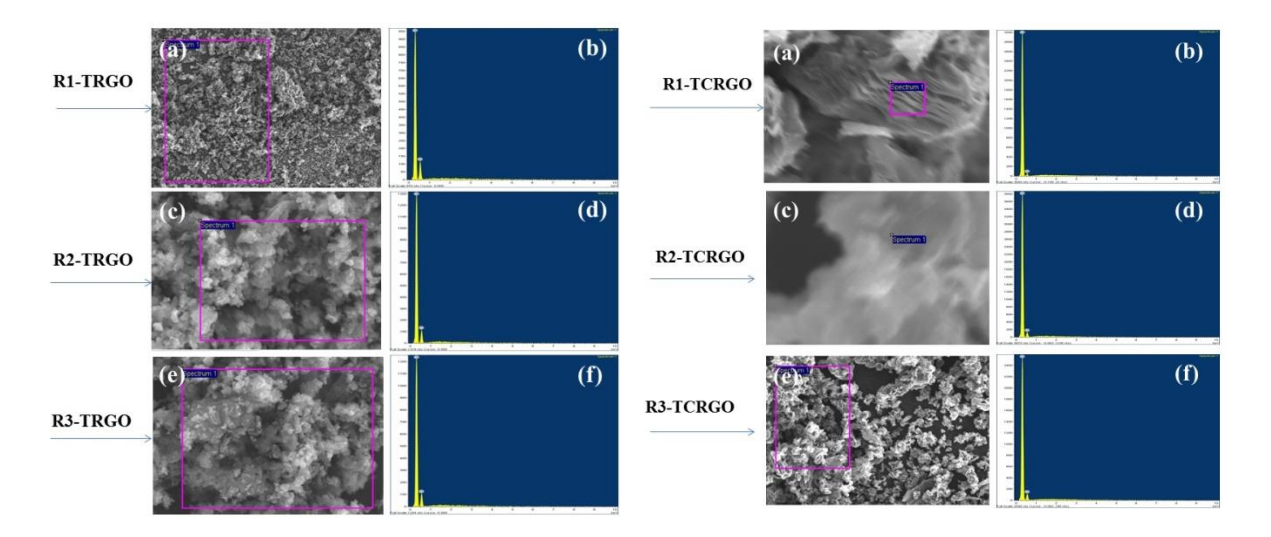


Fig. 3.2.12 EDS spectrum of the thermally reduced graphene oxide samples (left side) and thermally reduced of chemically reduced samples (right side) of reaction 1,2 and 3 respectively.

Fig. 3.2.12 Shows the EDS analysis images of the thermally reduced graphene oxide ((left side) samples of R1(a &b), R2(c &d) and R3 (e &f) respectively. These samples have C/O ratios 4.2,4.3 and 4.6 of thermally reduced at 300°C in the furnace (in air). Comparative graphite oxide samples the C/O ratios are increases which indicate the oxygen-related functional groups are removed. And also C/O ratios are decreased than chemically reduced samples. Fig. 3.2.12 Shows the EDS analysis images of the thermally reduced of chemically reduced graphene oxide ((right side) samples of R1(a &b), R2(c &d) and R3 (e &f) respectively. These samples have C/O ratios 12.9,9.2 and 7.6 of thermally reduced at 300°C in the furnace (in air). In this case, C/O ratios are increased comparatively chemically reduced samples and thermally reduced samples. But R3 reaction shows the less C/O ratio than the chemically reduced sample. All the C/O ratios are shown in table.3.2.10.

Table 3.2.10 C/O ratios of all thee samples of graphite oxides, chemically, thermally and multiples reduced of graphene oxide.

| Sample name | C/O ratio |
|--------------------|-----------|
| R1- graphite oxide | 2.1 |
| R2- graphite oxide | 1.94 |
| R3- graphite oxide | 1.95 |
| R1- CRGO | 6.8 |
| R2- CRGO | 8.5 |
| R3- CRGO | 12.1 |
| R1- TRGO | 4.2 |
| R2- TRGO | 4.3 |
| R3- TRGO | 4.6 |
| R1- TCRGO | 12.9 |
| R2- TCRGO | 9.2 |
| R3- TCRGO | 7.6 |

3.2.10 Bonding characteristics by FTIR

FTIR technique was used for the identification of the chemical bonding of materials. Fig 3.2.13 (a) shows the FTIR spectrum of Graphite Oxide for the reaction 1,2,3 which indicates the different intensity and peak position of functional groups. Bands at 3393cm⁻¹, 3357cm⁻¹ and 3380cm⁻¹ are represents the O-H stretching mode in the hydroxyl groups of R1, R2, and R3 graphite oxide samples respectively. 1725 cm⁻¹, 1723 cm⁻¹, and 1710 cm⁻¹ bonds are present in the reaction R1, R2, and R3 respectively. These bonds represent the ketone (C=O) will present in the carbonyl or carboxyl groups in the R1, R2 and R3 graphite oxide samples respectively. 1624 cm⁻¹, 1615 cm⁻¹, and 1608 cm⁻¹ bonds represent the stretching mode of monoxide C=C bonds or H-O-H (water molecules) bending mode of R1, R2, and R3 –GrO samples respectively. All the graphite oxide samples, We are dried at 100°C in the vacuum oven for 12h. So that mostly we expected absorbed water molecules are removed and may be presented in between the graphite oxide layers because we observed the less weight loss <100°C temperature. i.e these bond are may be formed by the C=C bonds. 1383cm⁻¹ bond represents the O-H deformation in the carboxyl group. It is present in the R1-GrO sample only and absents in the other two samples such as R2 and R3 samples.

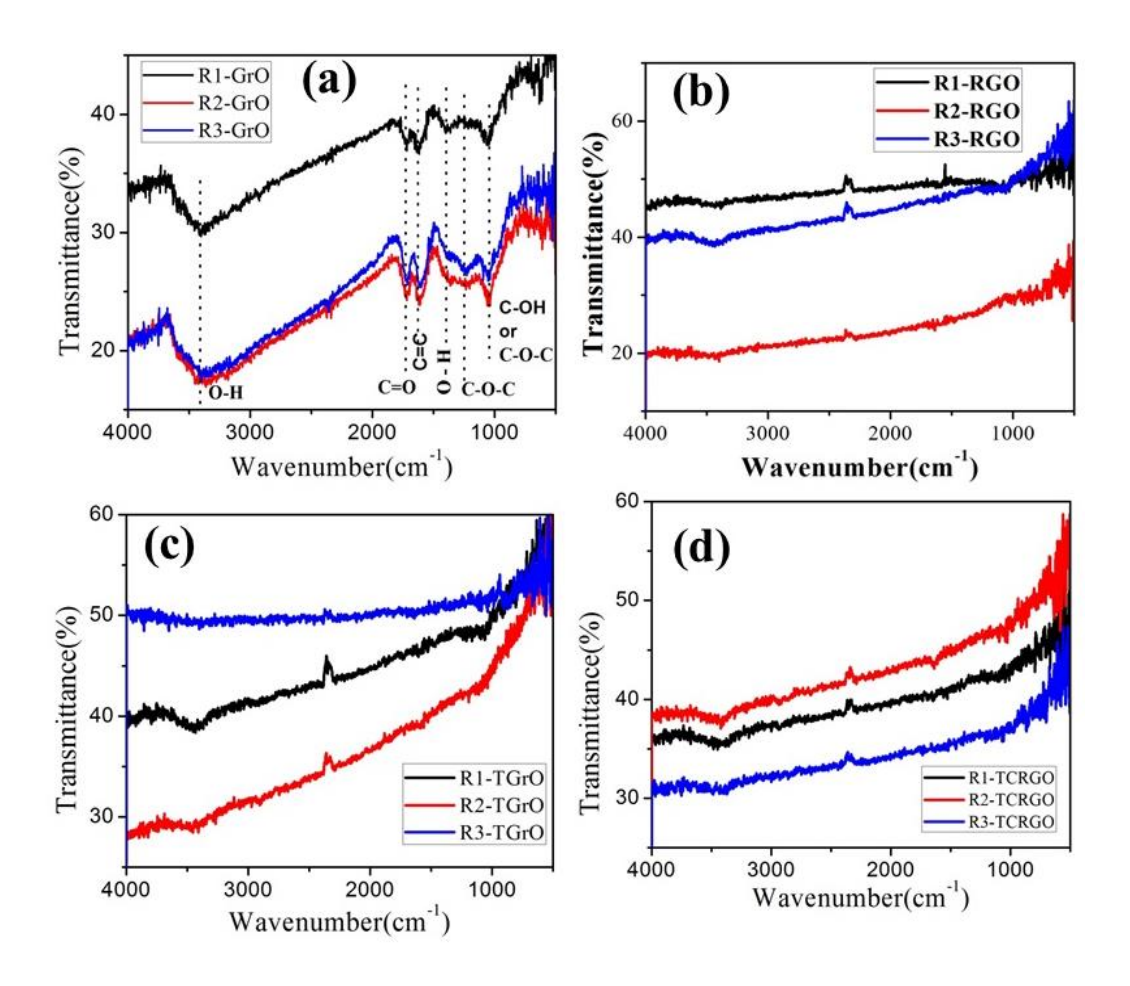


Fig .3.2.13. FTIR spectrum of different graphene-based materials of Reaction 1,2, and 3. (a) graphite oxide of Reaction 1,2, and 3, (b) Reduced graphene oxide of Reaction 1,2, and 3, (c) thermally reduced graphite oxide of Reaction 1,2, and 3 and (d) thermally reduced of chemically reduced samples of Reaction 1,2, and 3.

1240cm⁻¹ and 1231cm⁻¹ bonds represent the C-OH stretching mode of phenolic groups present in the hydroxyl groups. These bonds are presented in R2 and R3 – GrO samples respectively. This range band is not present in the R1 sample. R1 and R2 – GrO samples have bonded at 1053cm⁻¹. This indicates the C-O in C-OH or C-O-C bonds and R2 has a 1043cm⁻¹ bond which represents the edge phenol groups in hydroxyl.

In the case of chemically reduced samples shown in Fig 3.2.13 (b), all samples show the removal of oxygen-related functional groups, and also these samples show the still some hydroxyl groups related functional groups are presented. R1 –RGO has 1076cm⁻¹ peak which represents the basal plane phenol groups in hydroxyl groups and also presented at 3439cm⁻¹ band represents the hydroxyl groups, this bond position is redshifted competitive graphite oxide sample and it has low intensity. R2 –RGO samples show the redshift of hydroxyl groups presented with low intensity at 4351cm⁻¹. R3- RGO shows the similar to the R1-RGO samples. Fig.3.2.13 (c) and (d)

corresponding thermally reduced and thermally and chemically reduced samples. These samples show the removal of the Oxygen functional groups.

3.2.11 UV – analysis for electronic transition

UV-Vis spectroscopy is analytical technique, used for the electronic transition (conjugated system) of the compound. Fig 3.2.14 shows the UV spectrum, (a) - (d) for the graphene oxide, chemically, thermally and multi reduction of reaction 1,2 and 3 respectively. All samples show the aromatic phenol group in hydroxy is represents the 215 - 250 wavelength range small hump peaks are appearance this exhibits the $\pi \to \pi^*$ of C=C. These groups also identified in the FTIR analysis. The Fig 3.2.14 (a) shows the graphene oxide samples of reaction 1,2and 3, the graphene oxide samples exhibit the more aromatic peaks of phenolic groups with high intensity than reduction samples. The graphite oxide samples show the same, have high-intensity competitive to the phenolic groups intensity peak positions at $264 \text{nm}(\pi \to \pi^* \text{ of C=C})$, higher wavelength of these samples indicates the more conjugated system is formed that means lower energy gapes may be expected this may be affected by the drying temperature at 100°C for 12h in the vacuum furnace. these samples show the different intensity of each other. R3-GO sample has a higher intensity than other two samples. Fig 3.2.14 (b) shows the chemically reduced graphene oxide samples by hydrazine hydrate at 120°C in DIW solute reaction 1,2and 3. These samples exhibit the different absorption peaks position and intensity. R1-RGO sample has less intensity and absorption peak at 279nm is very broad. R3-RGO sample has a sharp intensity peak at 265nm and small shoulder at 268nm .R3-RGO sample exhibits the absorption peak at the 266.6nm and small shoulder at 273nm. Fig 3.2.14 (c) shows the thermally reduced graphene oxide samples at 300°C in the furnace in the atmosphere is air. These samples have absorption peaks at 266.4nm, 266.6nm and 267.8 nm of R1, R2, and R3-TRGO samples respectively. R2-TRGO sample has a higher intensity than R1 and R3-TRGO samples but

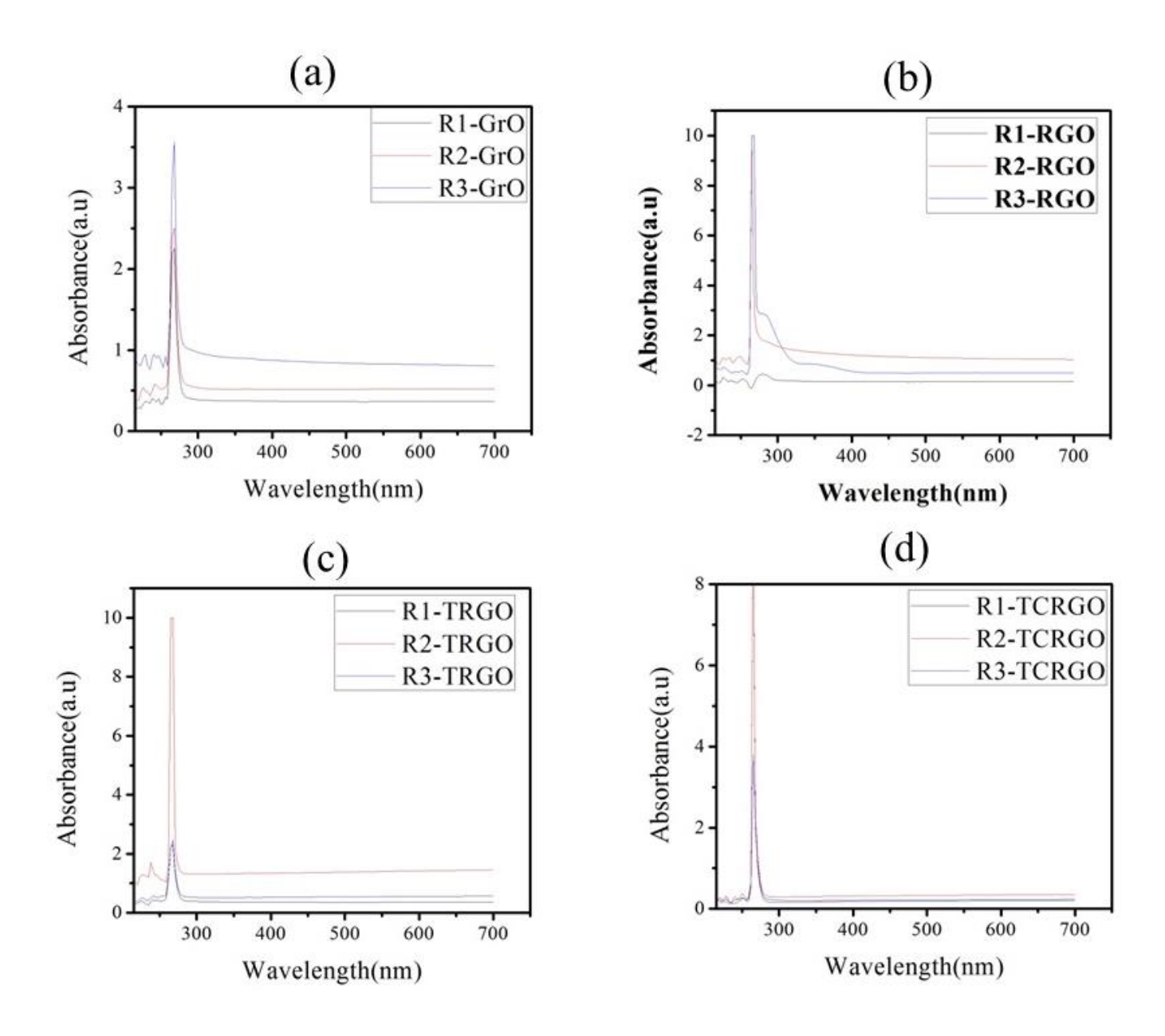


Fig .3.2.14. UV spectrum of different graphene-based materials of Reaction 1,2, and 3. (a) graphite oxide of Reaction 1,2, and 3, (b) Reduced graphene oxide of Reaction 1,2, and 3, (c) thermally reduced graphite oxide of Reaction 1,2, and 3 and (d) thermally reduced of chemically reduced samples of Reaction 1,2, and 3.

these samples have the same intensity. R2 – TRGO has a small shoulder at 270nm but this peak is absent in the case of R1 and R3- TRGO samples. Fig 3.2.14 (c) shows the thermally reduced of chemically reduced graphene oxide samples at 300°C in the furnace in the atmosphere is air. These samples show the same peak position at 265.3nm. R1 and R2 have the same intensity and small shoulder at 268nm and also higher intensity than R3-TCRGO sample and this sample do not have small shoulder peak.

3. 3 Effect of reaction temperature (at higher temperature) on the synthesis of the GO by MHM:

3.3.1 Synthesis of GO by MM

Taking the $<45\mu m$ size graphite powder is 2gm, H_2SO_4 is 96ml, and Na_2NO_3 is 2gm in a beaker within ice bath on a hot plate, and this mixture was stirring for 30minits. After that, we added KMnO₄ was 12gm slowly (within 90minits) during the stirring. The removed the ice both and increasing the temperature up to 35^0C and stirring for 2h. DIW 80ml was added to the mixture as drops within 30min during the stirring and then to stop the reaction for that we added 200ml of DIW and followed by the 10ml of H_2O_2 . This mixture was stirring for 10minits. At this time we observed that the solution was appearing in light yellow color. This solution was repeatedly washed with DIW and HCl up to obtained neutral PH and filtered. The obtained material was dried at 50^0C for 12h in a vacuum furnace. This process was same for the $70^0C,100^0C$, and 140^0C .

3.3.2 Structural Analysis by XRD

From the Fig.3.3.1 shows the oxidation temperature more effective parameter because observed that, variation in their structure showed in table 3.3.1. These samples show the different interplanar distance and crystallite size may be variation in the Oxygen-related functional groups or water molecules intercalated between the layers and variation in the number of functional groups, this effect explained later by the Raman and FTIR analysis. The graphite oxide synthesis at different temperatures such as 35°C and 70°C mostly shows the nearly equal values with different crystallite sizes showed in table 1. The interplanar distance 0.775nm,0.782nm corresponding 2θ values are 11.4 and 11.3 respectively for the 35°C and 70°C graphite oxides, indicates that these samples are well oxidized. Because the graphite has interplanar distance is 0.334nm, and crystallite size is 23.08nm showed in the previous chapter. And also the graphite has more intensity with a sharp peak; these samples have very less intensity and broadening in peaks which mean that graphite has more stacking layers and also large sheets. The broadening happens in the case of oxidized samples due to the sheet size reduced during the synthesis. The decreased in the intensity also gives the number of layers also decreased. 100°C and 140°C graphite oxide samples show the completely different from the 35°C and 70°C graphite samples. These samples the XRD peaks are very broad

and appearing at 2θ values are 24.05^{0} , and 24.62^{0} the corresponding d values are 0.369nm and 0.3612nm of 100^{0} C and 140^{0} C graphite oxide

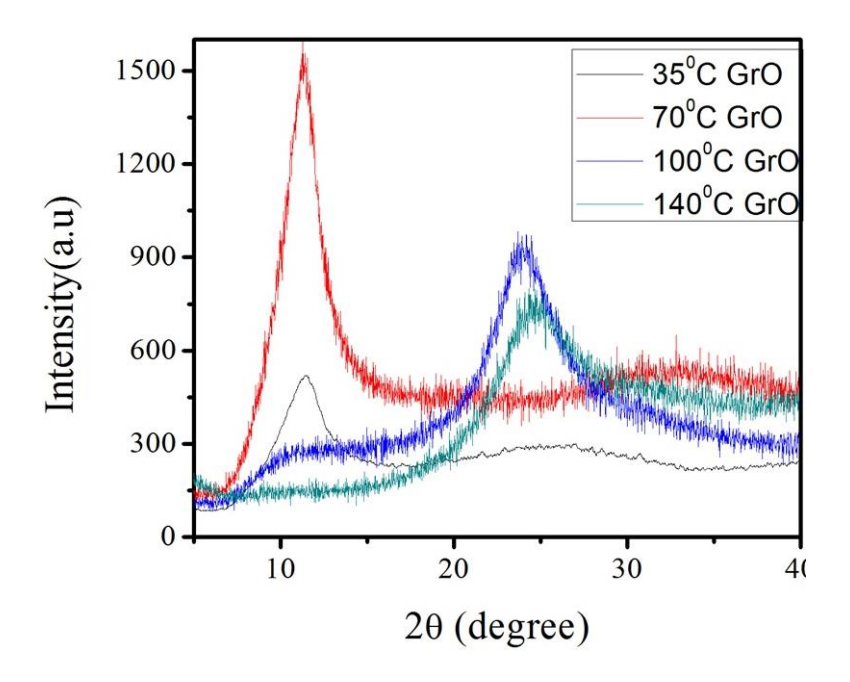


Fig.3.3.1 Shows the image of XRD for different oxidation temperature for the graphite oxide.

respectively. This spectrum looks like reduced graphene oxide. That means, in this case, maybe initially oxidation happing and then removed some oxygen functional groups. The initial oxidation means raising the temperature condition people represent as step 1 oxidation []. These samples still we called as graphite oxide samples because we did EDS for the all samples, we observed that C/O ratios are 1.3,1.3,2.3 and 2.2 for 35°C,70°C,100°C and 140°C respectively. These results correlated with the FTIR and Raman later sections.

Table.3.3.1 The interplanar distance and crystallite size of graphite oxides (XRD) by varying the oxidation temperature

| Sample name | 2θ (Degree) | Interplanar distance (d) nm | Crystallite size (D) nm |
|-------------|-------------|-----------------------------------|----------------------------|
| 35°C-GrO | 11.4 | 0.775 | 2.798 |
| 70°C-GrO | 11.3 | 0.782 | 3.464 |
| 100°C-GrO | 24.05 | 0.369 | 1.973 |
| 140°C-GrO | 24.65 | 0.361 | 1.924 |

3.3.3 Molecular structure and disorder by Raman analysis

Fig.3.3.2 shows the Raman spectrum of different oxidation temperature of the graphite oxides. All samples were taken in the form of powders. These samples show the different intensity and different band position showed in table 3.3.2. All four samples exhibit the D, G and 2D regions with broadening. In the case of the reaction temperature at 35°C sample graphite oxides, it has D band at 1349cm⁻¹, G band at 1595cm⁻¹ and 2D peak is a broad hump. The broadening and the G band redshift indicates this sample was completely oxidized. The red of G band due to the more functional groups such as hydroxyl, epoxy and water molecules. The second sample reaction temperature at 70°C shows the D peak at 1349cm⁻¹, G at 1588cm⁻¹ and 2D band show the broad and small peak hump was appearing. Comparative to the 35°C – GrO sample this sample shows the may be less formation of hydroxyl or epoxy or water molecules. These results later confirmed by FTIR and TGA analysis. The remaining two samples reaction did at 100°C and 140°C graphite oxide samples completely different from the above samples such as 35°C and 70°C graphite oxide samples.

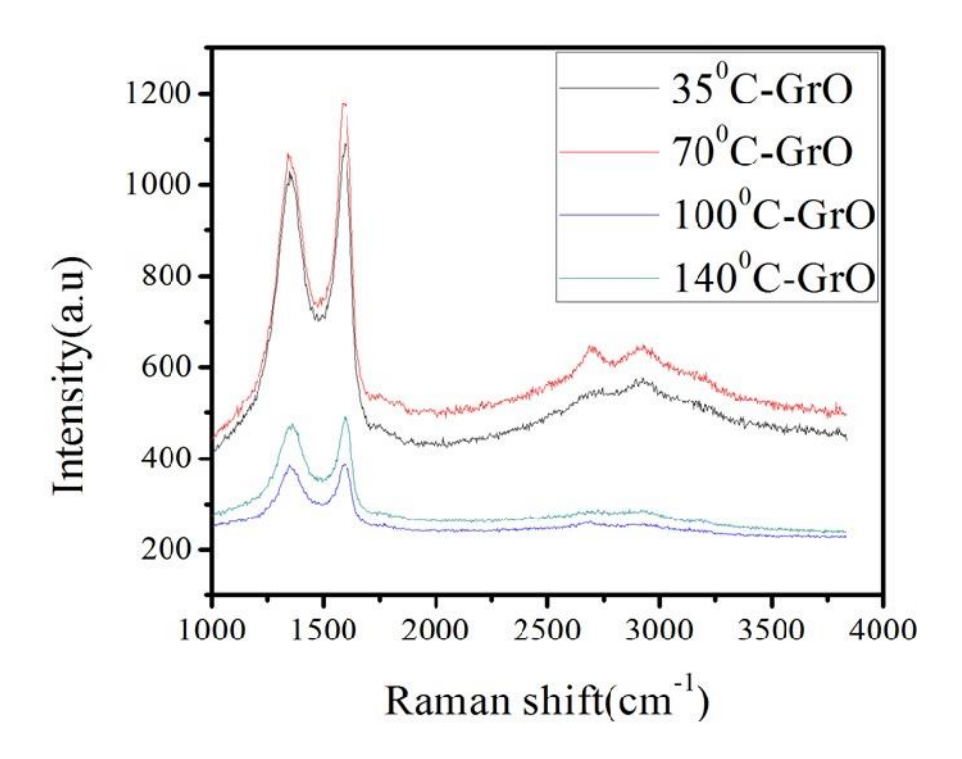


Fig. 3.3.2 Raman spectrum of the different oxidation temperature synthesized graphite oxide

Table 3.3.2 Raman band positions and their intensity ratios of graphite oxides by varying the oxidation temperature

| Sample name | D band | G band | 2D band | I_D/I_G |
|-------------|------------------|------------------|------------------|-----------|
| | cm ⁻¹ | cm ⁻¹ | cm ⁻¹ | |
| 35°C-GrO | 1349 | 1595 | broad | 0.93 |
| 70°C-GrO | 1349 | 1588 | broad | 0.91 |
| 100°C-GrO | 1354 | 1593 | broad | 0.99 |
| 140°C-GrO | 1356 | 1596 | broad | 0.97 |

3.3.4 Thermal and oxidation Analysis by TGA and DTA

Thermogravimetry analysis is used to measure the weight loss of materials. Figure 3.3.3(a) shows the TGA plot of combined samples such as 35, 70, 100 and 140°C for graphite oxide synthesis temperature. TGA curves show the different wights loss, the 100and 140 °C samples shows the same curve nature, these samples don't have any water-related groups and also have less oxygen-related functional groups, these samples exhibit the gradually decreased weight loss of the may be the removal of the carbon or more stable oxygen-related groups. But 35 and 70°C samples shows the different weight loss to each other. In the case of 35°C sample show the 50-185°C range weight loss is 27%, which may be due to the intercalated water molecules and stream. But at the 185-188°C

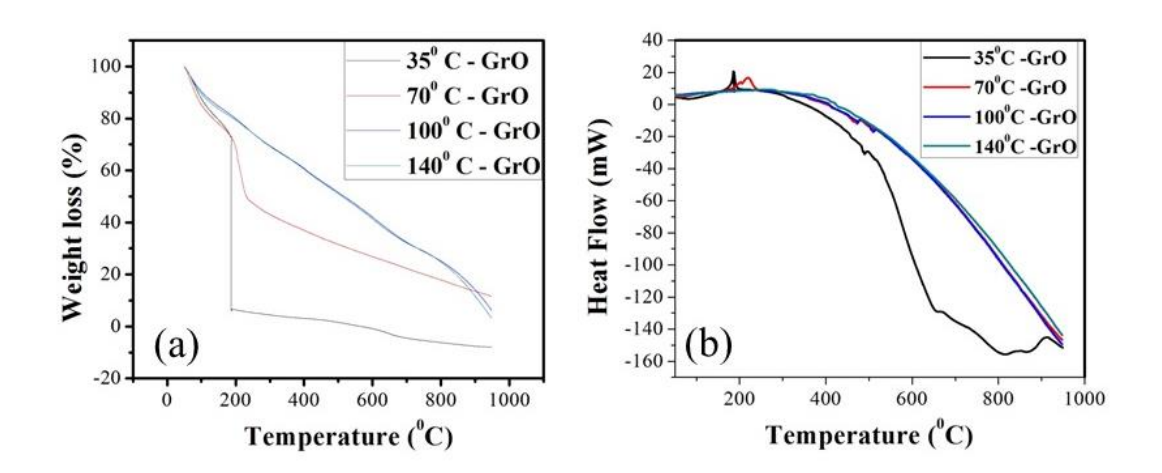


Fig.3.3.3 (a) TGA curves and (b) DTA curves of different reaction temperature of graphite oxide range, the weight loss is very drastically change was occurred, in this range, the weight loss is 67%. This indicated that more oxygen-related functional groups are formed. The 70°C graphite oxide

sample has weight loss is 26% in the range of 50-181°C and 24% weight loss occurred at the 181-230°C range.comparion to all samples 35°C graphite oxide sample has more oxygen-related functional groups. Fig. 3.3.3 (b) shows the DTA curves 35, 70, 100 and 140°C for graphite oxide synthesis temperature. The reaction temperature of 35° C graphite oxide sample has very sharp endothermic peak at 188°C and reaction temperature of 70° C graphite oxide sample has two peaks one is endothermic (very small peak) peak at 206 ° C and another peak at 220 ° C is exothermic (very broad intensity peak) and 100 and 140°C for graphite oxide synthesis temperature samples shows the thermally stable.

3.3.5 Bonding characteristics (FTIR)

FTIR spectroscopy is very useful for identification of carbon-oxygen related band of graphene oxide materials. Figure 4 shows the temperature-dependent of graphite oxide materials. These powder samples are prepared by the KBr pellets. From this figure clearly shows the 35°C and 70°C graphite oxide samples and also 100°C and 140°C graphite oxide samples, have same functional groups with different intensity and broadening of the peaks. Comparative all samples 35°C graphite oxide sample has more intensity and broadening band at 3421cm⁻¹, which indicated the vibrational stretching mode of hydroxyl and water molecules, the water molecule is appearing in graphite oxide as intercalated between layers or may be absorbed on the surface of the graphene sheets. More intensity of this peak may be attributed to water molecules due to the low-temperature reaction than other samples. All samples show the peaks at 2851, 2920cm⁻¹ which related to the C-H stretching vibrations of CH₂ groups. When comparative to all samples lowest temperature reaction of graphite oxide (35°C graphite oxide sample) has more intensity of these bands indicates the at this temperature more CH₂ or CH₃ groups are formed. 35°C and 70°C graphite oxide samples have 3869 and 3737cm⁻¹ bands are appearing but not in the high-temperature synthesis at 100°C and 140°C graphite oxide samples and also these bands intensity are more in 70°C graphite oxide sample than 35°C graphite oxide sample.

35°C and 70°C graphite oxide samples have more intensity and broadening peak of CO₂ at 2340cm⁻¹ than other two samples. Both 35°C and 70°C graphite oxide samples show the C=O related groups at 1717cm⁻¹ (C=O) and have the same intensity and broadening. But in the case of 100°C and 140°C graphite oxide samples, this band was shifted to lower wave number at 1707cm⁻¹ and also these samples also have the same intensity and broadening. This band indicates the formation of the carboxylic groups. 35°C and 70°C graphite oxide samples have the same band

position at 1623cm⁻¹ and intensity but 70°C graphite oxide sample has more broadening than 35°C graphite oxide sample. This band indicates the bending of water molecules and stretching vibrations of C=C (unoxidized graphitic domains). This band is not observing in 100°C and 140°C graphite oxide samples, these sample shows the band positions at 1577 and 1575cm⁻¹. this range indicates the there are no any oxygen-related groups and water molecules and these bands indicates the C=C network.

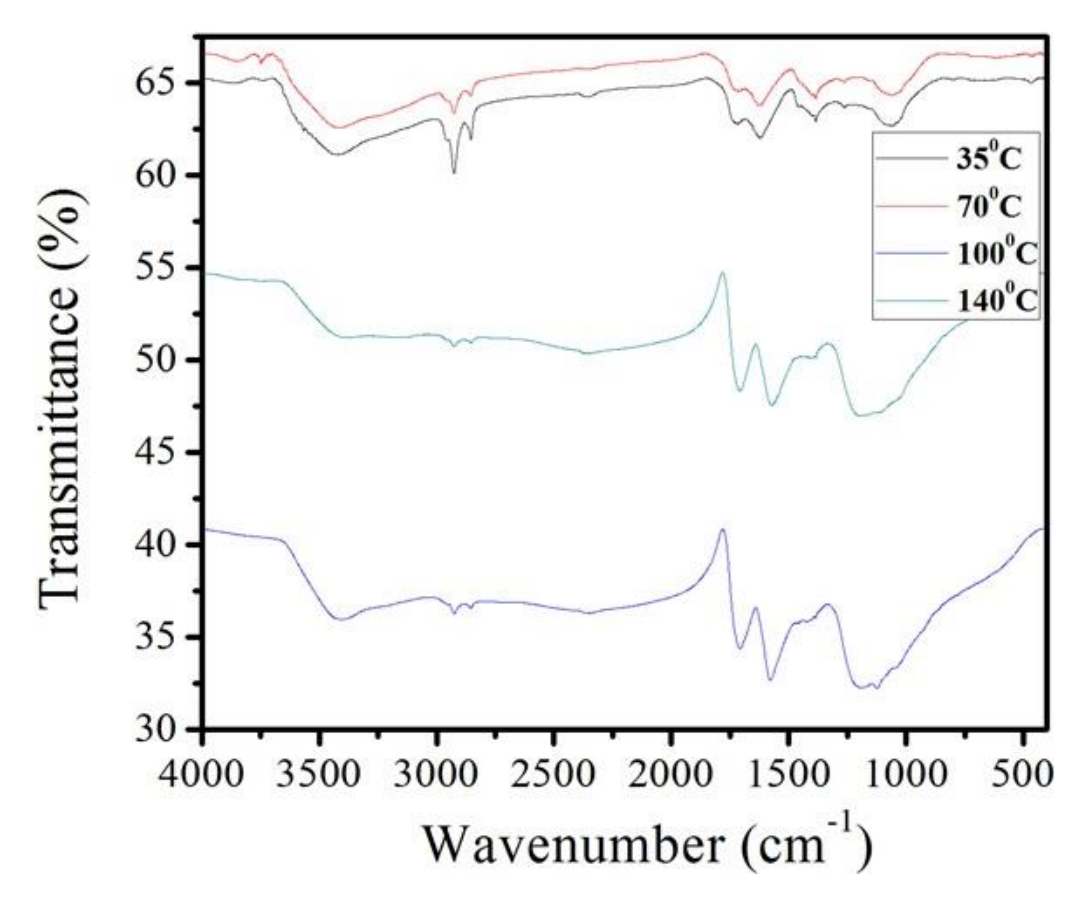


Fig 3.3.4. The FTIR spectrum for the different oxidation temperature of the graphite oxide

As shown in Fig. 3.3.4, 35°C and 70°C synthesized graphite oxide samples consist of 1456, 1399 and 1384cm⁻¹ bands, moreover 35°C graphite oxide sample has more intensity peaks than 70°C graphite oxide sample. these bands are observed in 100°C and 140°C graphite oxide samples when the spectrum was zoomed and also shows the very less intensity. The band position at 1262cm⁻¹ is observer in 35°C and 70°C graphite oxide samples. This band was disappeared in other two samples. 35°C and 70°C graphite oxide show the band at 1055cm⁻¹ with different broadening and same intensity, this band did not observe in 100°C and 140°C graphite oxide samples, but these samples

show the new band positions are 1194,1124 and 1042 cm⁻¹ with small intensity in the case of 140^{0} C graphite oxide sample 1042 cm⁻¹ was disappeared. 35^{0} C and 70^{0} C graphite oxide samples show the small intensity band positions, but not appearing in the other two samples.

3.3.6 Morphology analysis by FESEM

Figure 5 (a) and (b) shows the FESEM image of 35°C and 70°C graphite oxide samples, which shows the flat sheet-like morphology and (c) and (d) shows the very disorder nature and more ripel.

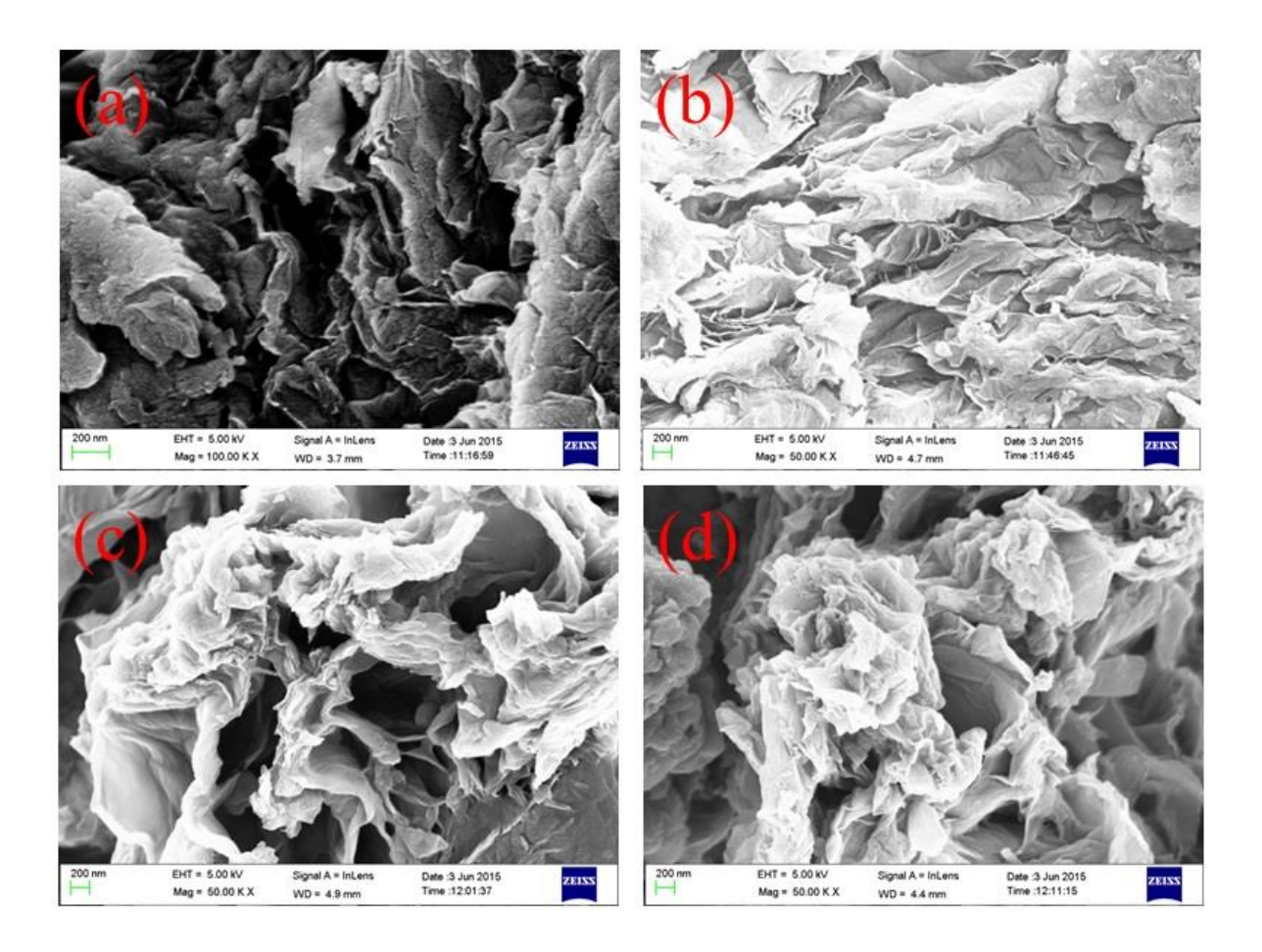


Fig3.3.5. The FESEM images for the different oxidation temperature of the graphite oxide

3.3.7 Morphology and structural Analysis by TEM

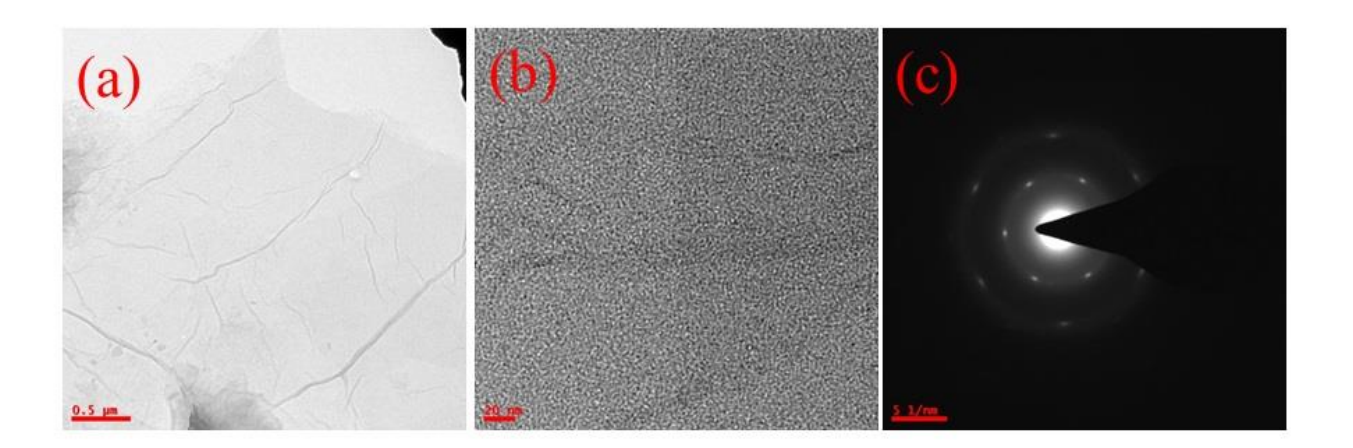


Fig 3.3.6. Shows the TEM (a), HRTEM (b) and SAED (c) images for the 35°C graphite oxide sample.

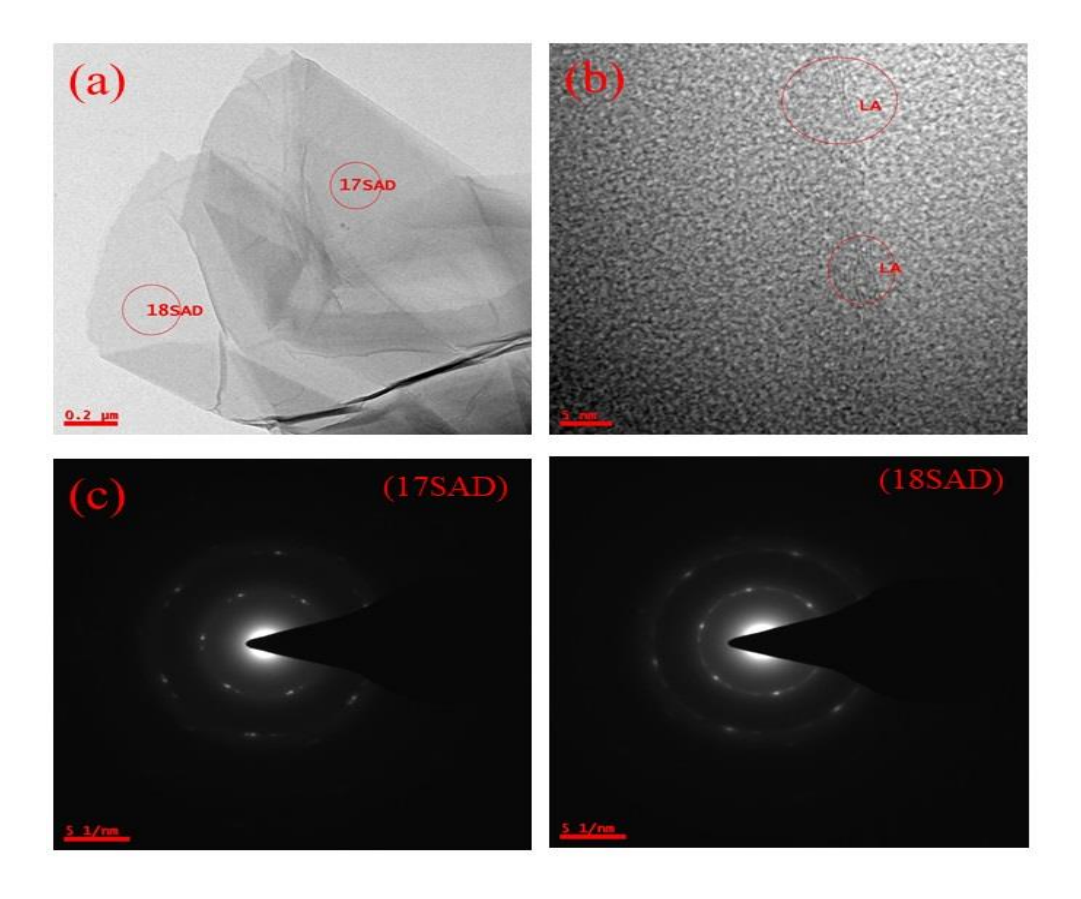


Fig 3.3. 7 TEM (a), HRTEM (b) and SAED (c) and (d) images for the 70°C graphite oxide sample.

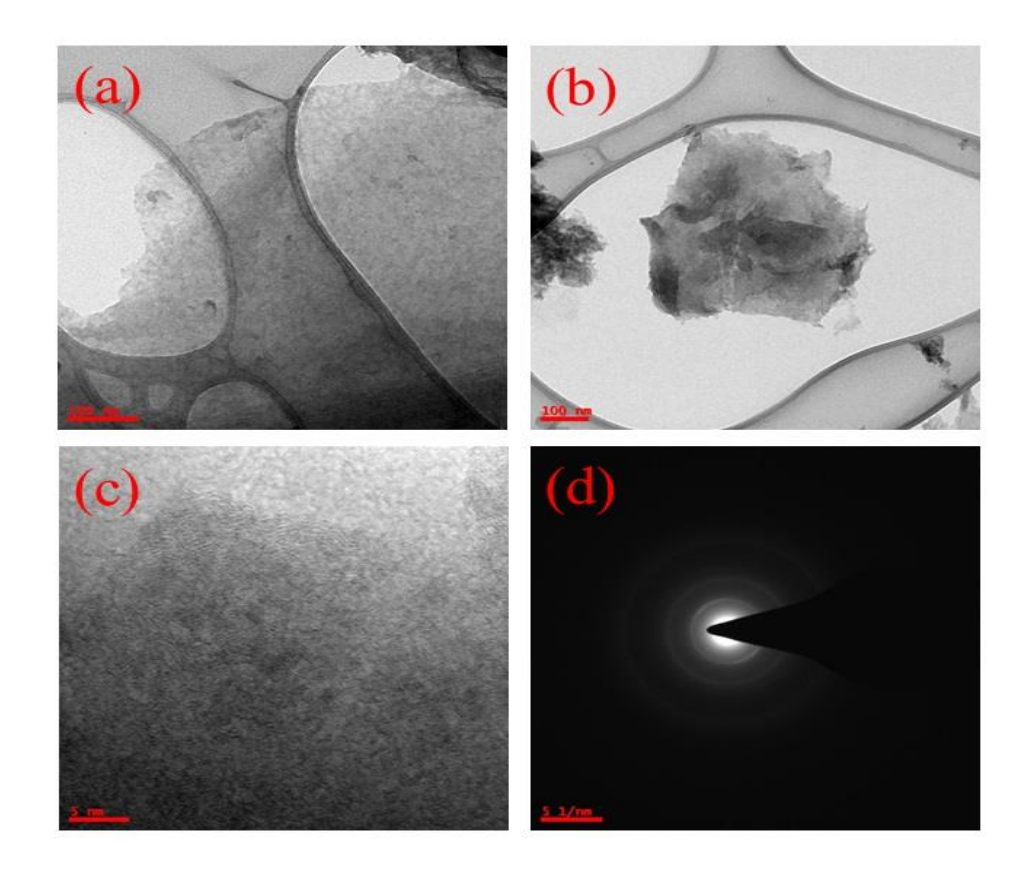


Fig 3.3.8. Shows the TEM (a) and (b) HRTEM (c) and SAED (d) images for the 100° C graphite oxide sample.

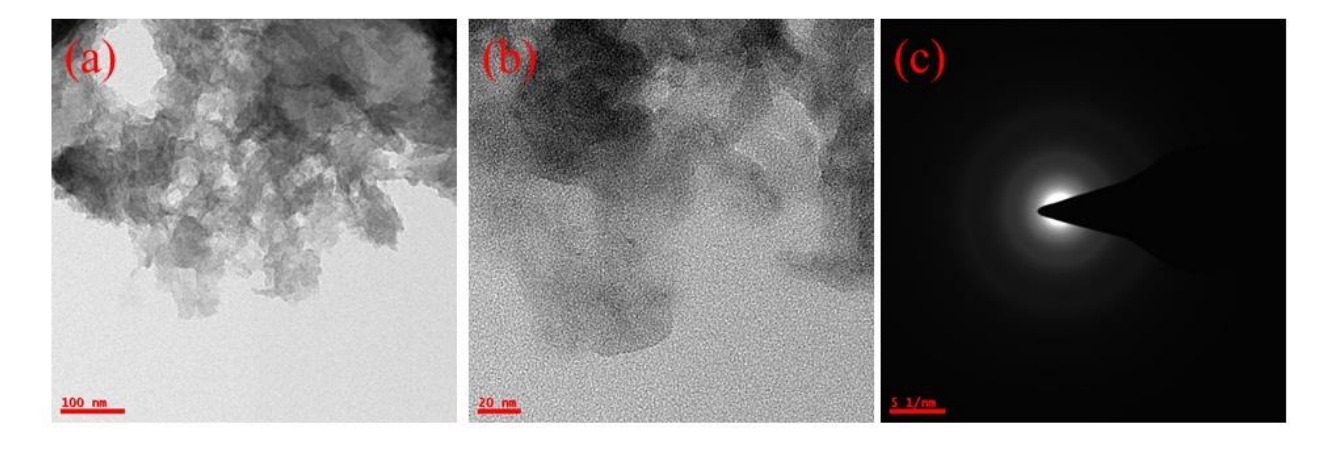


Fig 3.3.9. Shows the TEM (a), HRTEM (b) and SAED (c) images for the 140°C graphite oxide sample.

3.4 Effect of solvents on the exfoliation of reduced graphene oxide reduction (RGO)

In this section, the impact of solvents on the structural, morphology, bonding and thermal analysis of RGO by using XRD, TEM, FT IR, UV and TGA are discussed for the GO sample synthesized by reaction 3 as discussed in the previous section.

3.4.1 RGO Preparation

We took graphite oxide 250mg and 250ml DIW in a 500ml beaker and sonicated for 30mints obtained a clearer solution. Then Hydrazine hydrate 10ml was added to the graphene oxide solution then heated 120°C and stirred for 6h. This experimental was going on a hot plate by using the vegetable oil both. This is same for DMF solvent instead of DIW. After completion of the reaction, we observed that in the DIW, the solution appearing in black colored but the material looked like weight loss and formed on the surface of a solution but in the DMF, the solution completed in black colored and appearing good dispersibility. These samples were washed with DIW and obtained PH=7 and filtered with a vacuum pump and dried at 120°C in the Oven for 12h.

3.4.2 Structural analysis by XRD

XRD is a useful tool for the analyzing the crystal structure of graphite derived materials. In the XRD pattern of graphite has a sharp peak at $2\theta = 26.6^{\circ}$ corresponding to an interlayer distance (d) of 3.34Å. After oxidation of graphite has a sharp peak at $2\theta = 13.5^{\circ}$ and corresponding d=6.6 Å. The disappearance of the $2\theta = 26.6^{\circ}$ peak of graphite indicates the good oxidation occurs i.e. in this

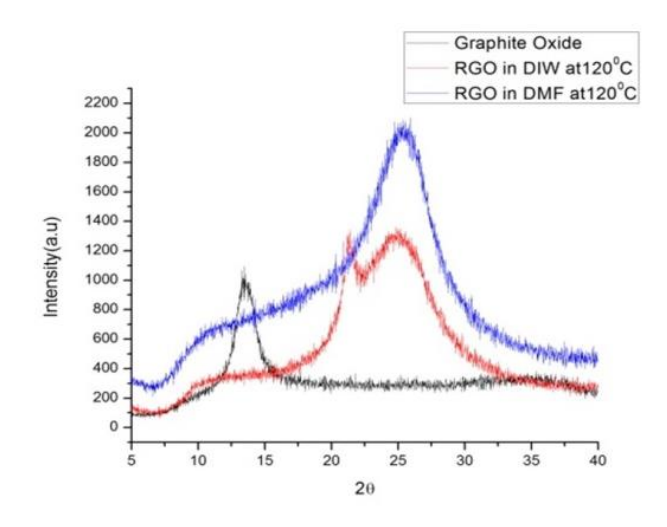


Fig.3.4.1. XRD pattern of graphite oxide and RGO of DIW and DMF

process can be attributed to the induction of Oxygen-contains functional groups into the carbon lattice during the oxidation. The interlayer distance 6.6 Å of graphite oxide obtained due to the removal of water molecules because dried at 100^{0} C compared with literature obtained graphite oxide d=8-9.5 Å dried at RT. After reduction, the peak at 13.5^{0} vanishes and a new peak at 21^{0} and 25^{0} appears. This can be indicating the removal of oxygen functional groups. In this reduction process, we did reaction temperature at high-temperature 120^{0} C in different solvents such as DIW and DMF. In the reduction in DIW, the XRD pattern shows the two peaks at 21^{0} and 25^{0} corresponding interlayer distance 4.2 Å and 3.57 Å. In this 21^{0} , shows the poly hydrocarbon templets. In DMF reaction $2\theta = 25.07^{0}$ corresponding d= 3.55 Å. Which indicates that it was fully reduced and there is no peak at 21^{0} and also indicate it has good crystallinity compared with DIW reaction.

3.4.3. Morphology analysis by TEM and FESEM

Transmission electron microscopy is used for to analyze the crystalline nature and morphology of graphene oxide and reduced graphene oxide. In the Fig.3.4.2 (a),(b) and (c) images are TEM, HR-TEM and SAED pattern of Graphite oxide respectively (a) shows the sheet-like morphology and also more disorder supported by Fig.3.4.2 (b) and(c). In Fig.3.4.2 (c) SAED pattern of shows the amorphous regions because due to the presence of sp³ carbon atoms formed during the oxidation and indicate the disorder. Fig 3.4.2 (d), (e) and (f) images are TEM, HR-TEM and SAED pattern of RGO in DIW respectively and (d) shows the sheet-like morphology and agglomerate sheets and good transparent. Fig 3.4.2 (f) shows the SAED pattern has crystalline nature indicate the removal of oxygen functional groups and formation of an sp² network for graphene sheet. Fig.3.4.2 (g),(h) and (i) images are TEM, HR-TEM and SAED pattern of RGO in DMF respectively. Fig.3.4.2 (g) shows the sheet-like morphology and more transparent. HR-TEM image Fig. 3.4.2 (h) shows the clearly exhibited the signature of single-layer graphene. Fig.3.4.2 (i) shows the hexagonal SAED pattern which indicates more removal of oxygen functional groups and indicates more formation of the sp² network.

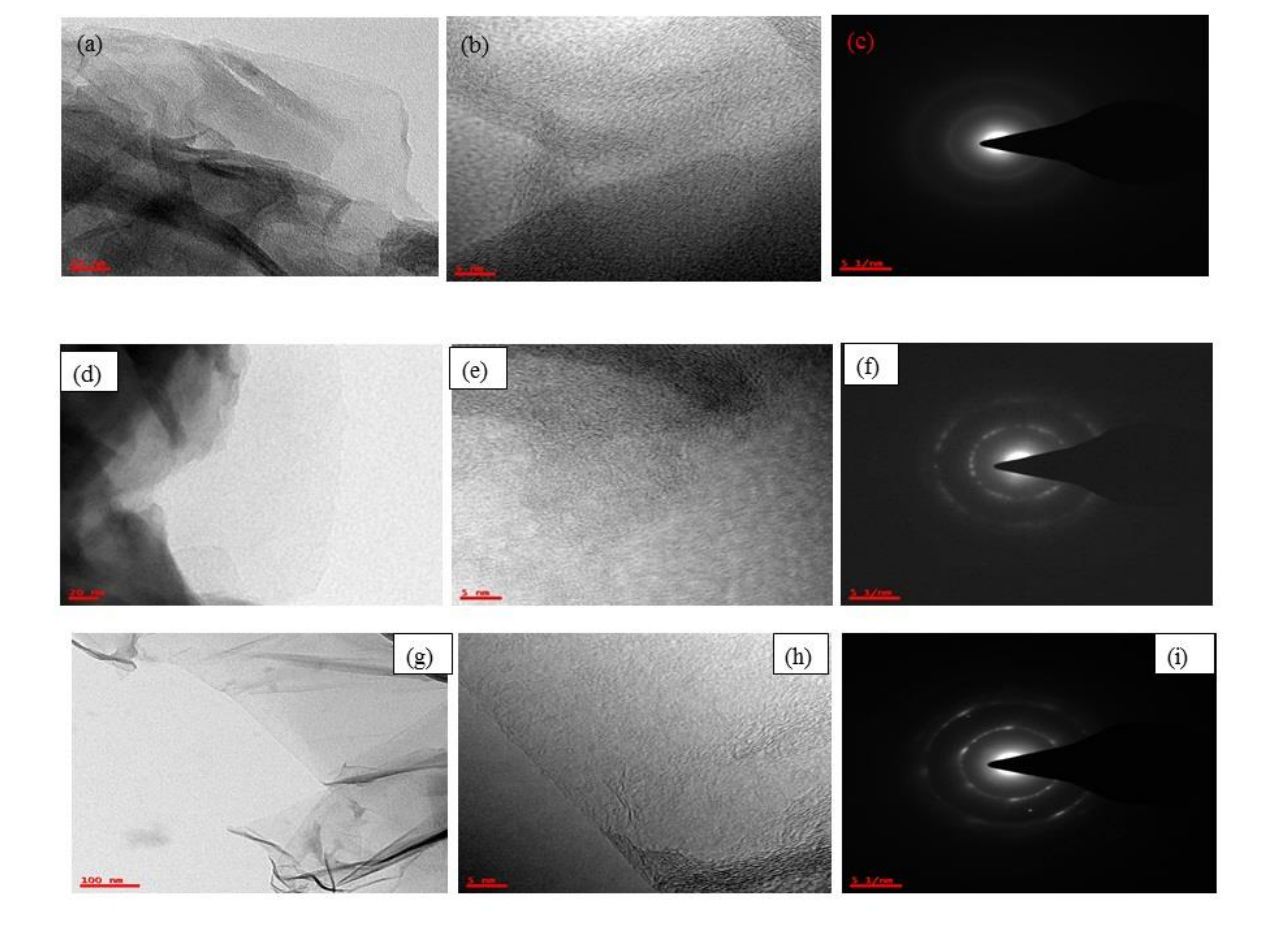


Fig.3.4.2 (a),(b) and (c) images are TEM, HR-TEM and SAED pattern of Graphite oxide respectively and (d),(e) and (f) images are TEM, HR-TEM and SAED pattern of RGO in DIW respectively and (g),(h) and (i) images are TEM, HR-TEM and SAED pattern of RGO in DMF respectively.

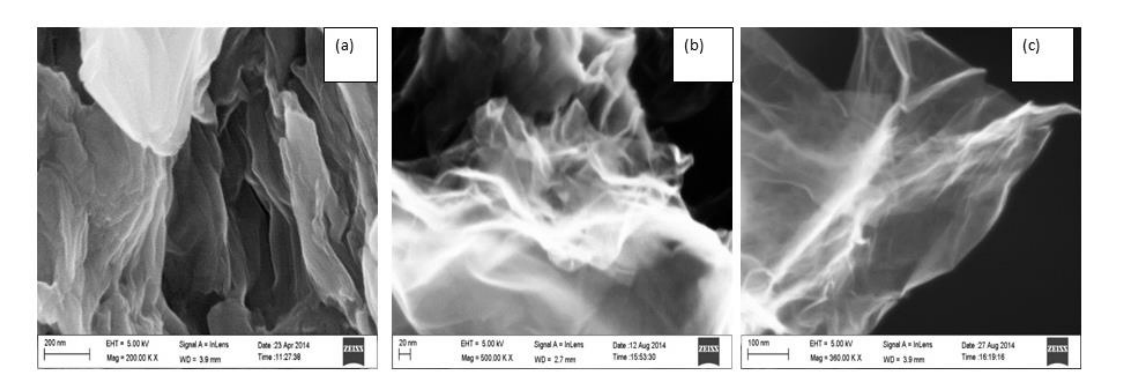


Fig.3.4.3. FESEM images of (a) graphite oxide , (b) RGrO in DIW and (c)) RGrO in DMF (all images from powders)

Fig. 3.4.3 (a) shows a FESEM image of graphite oxide(GrO) has the stacked layer structure. This can be supported by XRD results for good oxidation of graphite. Fig.3.4.3(b) and 3.4.3(c) show the good transparent and sheet-like morphology but a more agglomerate appearance in a reduction in DIW compare with DMF and transparent indicates the removal of oxygen functional groups at high-temperature reduction at 120°C.

3.4.5 Bonding characteristics analysis by FTIR

FTIR is good for to investigate the oxidation and reduction of graphene-based materials. In Fig. 3.4.4 graphite oxide spectrum shows as followed oxygen functional groups such as C-O group attributed to stretching vibration mode in the alkoxy group at 1050cm⁻¹, at 1405 cm⁻¹ arising from the C-OH carbonyl group, C=C skeletal ring of aromatic vibrations were located at 1618 cm⁻¹, at 1725 cm⁻¹ corresponding to the C=O stretch mode in the carboxyl group and 3418 cm⁻¹ from the O-H groups. After reduction with hydrazine hydrate at 120°C and dried at 120°C in the vacuum oven, the FTIR spectrum of reaction in DIW and DMF shows the varnish of all oxygen functional groups. These results indicate that the graphite oxide is successfully oxidized and reduced by the hydrazine hydrate at 120°C in both solvents such as DIW and DMF. success

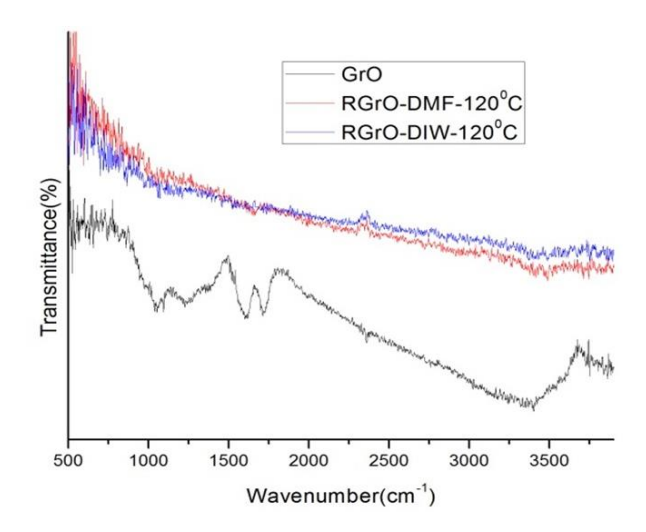


Fig.3.4.4. FTIR spectrum image of graphite oxide (black spectrum) and RGO(red spectrum of DIW and blue spectrum of DMF.

3.4.6 TGA Analysis

TGA is more suitable for the graphite oxide derivate materials to analyze the oxidation and reduction process.in Fig.3.2.5 shows the graphite oxide has the weight loss between $70^{\circ}\text{C} - 120^{\circ}\text{C}$ is 3% this due to the graphite oxide dried at 100°C . This indicates the very fewer water molecules are there compared with previous report dried at RT and 150°C - 280°C the weight loss is 28% due to the realizing CO, CO₂ and stream and 300°C - 900°C the weight loss is 22% due to the removing of more stable oxygen functional groups. After reduction of graphite oxide by Hydrazine hydrate at 120°C in different solvents such as DIW and DMF shows the thermally stable due to the removal of oxygen functional groups but in the case reduction in DIW shows the weight loss between 150°C - 280°C is 8%. This can indicate the more reduction happen in DMF compared with the DIW.

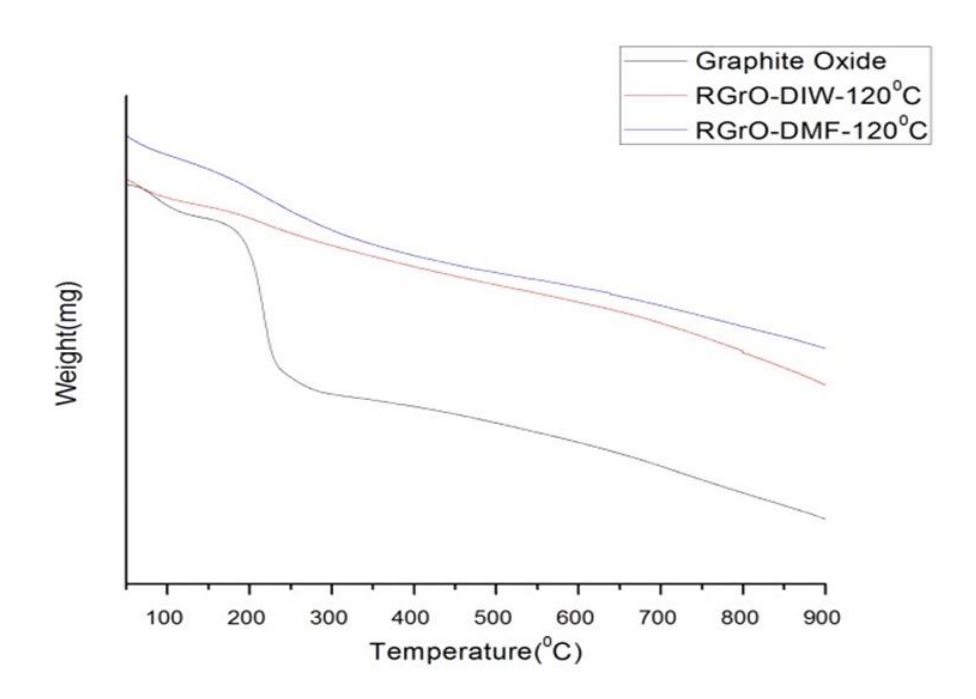


Fig.3.4.5. TGA images of graphite oxide (black curve) and RGO (red curve of DMF and blue curve of DIW).

3.4.7 UV Analysis

UV-Vis spectrum is sensitive to the structure and oxidation states. We performed UV-Vis absorption spectrum on graphite oxide dried at 100^{0} C and RGO samples indicate RGO-DIW and RGO-DMF reduction at 120^{0} C and also dried at 120^{0} C. Generally, previous reports show the graphite oxide has two peaks dried at $\leq 60^{0}$ C, ≤ 230 nm peaks indicates the conjugated π - π * (C=C)

transition and <300nm assigned for n- π (C-O) transition. In the Fig.3.4.6 (a) spectrum shows the graphite oxide has three peaks first one very small peak at 244nm and a broad peak at 263nm and very small hump at 314nm. This GO has higher wavelengths indicates the more population of sp² carbon atoms obtained due to the drying at 100^{0} C and reduction in DIW at 120^{0} C by hydrazine hydrate shows the <251nm peaks have too much very less intensity and at 265nm peak has more intensity comparable with graphite oxide and increased in wavelength. This indicates the graphite oxide well reduced by hydrazine hydrate at 120^{0} C in a DIW solvent. Fig.3.4.6 (c) shows the reduction in DMF at 120^{0} C has single broad and more intensity peak at 270nm this can indicate the complete reduction happen in the DMF solution compared with the reduction in a DIW solvent.

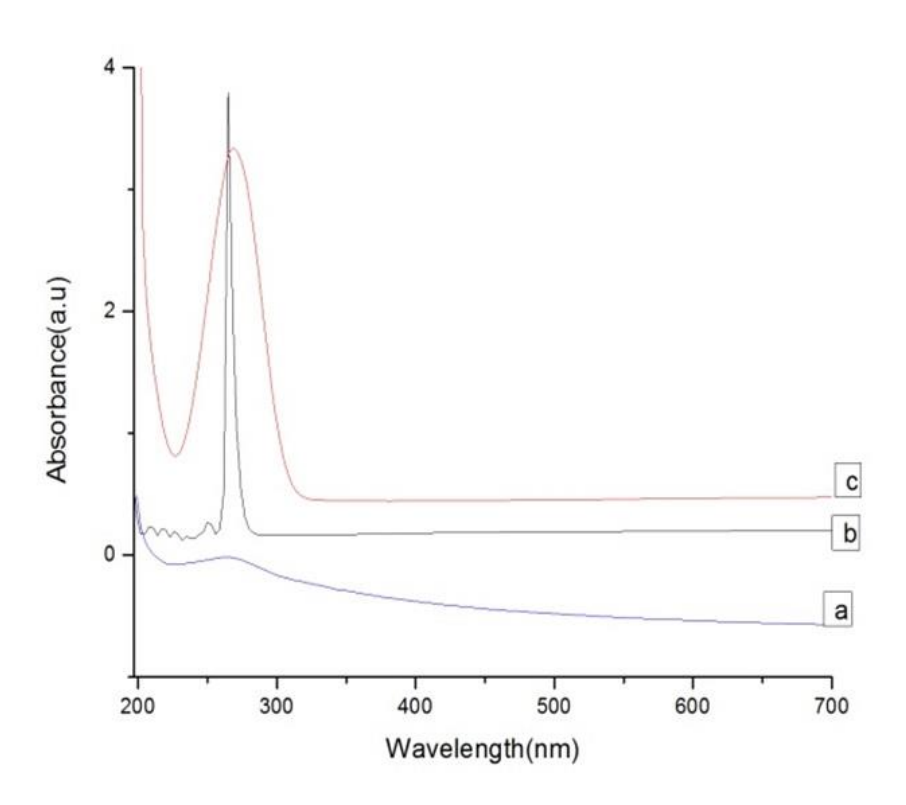


Fig.3.4.6. UV-Vis Spectrum of (a) graphite oxide,(b) and (c) are RGO samples of reduced in DIW and DMF by hydrazine hydrate at 120°C respectively.

3.5 Conclusions

In this chapter GO was synthesized by using the equal ratios of graphite: KMnO₄: H₂SO₄ (1:3:23) at lower oxidation temperature such as 45,40 and 35°C. Those are named as reaction1,2 and 3 respectively. All the GO samples were dried at 100°C in a vacuum oven. All these three GO samples were analysed by XRD, Raman, FT IR, TEM, UV and TGA for structure, bonding, morphology, molecular structure and thermal stability. Finally, all these three samples were reduced chemically by hydrazine hydrate, thermally and bothe chemically and thermally. As obtained RGO samples were analyzed by XRD, Raman, FT IR, TEM, UV and TGA for structural, bonding, molecular structure, morphology and thermal stability. In the second section of this chapter, three GO samples were synthesized at same ratios with higher oxidation reaction temperature. All the samples were analyzed by using XRD, Raman, FT IR, TEM, UV and TGA for structural, bonding, molecular structure, morphology and thermal stability. In the third section, the impact of solvents on the exfoliation of RGO was investigated supported by XRD, Raman, FT IR, TEM, UV and TGA for structural, bonding, molecular structure, morphology and thermal stability.

From XRD analysis, after oxidation, the interplanar distance was increased from the graphite samples so that all samples good oxidized. But these samples have different interplanar distances which indicate the different oxidation levels occurred even by using the equal ratios of graphite: KMnO₄: H₂SO₄ (1:3:23). this was happened due to the temperature and time. Reaction 1 synthesized GO contains more oxygen functional groups due to the higher interplanar distance. Reaction 1 synthesized GO shos higher intensity than other two samples which indicates this sample may have more crystallinity than other two samples. All the three GO samples (reaction 1, reaction 2 and reaction 3) showed different crystallite sizes (XRD), so that the crystallite size varies with the reaction temperature. After chemical reduction, the interplanar distance was decreased for all three GO samples which indicate the oxygen functional groups have removed some extent. All three samples show the nearly same peak position at 21° represents the hydrocarbons presence and 25° peak indicates the formation of graphene structure. Thermally reduced graphene oxides(RGO) obtained from reaction 1,2 and 3 GO, confirmed that the reaction 1 GI only contains the hydrocarbon-related groups, however reaction 2 and reaction 3 GO samples these groups are absent. Chemically and thermally reduced graphene oxides(RGO) show the structural deviation from the chemically reduced RGO samples. In the case of the RGO obtained from the chemical reduction with hydrazine hydrate shows the two peaks, on the other hand, chemically with thermally reduced graphene oxide shows show a single peak at $2\theta = 24$ and interplanar distance (d) = 0.36nm.

Raman analysis results shows the broadening of the G peak and D band and the 2D band is suppressed, this represents that the oxidation happened for all the reactions. Generally, the graphite oxide case G band position shows a redshift of the graphite position. GO obtains from the reaction (1) shows the blueshift of the G peak which indicates that it contains less epoxy, hydroxyl and water molecules. The blueshift can happen when the double bond related functional groups are formed. The reaction 3 based RGO show the better chemically reduction than other samples due to the blueshifted of the G band 2D band and also shows the higher value of I_D/I_G ratio. Thermally reduced samples completely different from the graphite oxide and chemically reduced graphite oxide samples. These samples did not contain the 2D band particularly comparative to CRGrO samples. I_D/I_G ratios decrease with chemically reduced samples which mean that formation of SP² carbon domains may be larger size comparative to CRGrO samples. G* band is absent in these samples comparative chemically reduced graphite oxides and also G+D band is more intense than CRGO samples. The G band position is red shifted compare to CRGO samples. In TCRGO samples, the RGO obtained by using the reaction 3 GO shows lower I_D/I_G ratio in comparison to the RGO obtained from reaction 1 and 2. Therefore, the reaction 3 is better for the synthesis of GO and also both chemically and thermally reduction process is more effective to obtain reduced graphene oxide (RGO).

FESEM analysis, results indicate that all three samples are shown the good intercalated sheet-like morphology which indicated the oxidation successfully happens. After chemical reduction three samples show the different morphology comparative to their oxidation samples. The RGO obtained from the reaction 3 GO show the high transference than other two samples.

TEM analysis results indicate that the GO synthesized by reaction shows some % of the crystallinity whereas other samples show the ring pattern. The chemically reduced graphene oxide samples obtained from the reaction 3 GO shows different morphology than the other two samples(reaction1 and 2 RGO samples). It consists of a very thin sheet-like morphology with different layers, single, double and few layers and also it has hexagonal diffraction spots.

TGA and DTA analysis result indicate that the GO obtained from the reaction 1,2 and 3 show the different weight loss and different exothermic peak position which indicate that these samples have different oxidation levels. RGO samples obtained from all these three GO did not show weight loss

and exothermic peaks which indicates the after reduction process all these samples are thermally stable.

EDS analysis results indicate that all three samples (R1-GrO, R2-GrO, and R3-GrO) show the nearly equal C/O ratios which indicate that the all samples are fully oxidized. But all three GO samples shows the different interplanar distance from the XRD analysis, different band position in Raman analysis and different weight loss and exotherm peak position from the TGA and DTA analysis. Therefore, we have concluded that though all these samples possess equal C/O ratios the formation of the oxygen-related functional groups is different. Further, the RGO obtained by using chemically reduction process shows higher C/O ratio than other two samples. So that, in the case of chemically reduced graphene oxide more oxygen-related function groups are removed than other two samples.

FTIR spectrum of obtained GO by using the reaction 1,2,3 indicates the different intensity and peak position of functional groups. The 1383cm⁻¹ band represents the O-H deformation in the carboxyl group. It is appeared in the R1-GrO sample only and not present in the other two samples such as R2 and R3 samples. 1240cm⁻¹ and 1231cm⁻¹ bands represent the C-OH stretching mode of phenolic groups present in the hydroxyl groups. These bonds are appeared in R2 and R3 – GrO samples and not present in the R1 sample. R2 GrO shows a peak position at 1043cm⁻¹ which represents the edge phenol groups in hydroxyl. All reduced samples indicate the removal of oxygen-related functional groups and however show some hydroxyl groups related functional groups are presented.

UV analysis results indicate that all GO samples(reaction 1,2 and 3) show the presence of the aromatic phenol group in hydroxy in the wavelength range 215-250nm. Small hump peaks appear and that confirms the $\pi \to \pi^*$ of the C=C and n- π for the C-O. All the GO obtained are oxidized and after reduction n- π transition peaks are not present.

Higher reaction temperature synthesized GO show very disordered structure with some graphitic ordering are present as observed from the (XRD) and TEM analysis results. Therefore, the very high temperature is not more suitable for obtaining a fully oxidized graphene oxide. We have concluded that GO synthesized at 35°C show all the characteristics of good graphene oxide and the same process was chosen as an optimum process for the following work.

Further, our experimental work from the solvents effects for obtaining the exfoliation of Go for reduction of RGO suggests that DMF is better than DI water to obtain less disorder, more graphitic ordered structure.

Chapter -4

Influence of the precursor graphite size on the structure, morphology, and bonding characteristic of the graphene oxide and reduced graphene oxide

4.1. Introduction

In the previous chapter, we have described the effect of different synthesis parameters on the synthesis of GO and RGO. This chapter mainly deals with the study of different sizes graphite on the synthesis of GO and RGO by MHM.

4.2 Synthesis of graphite oxide by different sizes precursor graphite

Graphite oxide was synthesized from the graphite powder by modified Hummer's method. In a typical experiment 4 g of graphite (2-15 μ m) powder was first added into 92 ml of the concentrated H₂SO₄ and then 2g of NaNO₃ was prepared in a 2000ml beaker by keeping in an Ice bath string for 30min.Under stirring, the mixture was cooled to 5°C using an ice bath then, KMnO₄ (12 g) was gradually added maintain the 5°C and continuing stirring, for 45mints. Then the Ice bath was removed and stirred for 1h at RT on a hot plate. The temperature raised from RT to 35°C and stirring for 4h. As the temperature increased from 35°C to 100°C at this stage 184 ml of DI water was added and stirred for 15 min. Further, the solution was diluted with 560ml of DI water. After that, 40 ml of 30% H₂O₂was added to the mixture to reduce the residual KMnO₄. Finally, cleaning was carried out with DI water several times and then with 35% HCl twice (each time 80ml) until pH value reached to 7. The obtained graphite oxide (GO) was collected by centrifuging and filtering process. Finally, the resulting graphite oxide (GO) was dried at 60°C for12 h in a vacuum oven. The same process was carried out for choosing another two sizes graphite powder as a precursor, one size is <45 and another size is 170-840 μ m.

4.3 RGO Preparation by chemical reduction process

In this process, 250mg of the obtained graphite oxide was taken in a 500ml beaker containing 250ml DI water and sonicated for 60min to obtain a clearer solution. Then, 10ml hydrazine hydrate was added to the graphene oxide solution and heated at 95°C with stirring for 6h. This experiment was carried on a hot plate by using the silicon oil both. After completion of the reaction, the solid material was filtered and washed with DIW and several times till PH=7. Finally, filtered and dried at 60°C by using a vacuum oven for 12h. Same reduction process also preferred for other two GO samples, those were synthesized by using same for <45µm and 170-840µm size graphite powders as source material.

4.4 Characterization of GO and RGO

4.4.1 Structural analysis by XRD

Fig.4.1 shows the XRD pattern of the different sizes graphite precursors. And all the different parameters as obtained from the XRD pattern are listed in table.1. All three samples have they similar 2θ values as shown in table.1. 2θ = 26.6° and corresponding interplanar distance are 3.3Å out of all these three sizes 170-840 and <45 µm graphites have more intensity than 2-15 µm

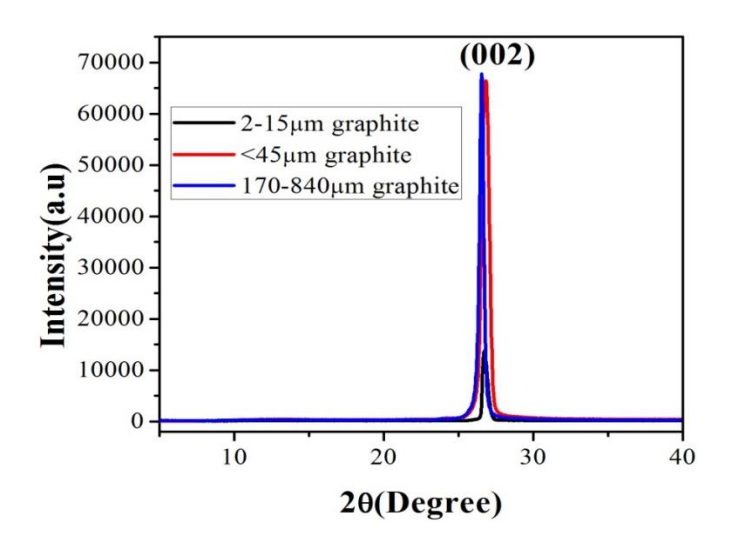


Fig.4. 1. XRD pattern of different sizes of graphite

due to its bigger sizes. The crystallite sizes are calculated by Debye Scherrer's formula from XRD data and are 21.3nm,13.5nm, and 24.7nm for 2-15,<45 and 170-840 μ m respectively. Therefore, 170-840 μ m graphite has larger crystallite size and < 45 μ m has the least crystallite size.

Table:4.1 Interplanar distance and crystallite size(XRD) of the different sizes of graphite

| Sample name | 2θ | d nm | D nm | Shape of the peak | FWHM |
|----------------|------|---------|---------|----------------------|------|
| 2-15µm | 26.7 | 0.324 | 21.3 | sharp | 0.38 |
| graphite | | | | | |
| <45µm | 26.8 | 0.324 | 13.5 | sharp | 0.60 |
| graphite | | | | | |
| 170-840µm | 26.4 | 0.38 | 24.7 | sharp | 0.35 |
| graphite | | | | | |

Fig.4.2. shows the XRD spectrum of all these graphite after oxidation process. As shown in Fig.4.2.and the interplanar distance(d) increases to 7.1,7.7 and 7 Å for graphite oxide from the parent graphite having sizes 2-15,<45 and 170-840 μ m respectively. The increase in the interplanar distance (d) for all the three graphite oxide indicates that intercalation of the water molecules and oxygen functional groups between the graphite layers. However, in the case of graphite oxide, synthesized from 170-840 μ m size graphite has another peak at $2\theta = 26.4^{\circ}$ with d = 3.4Å which indicates that 170-840 μ m GO is partially oxidized. Therefore, bigger size graphite is not fully oxidized under this conditions and hence the oxidation process of graphite is size dependent, i.e. the smaller size of graphite is fully oxidized within 4 hours' time of reaction whereas bigger size (170-840 μ m) graphite needs more time or a different ratio of chemicals to be fully oxidized. Also after oxidation, smaller size source i.e 2-15 μ m graphite oxide has more intensity peak thane other two sizes, which indicates that 2-15 μ m size, graphite oxide consist of more crystallinity than other two sizes synthesized GO.

Fig.4.3 shows the XRD spectrum after reduction of graphite oxide for all the three graphite oxide samples. It is seen that the interplanar distance(d) decreases from 7.5 to 4.5Å of all samples, which indicates the oxygen functional groups are subsequently removed and broad peaks represent that smaller crystallites are formed. Also, a small hump is noticed at 19-20⁰ (as shown in figure 3)

indicates some functional groups are present in the carbon backbone after reduction process or another phase may be present in the RGO.

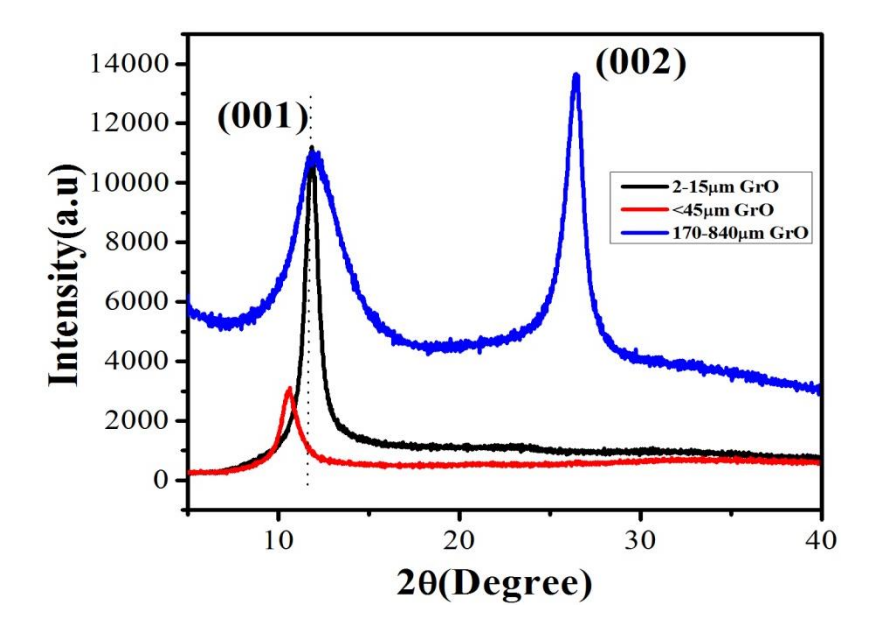


Fig. 4.2. XRD pattern of different sizes of graphite oxides with different source graphtes.

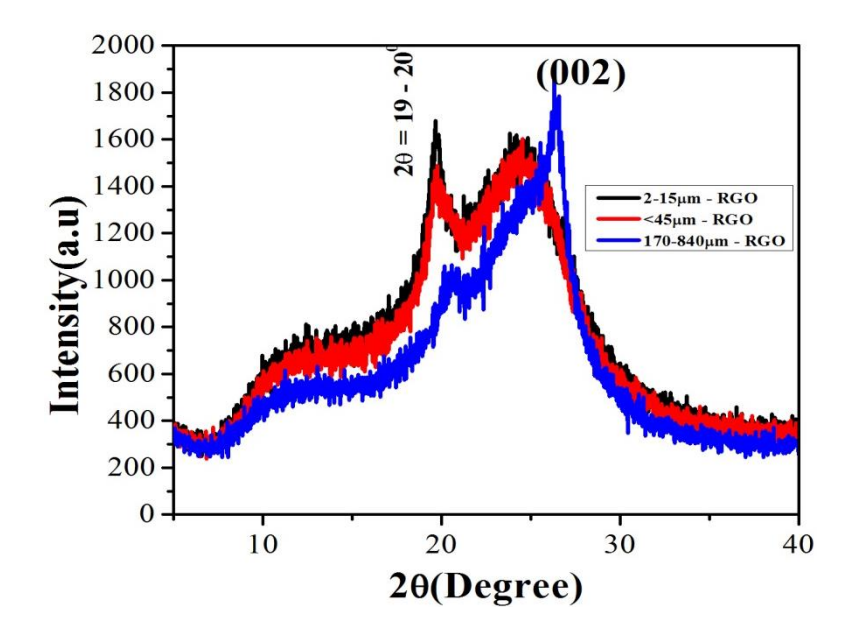


Fig.4.3. XRD pattern of different sizes of reduced graphene oxides.

4.4.2 TEM analysis of GO and RGO

Fig. 4.4.(a) - (c) shows the TEM images of all three graphite oxides. It is observed from Fig. 4.4(a)that less folding and disorder present in the smaller size graphite synthesized graphene oxide as comparative larger sizes source graphite synthesized graphene oxide. More thick sheet morphology and less transparent are observed from the reduced graphene oxide synthesized by using the 170-840µm graphite as compared to the smaller size graphite powder synthesized graphene oxide. From the SAED pattern (as shown in Fig.4.4) shows the hexagonal structure of two rings are observed and HRTEM clearly shows the lattice fringes <4 layers of 2-15 µm graphene oxide. Clearly, shows diffraction spots indicates the characteristic of crystalline order which also supported by XRD results. Fig.4.4.(b) shows the <45 µm graphite oxide has more folding comparative with 2-15 µm graphite oxide and SAED shows the ring like diffraction pattern indicates the polycrystalline nature of GO (as shown in Fig.4. 4 (b). HRTEM images show the more folding of lattice fringes of GO. Fig.4.4. (c) show the 170-840 µm graphite oxide TEM image represents the more thick sheet morphology and less transparency comparative to other sizes and also SAED and HRTEM show the multilayers nature of GO because of partially oxidized. Fig.4.4.(d) shows TEM image of 2-15 µm RGO has very less folding, flat sheet formation, and more transference in nature. The SAED pattern shows the sharp diffraction spots which further indicates the restoration of SP² hybridized carbon atoms by the chemical reduction. HRTEM image clearly conforms <3-4 layers are present in the samples. Fig.4.4.(e) shows the TEM image of <45 µm RGO, which clearly shows more folding with transparency in nature and SAED pattern shows the very fewer intensity spots with a hexagonal structure. Moreover, the HRTEM image conforms even having single layer lattice fringes, which are distributed randomly. Fig.4. 4.(f) shows the TEM image of 170-840 µm RGO has a thick sheet and SAED pattern has sharp spots of multilayer formation. Therefore, TEM results correlated with the corresponding XRD results and concluded that after oxidation and reduction smaller size graphite synthesized reduced graphene oxide has good crystallinity and less folding as compared to that of bigger sizes graphite powder.

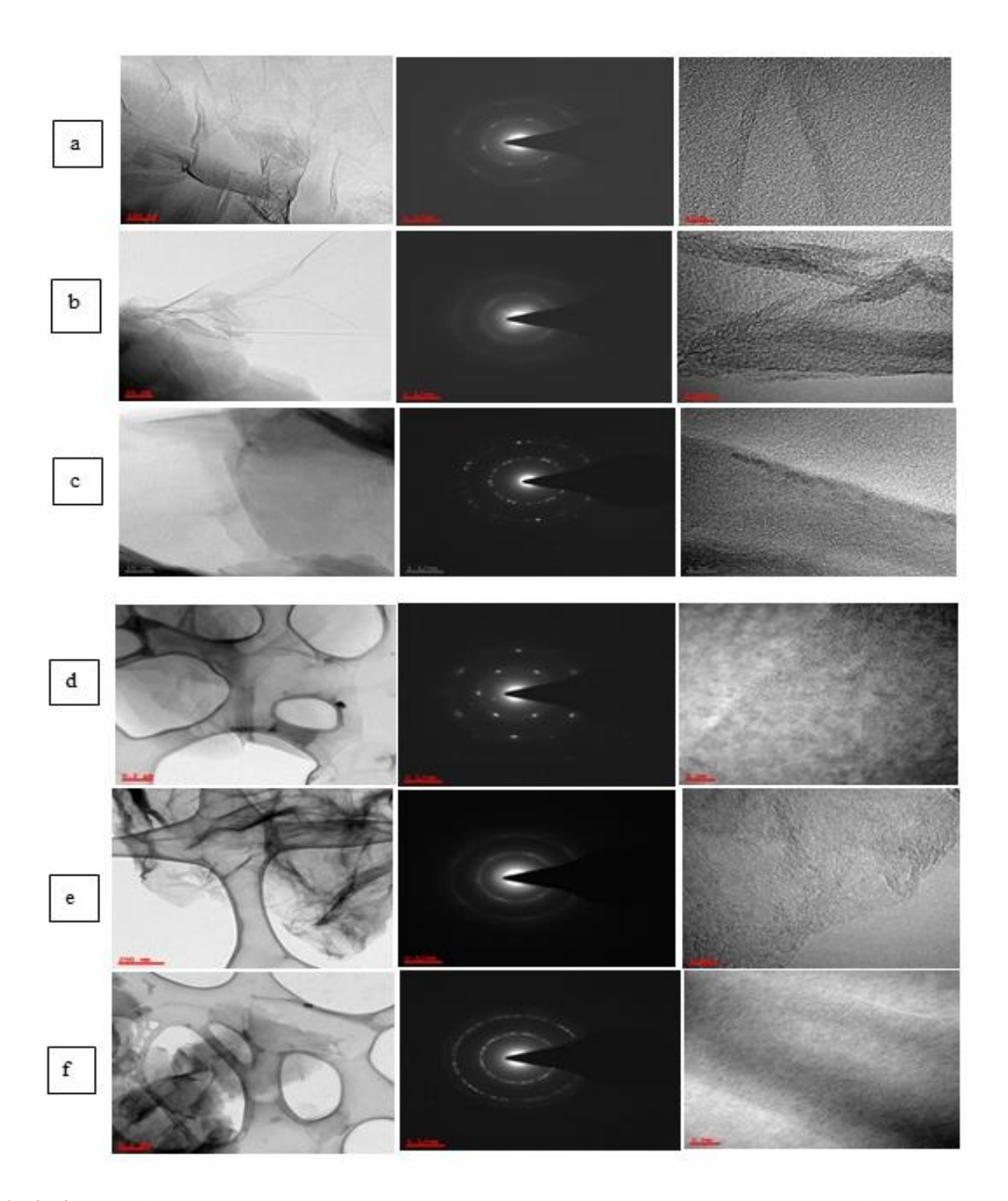


Fig.4. 4. TEM images (a),(b) and (c) are 2-15,<45 and 170-he 840 μ m GrOs corresponding SAD and HRTEM images. and TEM images (d),(e) and (f) are 2-15,<45 and 170-840 μ m RGO corresponding SAD and HRTEM images.

4.4.3 Morphology analysis by FESEM

The source graphite samples morphology are observed by using scanning electron microscopy and the graphite oxide and reduced graphene oxide samples are analyzed by FESEM. Fig.4.5 shows the

morphology the different precursor's graphite samples and the corresponding synthesized graphite oxide and reduced graphene oxide by SEM and FESEM. The graphite samples are seen by SEM, clearly shows the size of the samples as shown in Fig.4.5 (a-c) are values are 2-15 μ m, <45 μ m and 170-840 μ m respectively. Fig.4. 5 (d-f) shows the FESEM images of the synthesized graphite oxide samples of 2-15 μ m, <45 μ m and 170-840 μ m graphite oxide respectively. In which 2-15 μ m graphite oxide shows more charging than <45 μ m and 170-840 μ m graphite oxide. Which indicates the more oxidation occurs synthesis samples. Fig.4.5. (g-i), as shown in the Fig.4. 5 (g), the morphology of the 2-15 μ m RGO,<45 μ m RGO and 170-840 μ m RGO respectively. 2-15 μ m RGO has a flat sheet and transferent than <45 and 170-840 μ m RGO. Regarding the morphology of different size of RGO results of FESEM and TEM, they are supported each other.

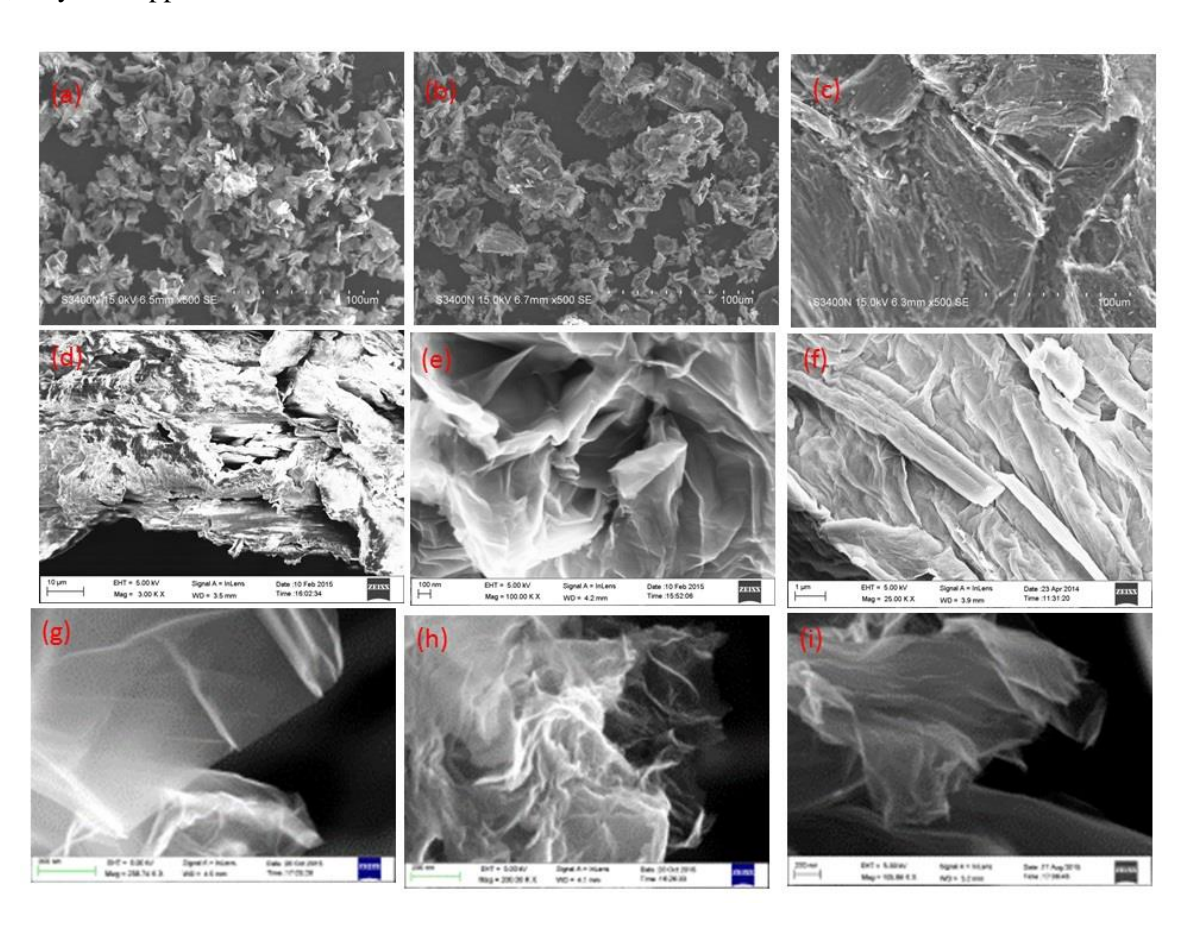


Fig.4.5 SEM images of (a) 2-15 μ m graphite (b) <45 μ m graphite and (c) 170-840 μ m graphite and FESEM images of (d) 2-15 μ m ,(e) <45 μ m and (f) 170-840 μ m graphite oxide. FESEM images of (g) 2-15 μ m,(h) <45 μ m and (i) 170-840 μ m reduced graphite oxide.

.

4.4.4 Raman Analysis GO and RGO:

Fig.4.6. shows the Raman spectrums of 2-15, <45 and 170-840 μ m graphite oxide. These samples have typical D band and G bands. The D band appears at 1354,1353 and 1355cm⁻¹ and G band at 1590,1585 and 1585 cm⁻¹ (I_D/I_G ratio are 0.95,0.88 and 0.78) for the 2-15,<45 and 170-840 μ m graphite oxides respectively. The $_D/I_G$ ratio are 0.95,0.88 and 0.78 for 2-15, <45 and 170-840 μ m

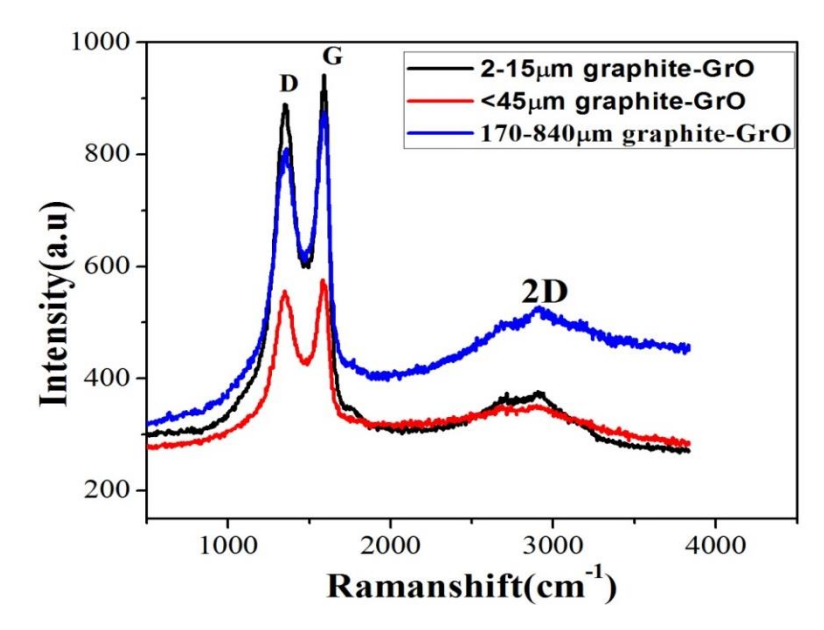


Fig.4.6. Raman spectrum of 2-15, <45 and 170-840μm graphite oxides.

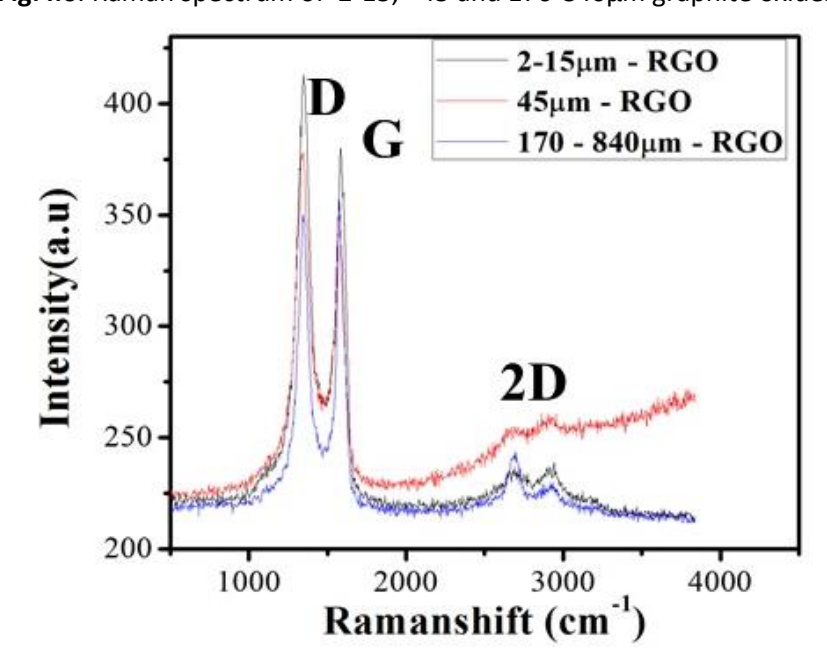


Fig..4.7 Raman spectrum of 2-15, <45 and 170-840μm reduced graphene oxides.

GO respectively. The broad and the peak shift to a higher wavenumber of the G band, the I_D/I_G ratio increase to indicate god oxidation of the sample. Therefore, 2-15 μ m graphite oxide is oxidized more

as compared to the other two samples due to the shift of G band to the higher wavenumber and increasing of the I_D/I_G ratio. Fig.4.7.shows the Raman spectrums of 2-15, <45 and 170-840 μ m reduced graphene oxide (RGO). The D band appears at 1348, 1342 and 13146 cm⁻¹ and G band at 1586, 1576 and 1580 cm⁻¹. The I_D/I_G ratio of the three RGO samples are 1.32, 1.26 and 0.99 of 2-15, <45 and 170-840 μ m reduced graphene oxides respectively. After reduction, the I_D/I_G ratio increase as compared to the GO samples. This indicates that the new created graphitic domain in RGO is number than that presented in the GO i.e. size of the sp² domain in GO decreases after chemical reduction. Therefore, 2-15 μ m RGO shows more I_D/I_G ratio in comparison to the other two sizes. Therefore the smaller size graphite consists of more formation of new sp² domains after chemical reduction. This result can be correlated to the XRD results, to the formation of the broad peak in XRD after reduction.

4.4.5 FTIR analysis for bonding characterization and functional groups

Fig.4.8 (a) shows the FTIR spectrum of 2-15, <45 and 170-840 μm graphite oxides. All three samples have similar peak positions of the functional groups with very small variation in the intensity and broad peaks. The three samples consist of the functional groups are, 3400cm⁻¹ of O-H stretching vibration of the hydroxyl groups and intercalated water molecules between graphite layers. 1724 cm⁻¹ indicates the C=O stretch mode in the carbonyl groups, 1620 cm⁻¹ contributes to the C=C skeletal vibration of unoxidized Graphitic domains or contribution from the stretching deformation of O-H vibration of intercalated water, 1380 cm⁻¹ indicates the OH deformation vibration of COOH groups, 1228 cm⁻¹ attributes to the C-O stretching peak of epoxy groups and 1051 cm⁻¹ indicates the C-O group of alkoxy of stretching vibration mode. All three samples attribute broad and more intensity peaks for the hydroxyl and epoxy groups and fewer intensity peaks are observed for carbonyl and carboxyl groups i.e. a large amount of hydroxyl and epoxy groups distributed on the basal plane of GO and a small amount of carboxyl and carbonyl groups formed at edges of GO sheets.

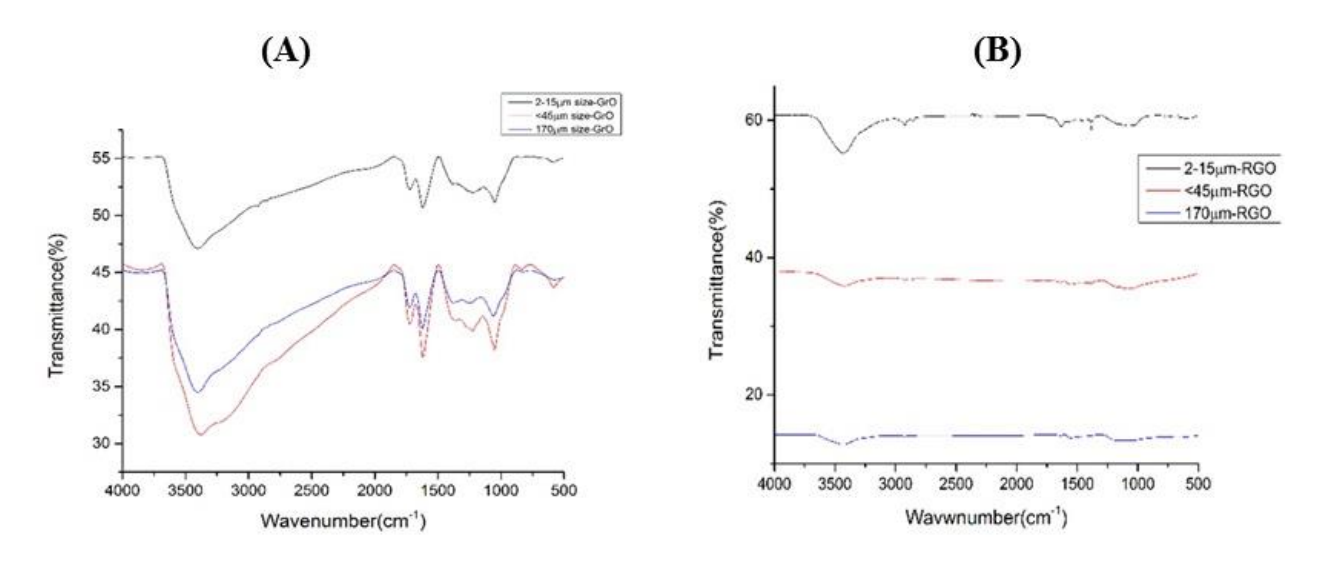


Fig.4.8. FTIR spectrum of (A) 2-15, <45 and 170-840 μ m Graphite oxides and (b) 2-15, <45 and 170-840 μ m reduced Graphite oxides

Fig.8 (b) shows the FTIR spectrum of 2-15, <45 and 170-840 μm reduced graphene oxides by hydrazine hydrate. It is seen that for all these three samples, the disappearance of 1724 cm⁻¹, 1228 cm⁻¹ and 1051 cm⁻¹ peaks of carbonyl, epoxy, and alkoxy respectively and also broadness is reduced. The removed from the hydrazine hydrate.

4.4.6 TGA analysis of GO and RGO

Fig.4.9 (a) shows the TGA spectrum of 2-15, <45 and 170-840 μm graphite oxides. These three samples show the weight loss at < 100°C and the wt% losses are 10.6, 11.5 and 8.3% it is also observed that between 130-300°C, the weight loss is 37.4, 32.8 and 24.4% for the 2-15, <45 and 170-840 μm graphite oxides respectively. These three samples show the different weight loss at<100°C and in between 130-300°C, which indicates the oxidation-dependent on the size of the graphite. At <100°C the weight loss due to the water molecules evaporation and between 130-300°C range weight loss represents the decomposition of oxygen-containing functional groups such as yielding CO, CO₂, and steam. <45 μm graphite oxides consists of more water molecules between the graphite layers in comparison to other two sizes graphite oxide. These water molecules can attribute to the more folding, polycrystalline and disorder of lattice fringes as seen in TEM analysis. There is an agreement between the XRD and FTIR results. At, 130-300°C range, more weight loss is observed 2-15 μm graphite oxide comparative other two sizes graphite oxides. i.e it consists of more oxygen-containing functional groups. Experimental results indicate the smaller size graphite easily

oxidized comparative to the bigger size graphite. Fig.4.9 (b) shows all the three RGO samples after the chemical reduction by hydrazine hydrate. As shown in Fig.4.9 (b) all those three samples thermally stable i.e. there is no sudden weight loss between 130-300°C range indicates the removal of oxygen functional groups. Hence, all are reduced graphene oxide.

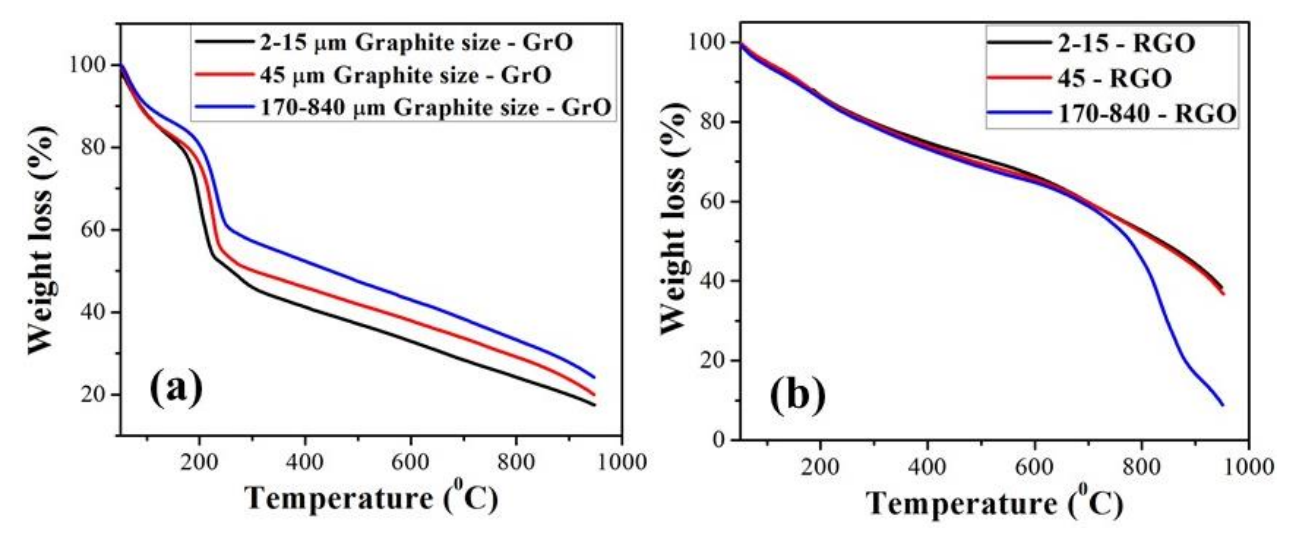


Fig. 4.9. TGA analysis spectrum of (a) 2-15, <45 and 170-840 μ m graphite oxides and (b) 2-15, <45 and 170-840 μ m reduced graphene oxides.

4.4.7 DTA analysis of GO and RGO

By using the DTA technique we can observe that material behavior through the endothermic (melting or boiling or sublimation of the material) process (or) exothermic (crystallization of the sample) process. Fig. 4.10 (a) shows the DTA curves of 2-15, <45 and 170-840μm graphite oxides samples. 2-15 μm graphite oxide exhibits the broad exothermic peak at 205°C (onset and offset temperature are 156 - 239°C). in the case of <45μm graphite oxide samples has a sharp exothermic peak at 227°C (onset and offset temperature range is 192 - 248°C). 170-840μm graphite oxides sample contains the sharp exothermic peak at 235°C (onset and offset temperature range is 198- 262°C). The exothermic peak indicates decomposition of the sample and crystallization. So that comparative higher size graphite oxide samples smaller size i.e 2-15μm sample has low crystallization temperature. Fig. 4.10 (b) shows the DTA curves of 2-15, <45 and 170-840μm reduced graphene oxides samples. In this case, RGO samples <45 and 170-840μm reduced graphene oxides samples shows the thermally stable but 2-15μm size RGO sample have two endothermic peaks such as 182°C and 186°C. So that, we may

be expected that due to the smaller size graphene sheet, it has a higher surface area that means the interaction between oxygen functional may be increased.

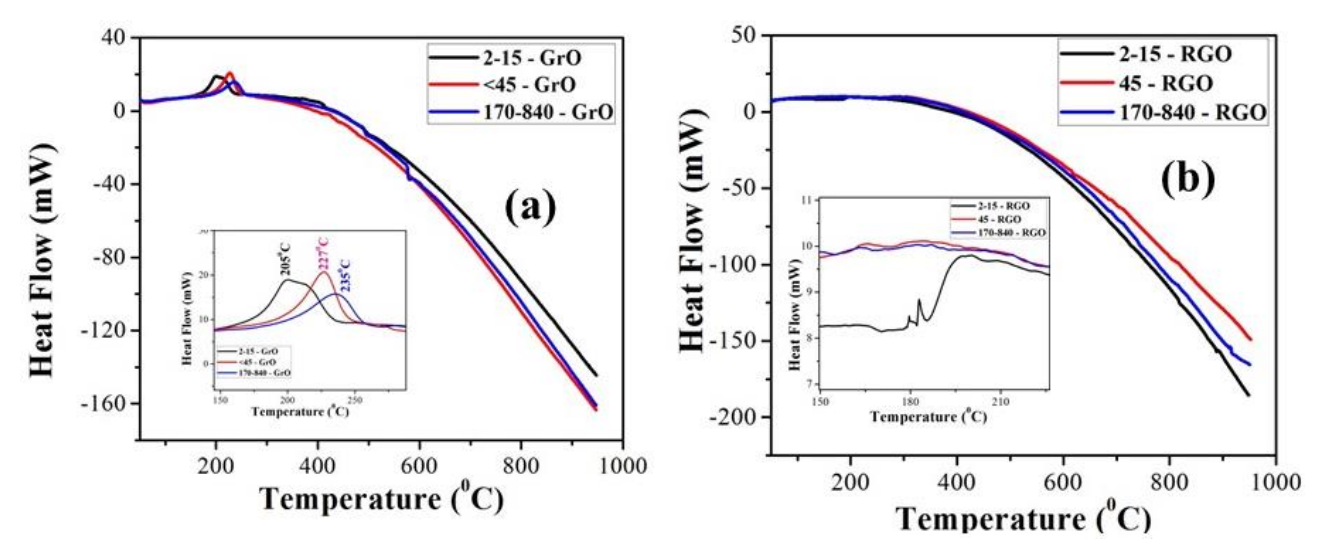


Fig. 4.10. DTA analysis spectrum of (a) 2-15, <45 and 170-840µm graphite oxides and (b) 2-15, <45 and 170-840µm reduced graphene oxides.

4.4.8 UV- Analysis of different graphite size synthesized GO and RGO

Fig.4.11. (a) Shows UV- spectra of the 2-15, <45 and 170-840 μ m graphite oxides as shown in Fig.4.11 (a), it shows two characteristic peaks those appear at 242nm, 249nm and 263nm for 2-15 μ m, <45 μ m and 170-840 μ m graphite oxide due to $\pi \to \pi^*$ transitions of the aromatic C -C bonds. Other characteristic peaks appear at 297nm, 310nm and 305m for 2-15 μ m, <45 μ m and 170-840 μ m graphite oxide due to n $\to \pi^*$ transitions of C=O bond. The above peaks around 250nm indicate the more epoxy groups are formed in the synthesis graphite oxide. The peak at 263nm indicates the electronic properties of the GO with different coverage of OH and O form epoxy groups, which are deeply affected by the charge distribution as well as by the formation of hydrogen bonds. Fig.4.11. (b) shows all the three RGO samples by hydrazine hydrate, absorption peaks are 269,270 and 270nm for the 2-15, <45 and 170-840 μ m reduced graphene oxides respectively. These peaks indicate the restoration of SP² carbons after the reduction process.

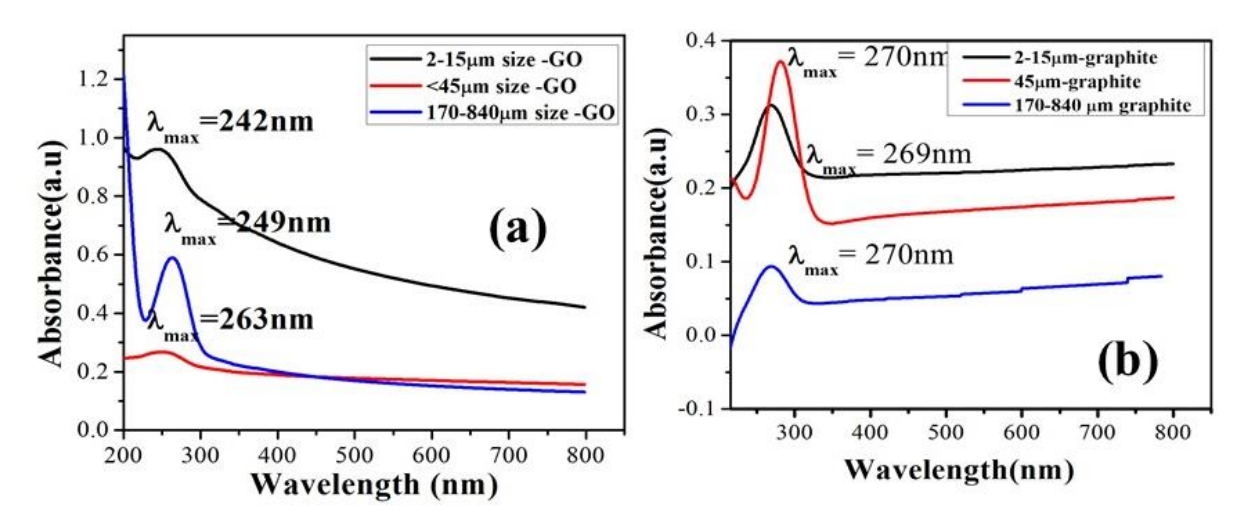


Fig.4.11. UV-Vis spectrum of (a) 2-15, <45 and 170-840µm graphite oxides and (b) 2-15, <45 and 170-840µm reduced graphene oxides.

4.5 Conclusion

Three different sizes graphite precursor (2-15 µm, <45 µm, and 170-840µm,) are oxidized by MHM and then corresponding RGO are synthesized by hydrazine hydrate process. The analysis from the XRD, TEM, and Raman indicates that size graphite (2-5 µm) consists of more crystallinity in the GO and RGO. It is concluded smaller size precursors graphite fully oxidized in comparison to the large size graphite source material. Hence oxidation of graphite to graphene oxide is size depended on the source graphite and also shows better quality of reduced graphene oxide than other sizes of Go and RGO. Morphology of the GO and RGO of different sizes and graphite after oxidation and reduction are observed in TEM and FESEM. Which indicates that smaller graphite has a flat surface and more transference then the bigger size of the graphite. from the TG analysis it is observed that different weight loss in the graphite oxide which suggest that weight loss also depends on the size graphite due \to the oxidation rate. After reduction, all the samples are seemed to be thermally stable due to the removing the oxygen functional groups. FTIR analysis indicates that all the three samples of GO and RGO have similar functional groups with different intensity. UV spectroscopy analysis shows different abortion peaks which indicated that all the sizes graphite oxidized differently. Also, UV spectroscopy results confirmed that all the three GO samples are successfully reduced to RGO. In the next chapter, we describe the fabrication of a novel nanocomposite (graphene/al2o3) material by choosing the best-known synthesis process parameters for synthesis GO and RGO from this chapter and previous chapter results.

Chapter 5

Influence of synthesis parameters on the synthesis of GO-Al₂O₃ nanocomposite by colloidal mixing process

5.1 Introduction

This chapter deals with the synthesis of prime-alumina nanocomposite by mixing the GO and RGO as described in the earlier chapter. From all the experimental results 2-15 μ m size of graphite have shown the good quality of graphene due to its good crystallinity, more transference, and easily reduction. So that this material has high hydrophilic nature due to good oxidation. And easier to prepare nanocomposite. In this chapter, we have described graphene-based alumina nanocomposite by using the colloidal mixing process. This process has some advantage uses-full of the controlling the defects and metastable phases of alumina.

5.2 source graphite oxide GO) and alumina nanoparticle for fabrication of nanocomposite

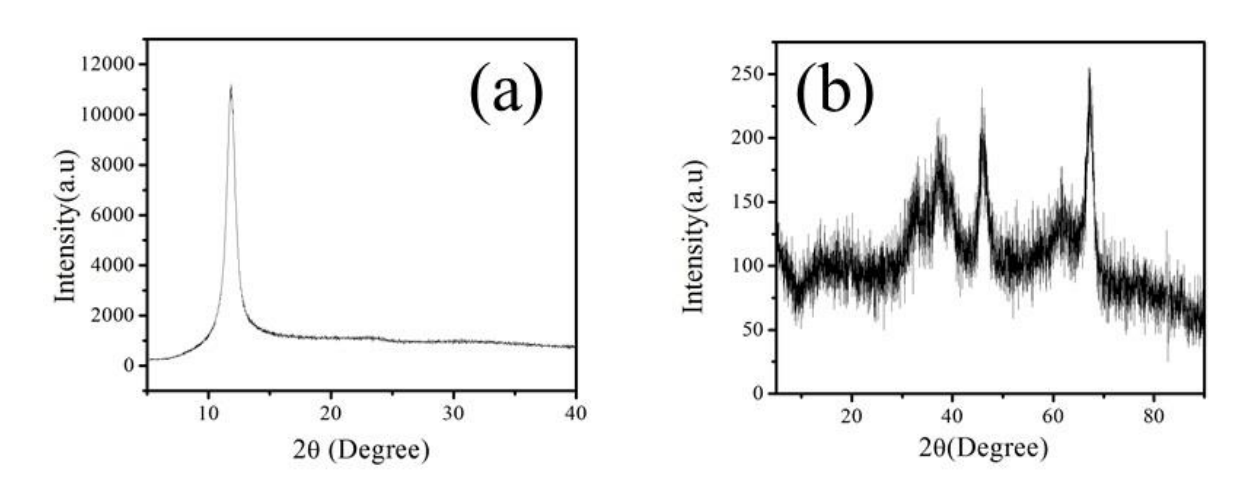


Fig. 5.1 XRD pattern of graphite oxide (a) and (b) nano alumina

Fig. 5.1(a) shows the XRD pattern of graphite oxide. The XRD peak at $2\theta = 12.9^{\circ}$, the interplanar distance is 7.1Å which is greater than graphite interplanar distance(3.3Å). This indicates the nature of oxidation. So that this material contained oxygen functional groups. This material was good

nature of hydrophilic. The Fig. 5.1(b) shows the XRD pattern of nano alumina. More intensity peaks of this material appear at 2θ = 32.5,37.5,45.2,61.5 and 66.7⁰ and corresponding interplanar distances are 2.8,2,4,1.9,1.5 and 1.34Å, the plane of these peaks are (220),(311),(400),(511) and (400) respectively.

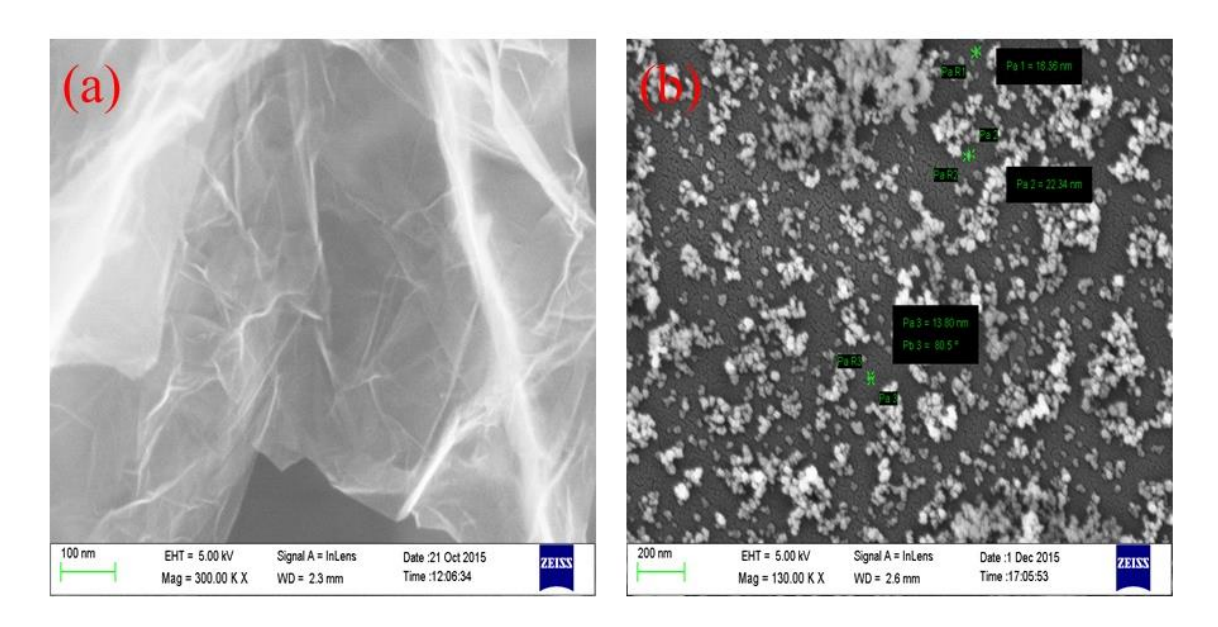


Fig. 5.2 FESEM images of graphene oxide (a) and (b) gamma phase nano alumina.

Fig. 5.2 (a) shows the FESEM image of graphene oxide. The sample was prepared by taking 50mg of graphite oxide dispersed in 50ml of DIW (con.1mg/ml), by 60 min. sonication and then one drop was cast on n-type Si wafer. As shown in Fig. 5.2(a) it clearly shows less folded sheet-like morphology with high transparency. Which indicates the very good quality of graphene oxide. The Fig. 5.2(b) shows the FESEM image of nano alumina, which was prepared, by taking 100mg of nano alumina powder in 50 ml of DIW by 35min. sonication. From that solution, one single drop was cast on Si substrate and then gold coating was done. This image clearly shows the fine nanoparticles indicates the average size, of 13nm with less agglomeration of gamma phase alumina.

Fig.5.3 shows the image of TEM, SAED, HRTEM and FFT profile of HRTEM of graphene oxide. This sample was prepared like the FESEM sample preparation instead of Si substrate using the holy carbon grid. The TEM image shows the large sheet-like, less folding and it appears with very high transparency. Which further indicates that very thin sheet of graphene was formed. The SAED pattern shows the two rings of hexagonal bright diffraction spots. So that the graphene oxide exhibits the graphitic nature. From the HRTEM image as shown in the Fig. 5.3(c),

1-5 graphene layers with interplanar distance is observed by the corresponding the FFT profile showed in Fig.5.3(d), the average the value is 0.52nm .this value less than XRD value because maybe the graphite oxide was dispersed in DIW and sonication cloud be the effect on the exfoliation of the graphene layers. But in the case of XRD sample, we have taken only graphite oxide powder. The SAED pattern clearly shows the two rings of hexagonal structure, which may indicate that the graphene layers are overlapping each other. From the TEM results, the graphene oxide shows the good quality of graphene.

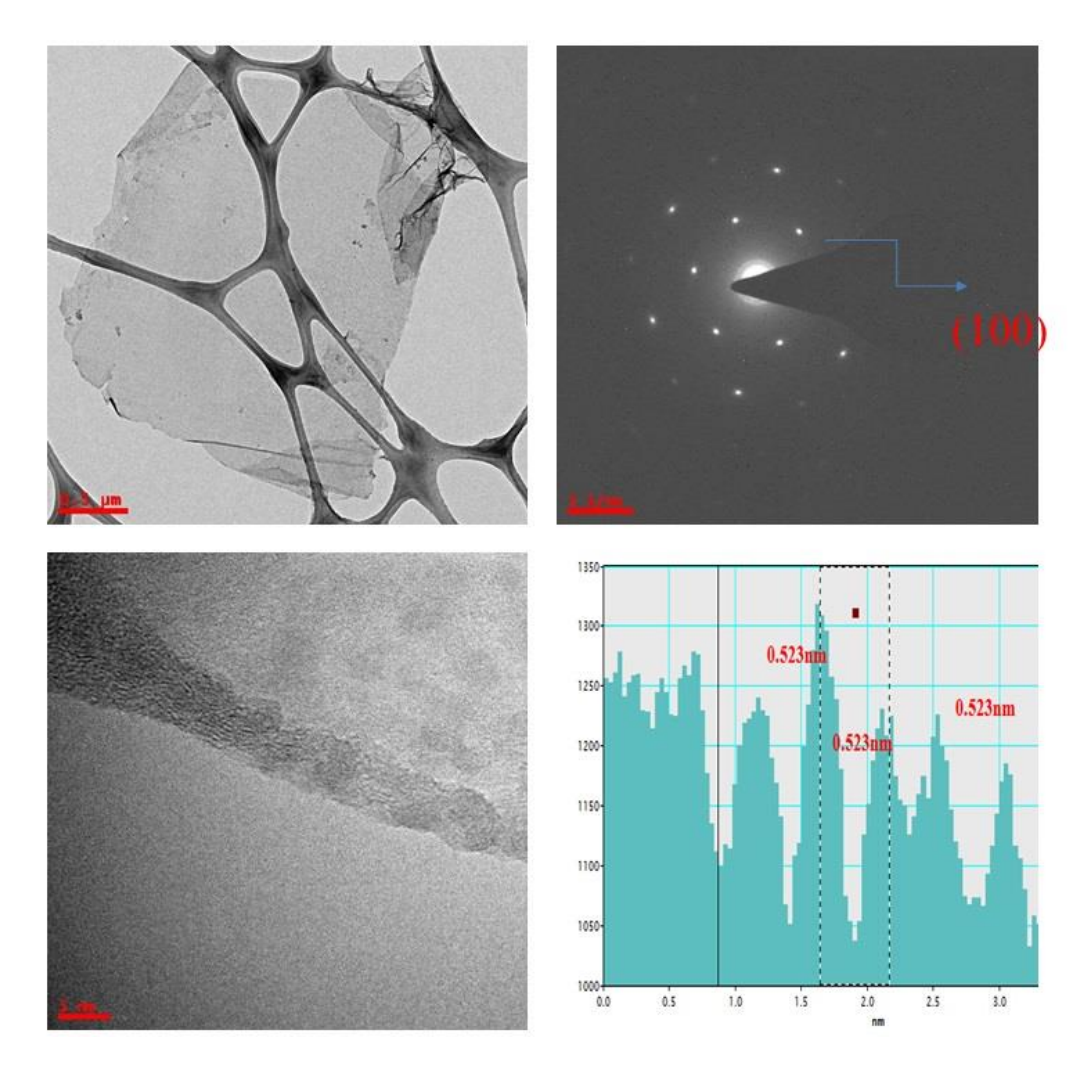


Fig. 5.3. TEM, SAED, and HRTEM images of graphene oxide(GO).

Fig.5. 4 shows the images of TEM, SAED, HRTEM and FFT profile of HRTEM of γ phase nano alumina. The sample preparation was carried out the same way for FESEM sample instead of Si substrate using the Cu grid. The TEM image shows that the γ phase alumina nanoparticles has nearly spherical shape and exhibits in less agglomeration. The SAED pattern clearly shows the polycrystalline nature. In this pattern, the 2^{nd} ring has a bright spot, which indicates the (400) plane.

This plane is identified by the measuring the interplanar distance (d) from the SAED pattern, the obtained value is 0.1916nm and comparison with XRD results, this value all most same.

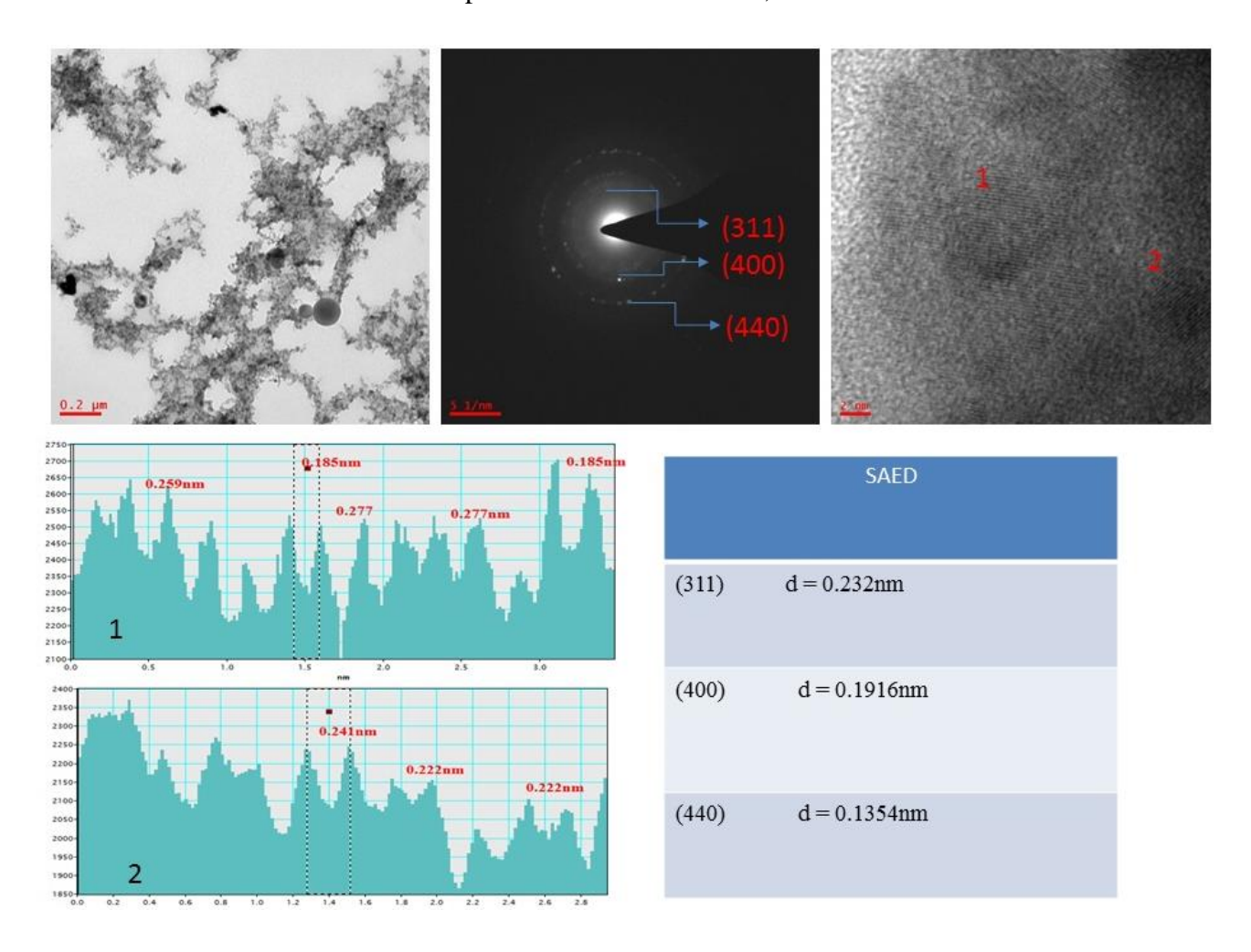


Fig.5. 4. The typical TEM, SAED, and HRTEM images of gamma phase nano alumina (γ -Al2O3).

The 3^{rd} ring of interplanar distance is 0.3154nm which similar to the XRD value. so the corresponding plane is identified as (440) and also measure the d value of the 1^{st} ring from the SAED pattern is 0.232nm. The corresponding plane is (311) and the HRTEM shows the alumina fringes indicated two areas such as the 1^{st} area of FFT showed in the figure, it has interplanar distance is 0.277nm and 2^{nd} area shows the 0.241nm, the corresponding planes are (220) and (311) respectively.

FTIR technically is very useful for identification of bonding of oxygen-related functional groups. Fig. 5.5 (a) shows the FTIR spectrum of graphite oxide, the sample was prepared as a pellet by KBr, for FTIR analysis. The spectrum contains the different oxygen-related functional groups as

shown in Fig.5.5(a). The broad and more intensity peak at 3401cm⁻¹, which corresponds to the –OH groups in the hydroxyl and water of stretching mode of vibrations. The bands at 2925 and 2854cm⁻¹ are related to the CH₂ group family. The sharp peak at 1719cm⁻¹ due to the formation of ketone group of C=O in the carbonyl or carboxyl groups. Very sharp and more intensity peak at 1622cm⁻¹ represents the unoxidized C=C bonds in the skeleton carbon network and also represents the intercalated water molecules of bending vibrations. The band at 1384cm⁻¹ represents the presence of deformed hydroxyl groups and the 1300-1100 cm⁻¹ range represents the carboxyl or ether related groups. The more intense and sharp peak at 1052cm⁻¹ indicates the epoxy or alkoxy functional groups. The presence of these oxygen-related groups indicated the higher level of oxidation for the graphite.

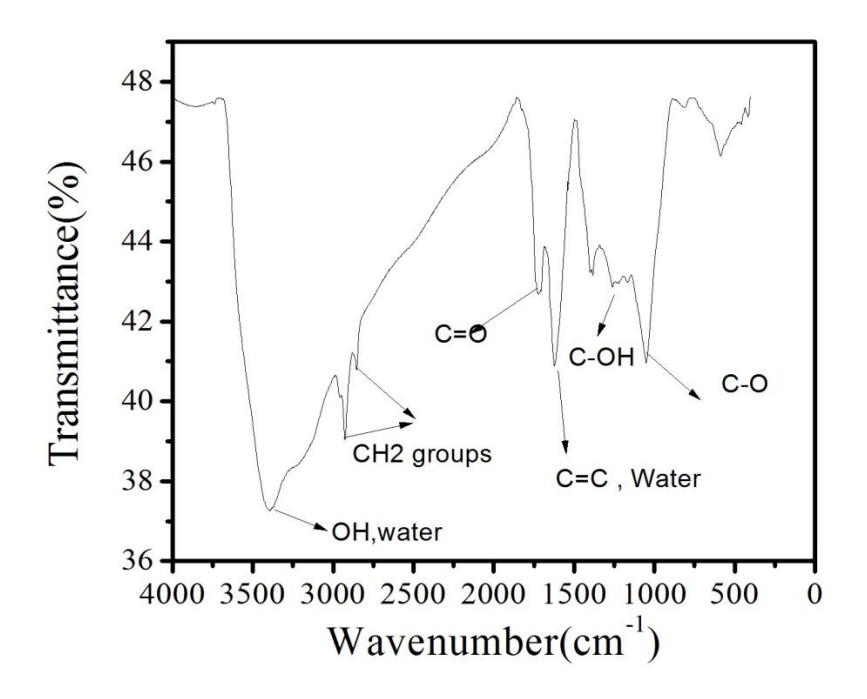


Fig. 5.5 FTIR spectrum of graphite oxide.

Fig. 5.5 shows the FTIR spectrum of alumina nanoparticles. In the spectrum, the sharp and broadband at 3465cm^{-1} indicate the –OH groups of hydroxyl or absorbed water molecules of stretching vibrations. Very small humps are appearing at range $2900\text{-}2800 \text{cm}^{-1}$ due to the CH₂ related groups. Another sharp peak at 1634cm^{-1} indicates the presence of bending vibrations of water molecules, the broad shoulder at 830cm^{-1} represent the tetrahedral sites of AlO₄ and the peak at 554cm^{-1} indicates the octahedral sites of AlO₆. The coordination of tetrahedral and octahedral presence indicates the γ phase nano alumina.

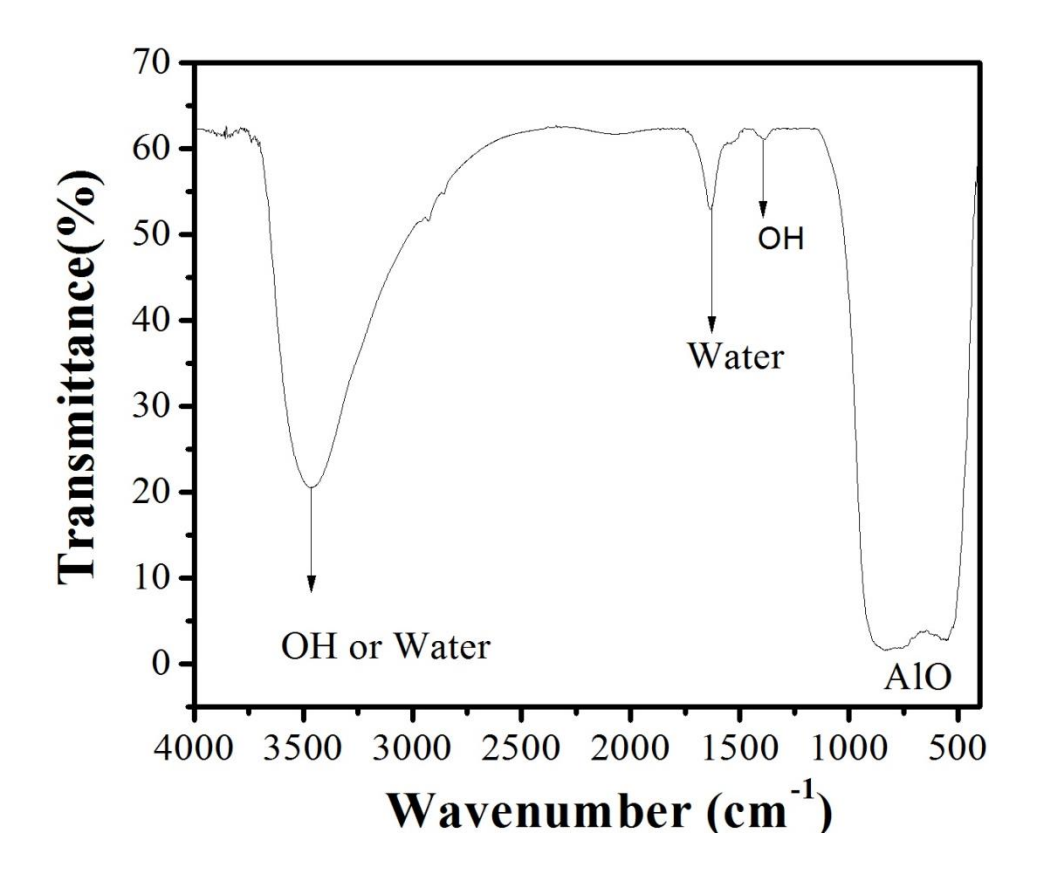


Fig.5. 6. FTIR spectrum of nano alumina.

5.3 preparation of GO/Al₂O₃ nanocomposite

GO/RGO - Alumina nanocomposite was prepared by the colloidal process. In this process, initially GO was dispersed in water by sonication then separately prepared alumina dispersed in water was mixed and mechanically stirring was carried out by varying the parameters such as temperature, additives, different weight percentages and are listed in table 5.1.

A set of six GO/Al₂O₃ nanocomposites were fabricated by different synthesis parameters and are listed in table 5.1. and as follows

- 1) R1 and R2 synthesis variation in **reaction temperature** without using any additives.
- 2) R2 and R3 synthesis for variation in **different weights** without using any additives.
- 3) R4 and R5 synthesis for variation in **different weights with using HCl** using as an additive.
- 4) R2 and R5 synthesis for variation in without HCl and with HCl.
- 5) R5 and R6 synthesis for variation in adding additives are HCl and Hydrazine hydrate.

Table 5.1 Different reaction parameters for synthesis of GO/RGO - Alumina nanocomposite by the colloidal process

| | R1 | R2 | R3 | R4 | R5 | R6 |
|-----------------------------------|-------|------------|------------|--------------------|------------|------------|
| GrO | 50mg | 50mg | 50mg | 1mg | 50mg | 50mg |
| DIW | 50ml | 50ml | 50ml | 20ml | 50ml | 50ml |
| Sonication time | 1h | 1h | 1h | 1h | 1h | 1h |
| | | | | | | |
| Alumina(13nm) | 25mg | 25mg | 50mg | 50mg | 25mg | 25mg |
| DIW | 25ml | 25ml | 50ml | 50ml | 25ml | 25ml |
| Sonication time | 35min | 35min | 35min | 35min | 35min | 35min |
| Ratio of | 2:1 | 2:1 | 1:1 | 1:50 | 2:1 | 2:1 |
| GO:Al ₂ O ₃ | | | | | | |
| Additive | •••• | ••••• | ••••• | HCl | HCl | Hydrazine |
| | | | | | | hydrate |
| Stirring time | 4h | 4h | 4h | 4h | 4h | 4h |
| Reaction | | | | | | |
| temperature | RT | 80^{0} C | 80^{0} C | $80^{0}\mathrm{C}$ | 80^{0} C | 80^{0} C |
| | | | | | | |
| Dried | RT | 80^{0} C | 80^{0} C | 80^{0} C | 80^{0} C | 80^{0} C |
| temperature | | | | | | |

5.4 Structural analysis by XRD:

Fig. 5.6 shows the XRD pattern of GO/Alumina nanocomposite of R1 and R2, as shown in Fig.5.6. Samples exhibit the similar pattern. Peak positions and intensity are same for both samples. So these conditions have no effect on the structure of the nanocomposite. Fig. 5.7. shows the XRD pattern of GO/Alumina nanocomposite of R2 and R3 for variation in weight of the alumina at constant GO without the additive. Comparative each other samples, both samples have same peak positions but the GO peak intensity are different. R3 sample has low intensity than R2 and also alumina peaks intensity more for R3 than R2. Hence, we observed that when the alumina quantity increased the GO peak intensity reduced.

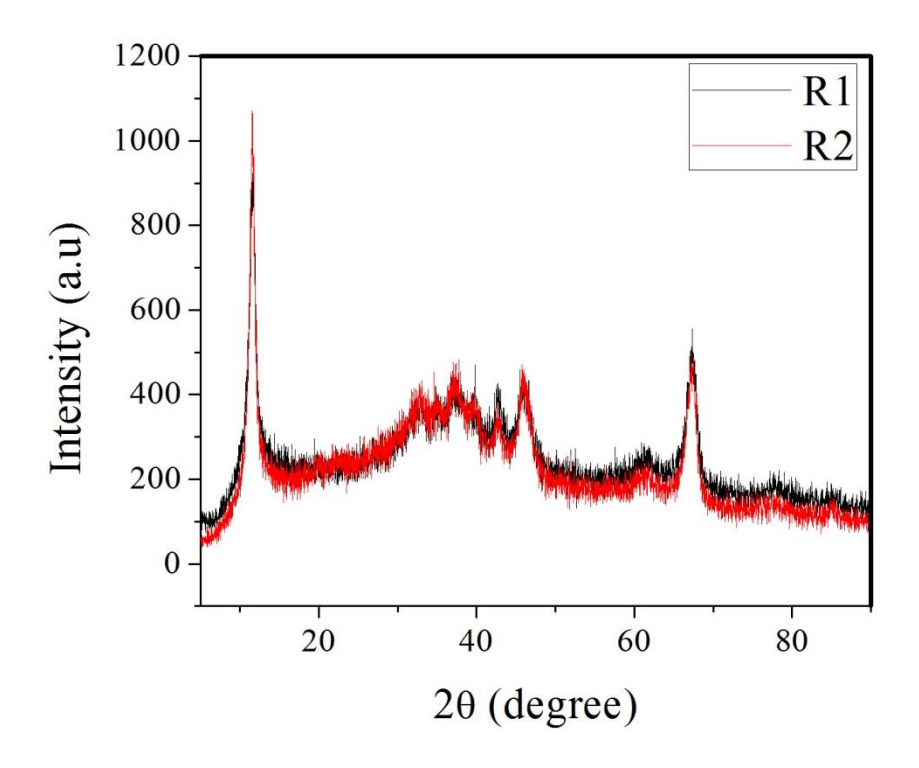


Fig.5.6 Comparative XRD of GO/Alumina nanocomposite of R1 and R2.

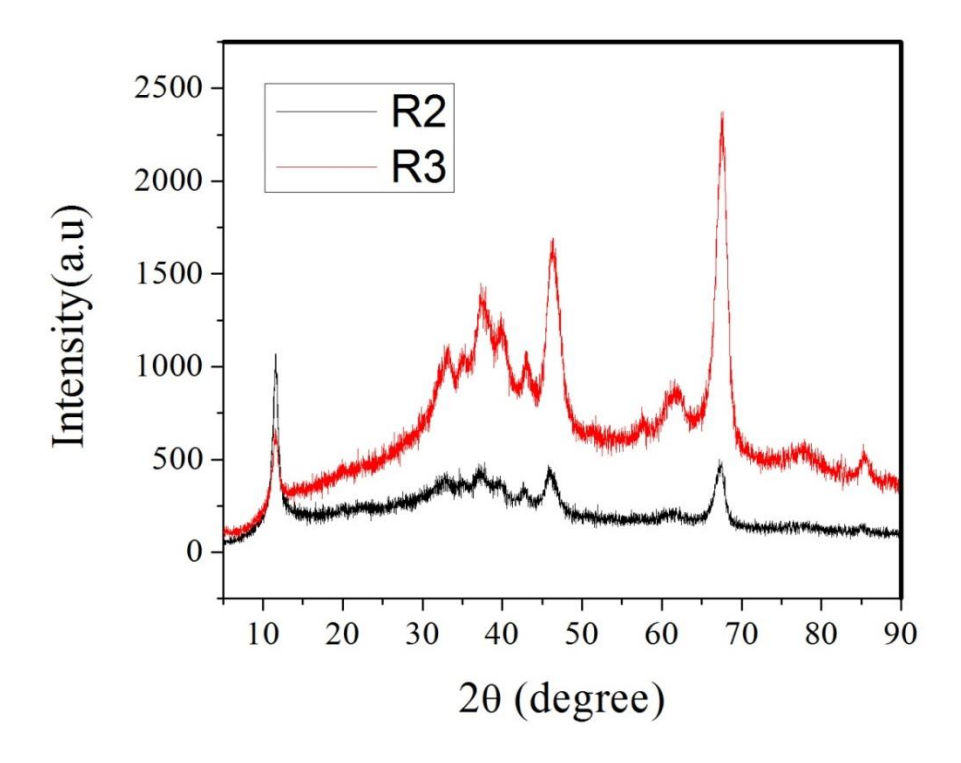


Fig. 5.7. Comparative XRD pattern of GO/Alumina nanocomposite of R2 and R3

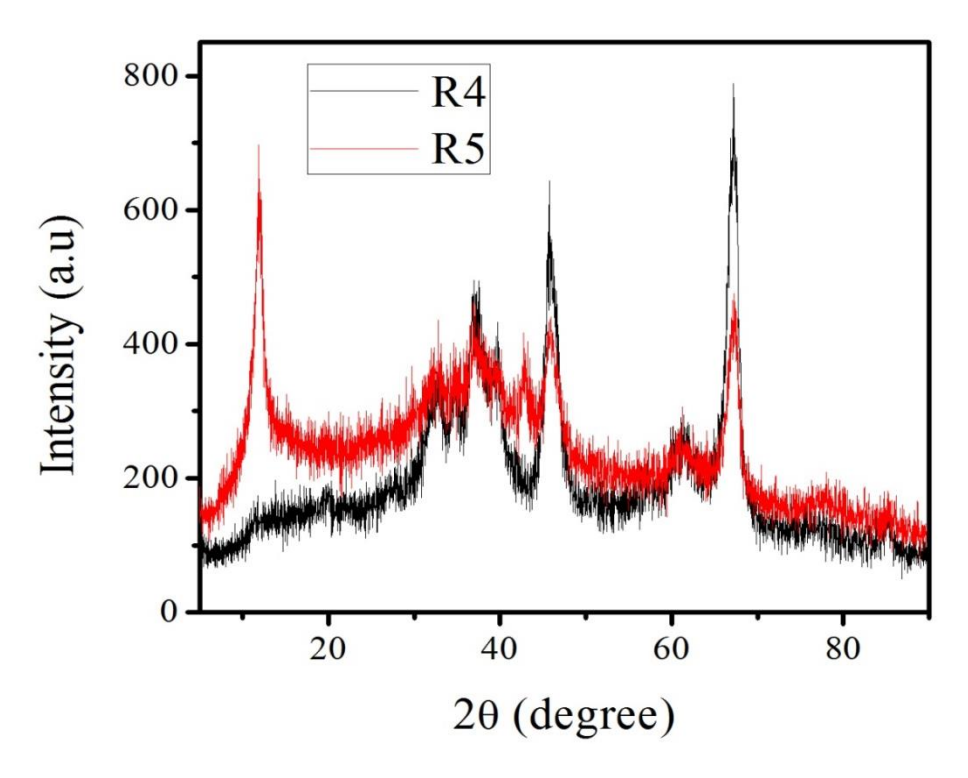


Fig.5.8. Comparative XRD pattern of GO/Alumina nanocomposite of R4 and R5

Fig. 5.8. shows the XRD pattern of GO/Alumina nanocomposite of R4 and R5 varying the different weight % of GO using HCl. R4 sample has very less quantity of the graphene oxide comparative to the R5. R4 sample does not show the GO peak but R5 sample shows the more intense peak of graphene oxide and alumina peaks intensities are high for the sample(R4) than R5. From this results, we concluded that no peak does not alumina –GO appear due to the very small amount was incorporated in the nanocomposite synthesis.that's why GO-peak is dominated by the alumina peaks intensity. The formation of the composite can be further analyzed by Raman, FTIR, and TEM.

Fig. 5.9 shows the GO/Alumina nanocomposite of R2 and R5, these samples are synthesized with 2:1 of GO to alumina nanoparticles and only the variation is that the R2 sample prepared without HCl as an additive and in R5 sample was synthesized by employing HCl as an additive. The spectrum as shown in Fig.5.9 clearly shows the same peak positions and intensity but only the difference in the GO peak intensity of both samples. R2 sample has high intensity than R5. This result indicates that HCl may be reacted with the oxygen functional groups in the GO sample. That's why the GO peak intensity may be reduced. This results will be correlated with the FTIR study in the next section

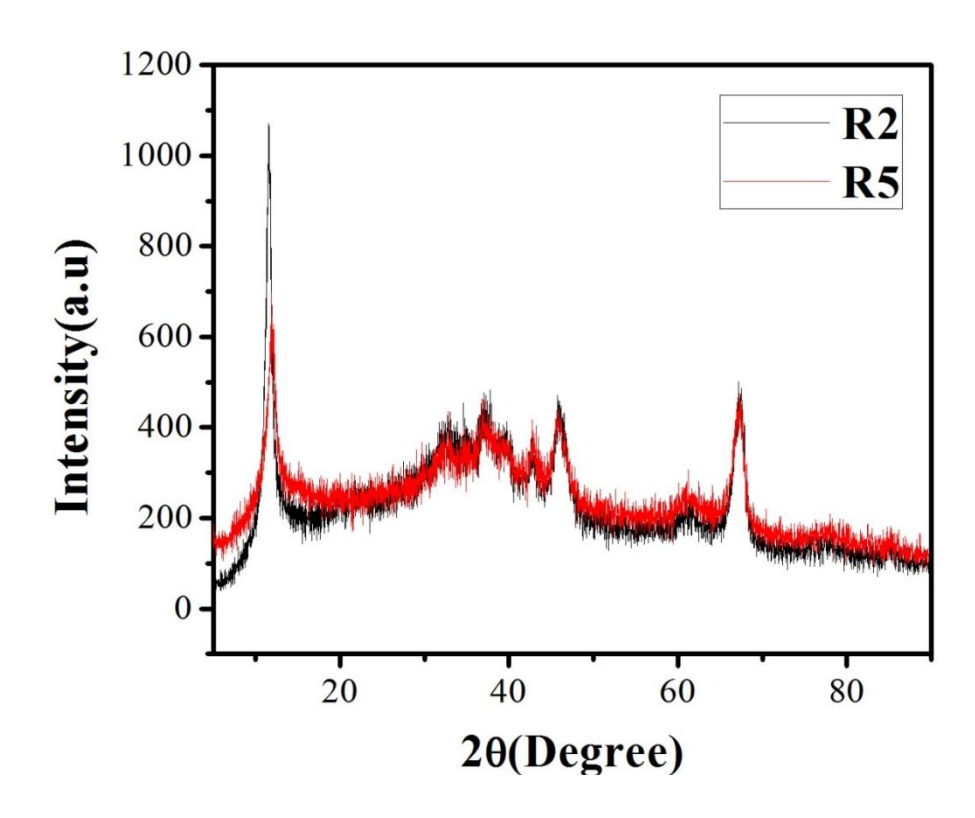


Fig.5.9 XRD pattern of GO/Alumina nanocomposite of R2 and R5

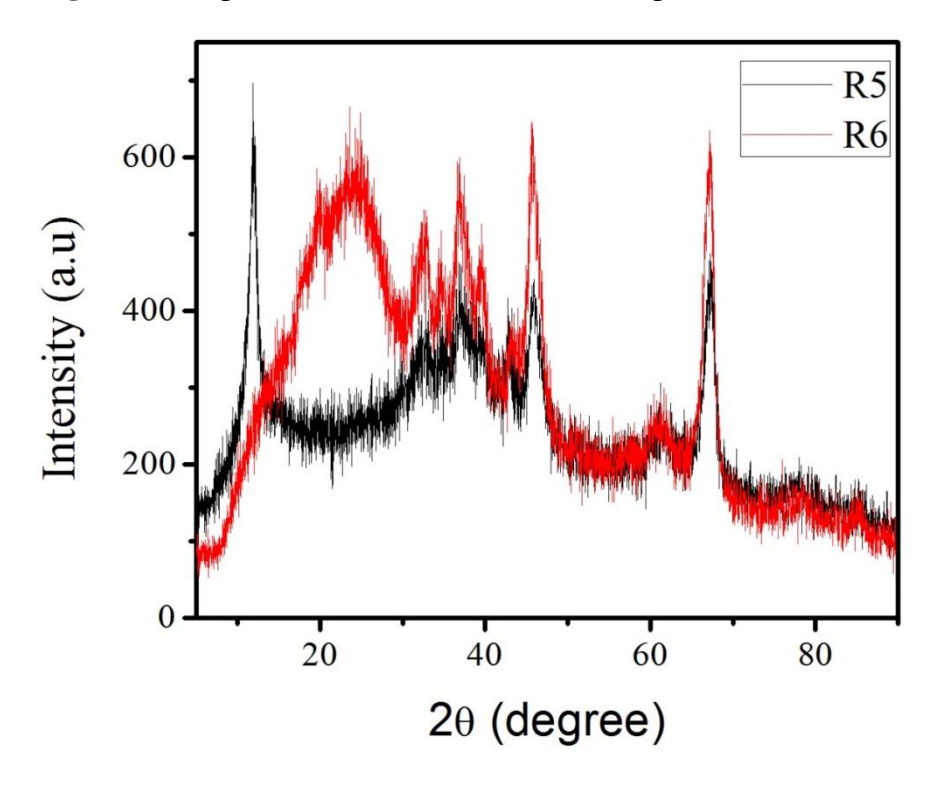


Fig.5.10. XRD pattern of GO/Alumina nanocomposite of R5 and R6

Fig.5.10 shows the XRD pattern of GO/Alumina nanocomposite of R5 and R6 samples. R5 and R6 samples are also synthesized at same synthesis parameters (2:1 ratio of GO and Al_2O_3 nanoparticles) but the additive such as HCl is used in R5 and hydrazine hydrate is used in R6. As shown in

Fig.5.10, the alumina peak positions appear the same way for both the R5 and R6 samples whereas R5 sample shows the graphene oxide peak but R6 sample shows broad RGO peaks. The alumina peaks intensity increases in R6 than R5 sample. Which indicates that some of the oxygen-related functional groups are removed in R6 sample due to the hydrazine hydrate additive. Therefore, from XRD analysis we concluded that only in case of R6 sample reduction occurs and RGO - Al₂O₃ nanocomposite is formed, whereas all other samples are still GO - Al₂O₃ based nanocomposites.

5.5 Bonding characteristics by FTIR

FTIR spectroscopy is a very used full technique to analyze the composite material. By using this technique, we can identify the functional groups such as oxygen-related groups in GO and newly formed bonds in the GO-based nanocomposites. Therefore, all the nanocomposites were analyzed by using the PerkinElmer FTIR in the wave number range 500 – 4000 cm⁻¹. Fig. 5.11 shows the FTIR spectrum of GO/alumina nanocomposite of R1 and R2. Both the samples are synthesized with different temperature, R1 was performed at room temperature (RT) and R2 synthesis was carried out at 80°C by the colloidal process. Both the samples show the mostly same functional groups and little bite change was observed in their band positions. As shown in Fig.5.11 also we observed little variation in their intensity and broadening of the band's properties.

It is observed that these nanocomposite materials have different band positions in comparison to the pure alumina bands and graphite oxide bands, further some bands are absent in the nanocomposite. For instance, C-H related groups at 2925cm⁻¹ and 2855cm⁻¹ are present in GO, but these peaks are absent in both R1 and R2 samples. Further, both GO and alumina does not show any C=O related functional groups but after formation of GO/alumina nanocomposites, these appear. Almost all the bands are 1264,1222 and 1166cm⁻¹ of GO, disappear after formation of the nanocomposite. The band in GO at 1052cm⁻¹ is red-shifted to at 1077cm⁻¹, which is related to Al-O-Al formation or (OH-Al=O) groups and also ketone group(C=O) at 1719cm⁻¹ of GO band completely disappearance after formation of GO/alumina nanocomposites.

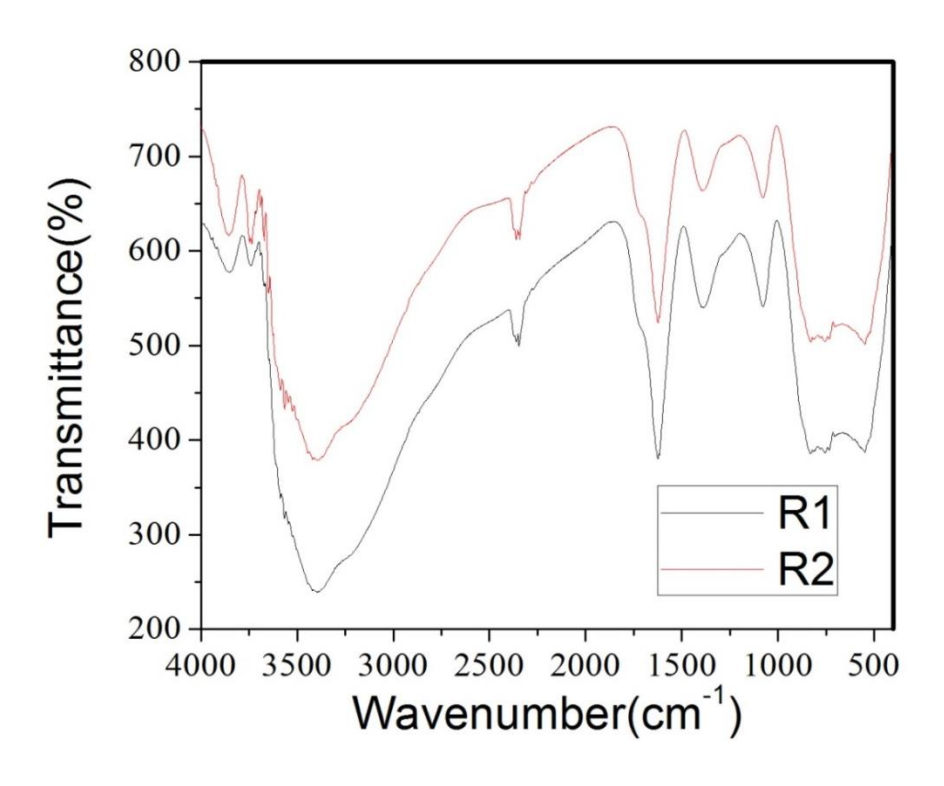


Fig.5.11 FTIR spectrum of GO/Alumina nanocomposite of R1 and R2

Fig. 5.13 shows the FTIR spectrum of R4 and R5 GO-alumina nanocomposite . in these case the band positions of R1 and R2 at 3402 and 3404cm⁻¹ are nearly equal but their peak intensity at 361 cm⁻¹ and 1258cm⁻¹ of R1 and 267 cm⁻¹ and 1134cm⁻¹ of R2 not same. The peak intensity decreasing and broadening may be due to the less presence of hydroxyl group or water molecules appear in R2 than R1, this may happen due to the different reaction temperature. CO₂ molecules band position at 2348cm⁻¹ for R1 and 2349cm⁻¹ for R2, and appears at 37 cm⁻¹ and 75cm⁻¹ for R1 and 45 cm⁻¹ and 82cm⁻¹ for R2 respectively. So R2 has more formation of CO₂ than R1. The band position at 1623cm⁻¹ is same for both the samples, R1 has a peak intensity at 248 cm⁻¹ and is 323cm⁻¹ and R2 has 205 cm⁻¹ and 342cm⁻¹. These band positions indicate the C=C and bending of the water molecules. The intensity of these peaks decrease in R2 sample represents that water molecules may be removed as compared to R1. The band's position appears at 1387 cm⁻¹ and 1383cm⁻¹ for R1 and R2, it is seen that a little bit peak shift but this range represents the deformation of OH bonds. The peak intensity and broadening at 85 cm⁻¹ and 148cm⁻¹ for R1 and 68 cm⁻¹ and 153cm⁻¹ for R2, show that the intensity decreases more for R2 than R1. The band positions appear at 1077 cm⁻¹ and 1076cm⁻¹ of R1 and R2 indicate the (OH)-Al=O asymmetric bends or Al-O-Al bond due to the symmetric bend modes. The intensity and broadening of the peaks at 72 cm⁻¹ and 158cm⁻¹ for R1, and 59 cm⁻¹ and 131cm⁻¹ for R2. Indicates that the peak intensity decreases more in R2 due to the different reaction temperature. The tetrahedral sites AlO4 intensity is more in R2 than R1 sample. From the XRD results of R1 and R2, it is seen that both samples show the similar intensity and same peak positions, here XRD is not very efficient to study the functional groups, and thus FTIR spectroscopy is more significance for the study, further, we can measure the bond and bond interaction i.e the functional groups interaction more clearly by the broadening of the peak.Fig.5.12 shows the FTIR spectrum of R2 and R3 GO-alumina nanocomposite. Both the samples are synthesized without additive and different wt% of alumina nanoparticles, R2 has more go wt% than

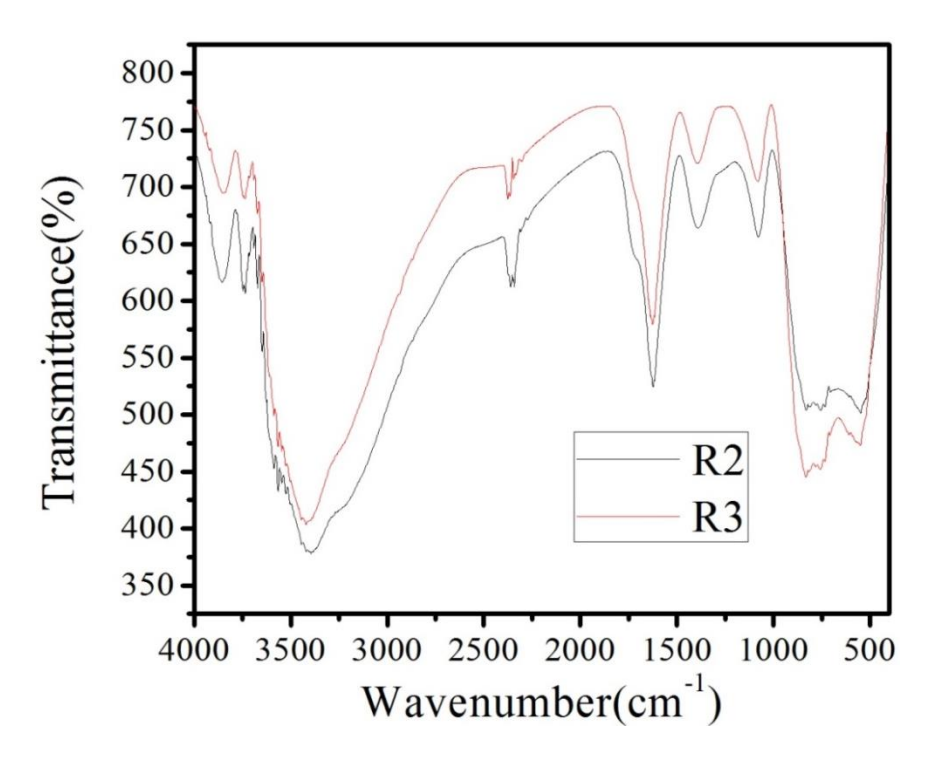


Fig. 5.12. FTIR spectrum of GO/Alumina nanocomposite of R2 and R3

R3 sample.therefore, these samples show different of OH and water molecules at 3404 cm⁻¹ and 3412 cm⁻¹ for bands. Both samples have same band position at 2349cm⁻¹ with different intensity, the intensity of R2 > R3 and broadening are also increased. The band at 1623cm⁻¹ is same for both the samples. The Al-O-Al band at 1076cm⁻¹ is same for R2 and R3 with little different intensity and broadening, R3 sample has more intensity and broadening comparative to R2 and also AlO₄ site intensity is also increased in R3 than R2. Because the GO content is more in R2 sample. We have used HCL as an additive and different weights of GO (1:50 for R4 and 2:1 for R5), these samples show different band position and also newly bands appear in FTIR spectra as shown in Fig.5.13. R4 sample contains very less quantity of graphene oxide than R5. R4 has a band at 3444cm⁻¹ and R5 has a band at 3392cm⁻¹ so these samples contain different OH and water molecules. Both samples

show same band position at 2354 cm⁻¹ for CO₂ with different intensity peak brooding. R4 sample band position at 1400cm⁻¹ indicates the carbon-hydrogen (CH₃),-carbon(C-C) and –Oxygen (C=O) deformation, and R5 shows a band position at 1388cm⁻¹ which indicates the OH deformation groups. R4 shows a band at 1639 cm-1 and R5 shows a band at 1615cm—¹. The intensity of the peak at 1264 and 1051cm⁻¹ corresponds to GO peaks. R5 shows a band at 1082cm⁻¹ which is related to the Al-O groups. Band of AlO₄ intensity is more for R4 than R5 sample.

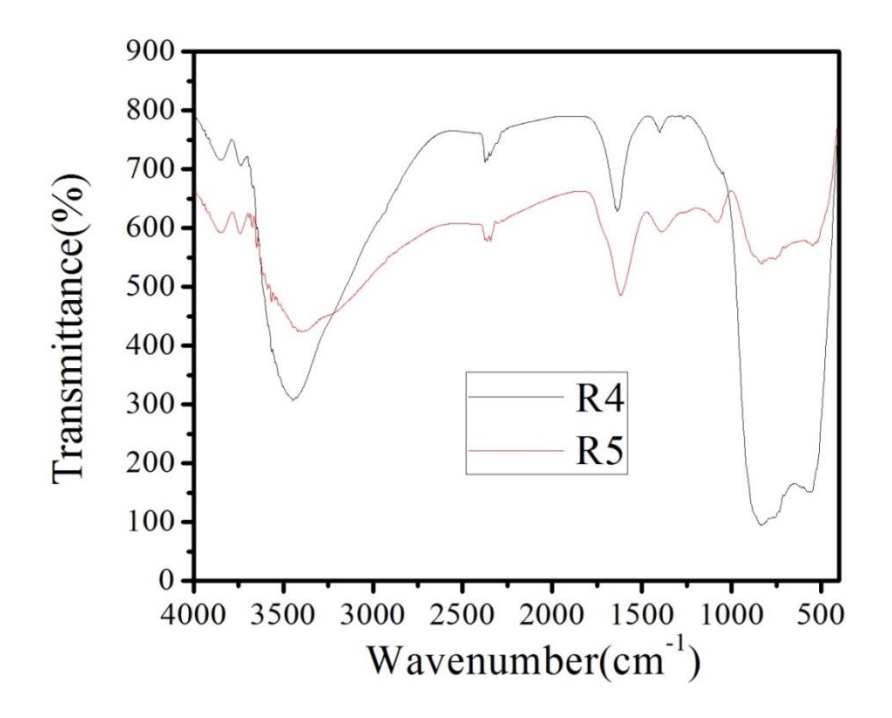


Fig. 5.13. FTIR spectrum of GO/Alumina nanocomposite of R4 and R5

Fig. 5.14 shows the FTIR spectrum of GO/alumina nanocomposite of R5 and R6. For HCl was used as an additive for R5 and hydrazine hydrate as an additive for R6, with same ratios of GO and Al₂O₃ nanoparticles, these two samples show the different bond formation also some of the new bands appear. R6 shows the removal of hydroxyl and water molecules due to the disappearance of the peak at 3401 cm⁻¹ in comparison to R5 sample. R5 sample shows the intensity and broad peak at 3392cm⁻¹. The band at 1623cm⁻¹ is not present for the R6 samples and a newly formed peak appears at 1546cm⁻¹ which is a C=C bond. And does not contain any oxygen-related groups. Both the

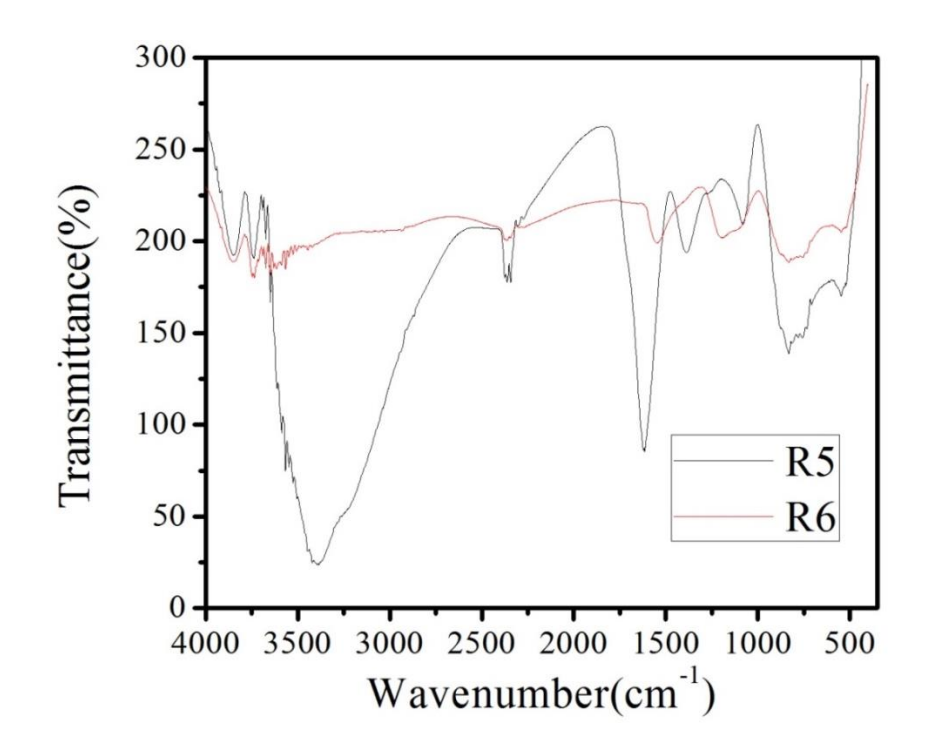


Fig. 5.14. FTIR spectrum of GO/Alumina nanocomposite of R5 and R6

samples show peak positions at 1615 cm⁻¹ and 1082 cm⁻¹. The peak at 1082 cm⁻¹ is not present in the R6 which indicates that OH related groups are completed remove. The peak intensity of the AlO4 of the R6 sample is similar to the alumina. Therefore RGO-Al2O3 nanocomposite formation happened only for the R6 sample which is synthesized by using hydrazine hydrate as an additive.

5.6 Morphology analysis by FESEM

FESEM is an analytical tool for identification of morphology of the materials. Fig.5.15 shows the FESEM images of GO/alumina for R1, with different magnification. As shown in Fig. 5.15, the alumina nanoparticles are attached to the graphene oxide sheet very uniformly. Because the alumina nanoparticles interact with the oxygen functional groups present in the GO.

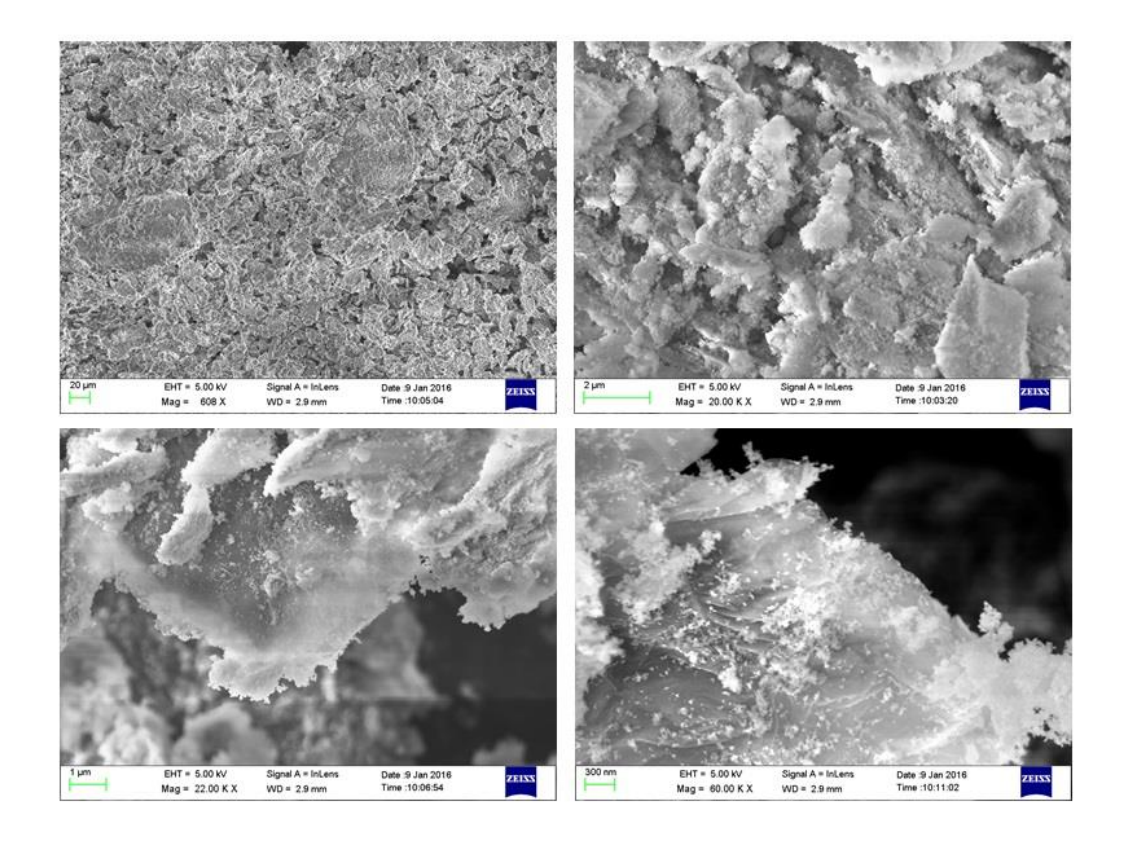


Fig. 5.15 shows the FESEM images of GO/Alumina nanocomposite synthesis at room temperature (R1).

Fig.5.16 shows the FESEM images of the GO/Alumina composite synthesis at 80°C (as shown in table 5.1) with different magnification images. As it is seen from Fig.5.16, that the alumina nanoparticles are embedded with the graphene oxide sheets. In this case, the graphene oxide sheets are more transference than R1 sample.

Fig. 5.17 shows the different magnification FESEM images of GO/Alumina composite (R5) synthesis at 80°C in the presence HCl as an additive. The low magnification image shows the bulk graphene flake with alumina nanoparticle. At medium magnification image shows the graphene oxide sheets completely covered with alumina nanoparticles and the high magnification image shows the alumina nanoparticles are situated on the graphene oxide sheet.

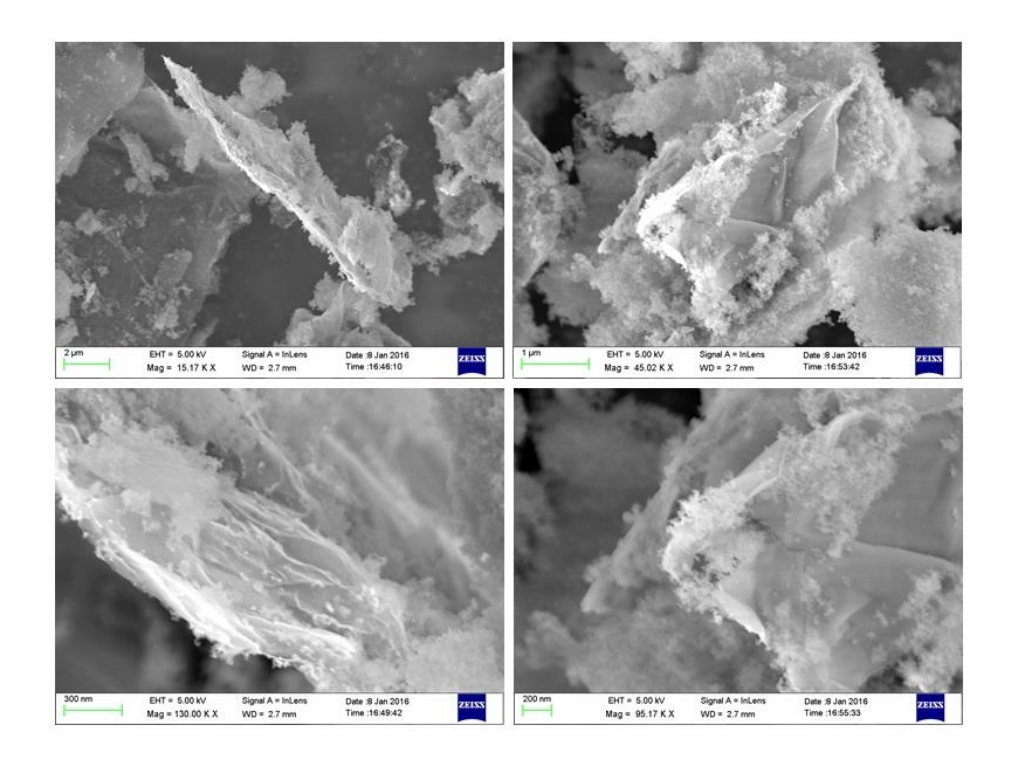


Fig. 5.16. shows the FESEM images of GO/Alumina nanocomposite synthesis at 80°C (R2)

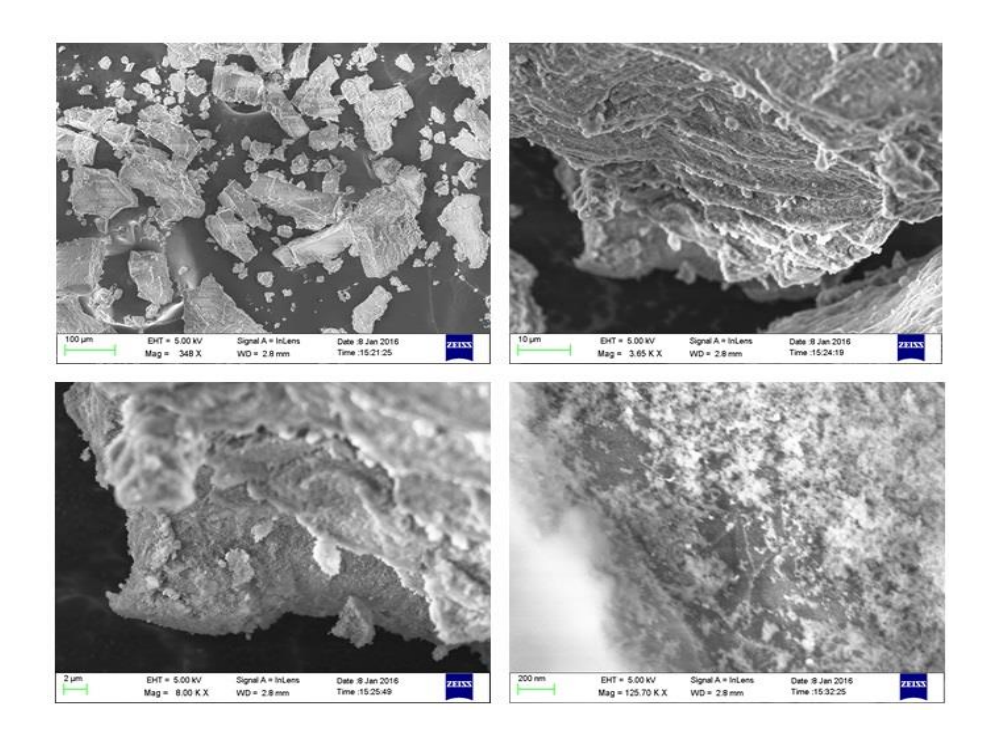


Fig.5.17. shows the FESEM images of GO/Alumina nanocomposite synthesis in the presence of additive as HCl at 80° C (R5).

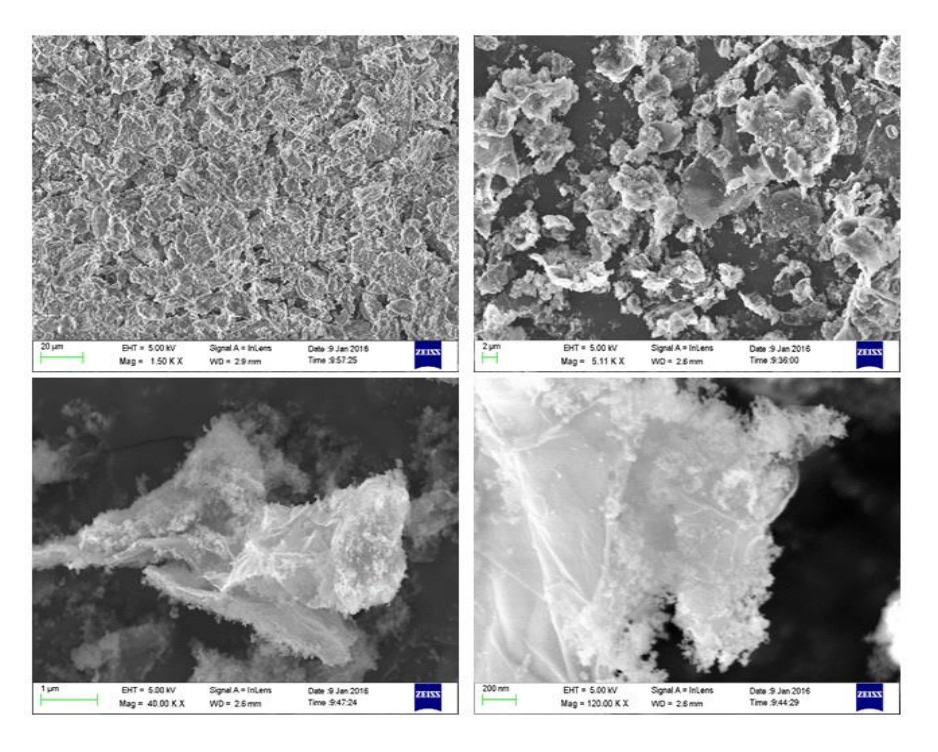


Fig.5.18.The FESEM images of GO/Alumina nanocomposite synthesis in the presence of additive as Hydrazine hydrate at 80°C (R6).

Fig.5.18 shows the different magnification FESEM images of GO/Alumina nanocomposite prepared in the presence of hydrazine hydrate as an additive at 80°C and the sample indicated as R6. This sample shows high transference than other samples. Because of reduction of GO to RGO. This sample indicates that a number of alumina nanoparticles are bonded to the graphene sheets uniformly, therefore FESEM analysis suggests that different morphological GO – Al2O3 and RGO - Al2O3 nanocomposite are synthesized by varying the reaction temperature and additives during the synthesis.

5.7 TEM analysis of the nanocomposite

Transition Electron Microscopy(TEM) can be used to gain more information about the structure and morphology of the materials. It can be very useful to identify the composite materials. All the nanocomposites are analyzed by using a TEM at 200KV acceleration voltage and bright field images were taken.

Fig.5.19 shows the TEM, HRTEM images and SAED pattern of the GO-alumina composite R1 for this purpose 1mg GO – Al2O3 nanocomposite was dispersed in 20ml of DI water and sonicated for one hour. Then one drop of the solution was cast on a lacy carbon grid and dried at 80°C on a hot

plate. As shown in Fig.5.19, the alumina nanoparticles are attached to the graphene oxide sheet. The HRTEM of the corresponding the TEM images contains the fringes of alumina and graphene oxide. In the HRTEM image, we had select two areas as area1 and area2 and calculated the interplanar distance (d) between two fringes by using fast Fourier transformation (FFT) profile as shown in

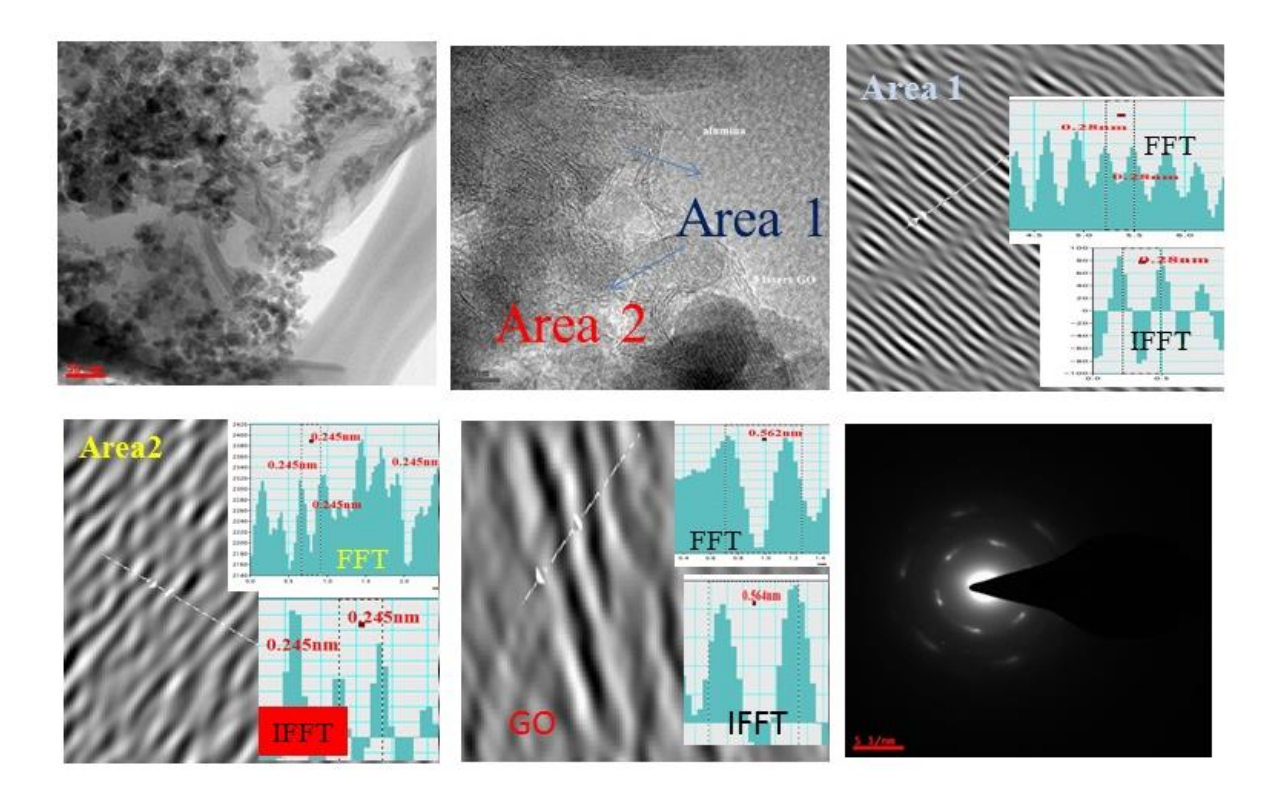


Fig.5.19 TEM images of GO-alumina nanocomposite of R1.(a) TEM image, (b) HRTEM image, (c) FFT, (d) IFFT, (e) SAED pattern of the R1 sample

Fig.5.19(c) and inverse fast Fourier transformation(IFFT) profile (Fig.5.19 (c)). We obtained the interplanar distance for area1, the value is 0.28nm and from the IFFT, the value is 0.28nm. hence, area1 in the figure 5.19 (b) corresponding to the γ phase alumina and agreed with the XRD data, d = 0.28nm. the corresponding plane is (220) at $2\theta = 32.4^{\circ}$, this is alumina peak. For area 2 interplanar distance from FFT, is 0.245nm and IFFT, d value is 0.245nm. this value indicates the (311) plane for γ alumina. In the HRTEM image, we choose the three layers of graphene oxide and the corresponding IFFT showed in the figure and obtained interplanar distance is 0.564nm and from the

FFT profile, d is 0.662 nm, which is less than as obtained from XRD data, this may be due to the graphene oxide formation of fewer layers comparative to the graphite oxide (in powder form). The

SAED pattern shows two rings with hexagonal diffraction bright spots. This indicates the good

quality of graphene oxide. In this image between two rings on the ring is also observed with fewer intensity spots of the polycrystalline ring which belongs to the alumina particles. Therefore, we concluded that the alumina nanoparticles interact with the oxygen functional groups present in the GO. Thus, TEM analysis indicates the formation of the GO- γ phase alumina nanocomposite.

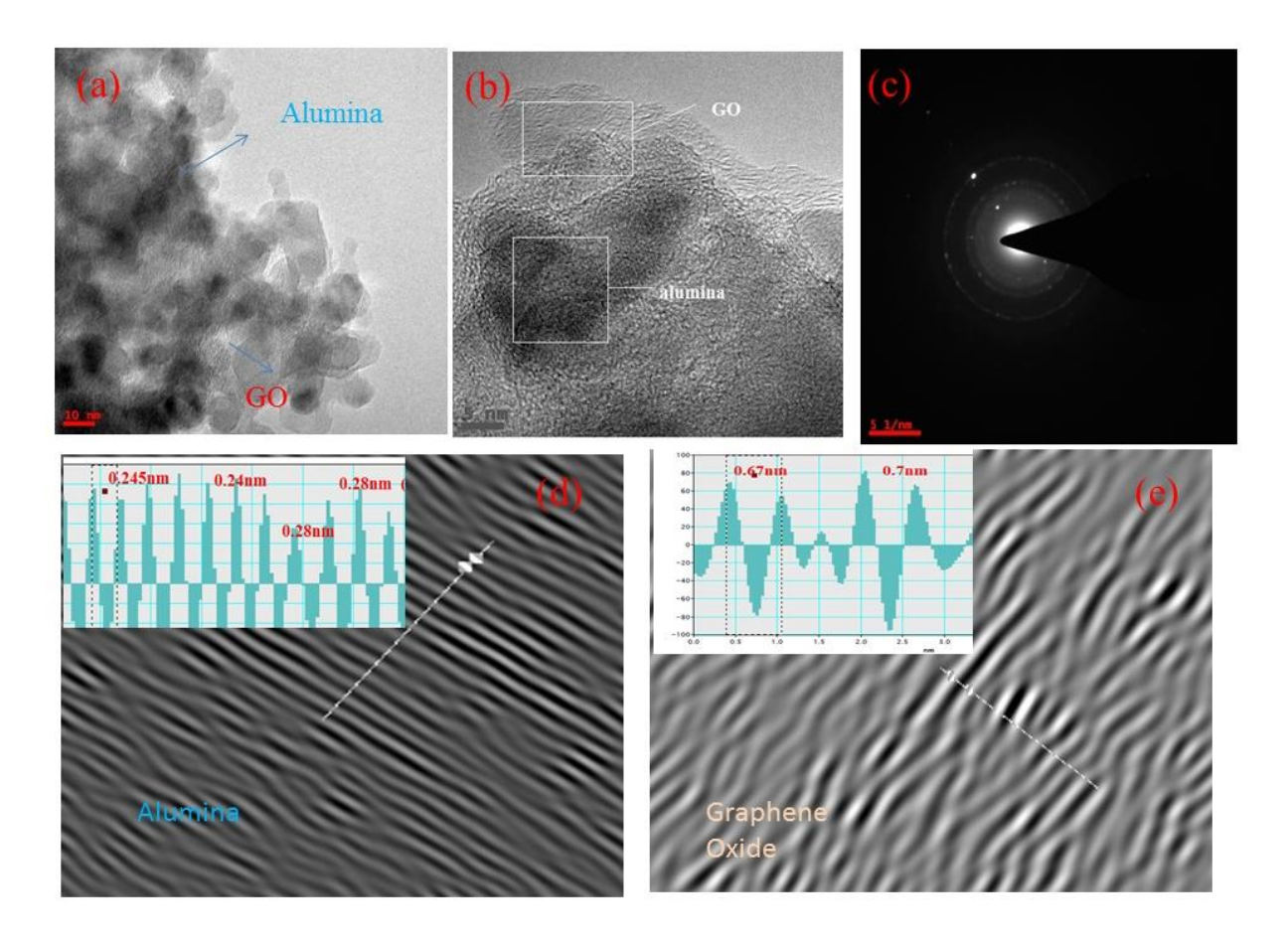


Fig. 5.20 TEM images of GO-alumina nanocomposite of R2.

Fig. 5.20 shows the TEM, HRTEM and SAED pattern of the R2 sample synthesis at 80° C without additive, this sample preparation is carried same way R1 sample discussed above. As shown in Fig.5.20, the alumina nanoparticles are embedded in graphene oxide sheets. And the graphene oxide fringes can be identified. Further, the alumina nanoparticles are more agglomerated than the R1 sample. The Fig.5.20 (b) shows the HRTEM of the corresponding TEM image. In this image, we have chosen two distinct areas and taken corresponding the IFFT profile as shown in the Fig.5.20 (d) and (e). the interplanar distance is nearly 0.7nm, this value coincided with XRD results and confirmed the GO. Another area, the fringes contain two types of interplanar distance such as d= 0.245nm and 0.28nm, those are γ phase alumina with (311) plane and (220) respectively. The Fig.5.20 (c) shows the SAED pattern of R2 sample, it appears as ring pattern with a light intensity

of diffraction spots. The ring pattern indicates the disordered present in the sample. The HRTEM clearly shows the graphene oxide fringes those are more disorder. This disorder may occur due to the high-temperature reaction and also due to the particles are mostly agglomerated. In the nanocomposite as shown in Fig.5.20 (a) .

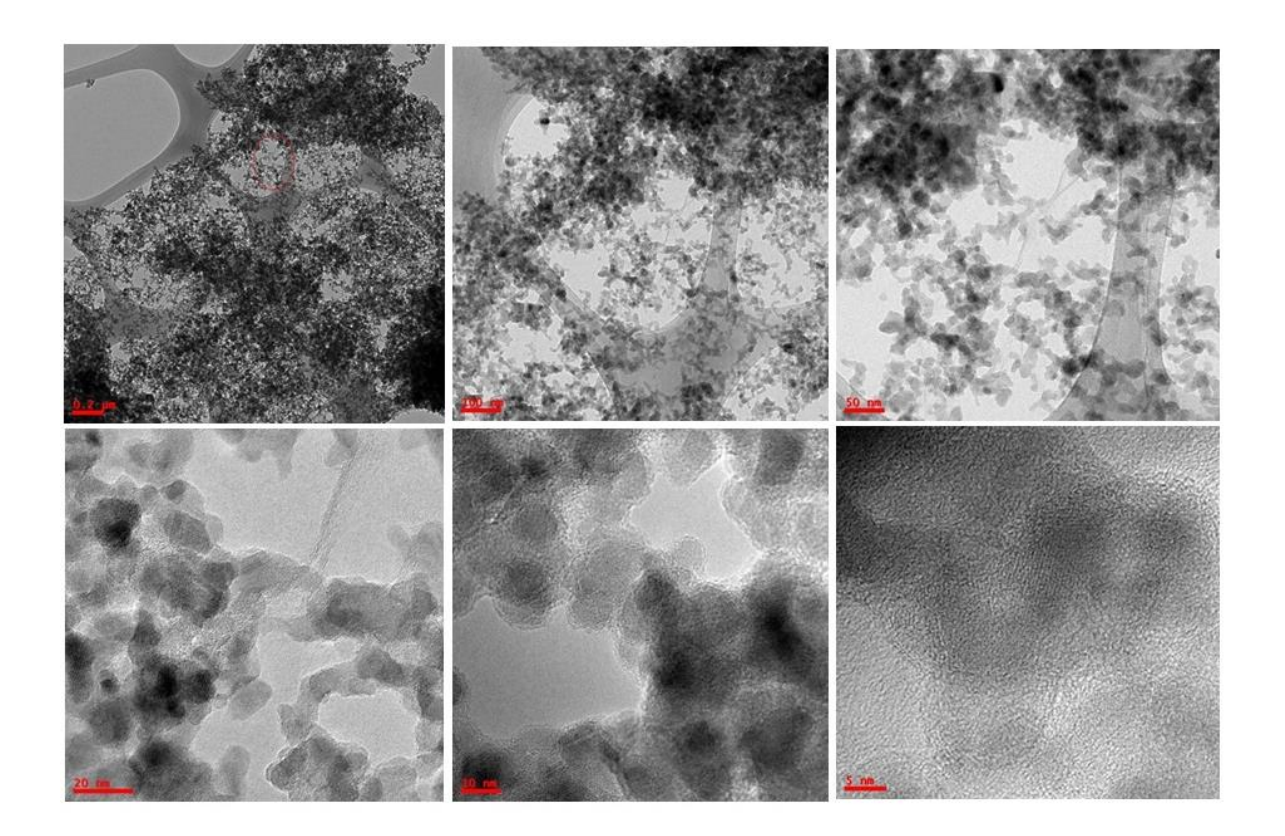


Fig.5.21 TEM images of GO-alumina nanocomposite of R3.

Fig.5.21 shows the different magnification images of TEM for the R3 sample, this sample preparation also same as mention the previous sample above. As shown in Fig.5.21 more alumina nanoparticles appear with very less GO content in the nanocomposite. In the higher magnification image as shown in Fig.5.21 (e and f), graphene oxide sheets are observed in the background of alumina nanoparticles and also clearly indicates the mixing of alumina nanoparticles with graphene oxide sheet. In the HRTEM image, as shown in Fig.5.21 (f) the graphene oxide fringes are appeared around the alumina nanoparticles. which indicates that the alumina nanoparticles are attached to the graphene oxide sheet. TEM analysis concludes that alumina nanoparticles are not sitting on the graphene sheet, but are bonded to each other by the covalent or electrostatic forces.

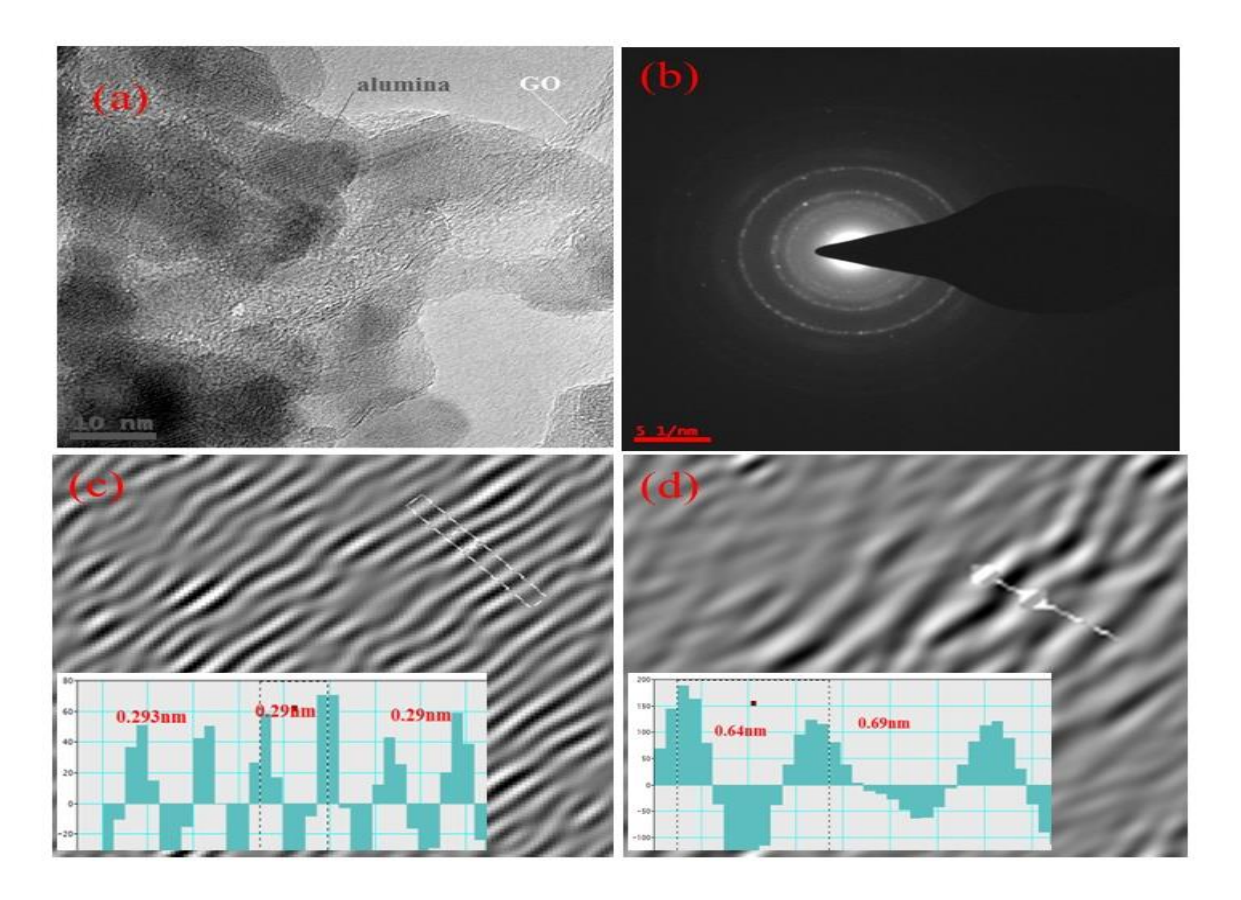


Fig. 5.22 TEM images of GO-alumina nanocomposite of R3.

Fig. 5.22 shows the HRTEM, SAED, and IFFT of HRTEM images of sample R3. As shown in Fig. 5.21 fine fringes of alumina and graphene oxides are clearly observed. The corresponding IFFT images as shown in Figure (c) and (d) respectively. The IFFT profile of alumina indicates the interplanar distance (d) is 0.29nm which is nearly equal to the (220) plane of γ phase of the nano alumina. The interplanar distance of graphene oxide is calculated by IFFT profile Fig.5.22(d), and value of d= 0.66 nearly. It confirmed that the GO/ γ phase alumina nanocomposite is formed. The SAED pattern shows the ring pattern, which indicates the disorder of the graphene sheets and alumina nanoparticles may be randomly attached to GO sheets.

Fig. 5.23 shows the TEM, HRTEM images and SAED pattern of the GO/alumina composite of R4. As shown in the Fig.5.23 (a) alumina nanoparticles are embedded in the graphene oxide sheets. From SAED pattern (Fig. 5.23 (b)), the diffraction pattern is clearly seen that indicates sample is polycrystalline nature. Fig. 5.23 (c) shows the HRTEM image, this image indicates the alumina fringes and graphene oxide fringes. Fig. 5.24 shows the TEM, HRTEM, SAED and IFFT profile of HRTEM image for R5. This sample was synthesized in the presence of HCl as an additive and reaction temperature at 80°C. as shown in Fig.5.24, the alumina nanoparticles are attached to the

graphene oxide sheet. This sheet appears as the highly transference and alumina nanoparticles are agglomerated as shown in Fig.5.24 (a). Fig.5.24 (b) HRTEM image clearly indicates the

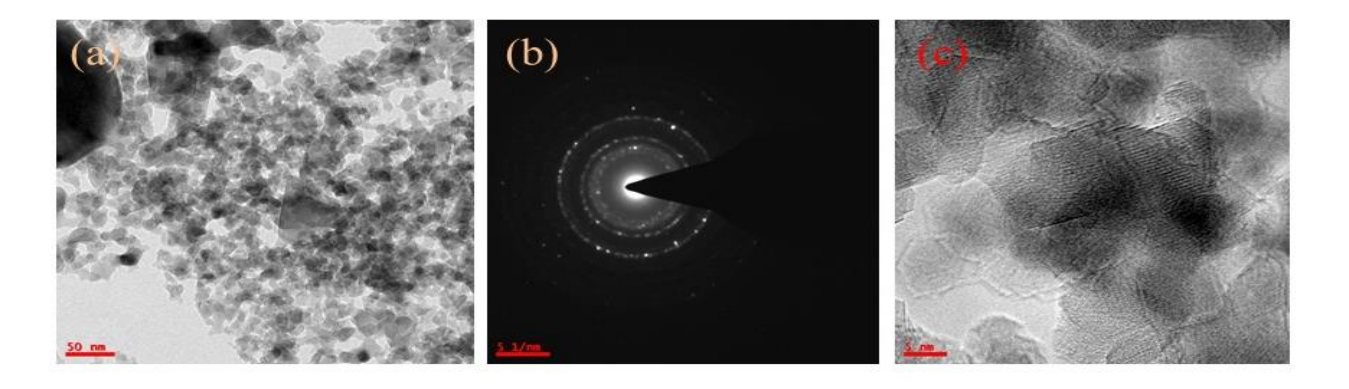


Fig. 5.23 TEM images of GO-alumina nanocomposite of R4

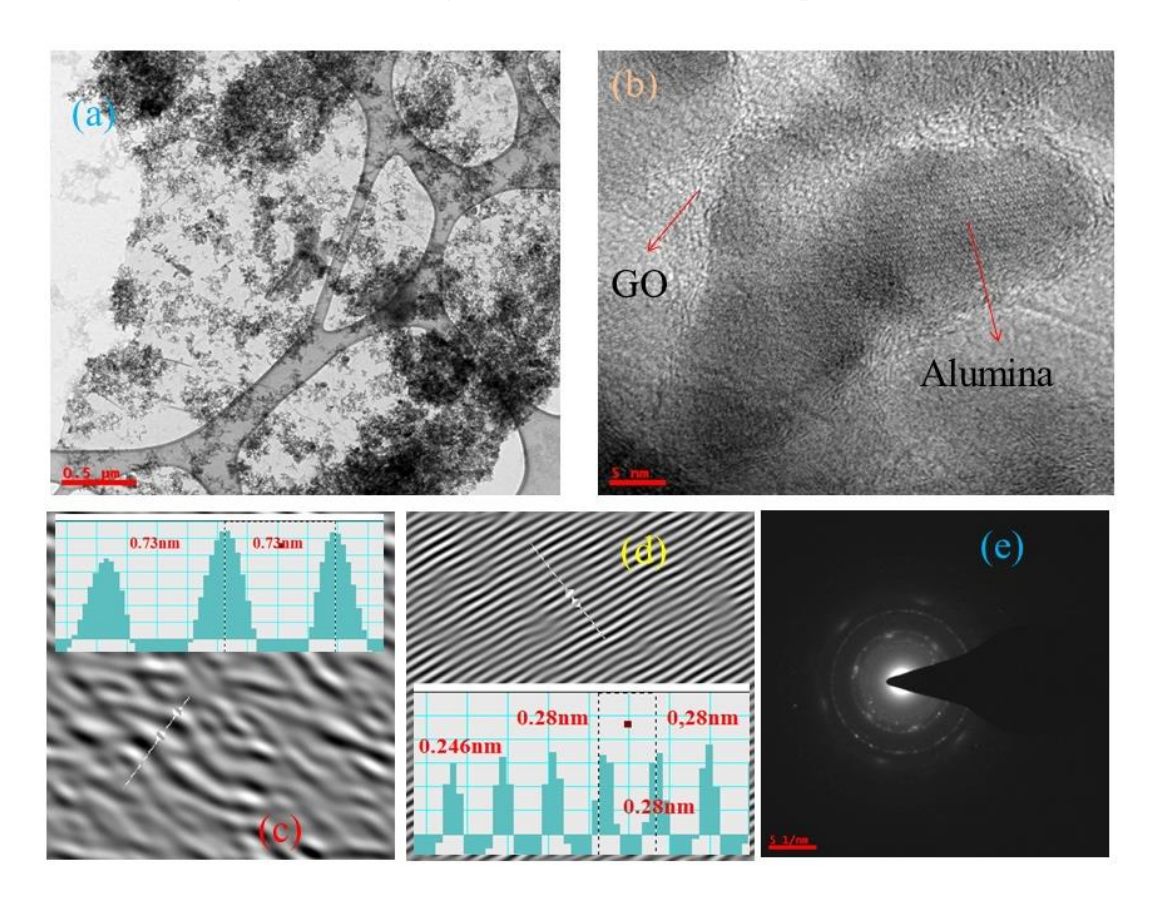


Fig. 5.24. TEM images of GO-alumina nanocomposite of R5

graphene oxide fringes and alumina nanoparticles. We observed that in the HRTEM image, around the nanoparticles graphene oxide fringes are present and hence looks like a core cell. In the HRTEM image, we have taken the IFFT profiles for the alumina and graphene oxide as indicated areas in Fig. 5.24 (c) represent the IFFT profile for the GO, as discussed in the, we observed the interplanar distance (d) is 0.73nm which is more than XRD results. Fig. 5.24 (d) indicates the HRTEM image of

IFFT for alumina nanoparticles, from this profile calculated interplanar distance (d) values, are 0.246nm and 0.28nm and the corresponding planes are (311) and (220) of γ phase nano alumina. The Fig. 5.24 (e) shows the SAED pattern of the sample R5, it clearly shows the formation of hexagonal diffraction spots with low intensity. Also, we have observed the alumina ring pattern. So in comparison with the previous sample, this sample has less disorder. TEM results evidence the formation of the GO/alumina nanocomposite.

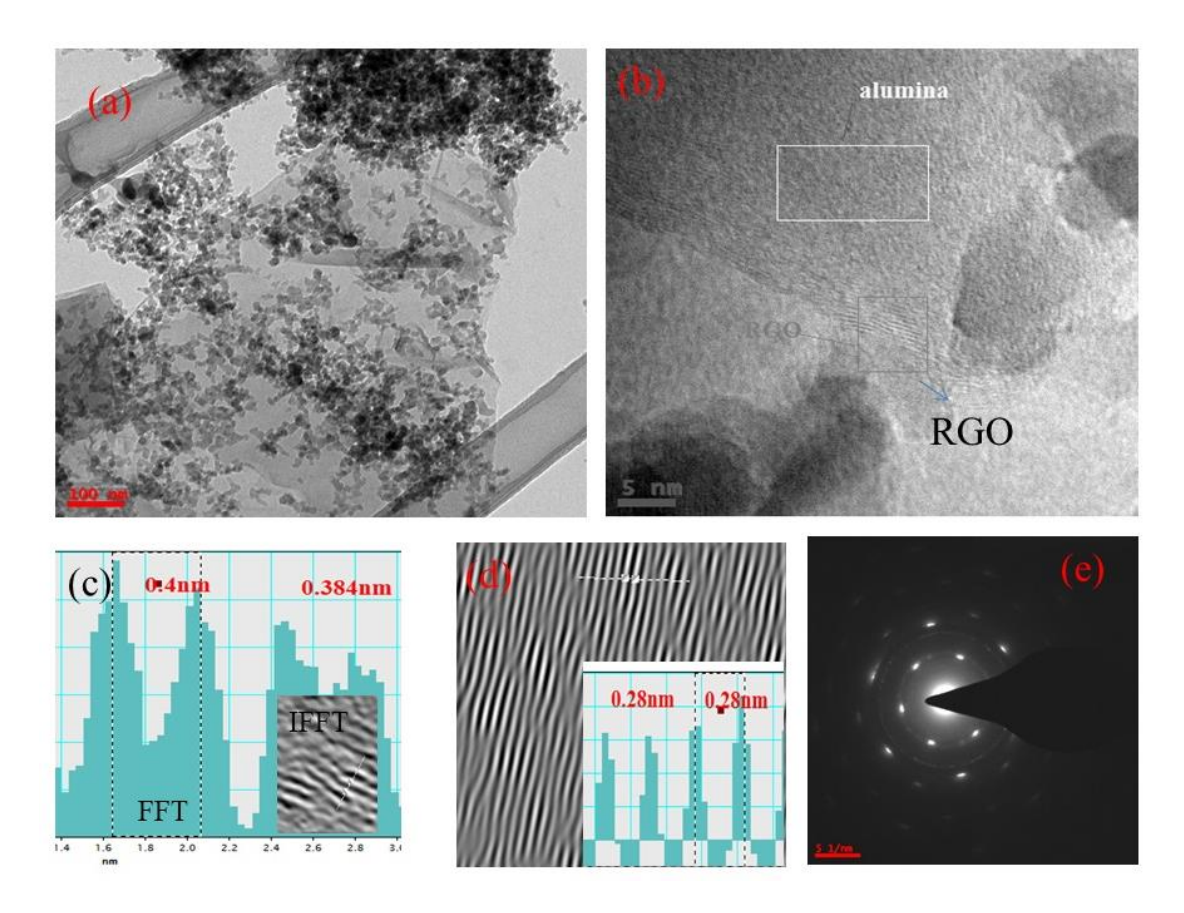


Fig. 5.25. TEM images of GO-alumina nanocomposite of R6

Fig. 5.25. The TEM, HRTEM images, and SAED pattern for R6, which was synthesized at 80°C in the presence of hydrazine hydrate as an additive. For TEM t1mg of the nanocomposite, power was dispersed with 20ml of ethyl glycol (EG) and sonicated for one hour. Then one droplet of this solution was cast on the Holly carbon grid and dried at 80°C on the hot plate. As shown in Fig.5.25 graphene –alumina nanocomposite is formed. And Fig.5.25 (b) clearly shows the graphene sheets are around the alumina nanoparticles. Fig.5.25 (c) shows the FFT profile of the selected area of the HRTEM image, which indicates that the interplanar distance is 0.4 nm and very well agreed with the XRD results. The inset the IFFT image clearly shows the appearance of RGO. The fig. 5.25 (d) indicates the IFFT image of the alumina area in HRTEM image, the interplanar distance is 0.28nm,

for the (220) plane of the γ phase alumina. The Fig.5.25 (e) shows the SAED pattern of the R6, which clearly shows the bright spots of hexagonal manner. This belongs to the RGO present in the composite and very low-intensity spots are arranged in polycrystalline nature indicates that alumina nanoparticle is a presence in the sample. Therefore, from TEM analysis we concluded that reduced graphene oxide (RGO) /Alumina nanocomposite.

5.8 Raman analysis of the nanocomposite

Raman technique is a very useful tool for the analysis of graphene-based composite materials. In this work, we have used the powder form the GO-alumina nanocomposites. We have analyzed these samples by using the micro Raman spectroscopy with a 532nm laser source.

Table:5.2 D,G band and I_D/I_G ratio of all the nanocomposite (R1 – R6)

| Sample name | D band (cm ⁻¹) | G band (cm ⁻¹) | I_D/I_G ratios |
|-------------|----------------------------|----------------------------|------------------|
| | | | |
| R1 | 1352 | 1590 | 0.97 |
| | | | |
| R2 | 1355 | 1590 | 0.98 |
| R3 | 1350 | 1590 | 0.97 |
| R4 | 1352 | 1599 | 0.95 |
| R5 | 1352 | 1590 | 0.94 |
| R6 | 1343 | 1585 | 1.04 |

Fig. 5.26 shows the Raman spectrum of all the synthesis of GO/alumina nanocomposites. Fig. 5.26 (a) shows the sample R1 and R2 of Raman spectra, these samples were prepared at different temperature variation such as R1 at RT and R2 at 80° C, without adding any additives. These samples have same G band position and I_D/I_G ratios are nearly same as shown in table 5.2 and the R2 sample has little bit increased the D band position and peak boarding than R1. may be due to the high-temperature reaction. The fig. 5.26 (b) shows the Raman spectra for R2 and R3 as seen similar

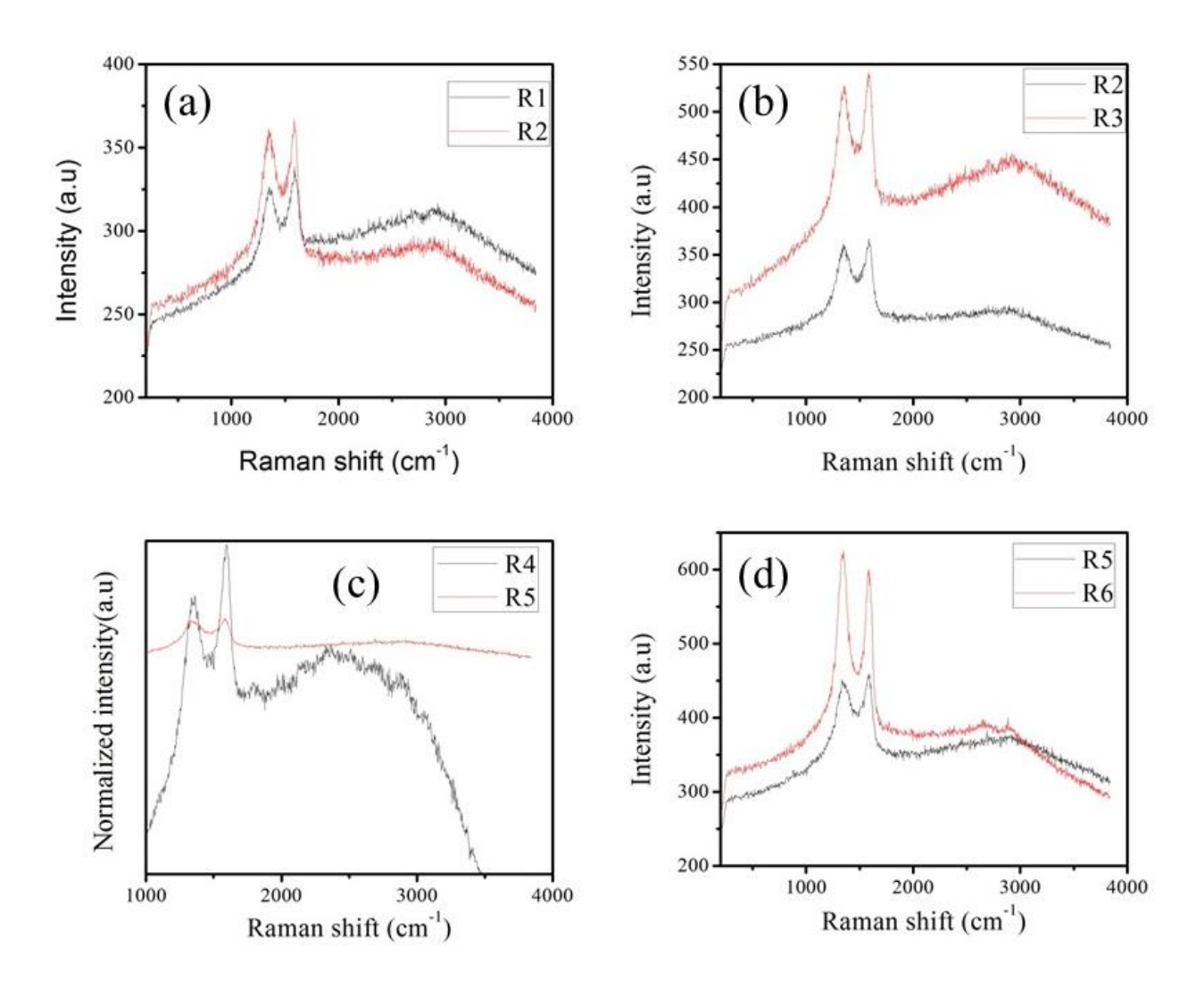


Fig. 5.26. The Raman spectrum of different GO/alumina reaction with the comparison.

peak positions and nearly equal I_D/I_G ratio. The Fig. 5.26 (c) shows the Raman spectra for R4 and R5 low and high content of GO in the presence of HCl for R4 and R5 respectively. These samples show the different G band positions as shown in table 5.2 and have same D band positions also R4 sample shows the more fluorescence significance than R5. The Fig. 5.26(d) shows the GO/ alumina nanocomposite synthesis at 80° C in the presence of an additive such as HCl for R5 and hydrazine hydrate for R6. These two samples show the different band position and intensity of the band, as shown in table 5.2. In case of R6 sample, the G and D band positions are blueshifted and also I_D/I_G ratio increases than R5.

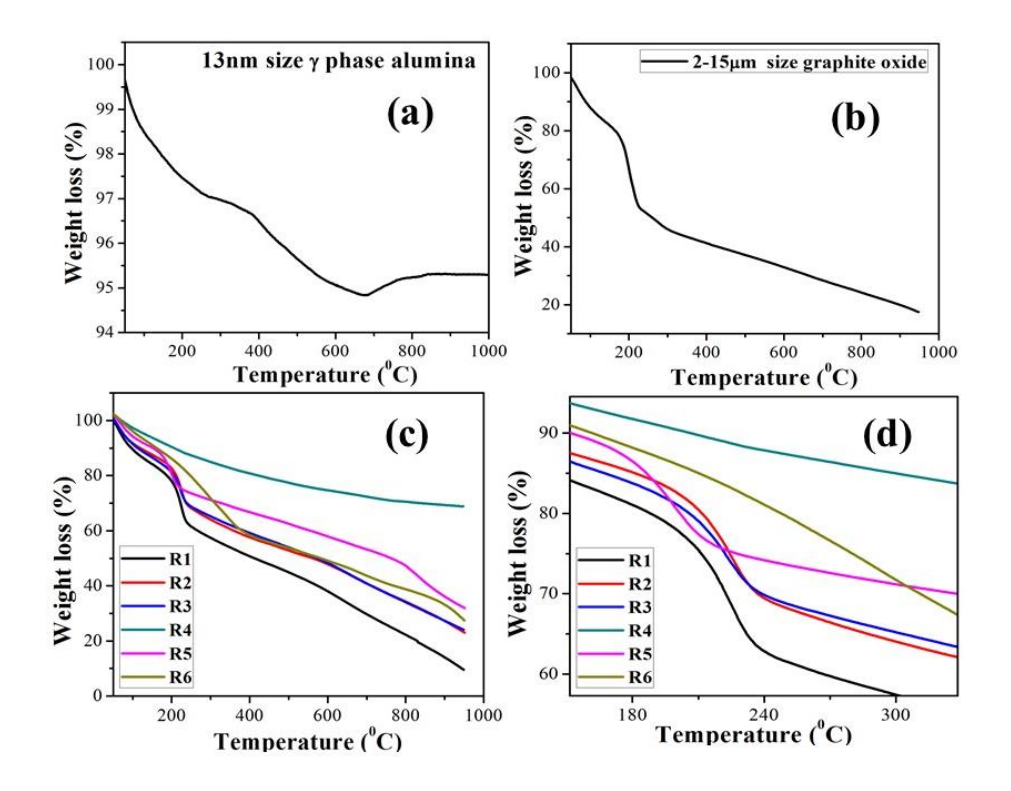


Fig. 5.27. The TGA curves of different GO/alumina reaction with the comparison (a) pure alumina, (b) graphite oxide (2-15 sample) (c) and (d) GO/ alumina nanocomposite and corresponding magnification respectively.

Fig.5.27 (a) shows the pure γ phase alumina TGA curve, this sample have different weight loss at 45 to 250°C (3%), 250 to 375 °C (0.4%), 375 to 681 °C (1.8%) and Fig.5.27 (b) 2-15 μm size graphite oxide . This sample was explained in the previous chapter. Fig.5.27 (c) shows TGA analysis of different synthesis parameter GO/alumina nanocomposite. R1: 55 to 178 °C (18.4%), 178 to 243 °C (62.5%), R2: 55 to 178 °C (14.5%), 178 to 243 °C (16%), R3: 55 to 178 °C (15.6%), 178 to 243 °C (14.4%), R5: 55 to 178 °C (12.7%), 178 to 243 °C (13.6%), R6:391.6 to 950 °C (31%). All samples show the different weight loss comparative to pure alumina and graphite oxide samples which indicate GO/alumina nanocomposite are formed in all samples but R4 and R6 samples show the thermally stable. so that R6 sample indicates the formation of RGO/ alumina nanocomposite. Fig.5.28(a) pure alumina DTA curve it shows the different endothermic peak positions are 445 °C,601°C,690°C,786°C, and 885°C. and Fig 5.28 (c) shows the different exothermic peaks such as R1: exothermic peak at 227°C, R2: exothermic peak at 228°C, R3: exothermic peak at 225°C R5: exothermic peak at 201°C.

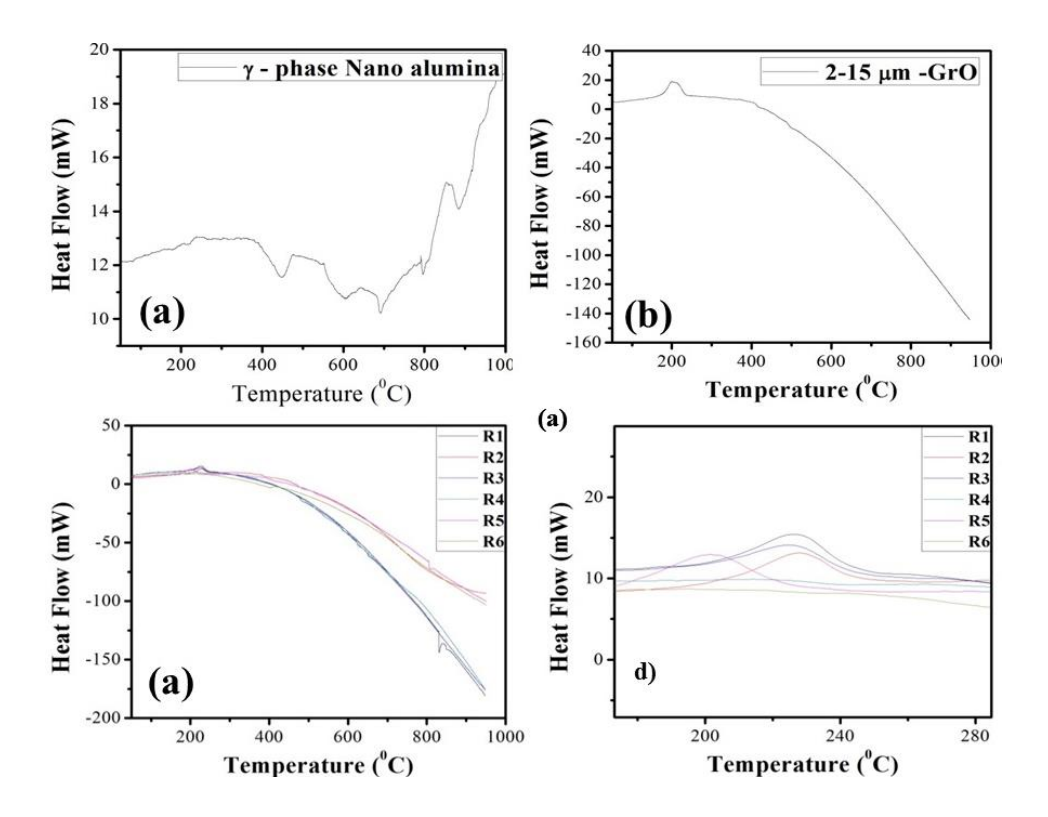


Fig. 5.28. The DTA curves of different GO/alumina reaction with the comparison (a) pure alumina, (b) graphite oxide (2-15 sample) (c) and (d) GO/ alumina nanocomposite and corresponding magnification respectively.

5.9 conclusion

A set of six nanocomposites are prepared by colloidal mixing process by varying the reaction temperature (at RT and 80° C) and different additives such as HCL and hydrazine hydrate. All the characterization results such as XRD, FESEM, FTIR, Raman, TGA/DTA and TEM are discussed in this chapter for all these nanocomposites. It is concluded that only when hydrazine hydrate was used as an additive GO is reduced during the synthesis process and RGO – Al2O3 nanocomposite is formed. All other cases GO – Al2O3 nanocomposites are only formed. In the next chapter, we described the effect of GO wt% in the formation of nanocomposites by using hydrazine hydrate as an additive.

Chapter 6

Influence of GO wt% in the formation of RGO-Al₂O₃ Nanocomposite

6.1 Introduction

This chapter deals with the influence of GO wt% on the formation of GO -Al2O3 / RGO- Al_2O_3 Nanocomposite. For this for this purpose, ~ 0.49 wt %, ~ 0.99 wt %, ~ 2.9 wt%, 4.8wt%, 9.1wt%, and 20wt%. GO was taken and a set of six nanocomposites with variation in GO wt% were synthesized by the colloidal process.

6.2 Preparation of different GO wt% in the formation of RGO-Al₂O₃ Nanocomposite

All the nanocomposites were synthesized by varying the different GOwt% such as 0.49, 0.99, 2.9, 4.8, 9.8 and 20wt% GO through the colloidal process as already discussed in the previous chapter.

Table 6.1 synthesis parameters for varying the GO wt% composite.

| process | 0.49% GO- PH | 0.99% GO PH | 2.9 % GO PH | 4.8% GO PH | 9.1% GO PH | 20% GO PH |
|---|--------------------|--------------------|-------------------|--------------------|-------------------|--------------------|
| DIW | 6.2 at 23°C | 6.35 At 23.5°C | 6.2 at 23°C | 6.1 at 22.1°C | 6.15 at 23°C | 6.35 at 23°C |
| GO + DIW | 5.01 At 22.9°C | 5.74 at23.6°C | 5.3 at 23.2°C | 5.44 at23.3°C | 5.4 at22.7°C | 5.47 at 23°C |
| Alumina +DIW | 5.6 at23°C | 6.1 at24°C | 5.35 at 23.3°C | 5.4 at 22.3°C | 5.39 at 23.3°C | 5.43 at 23.5°C |
| GO colloidal 1h sonication | 4.29 at25.9°C | 5.16 at26°C | 5.09 at 30.4°C | 4.95 at 26°C | 5.02 at 26.5°C | 4.9 at 27.9°C |
| Alumina colloidal 35min sonication | 5.62 at28.6°C | 5.28 at 27°C | 5.30 at 32.3°C | 5.35 at 25.9°C | 5.33 at 27.4°C | 5.53 at 24.6°C |
| Mix colloidal | 5.7 at 27.3°C | 5.34 at 25.8°C | 5.4 at 28.3°C | 5.45 at 25.7°C | 5.60 at 25.5°C | 5.64 at 25.3°C |
| Add hydrazine hydrate | 10.79 at 25.6°C | 10.93 at 25.3°C | 10.40 at 27°C | 10.23 at 24.9°C | 9.80 at 24.5°C | 10.02 at 24.8°C |
| After stirring for 4h at 80°C | 9.24 at 40°C | 9.3 at 40°C | 9.36 at 42.6°C | 9.35 at 47.7°C | 9.21 at 40.9°C | 9.24 at 40°C |

6.3 Structural analysis by XRD

Fig.6.1 shows the XRD spectrum of different GO wt% nanocomposites, these samples shows the different intensity of RGO and alumina peaks.small wt% of GO shows the less interplane distance at 0.5 nm for 0.49wt% (1 mg of GO). more interplane distance is increased up to 0.35 nm when this happened to GO content was increased, this more interplane represents the successfully obtained, reduced graphene oxide alumina nanocomposite, in these composites, γ phase nano alumina have different intensity with same peak positions, the interplanar of the alumina peaks are d = 0.28nm (220), 0.239nm(311), 0.228(222), 0.1974nm (400), 0.1395nm(440) and 0.114nm(444), these peaks are more dominant intensity peaks in γ phase alumina. During the formation of RGO alumina nanocomposite, in this composite, the alumina structure was not affected by the colloidal process.

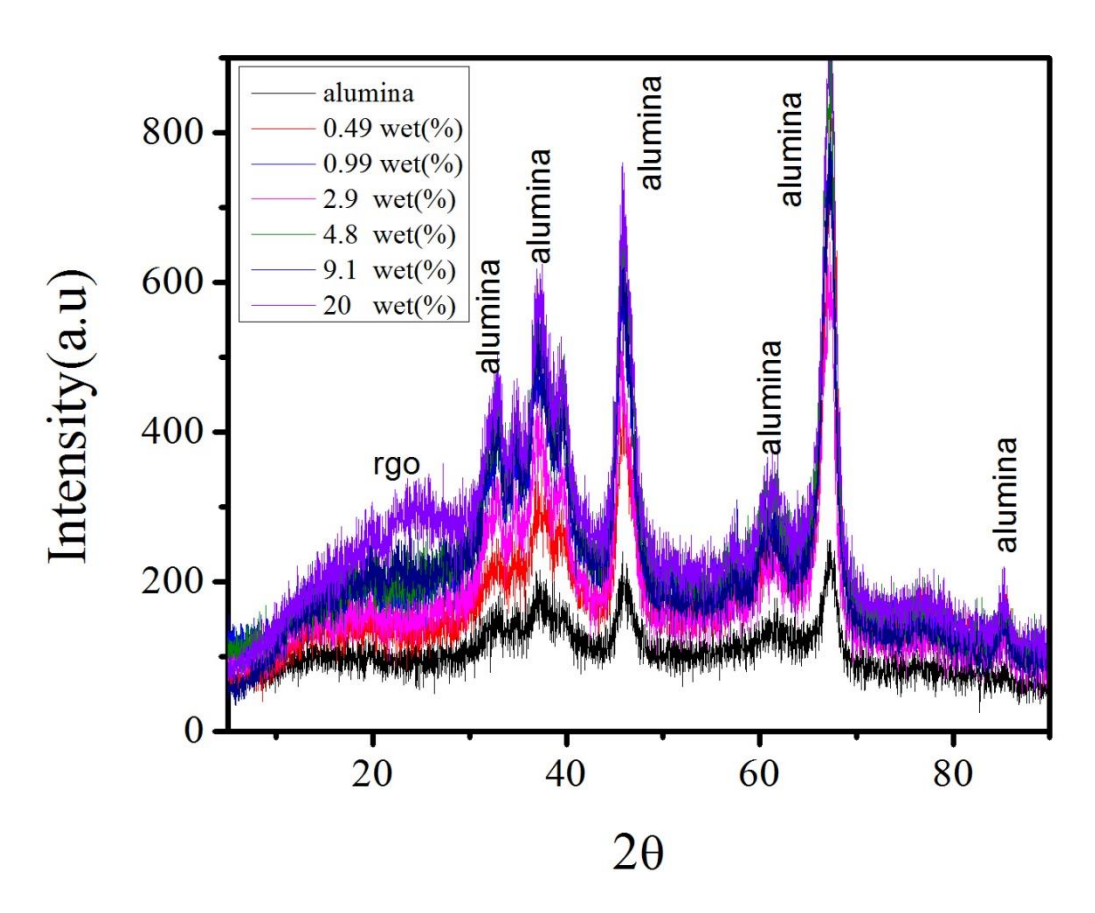


Fig.6.1 Typical XRD spectrum of different GO wt% nanocomposites

6.4 Raman Analysis of different GO wt% nanocomposites

Fig. 6.2 shows the Raman spectrum of different GO wt% nanocomposites. All samples exhibits D and G band with different band positions and ID /IG ratios showed in table 6.2.

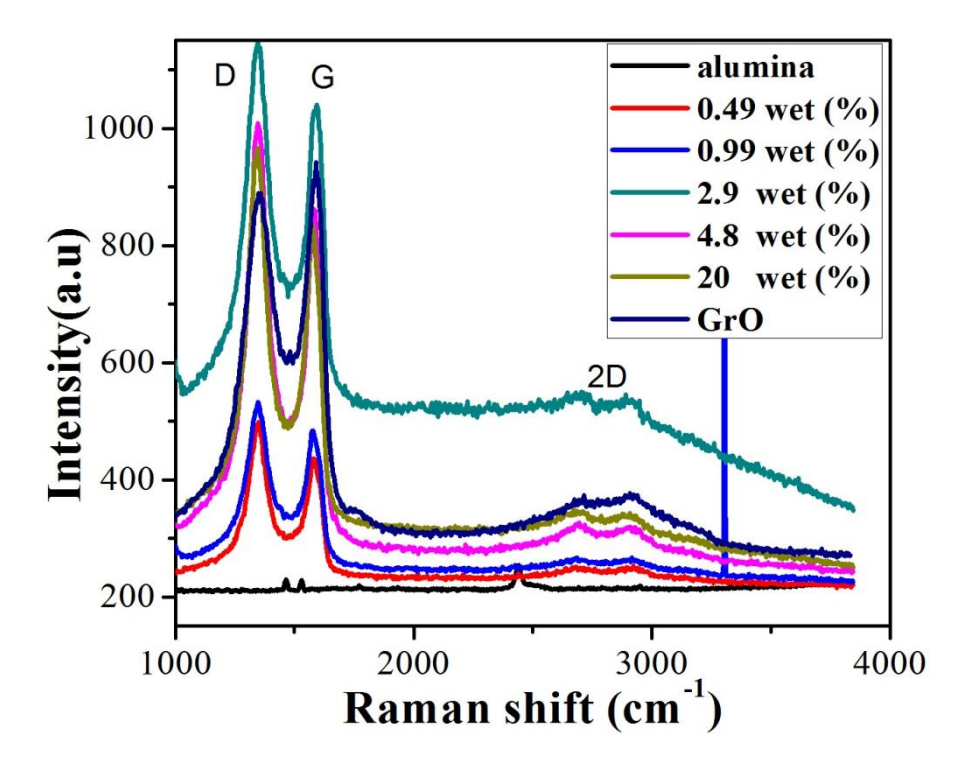


Fig.6.2 Raman spectrum of different GO wt% nanocomposites.

Table 6.2 . D, G band position and I_D/I_G ratios of different GO wt% nanocomposites

| Sample name | D(cm ⁻¹) | G(cm ⁻¹) | I_D/I_G |
|----------------|----------------------|----------------------|-----------|
| GO | 1354 | 1590 | 0.95 |
| 0.49wt% GO | 1347 | 1582 | 1.15 |
| 0.99wt% GO | 1346 | 1581 | 1.10 |
| 2.9wt% GO | 1348 | 1581 | 1.11 |
| 4.8wt% GO | 1345 | 1581 | 1.14 |
| 20wt% GO | 1343 | 1576 | 1.16 |

From the table 6.2, when increasing the GO content the D band and G band positions and I_D/I_G ratios are also varying. Comparative GO samples all the composite samples exhibit the higher I_D/I_G ratios and D band and G band positions are blueshifted showed in table 6.2. this indicates the removal of oxygen functional groups in GO and formed the RGO/ γ phase nanocomposite. When GO content was increased D and G band position are shifted to the lower wavenumber side.

Comparatively from all samples, 20wt% of GO content samples shows the higher blue shifted in the band position in the band position than in band position bonding formation may differ from the other samples.

6.5 FTIR Analysis of different GO wt% nanocomposites

Fig. 6.3 shows the FTIR spectrum for the different GO content nanocomposite. As shown in Fig. 6.3., the differential functional groups are present with varying intensity and broadening. Also, peak positions are shifted. The corresponding functional groups are listed in Table 6.3

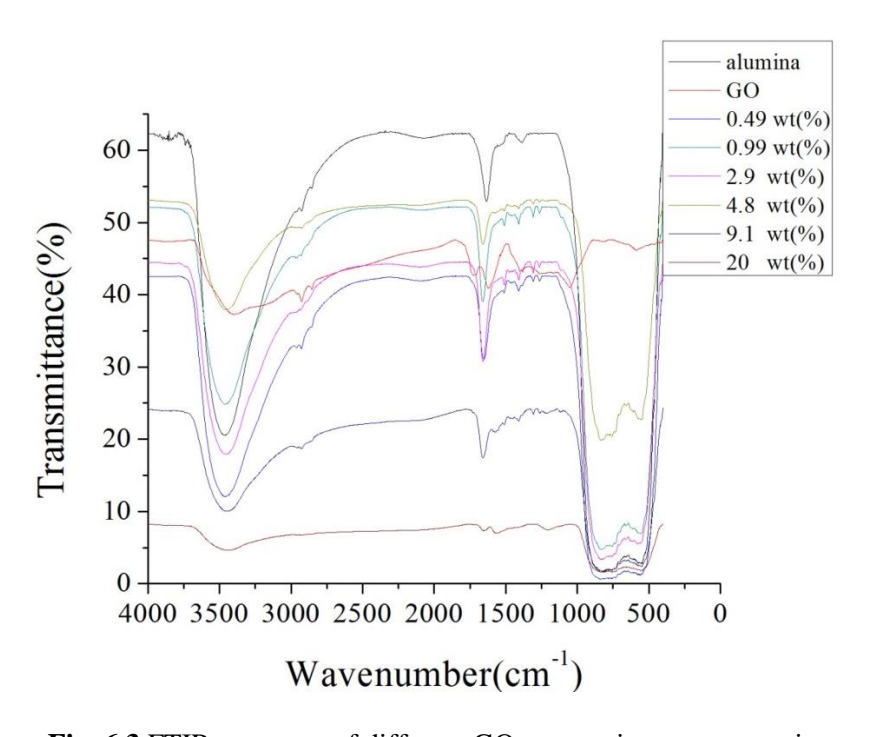


Fig. 6.3 FTIR spectrum of different GO content in nanocomposite

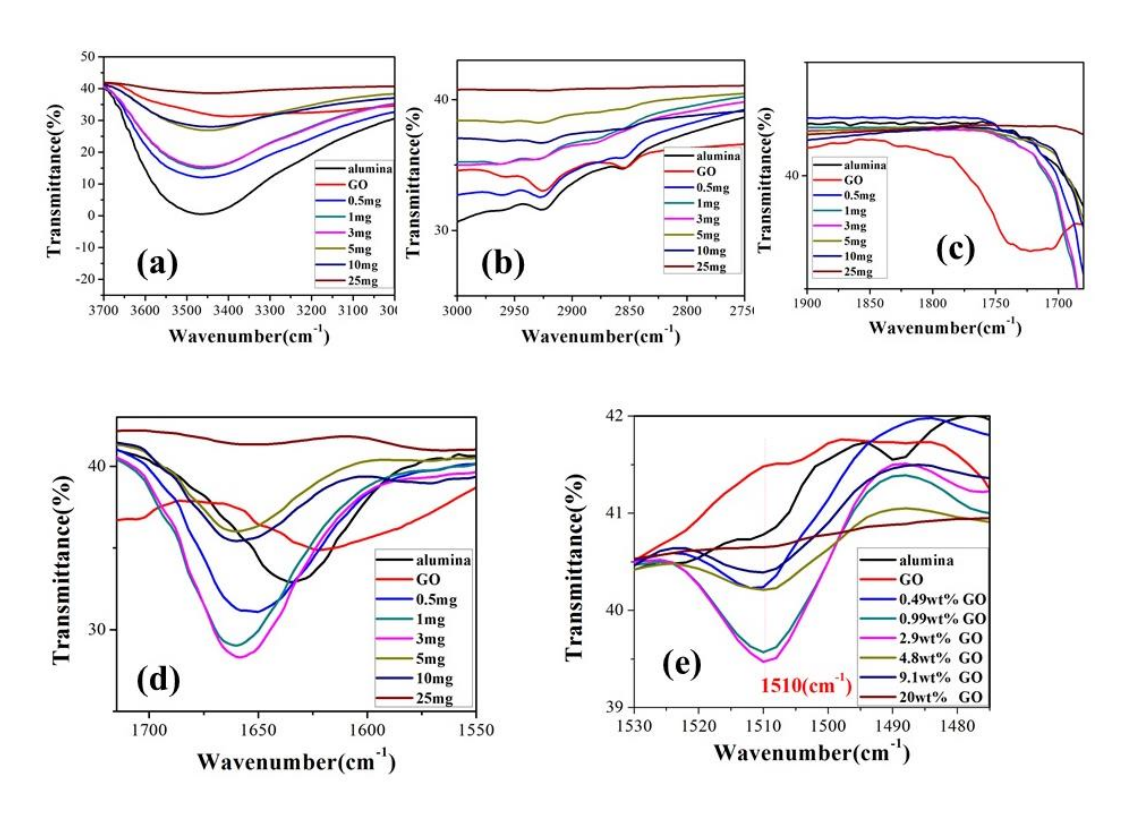


Fig. 6.4 (a) - (e) FTIR spectrum of different range (3000- 1400) for different GO content nanocomposite different .

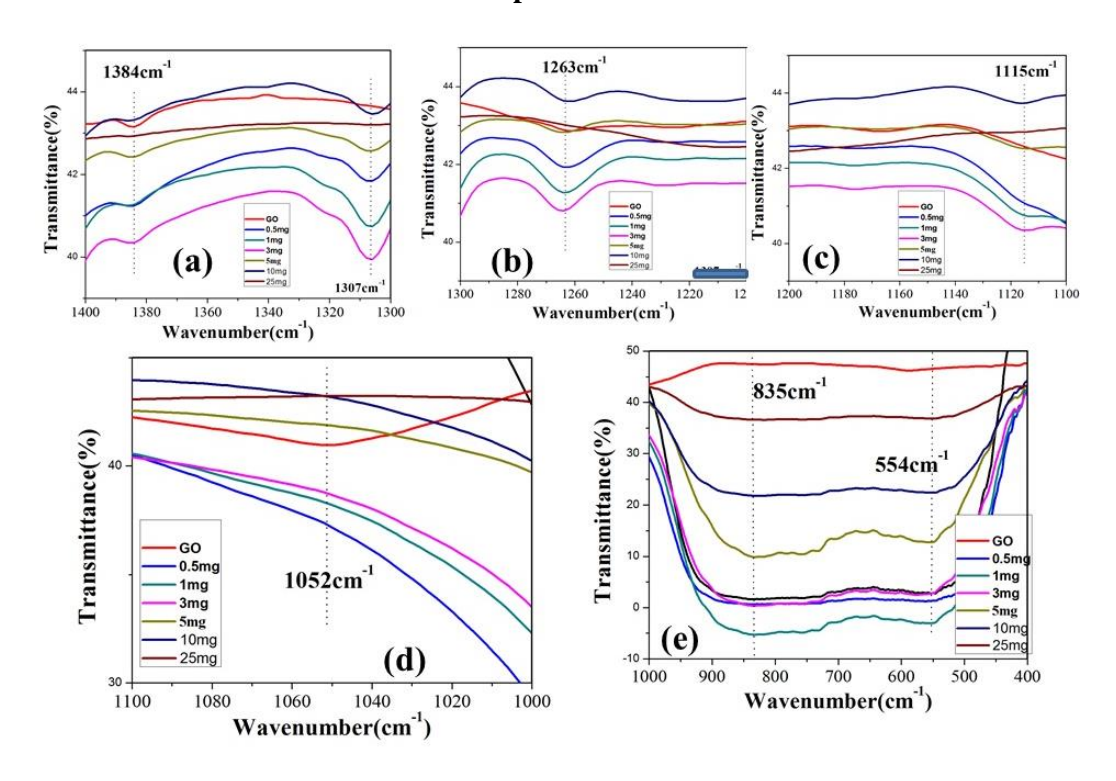


Fig. 6.5 (a) - (e) FTIR spectrum of different range (1400- 400) for different GO content nanocomposite different

As shown in Fig. 6.4 and 6.5, the band at 3465 cm⁻¹ which is related to the OH in hydroxyl group and water molecules, the corresponding bands are shown in table 6.3. It is observed that alumina shows more intensity and a sharp peak whereas GO shows the broad peak at 3401 cm⁻¹ in the case of composite peaks, these two peaks are disappeared and broadening also decreased. All samples show mostly CH₃ at 2925 cm⁻¹ this peak intensity also decreased when the increase in GO content, CH₂ related to another peak another peak is appeared in alumina and GO, with a small content of GO, this peak disappears when the GO content is increased. The band at 1719 cm⁻¹ represents the ketone group (C=O), this appears in the GO Sample, this peak is disappeared when the composite is formed, new peak positions are observed. Also, it is observed that when the GO wt% content increases, the peak position also decreases towards the lower wave number. The peak at 1622 cm⁻¹ represents the C=C or bending of water molecules when the composite is formed, this peak shifts to the higher wave number nearly at 1659 cm⁻¹ and also is seen that this peak intensity decreases when the GO content is increased. In the case of higher wt%, of GO, new peak forms at 1573 and also at 1562 cm⁻¹ for the 9.1 wt% and 20 wt% respectively. These range peaks are absent in the case of lower wt% of GO in the nanocomposites.

Table 6.3: the FTIR band positions for different GO content nanocomposite different.

| GO | 3401 OH | 2925 CH3 | 2854 CH2 | 1719 C=0 | 1622 C=C H2O | c=c | | | 1384 OH | | 1261 Pero xides | 1166 C-O | 1052 C-O- C | AlO 4 | AlO 6 |
|-------------|------------|-------------|-------------|-------------|--------------------|--------|------|--------|------------|------|-----------------------|-------------|-------------------|----------|----------|
| Al2O3 | 3465 | 2925 | 2855 | | 1634 | | | /22222 | 1394 | | | | | 830 | 554 |
| 0.49wt % | 3455 | 2924 | 2849 | | 1653 | | 1509 | 1407 | 1385 | 1305 | 1261 | | | 831 | 554 |
| 0.99wt % | 3455 | 2945 | 5575 | ****** | 1659 | | 1509 | 1410 | **** | 1305 | 1263 | **** | | 831 | 554 |
| 2.9wt% | 3455 | 2945 | **** | | 1658 | | 1510 | 1409 | | 1307 | 1263 | 1114 | | 831 | 573 |
| 4.8 wt% | 3448 | 2934 | 75555 | | 1661 | ****** | 1510 | 1409 | 1384 | 1307 | 1263 | 1114 | | 831 | 554 |
| 9.1wt% | 3444 | 2924 | 20202 | | 1660 | 1573 | 1510 | 1408 | | 1306 | 1262 | 1115 | | 831 | 549 |
| 20wt% | 3438 | 2924 | 2849 | **** | 1651 | 1562 | **** | **** | ¥ | 1306 | **** | **** | **** | 832 | 554 |

The peak appears at 1510 cm-1 for the nanocomposites synthesized at lower GO wt. %, and this peak are absent in nanocomposites those are synthesized at higher GO wt% samples such as 9.1

wt% and 20 wt% GO. Also, it is seen from the Fig. 6.3 that another new peak is formed at 1410 cm-1, and this peak is absent in sample containing higher GO wt% (20%).

OH, deformation of hydroxyl groups are present in the alumina and GO samples, when the GO contents increases, these peak intensity decreases and disappears at 20 wt% GO nanocomposite sample. 1337 cm-1 band is seen to be present only in alumina sample and this peak is not present in nanocomposites. 1306 cm-1 this peak is absent in both the alumina, GO and 20wt% nanocomposite sample, this peak intensity decreases when the GO content increases. The band at 1261cm-1 is present in the GO and absent in 20wt% GO sample, this band is redshifted when the GO content increases. 1166 cm-1 peak appears in the GO sample only, remaining all the nanocomposites, it does not appear. Similarly, 1114 cm-1 band is present in case of the 2.9, 4.8, 9.1 wt. % GO nanocomposites whereas this peak is not present in the pure GO sample. 1052 cm-1 band appears in GO sample only and not present in nanocomposites Both the 832 and 554cm-1 band represent the AlO4 and AlO6 and the intensities of these peaks reduce linearly with the GO content. Hence, FT IR results confirmed that nanocomposites are formed since extra bonds and peaks shifting are noticed in the nanocomposites samples.

6.6 TEM Analysis of different GO content nanocomposite

Fig.6.6(a) shows the TEM image of 0.49wt% GO content nanocomposite, from the figure it clearly shows that the γ – phase alumina nanoparticles are embedded to the graphene sheet and these particles are more agglomerated. Fig 6.6(b) shows the SAED pattern of the corresponding TEM image. The SAED pattern clearly shows the very low intensity of diffraction spots and also identifies the planes from the SAED pattern calculated the interplanar distance is 0.4364 nm, 0.2612 nm, and 0.1334nm. the corresponding planes are (002), (021) and (440). In which (002) represents the RGO in the composite and (021) and (440) are represents the γ – phase nano alumina. Fig 6.6 (c) shows the HRTEM images of the TEM image. From this image, it clearly shows the two different fringes, the graphene fringes are appearance around the alumina nanoparticles. So that it is clear evidence of the graphene – alumina nanocomposite is formed. We choose the graphene fringes FFT profile to calculate for interplanar distance shown in Fig 6.6 (d), the obtained interplanar distance is 0.28 nm which is related to the γ - phase alumina nanoparticles and the corresponding plane is (220). Fig 6.6 (e) showed the FFT profile of graphene fringes and obtained interplanar distance is 0.49 nm, (002). This distance related to the RGO in the nanocomposite.

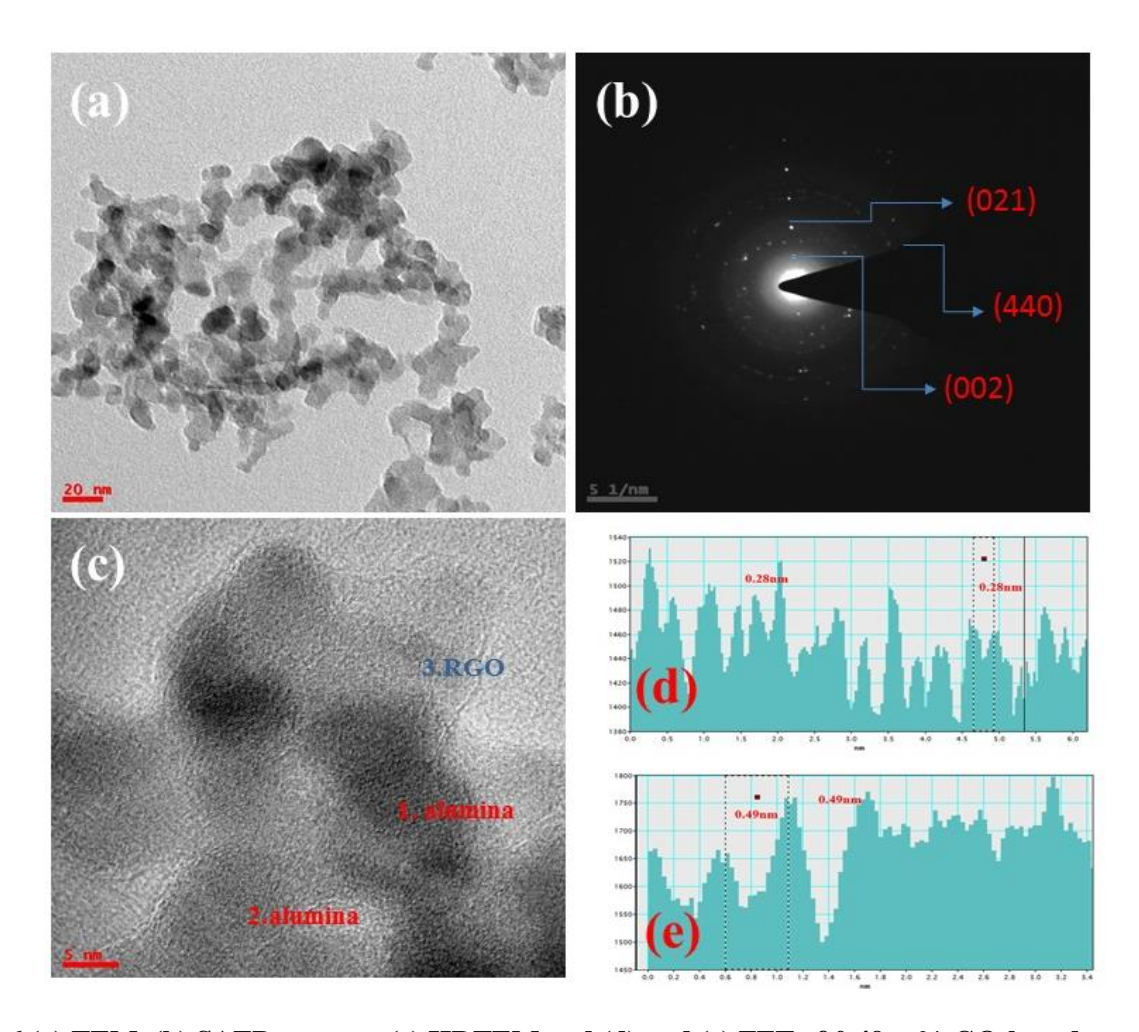


Fig. 6.6 (a) TEM, (b) SAED pattern, (c) HRTEM and (d) and (e) FFT of 0.49wt% GO-based nanocomposite.

Fig. 6.7 (a) shows the TEM image of 0.99 wt% GO sample.which indicates the γ – phase alumina nanoparticles are attached to the graphene sheet. In this sample, the γ – phase alumina nanoparticles are less agglomerated than 0.49 wt % of GO nanocomposite sample. Fig 6.7 (b) shows the SAED pattern of 0.99 wt % of GO sample. This pattern is similar to the 0.49 wt% GO SAED pattern, but the diffraction spots intensity was increased in the case of 0.99 wt % GO sample, from the SAED pattern we calculated the interplanar distance is 0.4038 nm which is related to the (002) plane of RGO in the nanocomposite and 0.2648 nm, 0.1888 nm and 0.1336 nm. Are related to the γ – phase nano alumina and corresponding planes are (221), (400) and (440) respectively.

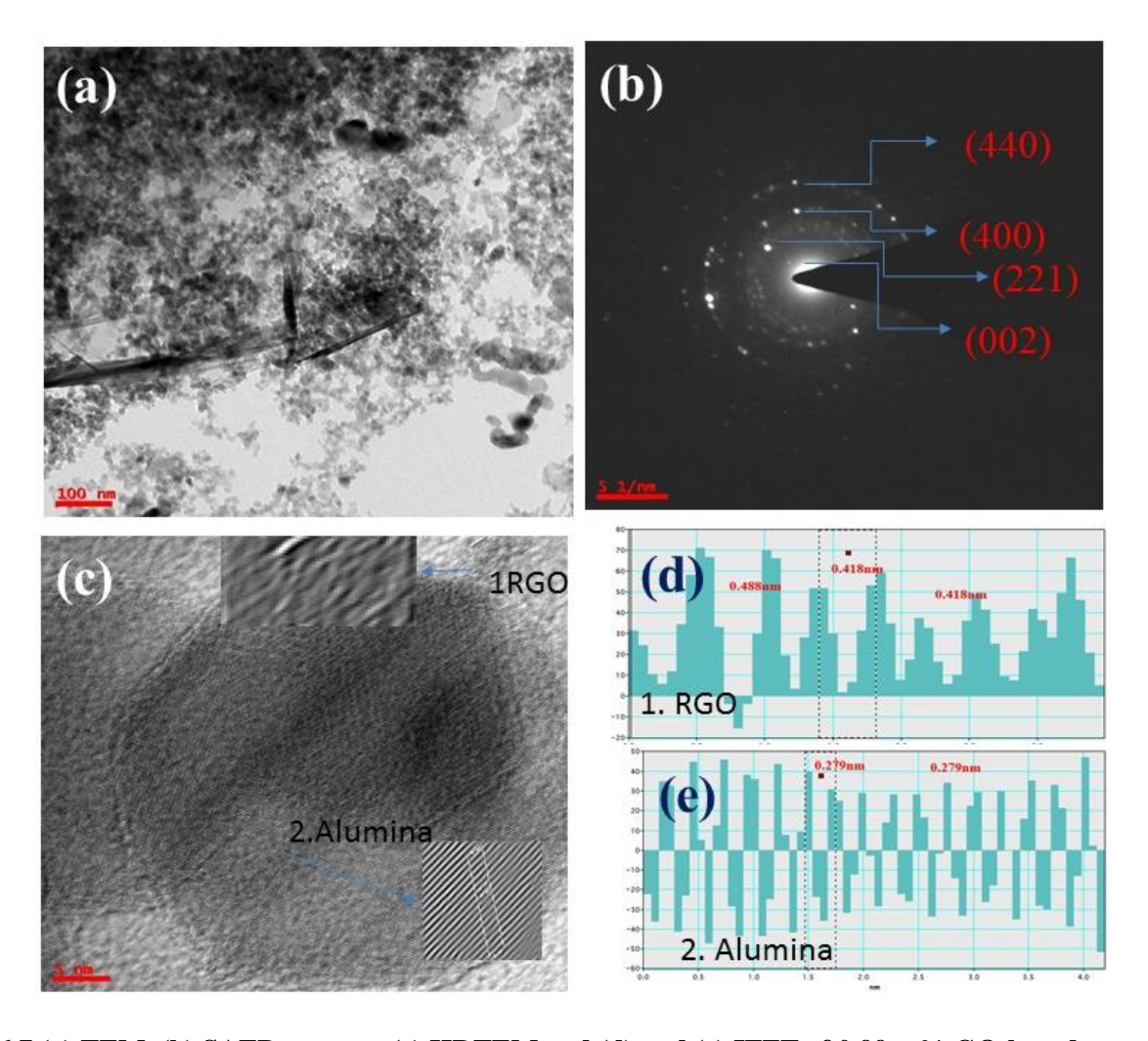


Fig. 6.7 (a) TEM, (b) SAED pattern, (c) HRTEM and (d) and (e) IFFT of 0.99wt% GO-based nanocomposite.

Fig. 6.7 (c) is the HRTEM image of 0.99wt% GO nanocomposite. This image clearly shows the core sell formation in the composite, the fringes of the γ - phase alumina nanoparticle are surrounded by the graphene fringes, in this image, we choose two areas. One area is indicated as 1 RGO and the second area is indicated by alumina, these fringes are clearly shown in inset images of IFFT. Fig.6.7 (d) shows the IFFT profile of area 1, the interplanar distance is 0.418 nm and IFFT of area 2 of the γ - phase nano alumina shown in Fig. 6.7 (e) from this figure, we obtained interplanar distance is 0.279 nm which is related to the (220) plane of the γ - phase alumina. This 0.99 wt% of GO composite, it represented as an RGO/ the γ - phase alumina nanocomposite. This sample has less agglomeration of alumina nanoparticles comparatively 0.49 wt% of RGO / the γ - phase alumina nanocomposite.

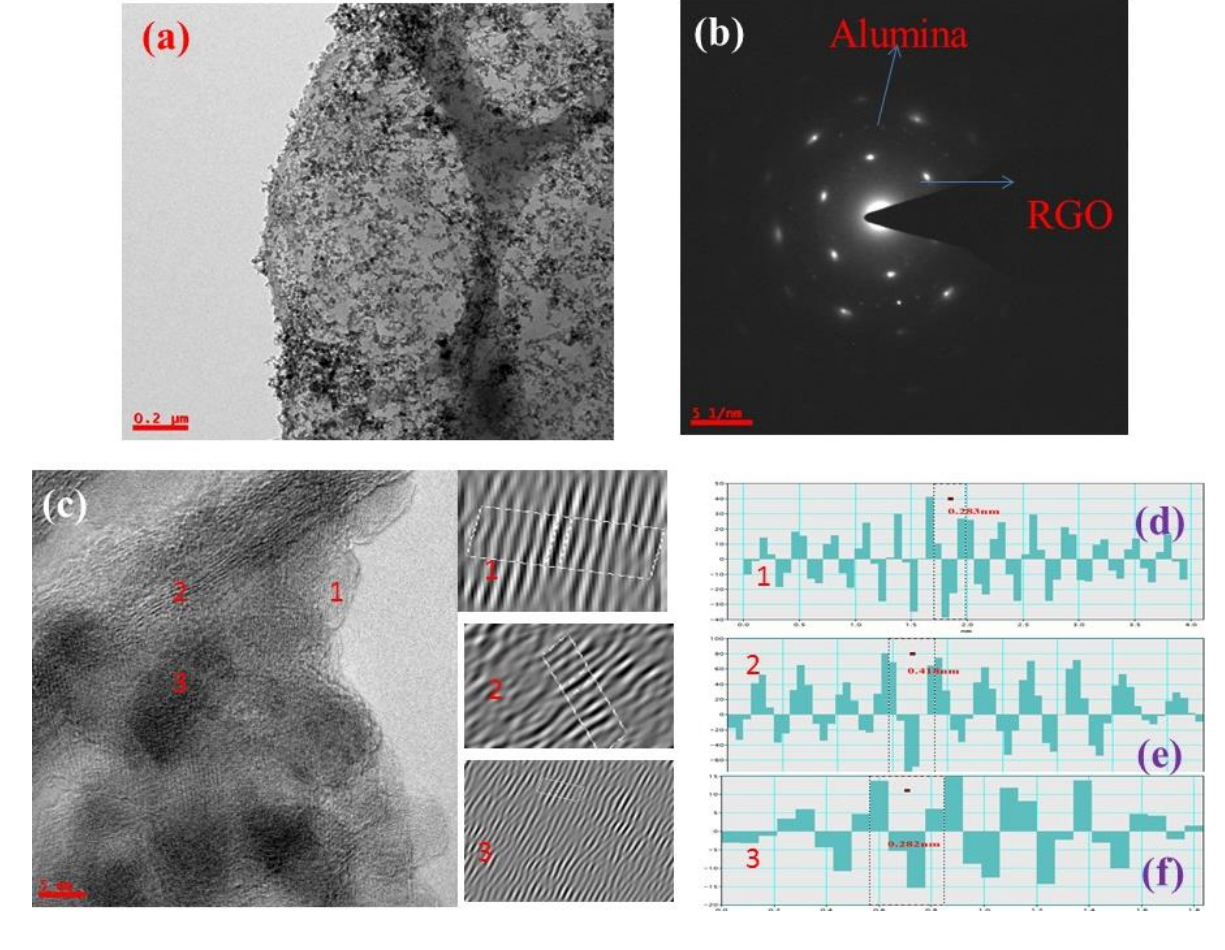


Fig. 6.8 (a) TEM, (b) SAED pattern, (c) HRTEM and (d) -(f) FFT of 20wt% GO based nanocomposite.

Fig.6.8 (a) shows the TEM image of 20 wt% of GO alumina nanocomposite. This figure clearly shows the γ - phase alumina nanoparticles are completely covered the graphene transference sheet with very less agglomeration. So that when the wt % increase of GO content, the γ - phase alumina agglomeration was reduced. that means the interaction between the γ - phase alumina nanoparticles and graphene oxide is more when GO content was increased. Fig.6.8 (b) shows the SAED pattern of the 20 wt% of GO alumina nanocomposite. The SAED pattern clearly indicates the hexagonal structure with bright diffraction spots, which indicates the RGO in the composite, and also less intensity of polycrystalline ring pattern appears which is regarding the γ - phase alumina. Compare to the low content of GO wt%, this sample shows the good formation of RGO/ γ - phase alumina nanocomposite. Fig.6.8 (c) shows the HRTEM image with an insert of IFFT images, from the HRTEM image, it clearly indicates the evidence for the formation of graphene-based, the γ - phase alumina nanocomposite. In this image, we choose three different areas, corresponding IFFT images showed in fig. 6.8 (d). shows the IFFT profile for the selected area 1, from this we observed the

interplanar distance is 0.283nm, and the corresponding plane is (220) which represents the γ - phase alumina nanoparticle fringes. Fig.6.8 (e) shows the IFFT profile for area 2, and the corresponding interplanar distance is 0.418 nm. Which is related to the RGO plane (002). Fig.6.8 (f) shows the image of IFFT profile for the area3. The interplanar distance is 0.282 nm, which indicates the (220) plane of the γ - phase alumina.

6.7 Conclusion:

Different GO/RGO-Al2O3 nanocomposites were synthesized by varying the GO wt. % (0.49, 0.99, 2.9, 4.8, 9.8 and 20 wt %) by using the optimum process parameters as discussed in the previous chapter. The as-obtained nanocomposites samples were analyzed by using XRD, FT IR, Raman, and TEM. Experimental results indicated that as the GO content increases more disorder and less agglomeration of the alumina nanoparticles are observed. Further, it is concluded that as the GO content increases the oxygen-related function groups are removed because of more interaction between the GO and alumina nanoparticles.

Chapter 7

Conclusions, Limitations and Scope of Future Work

In this thesis research work, the influence of the synthesis parameters such as oxidation reaction temperature (low and high) on the structure, morphology, bonding and properties of the graphene oxide(GO) and the corresponding chemically and thermally reduced graphene oxide(RGO) was studied by using the standard Modified Hummers synthesis method. In the second part of the thesis work, the influence of the different sizes source graphite on the synthesis of graphene oxide (GO) and corresponding reduced graphene oxide (RGO) was investigated by choosing the optimum synthesis parameters as obtained from the first part of the research work. The impacts of host graphite powder sizes on the structure, morphology, disorder, bonding and properties were also investigated by using the different analytical instruments. In the final part of the thesis work, a set of six GO/RGO-Al₂O₃ nanocomposite was synthesized by choosing γ -phase Al₂O₃ using the colloidal mixing process and the effects of the different additives such as HCl, Hydrazine hydrate and without any additives were investigated. The corresponding nanocomposites structure, morphology, bonding, interface and thermal stability were investigated by using different analytical instruments such as XRD, FESEM, TEM, FT IR, Raman spectroscopy and TGA/DTA for understanding the nanocomposite formation.

Graphene oxide was synthesized by varying the reaction temperature (low and high) by using the equal ratios of graphite, H₂SO₄, NaNO₃ and KMnO₄. All the samples were analyzed by using the XRD, FT IR, Raman, TEM, FESEM, UV and TGA/DTA for structural, molecular & bonding characteristics, morphological and thermal analysis. Experimental results indicated that oxidation reaction temperature has an effective role in the synthesis of GO. It was observed that low-temperature reaction showed the good quality of graphene oxide(GO) with better structural, less disorder and 2-3 layers of GO as compared to the higher reaction temperature. Further, the corresponding reduced graphene oxide (RGO) was obtained by using hydrazine hydrate and thermal reduction process, and experimental results confirmed that the RGO which was obtained by using the lower reaction temperature GO showed less disorder, more graphical structure, flat type and 2-3 layers as compared to the GO obtained at higher temperature.

Three different sizes graphite precursor (2-15 μ m, <45 μ m, and 170-840 μ m,) were oxidized by MHM method and then corresponding RGO were synthesized by the hydrazine hydrate reduction

process. The experimental results indicated that the smaller size precursor graphite was fully oxidized in comparison to the large size graphite as source material. Hence, oxidation of graphite to graphene oxide is size depended on the source graphite and also showed better quality of reduced graphene oxide than other sizes. Further, from the TGA and DTA analysis, it is observed that different weight loss and different exothermic peak position in the graphite oxide which suggest that weight loss also depends on the size graphite due to the oxidation rate. UV spectroscopy analysis shows different abortion peaks which indicated that all the sizes graphite oxidized differently. Hence, the precursor graphite size has a key role in the synthesis of GO and corresponding RGO.

A set of six GO/RGO-Alumina nanocomposites were prepared by colloidal mixing process by varying the reaction temperature (at RT and 80° c) and different additives such as HCL and hydrazine hydrate. From all the analytical analysis results such as XRD, FESEM, FTIR, Raman, TEM is TGA and DTA, it was concluded that only when hydrazine hydrate was used as an additive GO was reduced during the synthesis process and RGO – Al2O3 nanocomposite was formed. All other cases GO – Al2O3 nanocomposites formed. Hence, RGO-Alumina nanocomposite can be synthesized by using hydrazine hydrate as an additive during fabrication process by using a smaller size γ -phase alumina nanoparticles.

Different GO/RGO- Al2O3 nanocomposites were synthesized by using the optimum process parameters as obtained by varying the wt% GO (0.5, 1, 3, 5, 10 and 20 wt %) and all the samples were analyzed by using XRD, FT IR, Raman and TEM. Experimental results indicated that as the GO content increases more disorder and less agglomeration of the alumina nanoparticles are observed. Further, it was seen that as the GO content increases the oxygen-related function groups are removed because of more interaction between the GO and alumina nanoparticles.

In this thesis work, GO/RGO- alumina nanocomposites were synthesized and formation of the graphene-alumina nanocomposite was confirmed based on the structural, bonding, morphological and TGA/DTA analysis, however still to use such nanocomposites in practical application such as energy storage, memory devices and other applications, properties such as mechanical, catalytic and electrical are needed to be addressed. Therefore, the future scope of this thesis works to investigate the electrical, mechanical properties and the percolation threshold in order to utilize this nanocomposite for practical memory devices and energy applications.

References

- [1] U.Kreibig et al, "Optical Properties of Metal Clusters", *Springer*, **8**, 8, 699 (**1995**) **DOI:** 10.1002/adma.19960080823.
- [2] M. Gratzel, et al, "Photoelectrochemical cells", *Nature*, **414**,338 -344,(**2001**). **DOI**:10.1038/35104607
- [3] Murray CB et al "Synthesis and characterization of monodisperse nanocrystals and close-packed nanocrystal assemblies", *Annu Rev Mater Sci*, **30**,545–610, (**2000**) doi.org/10.1146/annurev.matsci.30.1.545
- [4] Mazzola L.et al "Commercializing nanotechnology", *Nat. Biotechnology*, **21**,1137–1143 (**2003**) **DOI**: 10.1038/nbt1003-1137
- [5] Paull R, et al," Investing in nanotechnology", *Nature Biotechnology*, **21**,1134–1147(2003). doi: 10.1038/nbt1003-1144
- [6] Taton TA, et al, "Nanostructures as tailored biological probes", *Trends Biotechnol*, **20**,277-279 ,(**2002**). doi: 10.1016/S0167-7799(02)01973-X
- [7] Whitesides GM et al, "The 'right' size in Nanobiotechnology" *Nature Biotechnology*, **21,**1161-1165, **(2003)**. doi:10.1038/nbt872.
- [8] Parak WJ, et al, "Biological applications of colloidal nanocrystals" **Nanotechnology**,**14**,15-27,(**2003**). doi: 10.1088/0957-4484/14/7/201
- [9] Pankhurst QA, et al "Applications of magnetic nanoparticles in biomedicine" *J Phys D: Appl Phys*, **36**:167–181, **(2003).** doi: 10.1088/0022-3727/36/13/201
- [10] Yan H et al "DNA-templated self-assembly of protein arrays and highly conductive nanowires", *Science.* **301**, 1882–1884 (2003). doi: 10.1126/science.1089389.
- [11] Keren K, "DNA-templated carbon nanotube field-effect transistor" *Science*, **302**,1380–1382, (**2003**) doi: 10.1126/science.1091022.
- [12] Bruchez M, et al "Semiconductor nanocrystals as fluorescent biological label" *science*, **281**, 2013–2016, **(1998).** doi: 10.1126/science.281.5385.2013
- [13] Chan WCW, Quantum dot bioconjugates for ultrasensitive nonisotopic detection", *science*, **281**, 2016–2018, **(1998).** doi: 10.1126/science.281.5385.2016.
- [14] Wang S, et al, "Antigen/antibody immunocomplex from CdTe nanoparticle bioconjugates", *Nano Letters*, **2**, 817–822, (**2002**). doi: 10.1021/nl0255193.
- [15] Mah C, et al,"Microsphere-mediated delivery of recombinant AAV vectors in vitro and in vivo". *Mol Therapy*, **1**, 239, (**2000**). doi: 10.1006/mthe.2000.0174.
- [16] Panatarotto D, et al, "Immunization with peptide-functionalized carbon nanotubes enhances virus-specific neutralizing antibody responses", *Chemistry&Biology*; **10**, 961–966, (**2003**). doi.org/10.1016/j.chembiol.2003.09.011
- [17] Edelstein RL, et al, "The BARC biosensor applied to the detection of biological warfare agents. Biosensors", *Bioelectron.*, **14**, 805–813, **(2000).** doi: 10.1016/S0956-5663(99)00054-8.
- [18] Nam JM, et al, "Nanoparticles-based bio-bar codes for the ultrasensitive detection of proteins", *Science*, 301, 1884–1886, (**2003**). doi: 10.1126/science.1088755
- [19] Yong-Tae Kim et al "Electrochemical Synthesis of CdSe Quantum-Dot Arrays on a Graphene Basal Plane Using Mesoporous Silica Thin-Film Templates", *Adv. Mater.*, **22**, 515–518, **(2010)**. DOI: 10.1002/adma.200902736
- [20]] Zhang G et al, "Fabrication of Heterogeneous Binary Arrays of Nanoparticles via Colloidal Lithography", *J. Am. Chem. Soc.*, **130** (**17**),5616–5617,(2008,) DOI: 10.1021/ja710771j
- [21] 21] Lee JY, et al, "Near-field focusing and magnification through self-assembled nanoscale spherical lenses", *Nature* **460**, 498–501, (**2009**). doi:10.1038/nature08173

- [22] Huang L, et al "Cuprite Nanowires by Electrodeposition from Lyotropic Reverse Hexagonal Liquid Crystalline Phase", *Chem. Mater.*, *14* (2), 876–880, (2002). DOI: 10.1021/cm010819r
- [23] Xia H, et al, "Preparation and properties of hybrid direct methanol fuel cell membranes by embedding organ phosphorylated titania sub microspheres into a chitosan polymer matrix", *J Power Sources*, **195**,4410–4113, **(2010).** doi:10.1016/j.jpowsour.2010.01.079
- [24] Yoon SM, et al, "Synthesis of Single Crystal Tetra(4-pyridyl)porphyrin Rectangular Nanotubes in Vapor Phase", *Angew. Chem. Int. Ed.*, **48**, 2506 -2509, **(2009)**. DOI: 10.1002/anie.200806301
- [25] Kim WY et al, "Understanding structures and electronic/spintronic properties of single molecules, nanowires, nanotubes, and nanoribbons towards the design of nanodevices" *J. Mater. Chem*, **18**, 4510–4521, (**2008**). DOI: 10.1039/b804359k
- [26] Kim KS et al, "Large-scale pattern growth of graphene films for stretchable transparent electrodes" Nature, **457**, 706–710, (**2009**). doi:10.1038/nature07719
- [27] Bae S et al. Roll-to-roll production of 30-inch graphene films for transparent electrodes", *Nature Nanotechnology*, **5**, 574–578, **(2010)**. doi:10.1038/nnano.2010.132
- [28] Dong X et al, "Synthesis of Triangular Silver Nanoprisms by Stepwise Reduction of Sodium Borohydride and Trisodium Citrate" *J. Phys. Chem. C*, **114** (5), 2070–2074, (**2010**). DOI: 10.1021/jp909964k
- [29] Pradhan D et al, "Vertical Growth of Two-Dimensional Zinc Oxide Nanostructures on ITO-Coated Glass: Effects of Deposition Temperature and Deposition Time", *J. Phys. Chem. C*, *112* (5), 1357–1364, (2008). DOI: 10.1021/jp076890n
- [30] D. Jariwala et al, "Carbon nanomaterials for electronics, optoelectronics, photovoltaics, and sensing", *Chem. Soc. Rev.*, 42, 2824-2860, (**2013**). DOI:10.1039/C2CS35335K
- [31] D.Jariwala, et al, "Carbon nanomaterials for electronics, optoelectronics, photovoltaics, and sensing", *Chem Soc Rev.*, **42**, 2824, (**2013**). doi: 10.1039/c2cs35335k.
- [32] Christopher S et al, Graphene. http://dx.doi.org/10.1016/B978-0-12-394593-8.00003-5 ,(**2013**) Elsevier Inc. (book)
- [33] R. Setton, P. et al, "Carbon Molecules and Materials" (**CRC Press, NewYork, 2002**) ISBN 9780415284424. (**book**)
- [34] M. Inagaki et al "New Carbon: Control of Structure and Functions" (Elsevier Science Ltd., Amsterdam, 2000) eBook ISBN: 9780080525709
- [35] P. Delhaés (ed.), Graphite and Precursors (Gordon and Breach Science Publishers, NewYork,2001)
- [36] F. Cirkel, C.M. Branch, Graphite: Its Properties, Occurrence, Refining, and Uses (Nabu Press, Charleston, SC 2010)
- [37] S.R.P. Silva (ed.), Properties of Amorphous Carbon (INSPEC, Institution of Electrical Engineers, London, 2003)
- [38] S.R.P. Silva, J. Roberts, G.A.J. Amaratunga (eds.), Specialist Meeting on Amorphous Carbon (World Scientific Publishing Company, Singapore 1998)
- [39] J. P. Sullivan, J. Robertson, O. Zhou, T. B. Allen, B. F. Coll, (eds.), Amorphous and Nanostructured Carbon, vol. 593 of Material Research Society Symposium Proceedings. Materials Research Society, Warrendale, PA 2000.
- [40] E. Ösawa (ed.), Perspectives of Fullerene Nanotechnology (Kluwer Academic Publishers, Netherland, 2002)
- [41] P. Ehrenfreund, et al "Fullerenes, and cosmic carbon". *Science*, **329**, 1159–1160, **(2010)**.DOI: 10.1126/science.1194855
- [42] T.W. Ebbesen (ed.), et al, "Carbon Nanotubes: Preparation and Properties" (Chemical Rubber, BocaRaton,1997)

- [43] M.S. Dresselhaus, et al, "Carbon Nanotubes: Synthesis, Structure, Properties, and Applications of Topics in Applied Physics", vol. 80 (**Springer, Heidelberg, 2001**)
- [44] K.S. Novoselov, et al, "Electric Field Effect in Atomically Thin Carbon Films", *Science* **306**, 666 669, (**2004**). DOI: 10.1126/science.1102896
- [45] A.K. Geim et al, "The rise of graphene", *Nat. Mater*, **6**, 183–191, **(2007)**. doi:10.1038/nmat1849
- [46] Novoselov K.S., et al, "Electric field effect in atomically thin carbon films", *Science*, **306**(**5296**), 666-669, (**2004**.). DOI: 10.1126/science.1102896
- [47] Balandin, A.A, et al "Superior thermal conductivity of single-layer graphene", **Nano. Lett. 8(3)**, 902–907, (**2008).** doi:10.1021/nl0731872
- [48] Boehm, H.P., et al "Nomenclature and terminology of graphite intercalation compounds" *Pure Appl. Chem*, **66(9)**, 1893–1901 (**1994**). doi:10.1351/pac199466091893
- [49] Liang, X., et al, "Electrostatic force assisted exfoliation of pre-patterned few-layer graphenes into device sites", *Nano Lett*, **9(1)**, 467–472, **(2008)**. doi:10.1021/nl803512z
- [50] Graphene: The Next Wonder Material?; Available from:
- http://www.acs.org/content/acs/en/education/resources/highschool/chemmatters/past-i ssues/archive-2012-2013/graphene.html
- [51] Sutter, P et al, "Epitaxial graphene: How silicon leaves the scene", *Nature Materials*, , **8(3)**, 171-172, (**2009**). doi:10.1038/nmat2392
- [52] Rollings, E., et al, "Synthesis and characterization of atomically thin graphite films on a silicon carbide substrate" *J. Phys. Chem. Solids*, **67(9-10)**, 2172–2177, (**2006**). doi:10.1016/j.jpcs.2006.05.010
- [53] Heer et al, "Epitaxial graphene", *Solid State Commun*, **143(1–2)**, 92–100, **(2007)**. doi:10.1016/j.ssc.2007.04.023
- [54] Alexander, M., et al "Density functional study of graphene overlayers on SiC", *Phys. Status Solidi B*, **245**(7), 1425–1435, (**2008**). doi:10.1002/pssb.200844031
- [55] Ni, Z.H., Chen, W., et al "Raman spectroscopy of epitaxial graphene on a SiC substrate" Phys. Rev. B Condens. Matter, **77**, 115416, (**2008**). doi:10.1103/PhysRevB.77.115416
- [56] Sutter, P.W., "Epitaxial graphene on ruthenium", *Nature Mater*, **7**, 406–411, (**2008**). doi:10.1038/nmat2166
- [57]. Seyller, T., et al "Epitaxial graphene: a new material", *Phys. Status Solidi B*, **245**(7), 1436–1446 (**2008**). doi:10.1002/pssb.200844143
- [58]. Sprinkle, M., Soukiassian, P., de Heer, W.A., Berger, C., Conrad, E.H.: Epitaxial graphene: the material for graphene electronics. Phys. Status Solidi RRL 3(6), A91–A94 (2009). doi:10. 1002/pssr.200903180
- [59] Li, X.S., et al., "Large-Area Synthesis of High-Quality and Uniform Graphene Films on Copper Foils", *Science*, **324**(**5932**), 1312-1314, (**2009**). doi: 10.1126/science.1171245
- [60] Wang, X., et al "Large-scale synthesis of few-layered graphene using CVD", *J. Chem. Vapor Deposition*, **15(1–3)**, 53–56, **(2009)**. doi:10.1002/cvde.200806737
- [61] Wang, Y., "Large area, continuous, few-layered graphene as anodes in organic photovoltaic devices", *Appl. Phys. Lett.*, **95**, 063302 (**2009**). doi:10. 1063/1.3204698
- [62] Dervishi, E., et al "Large-scale graphene production by the RF-CVD method". *Chem. Commun.* **27,** 4061–4063, (**2009**). doi:10.1039/B906323D
- [63] Chong-an, D., et al "Patterned graphene as source/drain electrodes for bottom-contact organic field-effect transistors", *Adv. Mater*, **20**(17), 3289–3293 (2008) doi:10.1002/adma.200800150
- [64] Chae, S.J., et al "Synthesis of large-area graphene layers on poly-nickel substrate by chemical vapor deposition: wrinkle formation" *Adv. Mater*, **21**(**22**), 2328–2333, (**2009**). doi:10.1002/adma.200803016

- [65] B.C. Brodie, "On the Atomic Weight of Graphite", *Phil. Trans. R. Soc. Lond*, **149**, 249-259, **(1859).** doi:10.1098/rstl.1859.0013
- [66] Minh-Hai Tran et al "Influence of graphite size on the synthesis and reduction of graphite oxide", *Current Applied Physics*, **14**, S74-S79, (**2014**). doi.org/10.1016/j.cap.2013.11.038
- [67] H.K. Jeong, et al, "Evidence of graphitic AB stacking order of graphite oxides", *J. Am. Chem. Soc*, **130(4)**, 1362 1366, **(2008). DOI:** 10.1021/ja0764730
- [68] L. Staudenmaier, et al "Verfahren zur Darstellung der Graphitsäure" *Chem. Ges.*, **31**, 1481 1487, **(1898)**. DOI: 10.1002/cber.18980310237
- [69] Dreyer D R, et al, "The chemistry of graphene oxide", *Chem. Soc. Rev.* **39** ,228–40 **(2010).** DOI: 10.1039/b917103g
- [70] W.S. Hummers et al "Preparation of Graphitic Oxide", *J. Am. Chem. Soc.*, **80**, 1339, (**1958**). DOI: 10.1021/ja01539a017
- [71] Syed Nasimul Alam, "Synthesis of Graphene Oxide (GO) by Modified Hummers Method and It's Thermal Reduction to Obtain Reduced Graphene Oxide (rGO)" *Graphene*, **6**, 1-18, (**2017**). doi.org/10.4236/graphene.2017.61001
- [72] Narasimharao K*, et al "Synthesis of Graphene Oxide by Modified Hummers Method and Hydrothermal Synthesis of Graphene-NiO Nano-Composite for Supercapacitor Application" J Material Sci Eng. **5: 6,** 1-4, **(2016).** DOI: 10.4172/2169-0022.1000284
- [73] LEILA .S, et al "Graphene Oxide Synthesized by using Modified Hummers Approach" *International Journal of Renewable Energy and Environmental Engineering*, **02**, 58-63, **(2014)**.
- [74] S. D. Perera, et al., "Hydrothermal synthesis of graphene-TiO2 nanotube composites with enhanced photocatalytic activity,", *ACS Catalysis*, **2**, 949–956, **(2012.) DOI:** 10.1021/cs200621c
- [75] Jianguo Song, Xinzhi Wang, and Chang-Tang Chang "Preparation and Characterization of Graphene Oxide" *Journal of Nanomaterials*, 1-6. (**2014**,) doi.org/10.1155/2014/276143
- [76] S Mohanty "Graphene: Synthesis, Properties, and Application" In the book Polymer Nanocomposites based on Inorganic and Organic Nanomaterials (139–194) © **2015** Scrivener Publishing LLC.
- [77] A. H. Castro Neto et al. "The electronic properties of graphene" *Rev. Mod. Phys.*, **81**, . 109 162, (**2009**) doi.org/10.1103/RevModPhys.81.109
- [78] Xia, F., et al., "Ultrafast graphene photodetector" *Nature Nanotechnology*, **4**, 839–843, (**2009**). doi:10.1038/nnano.2009.292
- [79] Mueller, T., et al., "Graphene photodetectors for high-speed optical communications", *Nature Photonics*, **4**, 297–301, (**2010**). doi:10.1038/nphoton.2010.40
- [80] Echtermeyer, T. J., et al., "Strong Plasmonic Enhancement of Photovoltage in Graphene", Nature Commun, **2**, 458, (2011). DOI:10.1038/ncomms1464 (2011)
- [81] Liu, M., et al., "A graphene-based broadband optical modulator", Nature, 474, 64–67, (2011) doi:10.1038/nature10067
- [82] Bao, Q. L., et al., "Atomic-Layer Graphene as a Saturable Absorber for Ultrafast Pulsed Lasers", *Adv Funct Mater*, **19(19)**, 3077–3083, **(2009)**. DOI: 10.1002/adfm.200901007
- [83] Bolotin, K. I. et al, "Ultrahigh electron mobility in suspended graphene", *Solid State Commun*, **146** (9-10), 351-355, (2008). doi.org/10.1016/j.ssc.2008.02.024
- [84] Du, X., et al., "Approaching ballistic transport in suspended graphene", *Nature Nanotechnology*, **3**, 491–495 (**2008**). doi:10.1038/nnano.2008.199
- [85] Schwierz, F., "Graphene transistors", *Nature Nanotechnology*, **5**, 487–496, (**2010**). doi:10.1038/nnano.2010.89

- [86] Farmer, D. B., et al., "Charge trapping and scattering in epitaxial graphene", *Phys Rev B*, **84**, 20541, (2011). doi.org/10.1103/PhysRevB.84.205417
- [87] Chen, J.-H., et al., "Defect Scattering in Graphene" *Phys Rev Lett*, **102**, 236805, **(2009)** doi.org/10.1103/PhysRevLett.102.236805
- [88] Chen, J.-H., et al., Intrinsic and extrinsic performance limits of graphene devices on SiO₂", *Nature Nanotechnology*, **3**, 206–209, **(2008)**. doi:10.1038/nnano.2008.58
- [89] Zhu, W., et al., "Carrier scattering, mobilities, and electrostatic potential in monolayer, bilayer, and trilayer graphene", *Phys Rev B*,**80**,235402,(**2009**).

doi.org/10.1103/PhysRevB.80.235402

- [90] Y.Zhu et al, "Graphene and Graphene Oxide: Synthesis, Properties, and Applications", *Adv.Mater.*, **22**, 3906, **(2010).** DOI: 10.1002/adma.201001068
- [91] Q. Lu, et al, "Excess energy and deformation along free edges of graphene nanoribbons," *Phys. Rev. B*, **81**, 155410, (**2010**). doi.org/10.1103/PhysRevB.81.155410
- [92] H. Chen, et al, "Mechanically Strong, Electrically Conductive, and Biocompatible Graphene Paper", *Adv.Mater.*, **20**, 3557, **(2008)**.DOI: 10.1002/adma.200800757
- [93] Zandiatashbar A, et al, "Effect of defects on the intrinsic strength and stiffness of graphene", *Nat Commun*, **5**, 3186, (**2014**). doi: 10.1038/ncomms4186.
- [94] Qin H, et al, "Mechanical properties of wrinkled graphene generated by topological defects", *Carbon*, **108**, 204–14, **(2016).** doi.org/10.1016/j.carbon.2016.07.014
- [95] E. Pop, et al, "Thermal properties of graphene: Fundamentals and applications", *MRS Bull.*, **37**, 1273 1281, (**2012**). doi.org/10.1557/mrs.2012.203
- [96] A.A. Balandin et al, "Thermal Conduction in Suspended Graphene Layers", *Fullerenes, Nanotubes, CarbonNanostr.*, **18**,474, **(2010**). doi.org/10.1080/1536383X.2010.487785
- [97]W.Cai et al, "Thermal Transport in Suspended and Supported Monolayer Graphene Grown by Chemical Vapor Deposition", *NanoLett.*, *10* (5),1645–1651, (2010). DOI: 10.1021/nl9041966 [98] J.H. Seol, , "Two-Dimensional Phonon Transport in Supported Graphene", *Science*, 328, (5975), 213-216, (2010). DOI: 10.1126/science.1184014
- [99] A.A. Balandin, et al, "Graphene-like Exfoliated Quasi- 2D thermoelectric crystals", CRC Press. 2012
- [100] J. Zhu, et al, "An overview of the engineered graphene nanostructures and nanocomposites" *RSC Adv.*, **3**, 22790, **(2013)**. DOI:10.1039/C3RA44621B
- [101] Andrea C, et al., "Science and technology roadmap for graphene, related two-dimensional crystals, and hybrid systems" *Nanoscale*, 7, 4598-4810, (2015), DOI:10.1039/C4NR01600A
- [102] G.E. Moore, "Cramming more components onto integrated circuits" *electronics*, **38**, 114-117, **(1965).**
- [103] M.Y. Han et al. "Energy Band-Gap Engineering of Graphene Nanoribbons", *Phys.rev.lett*, 98, 206805, (2007). doi.org/10.1103/PhysRevLett.98.206805
- [104] J.B. Oostinga et al, "Gate-induced insulating state in bilayer graphene devices", *Nat.Mater*, **7**,151 **7**,(2008). DOI:10.1038/nmat2082
- [105] Wu, Y., et al., IEDM Technical Digest, 23.8, 528, (2011)
- [106] Wu Y., et al, "High-frequency, scaled graphene transistors on diamond-like carbon". *Nature*, **472**, 74, **(2011)**. doi: 10.1038/nature09979.
- [107]Lin, et al., "Wafer-Scale Graphene Integrated Circuit", Science, **332**, 1294 -7, **(2011)** DOI: 10.1126/science.1204428
- [108] Kuzmenko, A. B. *et al*, "Universal Optical Conductance of Graphite", *Phys Rev Lett*, **100**, 117401, , **(2008).** doi.org/10.1103/PhysRevLett.100.117401
- [109] Nair, R. R., et al. "Fine Structure Constant Defines Visual Transparency of Graphene", *Science*, **320**, 1308, **(2008).** DOI: 10.1126/science.1156965

- [110] Mak, K. F., *et al.*, "Measurement of the Optical Conductivity of Graphene" *Phys Rev Lett*, **101**, 196405, **(2008).** doi.org/10.1103/PhysRevLett.101.196405
- [111] Wang, F., et al "Gate-variable optical transitions in graphene", *Science*, **320**(**5873**), 206-209, **(2008**). doi: 10.1126/science.1152793.
- [112] Mak, K. F., et al., "Seeing Many-Body Effects in Single- and Few-Layer Graphene: Observation of Two-Dimensional Saddle-Point Excitons", *Phys Rev Lett*, **106**, 046401, **(2011)**. **doi.org/10.1103/PhysRevLett.106.046401**
- [113] Xia, F., et al., "Ultrafast graphene photodetector", Nature Nanotechnology, **4**, 839–843, (**2009**). doi:10.1038/nnano.2009.292
- [114] Mueller, T., et al., "Graphene photodetectors for high-speed optical communications", *Nature Photonics*, **4**, 297–301, **(2010)**. doi:10.1038/nphoton.2010.40
- [115] E. W. Hill, et al, "Graphene Sensors", *IEEE Sens. J.*, **11**, 3161–3170, **(2011)**. Doi: 10.1109/JSEN.2011.2167608
- [116] N. L. Rangel et al, "Vibronics and plasmonics based graphene sensors", *J. Chem. Phys.*, **132**, 125102, **(2010)**. doi.org/10.1063/1.3364863
- [117] Y. Liu, et al, "Biological and chemical sensors based on graphene materials", *Chem. Soc. Rev*, **41**, 2283-2307, **(2012)**. DOI:10.1039/c1cs15270j
- [118] Q. Y. He, et al, "Graphene-based electronic sensors", *Chem. Sci*, **3**, 1764–1772,(**2012**), ... DOI:10.1039/C2SC20205K
- [119] S. M. Avdoshenko, , "Nanoscale eardrum: Graphene-based nanoscale sensors", *Nanoscale*, **4**, 3168–3174,(**2012**),. DOI: 10.1039/c2nr30097d
- [120] C. L. Wong, et al, "Characterization of nanomechanical graphene drum structures", *J. Micromech. Microeng*, **20(20)**, 115029, **(2010)**. doi.org/10.1088/0960-1317/20/11/115029
- [121] O. Frank, et al, "Development of a universal stress sensor for graphene and carbon fibres", *Nat. Commun*, **2**, 255, (**2011**). doi:10.1038/ncomms1247
- [122] G. Hwang, et al, "Graphene as thin film infrared optoelectronic sensor", *Isot: 2009 International Symposium on Optomechatronic Technologies*, 169–174, (2009)

DOI: 10.1109/ISOT.2009.5326118

- [123] K. W. C. Lai, et al, "Development of graphene-based optical detectors for infrared sensing applications," IEEE Sens., 398–401,(2011).doi.org/10.1109/ICSENS.2011.6127221
- [124] Andrea C. Ferrari et al. "Science and technology roadmap for graphene, related two-dimensional crystals, and hybrid systems" *Nanoscale*, **7**, 4598 4810, (**2015**).

DOI:10.1039/C4NR01600A

- [125] I. Surjati, "Increasing Bandwidth Dual Frequency Triangular Microstrip Antenna For WiMAX Application", *IJECS-IJENS*, **10**, 16–20, **(2010)**.
- [126] C. Di, et al, "Patterned Graphene as Source/Drain Electrodes for Bottom-Contact Organic Field-Effect Transistors", *Adv. Mater.* **20**, 3289–3293, **(2008).** DOI: 10.1002/adma.200800150
- [127] C. Sire, et al, "Flexible Gigahertz Transistors Derived from Solution-Based Single-Layer Graphene", *Nano Lett*, **12**, 1184–1188., **(2012).** DOI: 10.1021/nl203316r
- [128] B. Kumar, et al, "The Role of External Defects in Chemical Sensing of Graphene Field-Effect Transistors", *Nano Lett*, **13**, 1962–1968, (**2013**). DOI: 10.1021/nl304734g
- [129] C. Thiele and R. Das, http://www.IDTechEx.com (book)
- [130] B. Kumar et al, "Cathodes for Solid-State Lithium—Oxygen Cells: Roles of Nasicon Glass-Ceramics", *J. Electrochem. Soc.*, 157, A611-A616, (2010). doi: 10.1149/1.3356988.
- [131] C. Liu, "Graphene-based supercapacitor with an ultrahigh energy density", *Nano Lett.*, **10**, 4863–4868, (**2010**). DOI:10.1021/nl102661q.

- [132] T. Kim, et al, "Activated Graphene-Based Carbons as Supercapacitor Electrodes with Macroand Mesopores", *ACS Nano*, **7(8)**, 6899–6905, **(2013)**. DOI: 10.1021/nn402077v
- [133] Y. Jeon, et al, "Facile, scalable synthesis of edge-halogenated graphene nanoplatelets as efficient metal-free electrocatalysts for oxygen reduction reaction", *Sci. Rep.*, **3**, 1810, **(2013). doi:** 10.1038/srep01810
- [134] L. Dong, et al "Graphene-supported platinum and platinum-ruthenium nanoparticles with high electrocatalytic activity for methanol and ethanol oxidation", *Carbon*, **48**, 781–787,(**2010**). doi.org/10.1016/j.carbon.2009.10.027
- [135] J. Kim, et al, "Water Processable Graphene Oxide: Single-Walled Carbon Nanotube Composite as Anode Modifier for Polymer Solar Cells Adv", *Energy Mater.*, **1(8)**, 1052–1057, **(2011)**. **DOI:** 10.1002/aenm.201100466
- [136] P. Robaeys, et al, "Enhanced performance of polymer: fullerene bulk heterojunction solar cells upon graphene addition", *Appl. Phys. Lett*, **105**, 083306, (**2014**). doi.org/10.1063/1.4893777 [137] J. Haskins, et al, "Control of Thermal and Electronic Transport in Defect-Engineered Graphene Nanoribbons", *ACS Nano*, **5(5)**, 3779–3787, (**2011**). DOI: 10.1021/nn200114p
- [138] H. Sevinçli, et al., "A bottom-up route to enhance thermoelectric figures of merit in graphene nanoribbons", *Sci. Rep.*, **3**, 1228, (**2013**) **doi:** <u>10.1038/srep01228</u>
- [139] J. Kwon, et al, "A high-performance PZT ribbon-based nanogenerator using graphene transparent electrodes", *Energy Environ. Sci.*, 5, 8970–8975, (2012). DOI:10.1039/C2EE22251E
- [140] F. Bonaccorso, et al, "2D materials. Graphene, related two-dimensional crystals, and hybrid systems for energy conversion and storage", *Science*, **347**(**6217**), 1246501, (**2015**). doi: 10.1126/science.1246501.
- [141] R. J. Young, et al, "The mechanics of graphene nanocomposites: A review", *Comput. Sci. Technol.*, **72**, 1459–1476, (**2012**). DOI: DOI 10.1016/j.compscitech.2012.05.005
- [142] S. Vadukumpully, et al, "Flexible Conductive Graphene/Poly (Vinyl Chloride) Composite Thin Films with High Mechanical Strength and Thermal Stability," *Carbon*, **49**, 198-205, (**2011**). doi:10.1016/j.carbon.2010.09.004
- [143] F. He, et al, "High Dielectric Permittivity and Low Percolation Threshold in Nanocomposites Based on Poly(vinylidene fluoride) and Exfoliated Graphite Nanoplates", *Adv. Mater.*, 21, 710–715, (2009). **DOI:** 10.1002/adma.200801758
- [144] C.-C. Teng, et al, "Thermal Conductivity and Structure of Non-Covalent Functionalized Graphene/epoxy composites," *Carbon*, **49**, 5107-5116. (**2011**). doi:10.1016/j.carbon.2011.06.095 [145] S. Wang, et al, "Thermal Expansion of Graphene Composites" *Macromol*, 42(14), 5251–5255,(2009). **DOI:** 10.1021/ma900631c

- [146] M. A. Rafiee, et al, "Graphene Nanoribbon Composites", *ACS Nano*, **4**, 7415–7420, (**2010**). DOI: 10.1021/nn102529n
- [147]Y.Fan,et al"Preparation and electrical properties of graphene nanosheet/Al₂O₃ composites", *Carbon*, 48, 1743–1749,(2010). DOI: 10.1016/j.carbon.2010.01.017
- [148] C. Ramirez, et al, "Electrical conductivity maps in graphene nanoplatelet/silicon nitride composites using conducting scanning force microscopy" *Carbon*, **49**, 3873–3880, **(2011)**, doi.org/10.1016/j.carbon.2011.05.025
- [149] M. Melucci, et al, "Graphene–organic hybrids as processable, tunable platforms for pH-dependent photoemission, obtained by a new modular approach", *J. Mater. Chem.*, 22, 18237–18243, (2012). DOI:10.1039/C2JM33349J
- [150] H. Hu, et al, "Ultralight and highly compressible graphene aerogels", *Adv. Mater.*, **25**, 2219–2223, (**2013**). DOI:10.1002/adma.201204530
- [151] S. Park, et al, "Graphene oxide papers modified by divalent ions- enhancing mechanical properties via chemical cross-linking." *ACS Nano*, **2** (3), 572–578, (2008). DOI: 10.1021/nn700349a [152] Thiele, H. et al, "Graphit und Graphitsaure", *Z. Anorg. Allg. Chem* (*ZAAC*). **190** (1), 145–160, (1930), DOI: 10.1002/zaac.19301900114
- [153] Hofmann, U. et al., "Die Konstitution der Graphitsaure und ihre Reaktionen", *Liebigs Ann. Chem.*, **510** (1), 1–41, (1934). DOI: 10.1002/jlac.19345100102
- [154] Ruess, G. "Über das Graphitoxyhydroxyd (Graphitoxyd), Chem., 76(3-5), 381 -417, (1946)
- [155] Clauss, A et al., "Untersuchungen zur Struktur des Graphitoxyds", Z. Anorg. Allg. Chem. **291** (5–6), 205–220, (**1957**). **DOI**: 10.1002/zaac.19572910502
- [156] Nakajima, T et al, "Formation process, and structure of graphite oxide", *Carbon*, **32**, 469 -475, **(1994).** doi.org/10.1016/0008-6223(94)90168-6
- [157] ayrat.M.Dimiev et al "Mechanism of Graphene Oxide Formation", ACS Nano, 8 (3) ,3060–3068 '(2014). **DOI:** 10.1021/nn500606a
- [158] Gongkai Wang et al. "Tailoring oxidation degrees of graphene oxide by simple chemical reactions" *Appl. Phys. Lett.* **99**, 053114 , (**2011**) . https://doi.org/10.1063/1.3622637
- [159] Jesus Guerrero et al "Graphene oxide powders with different oxidation degree, prepared by synthesis variations of the Hummers method", *Materials Chemistry and Physics*, **153**, 209-220, **(2015)**. https://doi.org/10.1016/j.matchemphys.2015.01.005
- [160] Tong Hun Kang et al "Hidden Second Oxidation Step of Hummers Method", *Chem. Mater.* **28**, 756–764, **(2016)**. **DOI:** 10.1021/acs.chemmater.5b03700
- [161] Kaiser AB et al "Electronic transport properties of conducting polymers and carbon nanotubes", *Rep Prog Phys*, **64(1)**, 1–49, **(2001)**.
- [162] Kopelevich Y et al, "Graphene physics in graphite", *Adv Mater*,**19(24)**,4559–63,**(2007)**. DOI: 10.1002/adma.200702051
- [163] Zhao J, et al, "Efficient preparation of large-area graphene oxide sheets for transparent conductive films", ACS Nano, 4(9), 5245–52, (2010). DOI: 10.1021/nn1015506
- [164] Becerril HA, et al, "Evaluation of solution-processed reduced graphene oxide films as transparent conductors", *ACS Nano*, **2(3)**, 463–70, **(2008)**. **DOI:** 10.1021/nn700375n
- [165] Xingfa Gao et al. "Hydrazine and Thermal Reduction of Graphene Oxide: Reaction Mechanisms, Product Structures, and Reaction Design," *J. Phys. Chem. C*, **114**, 832–842, (**2010**). **DOI:** 10.1021/jp909284g
- [166] Ning-Jing Song et al. "Thermally reduced graphene oxide films as flexible lateral heat spreaders", *J. Mater. Chem. A.*, **2**, 16563–16568, (**2014**). DOI: 10.1039/c4ta02693d
- [167] Sasha Stankovich an et al "Synthesis of graphene-based nanosheets via chemical reduction of exfoliated graphite oxide", *carbon*, **45**,1558 1565, (**2007**). doi:10.1016/j.carbon.2007.02.034 [168] Dan Li et al "Processable aqueous dispersions of
- graphene nanosheets", nature nanotechnology, 3, 101 105, (2008). doi:10.1038/nnano.2007.451

- [169] T.T.Dang et al. "Superior dispersion of highly reduced graphene oxide in N, N-dimethylformamide," *Journal of Colloid and Interface Science*, **376**, 91–96, (**2012**). DOI: 10.1016/j.jcis.2012.03.026
- [170] Prerna Bansal, et al "Effect of Reaction Temperature on Structural and Optical Properties of Reduced Graphene Oxide" *International Journal of Materials, Mechanics, and Manufacturing*, **2(1)**, 18 20, **(2014)**. DOI: 10.7763/IJMMM.2014.V2.90
- [171] Cristina Botas et al "The effect of the parent graphite on the structure of graphene oxide", Carbon, 50, 2 7 5 2 8 2, (2 0 1 2). doi.org/10.1016/j.carbon.2011.08.045
- [172] Cristina Botas et al "Optimization of the size and yield of graphene oxide sheets in the exfoliation step", **Carbon**, 6 3, 5 6 2 5 9 2, (2 0 1 3). DOI10.1016/j.carbon.2013.06.096
- [173] Minh-Hai Tran et al "Influence of graphite size on the synthesis and reduction of graphite oxide", *Current Applied Physics*, **14**, S74-S79, **(2014)**. doi.org/10.1016/j.cap.2013.11.038
- [174] Haiyang Xian et al "Effect of Particle Size of Natural Flake Graphite on the Size and Structure of Graphene Oxide Prepared by the Modified Hummers Method", *Materials Science Forum*, **814**, 185-190, **(2015).** DOI:10.4028/www.scientific.net/MSF.814.185
- [175] Haoran Yu et al "The importance of raw graphite size to the capacitive properties of graphene oxide" RSC Adv., 6, 17023–17028, (2016). DOI:10.1039/C5RA24501J
- [176] Kai Wang et al "Preparation of graphene nanosheet/alumina composites by spark plasma sintering", *Materials research bulletin*, **4**, 315–318, (**2011**). 10.1016/j.materresbull.2010.11.005 [177] Yuchi Fan, et al, "Highly Conductive Few-Layer-Graphene/Al2O3 Nanocomposites with Tunable Charge-Carrier Type," *Adv. Funct. Mater*, **22** (**18**), 3882 -3889, (**2012**). **DOI:** 10.1002/adfm.201200632
- [178] Harshit Porwal et al "Graphene Reinforced Alumina Nano-Composites" *C A R B O N*, **6 4**, 3 5 9 3 6 9, **(2 0 1 3)**. http://dx.doi.org/10.1016/j.carbon.2013.07.086
- [179] Agnieszka et al, "New Reduced Graphene Oxide/Alumina(RGO/Al2O3)Nanocomposite: Innovative Method of Synthesis and Characterization" *Int. J. Appl. Ceram. Technol*, **12** (3), 522 528, (2013). DOI: 10.1111/ijac.12183
- [180] Ben Lee et al "Simultaneous strengthening and toughening of reduced graphene oxide/alumina composites fabricated by molecular-level mixing process" *C A R B O N*, **7 8**, 2 1 2 2 1 9, (**2 0 1 4**) DOI: http://dx.doi.org/10.1016/j.carbon.2014.06.074
- [181] A.M.Jastrzebska et al "Synthesis of the RGO/Al2O3 core-shell nanocomposite flakes and characterization of their unique electrostatic properties using zeta potential measurements" *Applied Surface Science*, **362**, 577 594, **(2016)**. https://doi.org/10.1016/j.apsusc.2015.10.125
- [182] Kaleem Ahmad, Wei Pan and Hui Wu "High-performance alumina-based graphene nanocomposites with novel electrical and dielectric properties" *RSC Adv.*, **5**, 33607–33614, (**2015**). DOI: 10.1039/C5RA01481F